

CRANFIELD UNIVERSITY

SITI JUITA MASTURA MOHD SALEH

MODELLING AND ANALYSIS OF THIN-WALLED STRUCTURES  
FOR OPTIMAL DESIGN OF COMPOSITE WING

SCHOOL OF AEROSPACE, TRANSPORT AND  
MANUFACTURING  
Centre for Aeronautics

PhD

Academic Year: 2012 - 2017

Supervisor: Professor Shijun Guo  
May 2017

CRANFIELD UNIVERSITY

SCHOOL OF AEROSPACE, TRANSPORT AND  
MANUFACTURING  
Centre for Aeronautics

PhD

Academic Year 2012 – 2017

SITI JUITA MASTURA MOHD SALEH

MODELLING AND ANALYSIS OF THIN-WALLED STRUCTURES  
FOR OPTIMAL DESIGN OF COMPOSITE WING

Supervisor: Professor Shijun Guo  
May 2017

This thesis is submitted in partial fulfilment of the requirements for  
the degree of PhD

© Cranfield University 2017. All rights reserved. No part of this  
publication may be reproduced without the written permission of the  
copyright owner.

## **ABSTRACT**

At present, the option for composite usage in aircraft components and the associated manufacturing process is largely based on experience, knowledge, benchmarking, and partly market driven. Consequently, a late realisation involving the design and manufacture, and an inevitable iterative design and validation process has led to high costs. The aim of this research is to develop a Knowledge-Based Optimisation Analysis Tool (K-BOAT) for optimal design of composite structures, subject to multi design constraints. Extensive study has been carried out on composite structure design, modelling, testing and analysis method to optimise a design of a composite wing panel during the preliminary design stage. This approach will allow the maximum knowledge input and interface between users (design engineers) with the design tool, rather than be left to the optimiser to provide a solution. The K-BOAT will build a set of parameters in the initial design, including the ratio of component dimensions, layers of different fibre angles, and bending-torsion coupling of a panel and a wing box. This framework offers a guideline for the design engineers to understand and expect the optimal solution of composite structures at the early design stage. This research focused on the optimal design of aircraft composite wing skin. The first level involved the initial analysis of the composite wing by using a low fidelity model based on thin-walled structural analysis method. The second level focused on the optimal design of the wing skin using the analytical method and validation using the high fidelity finite element (FE) method. In-house computing programs and commercial software are used for this level of study. In the third level, the FE model has been used to present a baseline structure to perform further detailed analysis and optimisation. The study is related to an industrially funded project. A case study of a practical wing structure in the project has indicated an improvement in aircraft aeroelastic stability by 30.5% from the initial design. Validation of the real industrial application proved that K-BOAT is applicable to the conceptual and preliminary phases in aircraft design.

**Keywords:** Composite structure, aircraft wing structure, optimal wing design, knowledge-based, optimisation tool.

## **ACKNOWLEDGEMENTS**

To the Almighty, all the praises and thanks to Allah the Giver of the bountiful blessing to me and my family throughout this journey.

A massive thank you to my supervisor, Professor Shijun Guo. His endless support both in academic and personal life are the reasons why I keep going, even during a very tough time. Thank you for converting my mistakes into lessons and my skills into strengths. And thank you for your valuable guidance until the very end.

To my dear husband who has sacrificed his job for me, to be here to support me. No words can describe how much you mean to me. No one else can take your place. You are my life, my heart, my soul.

Mom and dad, my biggest fans. I was raised to always believe that I could do anything I set my mind to. You taught me how to live and how to survive. Thousand miles apart, but we are always, always close at heart.

Blood is thicker than water. Thanks to my brother and sister for getting in touch with me every day. And a big hug to my sister for flying all the way from Malaysia to England to support me during this intense time. The moment she slept in the sleeping bag under my desk to accompany me, staying overnight at my office will always be cherished!

My staunch friends, Ogie, Kak Rohafiz and Ariel. These good friends always stood by side during my thick and thin. May you always be in His blessing. Only Allah can repay your good deeds.

I am deeply indebted to my friend, Hao Li who has supported me greatly and was always willing to help me with my research subject. I wish you all the best in your PhD journey. My Warlord, Si Chen, your computer skills and your unique tools helped me every time my machine gave me trouble. To Romans Kirenskis and Dami, thank you for letting me use your desktop when it was really in needed. Thank you lads.

And to Ministry of Education Malaysia and Universiti Tun Hussein Onn Malaysia, thank you for the three year sponsor and financial support.

# TABLE OF CONTENTS

ABSTRACT .....	i
ACKNOWLEDGEMENTS.....	ii
LIST OF FIGURES.....	vi
LIST OF TABLES .....	xii
LIST OF NOMENCLATURE AND ABBREVIATIONS .....	xv
1 INTRODUCTION.....	1
1.1 Overview and Motivation.....	1
1.2 Problem Statement .....	2
1.3 Aim and Objectives .....	2
1.4 Research Methodology .....	3
1.5 Research Novelty.....	4
2 LITERATURE REVIEW .....	5
2.1 Composite Laminate and Box in Aircraft Structure .....	5
2.1.1 Composite Laminate .....	5
2.1.2 Composite Box Structures.....	6
2.2 Overview of Engineering Design Optimisation Approaches.....	11
2.2.1 Classification of Engineering Design Optimisation .....	11
2.2.2 Knowledge-Base (KB) Definition and Technique .....	12
2.2.3 The Importance of Knowledge-Based System (KBS).....	14
2.2.4 Engineering Design Optimisation Approaches .....	15
2.2.5 Expert-Based Optimisation Approach .....	16
2.2.6 Design of Experiment-Based Optimisation Approach .....	17
2.2.7 Algorithmic Optimisation Approach .....	17
2.3 Optimisation of Composite Wing Structure .....	18
2.4 Aeroelastic Tailoring .....	20
2.5 Manufacture Constraint in Composite Structure Optimisation .....	22
3 KNOWLEDGE-BASED OPTIMISATION ANALYSIS TOOL (K-BOAT) .....	26
3.1 Phase 1: Classify (Requirement) .....	27
3.2 Phase 2: Identify .....	28
3.3 Phase 3: Analyse .....	29
3.4 Phase 4: Optimise.....	30
4 THEORETICAL STUDY .....	31
4.1 Mechanics of Composite Plate .....	31
4.1.1 Strain-Displacement Relations of a Composite Plate.....	31
4.1.2 Stress-Strain Relations.....	36
4.1.3 In-plane Resultant Forces .....	40
4.1.4 Resultant Moments .....	42
4.1.5 Laminate Equivalent Engineering Elastic Constant.....	44
4.2 Thin-walled Composite Beams: Single-Cell and Double-Cell .....	46
4.2.1 Displacement Field of a Composite Box Beam .....	46

4.2.2 Force-Deformation Relationships.....	49
4.3 Optimisation Method.....	51
5 ANALYSIS OF COMPOSITE PLATES AND THIN-WALLED COMPOSITE BEAMS.....	54
5.1 Composite Laminate Analysis.....	54
5.1.1 Equivalent Elastic Constant-Stiffness Relationship.....	54
5.1.2 Mathematical Equation: $E_x$ , $E_y$ and $G_{xy}$ Membrane Mode and Bending Mode.....	66
5.2 Composite Box Analysis.....	71
5.2.1 Composite Laminate and Box Relation.....	74
5.2.2 Laminate, Single-Cell Box and Double-Cell Box Relationship.....	78
5.3 A Matrix Element Analysis.....	80
5.3.1 Principal Findings.....	91
5.4 Coupling Stiffness Analysis.....	92
5.4.1 Coupling Stiffness Formula.....	92
5.4.2 BOXMX Program.....	95
5.4.3 FE Analysis.....	95
5.4.4 Discussion.....	101
5.4.5 Conclusion.....	102
5.5 Cut-out Analysis of Aluminium and Composite Box.....	104
5.6 Design Composite Box in Laminate Level.....	112
5.6.1 Method 1: Use Ten-Percent Rule.....	112
5.6.2 Method 2: Use Laminate and Thin-Walled Beam Theory (1-dimensional to 2-dimensional box).....	114
5.6.3 Method 3: Use Thin-Walled Beam Theory and FE Model (2-dimensional to 3-dimensional box).....	122
6 STRESS, BUCKLING, FREE VIBRATION AND AEROELASTIC ANALYSIS OF COMPOSITE WING.....	132
6.1 General Information.....	133
6.2 Skin Laminate Properties.....	135
6.3 Stiffness Analysis.....	137
6.3.1 Wing Box Sections.....	137
6.3.2 Stiffness Evaluation using BOXMX Program.....	139
6.3.3 Stiffness Evaluation using NASTRAN.....	143
6.3.4 Comparison of Results Using BOXMX Program and NASTRAN ...	151
6.4 FE Modelling and NASTRAN Analysis.....	154
6.4.1 Stress and Strain.....	154
6.4.2 Buckling Analysis.....	159
6.4.3 Modal Analysis.....	161
6.4.4 Flutter Analysis.....	164
6.4.5 Effect of Stringer Addition to Flutter Speed.....	168

7 OPTIMISATION OF COMPOSITE WING SUBJECT TO MULTI DESIGN AND MANUFACTURING CONSTRAINTS.....	174
7.1 Wing Optimisation.....	174
7.2 Result.....	177
7.2.1 Convergence History.....	177
7.2.2 Flutter Speed.....	180
7.2.3 Laminate Layup.....	182
7.2.4 Natural Modes and Frequency.....	186
8 CONCLUSIONS AND SCOPE FOR FUTURE WORK.....	189
8.1 Conclusions.....	189
8.2 Scope for Future Work.....	190
REFERENCES.....	191
APPENDICES.....	200
Appendix A: ABD Matrix Program (Example data file).....	200
Appendix B: BOX Program (Example data file).....	203
Appendix C: Comflut Program (Example data file).....	205
Appendix D: Optimisation (MATLAB Code).....	210
1) Material Input Data.....	210
2) Layup Process.....	212
3) Flutter Speed Process.....	213
4) Pre-process Optimisation.....	214
5) Post-process Optimisation.....	214
6) NASTRAN Input Data.....	215
7) NASTRAN Input for Optimisation.....	216
8) Optimisation Code (Flutter).....	217

## LIST OF FIGURES

Figure 2.1 Torque, transverse and axial loads acting on a beam .....	7
Figure 2.2 The normal forces $N$ , transverse shear forces $V_y$ and $V_z$ , bending moment, $M_y$ and $M_z$ and torque, $T$ acting on a beam .....	7
Figure 2.3: Example of Composite Laminate.....	10
Figure 2.4: Example of Single-Cell Box [12].....	10
Figure 2.5: Example of Double-Cell Box [17].....	10
Figure 2.6: Methods of Knowledge-Base [20].....	13
Figure 2.7: Basic for AI Problem Solving .....	14
Figure 2.8 An overview of engineering design optimisation approaches .....	16
Figure 2.9 MCLACA flowchart [41] .....	19
Figure 2.10 Example of section geometry definition of stringers .....	23
Figure 3.1 K-BOAT Framework .....	27
Figure 4.1 Undeformed (a) and deformed (b) geometry of laminate .....	32
Figure 4.2 Modulus, strain and stress variation through the laminate thickness [64] .....	37
Figure 4.3 Force intensity on a composite plate .....	40
Figure 4.4 Moment intensity on a composite plate .....	42
Figure 4.5 Coordinate systems and kinematic variables for thin-walled shell...	46
Figure 5.1 $E_x$ for $LU$ and $LB$ membrane and bending mode at different ply angle .....	56
Figure 5.2 $E_y$ for $LU$ and $LB$ membrane and bending mode at different ply angle .....	57
Figure 5.3 $G_{xy}$ for $LU$ and $LB$ membrane mode and bending mode at different ply angle .....	58
Figure 5.4 Percentage different $LU$ and $LB$ for $E_x$ , $E_y$ and $G_{xy}$ membrane mode .....	59
Figure 5.5 Percentage different $LU$ and $LB$ for $E_x$ , $E_y$ and $G_{xy}$ bending mode	60
Figure 5.6 $EI$ for $LU$ and $LB$ .....	61
Figure 5.7 $GJ$ for $LU$ and $LB$ .....	61
Figure 5.8 $CK$ for $LU$ and $LB$ .....	62



Figure 5.9 Individual element for $[A]$ $LU$ and $LB$ .....	64
Figure 5.10 Individual element for $[D]$ $LU$ and $LB$ .....	65
Figure 5.11 $EI$ $LU$ and $LB$ for single-cell and double-cell box .....	72
Figure 5.12 $GJ$ $LU$ and $LB$ for single-cell and double-cell .....	73
Figure 5.13 $CK$ $LU$ and $LB$ for single-cell and double-cell .....	73
Figure 5.14 Laminates and composite box used in this analysis .....	74
Figure 5.15 The relationship between laminate equivalent engineering elastic constants, single-cell and double-cell box .....	78
Figure 5.16 Graph $Ex$ for $LU$ and $LB$ .....	80
Figure 5.17 $a_{11}$ for $LU$ and $LB$ .....	81
Figure 5.18 Element $A_{11}$ of $A$ Matrix for $LU$ and $LB$ .....	82
Figure 5.19 Element $A_{12}$ of $A$ Matrix for $LU$ and $LB$ .....	82
Figure 5.20 Element $A_{13}$ of $A$ Matrix for $LU$ and $LB$ .....	82
Figure 5.21 Element $A_{22}$ of $A$ Matrix for $LU$ and $LB$ .....	83
Figure 5.22 Element $A_{23}$ of $A$ Matrix for $LU$ and $LB$ .....	83
Figure 5.23 Element $A_{33}$ of $A$ Matrix for $LU$ and $LB$ .....	83
Figure 5.24 Graph of $A$ elements .....	84
Figure 5.25 Graph $A_{22}$ $A_{33}$ .....	85
Figure 5.26 Graph $A_{232}$ .....	85
Figure 5.27: Graph $A_{22}A_{33} - A_{232}$ .....	85
Figure 5.28 Graph $A_{11}A_{22}A_{33}$ .....	86
Figure 5.29 Graph $2A_{12}A_{23}$ $A_{13}$ .....	87
Figure 5.30 Graph $-A_{22}A_{132}$ .....	87
Figure 5.31 Graph $-A_{33}A_{122}$ .....	87
Figure 5.32 Graph $A_{11}A_{232}$ .....	88
Figure 5.33 Breakdown of $A$ Matrix elements for $LU$ .....	88
Figure 5.34 Breakdown of $A$ Matrix elements for $LB$ .....	89
Figure 5.35 $Ex$ and $a_{11}$ correlation in a figure form .....	90
Figure 5.36 Reference axis. Coordinate for $x$ , $y$ and $z$ direction .....	92

Figure 5.37 Closed, single-cell cross section box beam.....	93
Figure 5.38 Method 1. Input example using layup properties .....	96
Figure 5.39 Method 2. Input example using equivalent stiffness .....	96
Figure 5.40 Result for Case 1.....	97
Figure 5.41 Result for Case 2.....	98
Figure 5.42 Result for Case 3.....	99
Figure 5.43 Result for Case 4.....	100
Figure 5.44 Example of CUS layup for circular tube and box beam cross section .....	102
Figure 5.45 Cut-out location and dimension. R = radius.....	104
Figure 5.46 Isometric view.....	105
Figure 5.47 Bottom view. Box with mesh .....	105
Figure 5.48 Loads applied at each box .....	106
Figure 5.49 Torsion results using aluminium.....	107
Figure 5.50 Graph of torsional stiffness for each case .....	108
Figure 5.51 Torsion results for composite boxes.....	109
Figure 5.52 Graph of torsional stiffness for each case .....	110
Figure 5.53 <b>GJ</b> reduction due to cut-out for aluminium and composite .....	111
Figure 5.54 Bending stiffness for laminate, box CUS and box CAS at different ply angle mixtures .....	113
Figure 5.55 Torsional stiffness for laminate, box CUS and box CAS at different ply angle mixtures .....	113
Figure 5.56 New conceptual framework for design tool to calculate bending stiffness, <b>EI</b> , torsional stiffness, <b>GJ</b> and coupling coefficient, <b>mx</b>	121
Figure 5.57 Coupling coefficient against laminate for different ply orientation	122
Figure 5.58 Example of bending moment load and boundary condition .....	123
Figure 5.59 Example of applied torque and boundary condition.....	124
Figure 5.60 Box section with cut-out (left) and without cut-out (right).....	125
Figure 5.61 Dimension of box with hole .....	125
Figure 5.62 Bending stiffness results from NASTRAN .....	127
Figure 5.63 Bending stiffness results box with and without cut-out .....	127

Figure 5.64 Torsional stiffness results from NASTRAN.....	128
Figure 5.65 Torsional stiffness results for box with and without cut-out .....	128
Figure 5.66 <i>EI</i> and <i>GJ</i> percentage reduction due to cut-out .....	129
Figure 5.67 Different box dimensions for bending stiffness analysis .....	130
Figure 5.68 Different taper ratio for torsional stiffness analysis.....	131
Figure 6.1 FE model of baseline wing .....	133
Figure 6.2 Locations of skin composite laminates from root to tip .....	135
Figure 6.3 Composite wing skin thickness distributions (min t=1.46mm, max t=9.15mm).....	136
Figure 6.4 Wing box sections along the span.....	137
Figure 6.5 Bending stiffness result from BOXMX Program .....	141
Figure 6.6 Torsional stiffness distribution from BOXMX Program .....	142
Figure 6.7 End condition and applied bending moment and torque .....	143
Figure 6.8 Bending stiffness of the baseline wing sections from NASTRAN ..	145
Figure 6.9 Bending stiffness distribution from NASTRAN .....	147
Figure 6.10 Torsional stiffness of the baseline wing sections from NASTRAN .....	148
Figure 6.11 Torsional stiffness distribution from NASTRAN.....	150
Figure 6.12 Bending stiffness result BOXMX Program vs NASTRAN.....	151
Figure 6.13 Percentage difference of <i>EI</i> between NASTRAN and BOXMX Program .....	151
Figure 6.14 Torsional stiffness distribution BOXMX vs NASTRAN.....	152
Figure 6.15 Percentage difference of <i>GJ</i> between NASTRAN and BOXMX Program .....	152
Figure 6.16 Aerodynamic load distribution under 2.5 load factor (total aerodynamic force=710000N).....	154
Figure 6.17 Deflection along span (Max. 1.56m).....	154
Figure 6.18 Maximum principal stresses in the upper and lower skins, and spars along the span (Max. 396 MPa) .....	155
Figure 6.19 Minimum principal stresses of upper and lower skins, and spars along the span (Max. -216MPa).....	156

Figure 6.20 Maximum principal strains of upper and lower skins, and spars along the span (Max. 6994 $\mu\epsilon$ ) .....	157
Figure 6.21 Minimum principal strains of upper and lower skins, and spars along the span (Max. -3982 $\mu\epsilon$ ).....	158
Figure 6.22 Buckling analysis results under 2.5 load factor .....	160
Figure 6.23 The first ten natural frequencies and modes .....	163
Figure 6.24 V-g plot of flutter analysis 4 modes .....	165
Figure 6.25 V-g plot of flutter analysis for damping, $g$ greater than 1.....	165
Figure 6.26 V-f plot of flutter analysis for baseline wing (6 modes) .....	166
Figure 6.27 NASTRAN T1 has been chosen for this analysis .....	168
Figure 6.28 Example of stringers location .....	169
Figure 6.29 Cross-section of the stringer .....	170
Figure 6.30 Example of stringers location at wing tip .....	173
Figure 7.1 Wing division for optimisation.....	175
Figure 7.2 Optimisation process using ABD Matrix Program, MATLAB and NASTRAN .....	176
Figure 7.3 The <i>fmincon</i> , MATLAB optimiser has been used in this optimisation .....	177
Figure 7.4 Result Box 1 .....	178
Figure 7.5 Result Box 2.....	178
Figure 7.6 Result Box 3.....	178
Figure 7.7 Result Box 4.....	179
Figure 7.8 Result Box 5.....	179
Figure 7.9 Result Box 6.....	179
Figure 7.10 Result Box 7 .....	180
Figure 7.11 Flutter speed results for initial and optimised layup.....	181
Figure 7.12 The percentage difference between initial and optimised layup design .....	181
Figure 7.13 The optimised composite wing cover panel subject to multi design constraints.....	188



## LIST OF TABLES

Table 2.1 Niu practical design guideline.....	23
Table 3.1 K-BOAT Phase 1: Classify (Requirement).....	28
Table 3.2 Phase 2 K-BOAT: Identify .....	29
Table 3.3 Phase 3 K-BOAT: Analyse .....	29
Table 3.4 Phase 4 K-BOAT: Optimise.....	30
Table 4.1 [a], [d] compliance matrix elements for a composite laminate .....	45
Table 4.2 Laminate engineering elastic constants.....	45
Table 4.3 Example of optimisation methods [91,92].....	52
Table 5.1: Material properties and dimension.....	54
Table 5.2 $E_x$ membrane and bending mode .....	56
Table 5.3 $E_y$ membrane and bending mode .....	58
Table 5.4 $G_{xy}$ membrane mode and bending mode .....	59
Table 5.5: $E_x$ membrane mode for $LU$ and $LB$ .....	67
Table 5.6: $E_x$ bending mode for $LU$ and $LB$ .....	67
Table 5.7 $E_y$ membrane mode from $LU$ and $LB$ .....	68
Table 5.8: $E_y$ bending mode for $LU$ and $LB$ .....	69
Table 5.9: $G_{xy}$ membrane mode for $LU$ and $LB$ .....	70
Table 5.10: $G_{xy}$ bending mode for $LU$ and $LB$ .....	70
Table 5.11: Bending Stiffness for Laminate 8 Layers, Laminate 16 Layers and Box .....	75
Table 5.12: Torsional Stiffness for Laminate 8 Layers, Laminate 16 Layers and Box.....	76
Table 5.13: Value of $E_x$ membrane, $E_x$ Bending and $E_x$ from EI for Laminate	77
Table 5.14 Layup for coupling study.....	94
Table 5.15 Result comparison between formula and BOXMX Program .....	95
Table 5.16 Maximum displacement results for Method 1 and Method 2 .....	101
Table 5.17 Example of input for formula and BOXMX Program .....	103
Table 5.18 Laminate layup of baseline wing model used in case study .....	107

Table 5.19 Torsional stiffness and $GJ$ reduction percentage due to cut-out (aluminium).....	108
Table 5.20 Torsional stiffness and $GJ$ reduction percentage due to cut-out (composite).....	109
Table 5.21 $GJ$ reduction percentage due to cut-out for aluminium and composite .....	110
Table 5.22 Ply angle mixtures .....	113
Table 5.23 Bending stiffness formula from laminate and beam theory.....	116
Table 5.24 Torsional stiffness formula from laminate and beam theory .....	118
Table 5.25 Coupling stiffness formula from laminate and beam theory.....	120
Table 5.26 Material properties for aluminium .....	126
Table 5.27 Material properties for composite .....	126
Table 5.28 The percentage of $EI$ and $GJ$ reduction due to cut-out .....	129
Table 5.29 Bending stiffness result for width to length ratio study.....	130
Table 5.30 Torsional stiffness results for taper ratio study .....	131
Table 6.1 General parameters of baseline wing .....	133
Table 6.2 Material properties of baseline wing .....	134
Table 6.3 Mass data .....	134
Table 6.4 Equivalent elastic properties of skin composite laminates.....	136
Table 6.5 Laminate layup and stacking sequences.....	138
Table 6.6 Bending stiffness of the wing box sections from BOXMX Program	141
Table 6.7 Torsional stiffness of the box sections from BOXMX Program .....	142
Table 6.8 Applied bending moment and bending rotation of each section .....	146
Table 6.9 Bending stiffness results from NASTRAN .....	147
Table 6.10 Applied torques and twist of the wing box sections .....	149
Table 6.11 Torsional stiffness results .....	150
Table 6.12 Buckling factor ( $BF$ ) and buckling status .....	159
Table 6.13 Flutter results summary .....	166
Table 6.14 Mechanical properties of AI 2024 .....	169
Table 6.15 Web and flange sections .....	171

Table 6.16 Bending stiffness, <i>EI</i> for stringers .....	172
Table 6.17 Flutter speed and frequency with and without stringers.....	173
Table 7.1 Flutter speed result for initial and optimised design.....	180
Table 7.2 Initial laminate layups subject to manufacturing constraints .....	183
Table 7.3 Optimised laminate layups subject to manufacturing constraints ...	184
Table 7.4 Trimmed optimum laminate layup for manufacturing considerations .....	185



## LIST OF NOMENCLATURE AND ABBREVIATIONS

$[A]$	In-plane stiffness matrix
$A_e$	Enclosed area of the cross section
$A_{sk}$	Section area of stringer skin
$A_{st}$	Section area of stringer
$ABO$	Approximation-Based Optimisation
$ACA$	Ant Colony Algorithm
$AI$	Artificial Intelligent
$A(s)$	Reduced axial stiffness
$b$	Laminate width
$b_{fl}$	Stringer flange width
$b_w$	Stringer web width
$[B]$	Membrane-bending coupling stiffness matrix
$B(s)$	Reduced coupling stiffness
$c$	Circumference
$CAS$	Circumferentially asymmetric stiffness
$CK$	Coupling stiffness
$CLT$	Reduced shear stiffness
$C(s)$	Composite laminate theory
$CUS$	Circumferentially uniform stiffness
$d$	Cross-section dimension of a thin-walled shell
$[D]$	Bending stiffness matrix
$E_1$	Longitudinal modulus
$E_2$	Transverse modulus
$E_x$	Young's modulus in $x$ direction
$E_y$	Young's modulus in $y$ direction
$EI$	Bending stiffness
$f$	Natural frequency
$FE$	Finite Element
$FRP$	Fibre Reinforced Plastic/Polymer
$G_{12}$	In-plane shear modulus
$G_{xy}$	Shear modulus in $xy$ direction
$GA$	Genetic Algorithm
$GB$	Gradient-Base
$GJ$	Torsional stiffness
$h$	Height of the thin-walled shell
$I$	Area moment of inertia

$J$	Polar moment of inertia
$k_{xx}$	Bending moment curvature in $x$ direction
$k_{xy}$	Bending moment curvature in $y$ direction
$k_{yy}$	Twisting moment curvature
$KB$	Knowledge-Base
$K - BOAT$	Knowledge-Based Optimisation Analysis Tool
$L$	Length of the thin-walled shell
$L_B$	Symmetrical and balance layup
$L_U$	Symmetrical and unbalance layup
$m_x$	Shear coupling coefficient in $x$ direction
$m_y$	Shear coupling coefficient in $y$ direction
$M$	Bending moment
$M_{xx}$	Resultant moment intensity about $y$ axis
$M_{xy}$	Twisting moment intensity about $xy$ axis
$M_{yy}$	Resultant moment intensity about $x$ axis
$MCLACA$	Multi City-Layer Ant Colony Algorithm
$MCLACO$	Multi City-Layer Ant Colony Optimisation
$MDO$	Multidisciplinary-Design-Optimisation
$MIGA$	Multi-Island Genetic Algorithm
$N_{xx}$	Resultant in-plane force intensity in $x$ axis
$N_{xy}$	Shear force intensity in $xy$ axis
$N_{yy}$	Resultant in-plane force intensity in $y$ axis
$P_{cr}$	Critical buckling load
$PS$	Permutation Search
$[\bar{Q}]$	Reduced transform stiffness matrix
$R$	Curvature radius of the shell middle wall
$s$	Circumferential coordinate
$t$	Thickness
$t_{fl}$	Stringer flange width
$t_w$	Stringer web thickness
$T$	Torque
$U$	Strain energy density
$UD$	Unidirectional
$V_f$	Flutter speed
$W$	Displacement before deformation in $z$ direction
$W_0$	Displacement after deformation in $z$ direction
$z$	$z$ coordinate from reference axis

$\epsilon_{xx}$	Transverse normal strain in $x$ direction
$\epsilon_{yy}$	Transverse normal strain in $y$ direction
$\epsilon_{zz}$	Transverse normal strain in $z$ direction
$\sigma_{xx}$	Normal stress in $x$ direction
$\sigma_{yy}$	Normal stress in $y$ direction
$\sigma_{zz}$	Normal stress in $z$ direction
$\gamma_{xy}$	Transverse shear strain in $xy$ plane
$\gamma_{xz}$	Transverse shear strain in $xz$ plane
$\gamma_{yz}$	Transverse shear strain in $yz$ plane
$\tau_{xy}$	Shear stress
$u$	Displacement before deformation in $x$ direction
$u_1$	Axial displacement
$u_0$	Displacement after deformation in $x$ direction
$v$	Displacement before deformation in $y$ direction
$\nu_{12}$	Poisson's ratio in fibre direction
$\nu_2$	Tangential displacement
$\nu_{21}$	Poisson's ratio in off-fibre direction
$\nu_0$	Displacement after deformation in $y$ direction
$\nu_{xy}$	Poisson's ratio in $xy$ plane
$\nu_{yx}$	Poisson's ratio in $yx$ plane
$\Gamma$	Closed contour
$\Phi$	Strain energy
$\varphi$	Twist angle

# 1 INTRODUCTION

## 1.1 Overview and Motivation

Carbon fibre reinforced composite has great potential to improve aircraft structure efficiency due to the high specific modulus and variable directional stiffness characteristics. For example, aeroelastic tailoring technique has been applied to optimise composite wing structures. It may also be applied to design a composite wing of high aspect ratio for large aircraft to achieve maximum aerodynamic efficiency.

The aim of this research is to develop a methodology and a Knowledge-Based Optimisation Analysis Tool (K-BOAT) for composite structural design, especially wing structures subject to multi constraints. It can be used in the early stages of aircraft design. The methodology includes three levels of design procedure: starting from the top level in the conceptual design phase structural layout and initial analysis using a low fidelity model, based on the thin-walled structure analysis method. Different types of components may be selected to suit various parts of the structure according to external and internal loading conditions and design constraints. At the second level, the study focuses on the optimal design of the primary structure and components, adopting the analytical method and validation using the high fidelity finite element (FE) method. In-house computing programs and commercial software are used at this level of study. In the third level, the FE model will be used to represent a baseline structure to perform further detailed analysis and optimisation.

Based on the methodology, the K-BOAT will be developed to optimise and assess the structural configurations in compliance with practical and low-cost composite manufacture process options. The tool will include a knowledge data base, including various materials, structure types and laminate layups, along with manufacturing limitations as design options and constraints.

## **1.2 Problem Statement**

Composite materials have become a viable and yet practical option in aircraft primary structures due to the ability to tailor their properties. However, demand to minimise the manufacturing process and reduce the maintenance cost is somehow increasing. This problem has arisen because currently there is insufficient available tool that can be used by designers during the early stage of design. Up to this stage, early decision-making is primarily based on experience or part benchmarking, with some determined by political decision. As a result, problems identified in the future will be very costly, incurring unnecessary development cost due to iterative design solutions and naturally the testing process will increase. The necessity to develop the optimisation tool for optimal design in compliance with practical design at the early design stage is identified in this thesis. Based on the methodology, an analysis tool for structural assessment and configuration with a practical manufacturing option is developed which contains knowledge-data base and optimisation procedure for material layup, types of material, types of structure as well as manufacturing constraints as design options and limitations.

## **1.3 Aim and Objectives**

The aim of this research is to develop a methodology and analysis tool that can be used as a guideline for the design engineer at early design stage. The tool is called “Knowledge-Based Optimisation Analysis Tool” or K-BOAT. This tool comprises the knowledge-based optimal design methodology for composite structure, subject to multi-design and manufacturing constraint. The research objectives in particular include:

1. To develop a methodology and Knowledge-Based Optimisation Analysis Tool (K-BOAT) framework, based on theoretical study and literature review.
2. To demonstrate the K-BOAT tool for composite aircraft wing by using low-fidelity and high-fidelity methods.
3. To investigate the macromechanics of fibre reinforced ply, composite laminate and FRP sections by carrying out the stiffness analysis on a generally orthotropic ply, stiffness matrices of a laminate and closed section thin-walled beam.
4. To identify the effect of bending stiffness, torsional stiffness and bending-coupling stiffness when laminate layup is extended to a box structure.

5. To create the FE model of a composite wing panel and perform optimisation of the wing panel skin, including the practical design constraints by applying K-BOAT.

## **1.4 Research Methodology**

Research methodology is divided into three levels of design procedure. The first level involved the initial analysis of the composite wing by using a low fidelity model, based on the thin-walled structure analysis method. In this level, material selection and structural configuration are obtained. Different types of structure are selected due to structural strength and stiffness, which are then analysed at variable loading conditions and based on design constraints. K-BOAT is developed at this stage. This tool will allow and be a guideline for the design engineer to obtain the design option and make a quick assessment at the early design stage.

In the next design procedure levels, research focused on the optimal design of the wing skin by adopting the analytical method, and validation using high fidelity finite element (FE) method. In-house computing programs and commercial software are used to this level of study. For the design requirement, study focussed on stiffness and structural strength. For practical design constraints, the study focussed on manufacturability process and design feasibility. FE analysis were carried out to validate the theory.

In the final level, the FE model has been used to present a baseline structure to perform further detailed analysis and optimisation. A case study of a new composite wing design was performed. In this level, in-house programs NASTRAN and CATIA were run and used. Computer programming such as FORTRAN and MATLAB has been used to aid the research analysis throughout the study duration.

## 1.5 Research Novelty

1. Development of a Knowledge-Based Optimisation Analysis Tool called K-BOAT. This tool has been demonstrated during the study and an optimised wing with multi design and manufacturing constraint has been designed. Results show that the flutter speed for optimised design has increased by 30.5% compared to initial design.
2. Knowledge addition to composite laminate. There is no clear explanation as to why coupling in symmetrical and balance layup is zero. Detailed research on individual element for stiffness matrix has been carried out. Analysis shows that the extension-shear coupling is eliminated in symmetrical balance layup by the plus and minus fibre angle, which contributes to the additional knowledge to shear theory.
3. Develop correlation between composite laminate, single-cell box structure and double-cell box structure of the same material, with the same properties have been developed. The relationship pattern will be a guide for the design engineer to predict the properties of the final product during the material selection process. By understanding this relationship, designers will be able to tailor the composite layup and stacking sequence as desired.
4. Develop correlation between laminate 1-dimensional, 2-dimensional and 3-dimensional beam structure. A new conceptual framework for design tool has been developed to correlate 1-dimensional to 2-dimensional beam structure. FE model was created to represent and correlate 2-dimensional and 3-dimensional beam structure. Relationships amongst composite laminates and composite wing box structures of the same material have been developed. These correlations will be guidelines for the design engineers to predict the stiffness of the wing box structure during the material selection process and laminate design stage.

## **2 LITERATURE REVIEW**

### **2.1 Composite Laminate and Box in Aircraft Structure**

The primary functions of aircraft structures are to protect passengers, payload, the entire aircraft system and environmental condition that encounter flight [1]. Aircraft structures also play important roles to provide the aerodynamic shape, to resist or transmit the applied load and be able to withstand their rigidities at all times during take-off, flying and landing. Composite materials are nowadays well known for their exceptional ability to produce high strength to weight, and high stiffness to weight ratio component [2]. The research of composite mechanics has continued over the decades, and theories relating to composite properties are continuously growing and developing. The ability to flexibly tailor the structure layup and its superior fatigue characteristic makes composites a suitable candidate in material selection for primary aircraft structures. The anisotropic properties of composites have provided significant advantages for the researchers and designers to develop further theories for design optimisation.

#### **2.1.1 Composite Laminate**

Over the years, special characteristics of composite materials have been continually discovered, due to researchers in recent times concentrating on their interesting behaviour. The continuous development of possible performance, and information on the possibility of the material strength and stiffness improvement, making research in this area highly pertinent and relevant. Composite material is essentially an anisotropic material. Tsai and Wu developed the strength criterion for anisotropic materials from a scalar function of the two strength tensors [3]. The basic understanding of dissimilarity between isotropic and anisotropic material is the presence of coupling in anisotropic material makes composite behaviour more complex [4]. Basically, the coupling occurrence in anisotropic material degrades the stiffness of the laminate. However, in some occasion, laminate is purposely designed to produce coupling so that the desired design objectives can be achieved. An example of this is the twist design of a helicopter rotor blade.

Extensive research related to the effect of coupling and various methods to eliminate the stiffness degrading coupling can be found in the literature. Sharma et al. [2] concluded



that coupling for cross-ply antisymmetric layup can be eliminated by a suitable choice of layup combination, stacking sequence and thickness ratio. It is proved that those factors are independent of the material properties of composite laminate. York [5] uses numerical equation and Classical Laminate Theory (CLT) to derive the presence of extension-shear coupling in 21 plies of composite laminate. York then illustrates the manufacturing method on how to construct a flat composite laminate without in-plane or out-of-plane coupling, under elevated temperature curing process, using up to 21 plies.

Bartholomew [6] showed that the bending coupling is easier to remove compared to membrane bending when using orthotropy ply. CLT is applied in the research with variation of laminate stacking layup.

J. Li and D. Li [7] derived the extension-shear coupled laminate by using CLT. It is shown that with the existence of hygro-thermal shearing distortion (HTSD), no standard form of extension-shear coupling appeared. This finding is achieved using a constrained optimisation method. Research has been conducted in a satisfactory manner and without the material dependent requirement.

The drawback of composites compared to isotropic materials is during manufacturing, part maintenance or repair, the process using mechanical joints which can degrade the stiffness of the laminate. Experiments run by Nakayama et al. [8] showed that the stiffness of the plate changed over the bearing stress-strain test. The result was verified by finite element analysis. The reliability-based fitting factor developed by combining the finite element damage analysis together with stochastic technique. For an easier composite repair technique, Bendemra et al. [9] discovered the tapered scarf repair. Influences of joint materials and parameter have been investigated at critical stress conditions. The tapered scarf repair experiment was conducted in the stepped-lap joint, with the addition of adhesive bond line to confirm the joint design parameter, including thickness of adhesive and ply, stacking sequence and layup and the taper angle. Results have been confirmed with linear finite element analysis.

### **2.1.2 Composite Box Structures**

The application of a composite wing box in structure design is much more widespread now, compared to previous years. Lately, aircraft structural engineers favour the use of

composite material. The high-strength and high-stiffness to weight ratio are the beneficial points for this material's selection. The elastic properties of the material can be optimised for a laminate, as well as for a composite box. The analysis of a composite box however is more complex than the analysis of a composite plate. A wing box can be a single-cell, two-cell or multi-cell, depending on the requirement by customer or manufacturer. In this research, both single-cell and double-cell box are evaluated in order to determine which option is stronger and stiffer and hence develop a new theory regarding the finding. Figure 2.1 shows the example of torque, transverse and axial loads acting on a beam while Figure 2.2 illustrates the example of forces, bending moment and torque acting on a beam structure.

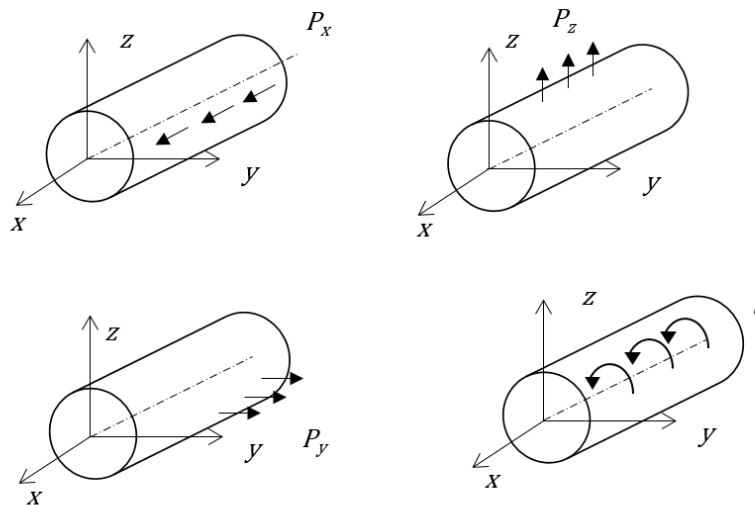


**Figure 2.1 Torque, transverse and axial loads acting on a beam**

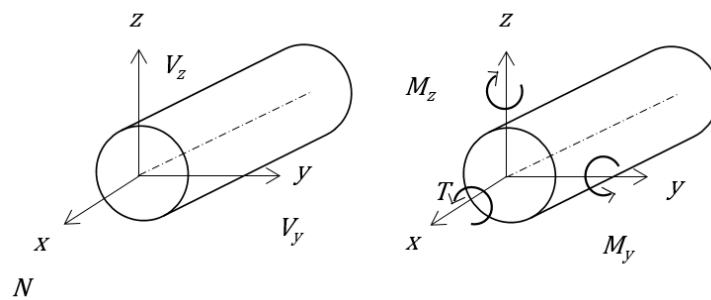


**Figure 2.2 The normal forces  $N$ , transverse shear forces  $V_y$  and  $V_z$ , bending moment,  $M_y$  and  $M_z$  and torque,  $T$  acting on a beam**

### **2.1.2.1 Development of Stiffness Relation for Composite Laminate, Single-Cell Composite Box and Double-Cell Composite Box**

Previous study regarding composite laminate theory and laminate closed-cell beam were mainly contemplated by materials and structural researchers. Mansfield [10] carried out an analysis of a two-cell thin walled anisotropic tube. The tube wall laminate used had asymmetry, hence analysis was formed on the presence of coupling between shear stress, direct stress and direct strain. In his research, Mansfield derived theories for a single-cell box and a double-cell box, which are subject to longitudinal tension, bending and torsion. Banerjee and Williams [11] derived analytical expressions for bending-torsion coupled and a Timoshenko composite beam elements, which had been proven to reduce around 87% time saving compared to the normal matrix inversion method when computing natural frequencies.

Armanios and Badir [12] derived the equation of motion for their research regarding anisotropic thin-walled beam, where analysis of free vibration was applied to types of laminate cases, which have Circumferentially Uniform Stiffness (CUS) or asymmetry layup and Circumferentially Asymmetric Stiffness (CAS) or symmetry layup. They highlighted that CUS produces extension-twist and bending-transverse shear coupling, whereas CAS produces bending-twist and extension-transverse shear coupling [13]. The effect of a different stacking sequence on free vibration analysis was examined.

Further research on anisotropic thin-walled beam closed-section has been continued by Berdichevsky et al. [14]. Theory was based on a two-dimensional closed section box. It is based on anisotropy materials properties and the displacement equation has been published in this research. In composite laminate, shear stiffness is generally very low, and this can affect the behaviour of composite beams: the same as the elastic couplings. Bauchau et al. [15] conducted an experiment to validate the theory of composite beam twist and strain distribution and used two methods to estimate warping deformation and warping constraints. His method used the St. Venant warping and Eigenwarping approaches. Results show that theory has good agreement with the experimental results.

Chandra and Chopra present a research paper regarding the effect of structural behaviour of double-cell beam [16]. The theory adopted in this paper was applied to

composite rotor blades, in the presence of elastic couplings. The Vlasov composite laminate theory was expanded by Chandra and Chopra to a two-cell box structure. Analysis was performed by taking into account the cross-section transverse shear deformation. The warping function was adopted in their analysis and shear stiffness of the closed contour section was also included in their research.

Badir extended the variation of consistent single-cell composite beams from his previous work [17]. In this paper the theory for static response of double-cell anisotropic thin-walled beam, subject to extension, bending and torsion were developed. Badir developed the theory using variationally and asymptotically convergence method to calculate the static response for this type of anisotropy closed-cell.

All significant theories and related analysis were adopted and applied to this research in order to find one common factor that relates to the structure rigidity for composite laminate, closed-section single-cell beam and double-cell beam box.

#### **2.1.2.2 Torsional and Bending Rigidity for Laminates, Single-Cell Box and Double Cell Box**

Theories for composite stiffness and strength structure are extensively studied in this thesis. Assumptions are considered and taken into account in relating the torsional and bending rigidity of composite in these three different forms. An analytical model, displacement field, kinematic equation, force-deformation relationships in kinematic variables are studied. The equations of motion are integrated to obtain the formula to calculate the axial force, torsional moment and bending moment in order to obtain the torsional stiffness and bending stiffness. Figure 2.3, Figure 2.4 and Figure 2.5 show the examples of composite laminate, single-cell box and double-cell box, respectively.

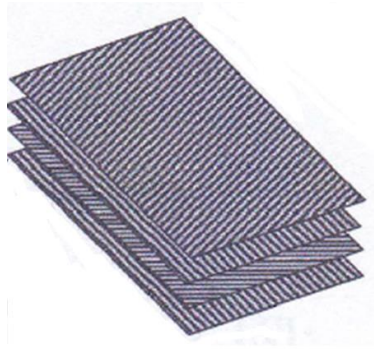


Figure 2.3: Example of Composite Laminate

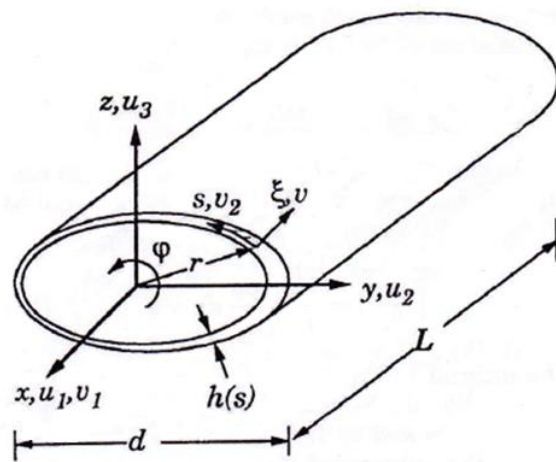


Figure 2.4: Example of Single-Cell Box [12]

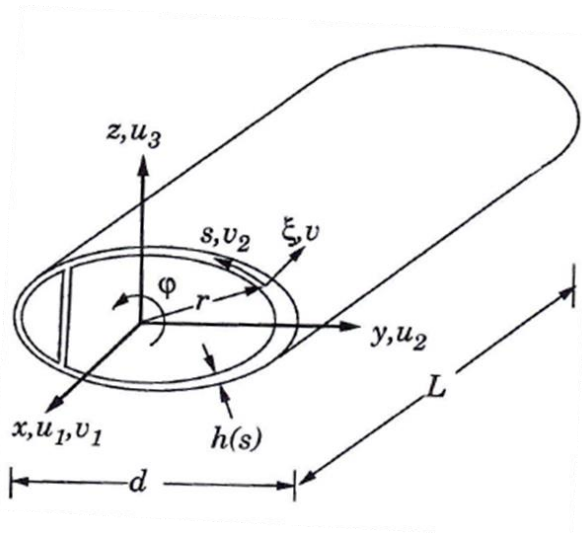


Figure 2.5: Example of Double-Cell Box [17]

## **2.2 Overview of Engineering Design Optimisation Approaches**

Design is the main step in manufacturing products or components, where most of the important decisions are made at this stage which will determine the final quality, safety, cost and delivery of a product. Since 1980, analysis techniques have been made available, which can guide designers towards products that are easy to manufacture and assemble. The availability of these techniques has created a revolution in the manufacturing industry, which has led to the reduction of product cost, manufacturing time and ease suppliers, lowered inventory and more importantly improved the product quality [18]. At the early stage of product design, the most essential steps are to define manufacturing and assembly problems and their limitations. The next step is to use Design for Manufacture and Assembly (DFMA) to arrive at the final product and ascertain if improvement is required: the process will return to the design engineer for design enhancement.

### **2.2.1 Classification of Engineering Design Optimisation**

A classification of the engineering design optimisation problems is essential in order to make decisions and choose the right approach for a given problem. Roy et al. [19] have developed the classification of engineering design optimisation based on five basic schemes and two viewpoints. The basic schemes are: design variables, constraints, objective functions, problem domains and the environment for the design.

1. Design variables: the number of design variables, their nature, permissible values and mutual dependencies that can affect the overall complexity of the optimisation task.
2. Design constraints: can be linear or nonlinear in nature.
3. Objective functions: to evaluate a design solution within the context of optimisation.
4. Problem domains: give different physics consideration within the optimisation such as aircraft design, requires significant effort and makes the optimisation more complex than single domain optimisation.
5. Environment optimisation: involves considerations like uncertainties in the design, level of knowledge available regarding the design solutions, importance of designer involvement and the nature of the environment.

The two viewpoint classifications of engineering design optimisation are design evaluation effort and the degrees of freedom of the design problem.

### **2.2.2 Knowledge-Base (KB) Definition and Technique**

Knowledge-base (KB) consists of data repository that provides information based on the way it is programmed. The rules programmed in the KB will form the repository pattern. The system in KB will not expand beyond their programming and will only do what it is designed to do. KB associates knowledge as well as numeric. Results produced are based on calculated values that are programmed.

Ke Wang et al. [20] define that the methods of KB consist of three steps as shown in Figure 2.6. The first step is to recognize the reaction centres for each reaction. The reaction classifications are based on these atom centres. All atoms with bonds being built or broken during the reaction are referred as reaction centres. The second step is to define the hierarchy of the reaction patterns. The feasibility of a reaction depends on many factors, where the structures and conditions are most influential. Structures of the reactants are the key factors that determine reaction occurrence. The conditions are the external factors that control the direction and extent of the reaction. The third step is to organize the generic reaction knowledge. A frame system has been built to store the Generic Reaction Knowledge-Base (GRKB) data, retrieve the new information from this GRKB and to implement linking to the original reaction data.

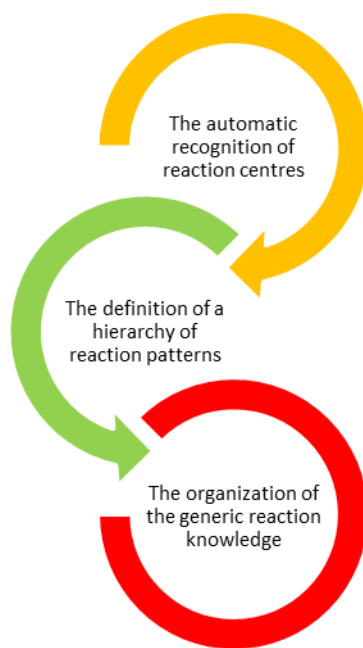


**Figure 2.6: Methods of Knowledge-Base [20]**

Bobbie [21] found that KB data can be formed into the same class or group by using the same information of data objects that they are related to. If data in the group did not match, they will isolate and leave weak linkage between them. Velasquez [22] states that by supporting the domain expert, the pattern repository is validated or rejected. Rules on how to use pattern are then created.

KB system uses Artificial Intelligent (AI) in problem solving algorithms. AI is a technology of computer science that develops intelligence into computer system and enables the machine and software to perform tasks that usually involve human intelligence. It uses step-by-step reasoning when solving puzzles and makes logical deductions. AI is broadly applied in science and technology fields, including robotics, computer games, expert systems and neural networks. The basic of AI problem solving is shown in Figure 2.7



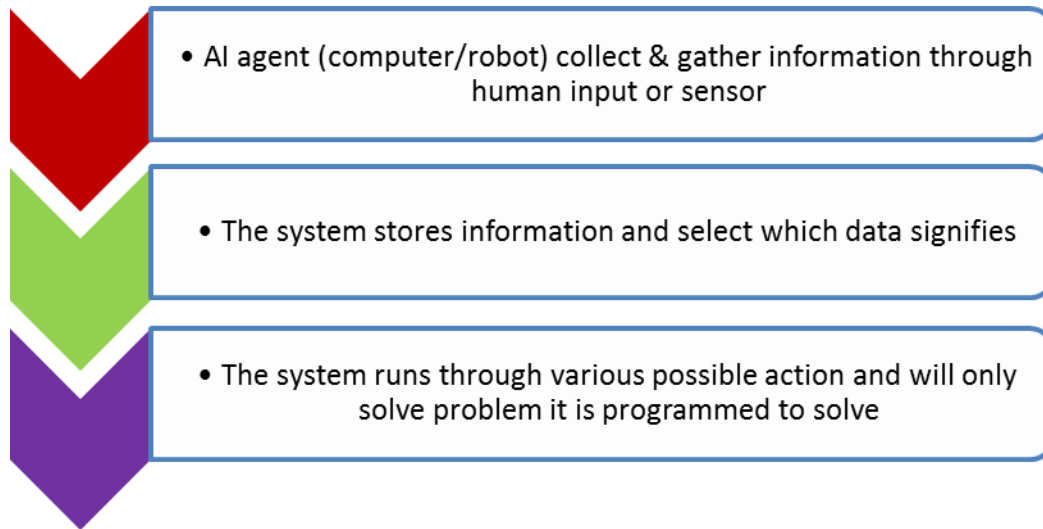


**Figure 2.7: Basic for AI Problem Solving**

### **2.2.3 The Importance of Knowledge-Based System (KBS)**

There are numerous reasons why a KB system becomes a useful tool. Velasquez states that a KB system has emerged as a technology to support system (software and hardware) that rely on expert knowledge, imprecise or incomplete data and deductive or inference machine.

By using KBS, the quality of goods and improvement in services can be increased with the cost decreased. KBS offers expertise to personnel with less experience in related areas. It avoids delay and provides expertise whenever the expert is unavailable. KBS also merges the different source of knowledge into one repository and the data recorded will provide a reliable database for future analysis. KBS is a significant tool as the knowledge is encoded into the system and hence provides consistency and availability over time. KB has been applied to maintain the knowledge extracted from web data and derived new tools called Web Using Mining (WUM).

Chapman [23] applied a KB engineering system to the automotive industry to reduce project costs for body-in-white (BIW). The system responded dynamically in connection with the constraints applied within a rapid timeframe and product cycle factors. Ong and Keane [24] demonstrated a Domain Knowledge Based Search Advisor on aircraft wing design domain. The search advisor contains the knowledge of repetitive performance on design domains that help designers in their search events. Curran et al. [25] introduced the evolution of multidisciplinary engineering knowledge, containing design and

production input called Knowledge Nurture for Optimal and Multidisciplinary Analysis and Design or KNOMAD. Choi [26] implement a KB engineering system to estimate the weight of aircraft composite structures and manufacturing cost. The structural analysis, weight estimation and cost estimation use finite element optimisation, geometry based and process based method respectively. Fuzzy logic is used for cost estimation.

Li et al. [27], Rocca [28] and Verhagen et al. [29] have provided critical reviews to identify the product development in KB: the effectiveness of this system, the theoretical foundation and research issues arise within KB. Thuraishingham [30] came out with a new idea of a Multilevel Secure Database Management System (MLS/DBMS) that defines the difficulties in designing the system. A new design for MLS/DBMS is proposed. Methods on how multilevel security concepts can be applied to a Knowledge-Based Management System (KBMS) is described. Multilevel security is highly recommended to incorporate into severe database management security systems such as military applications.

From research, the author found that KB is an expert tool that can provide solutions in multi areas. Therefore, in this research, the author uses KB system to create a novel analysis tool to optimise the design of composite wing structure, subject to multi constraint. The tool is called a Knowledge-Based Optimisation Analysis Tool or K-BOAT.

#### **2.2.4 Engineering Design Optimisation Approaches**

The conventional method for engineering design optimisation involves a step by step approach, which is time consuming and the process of identifying the right combination of product parameter is usually done manually and associated process parameters for the best solution. However, there are limitations using the manual approach as this method does not allow thorough exploration of the solution space to find the optimum design, resulting in sub-optimal designs. In the industry, the identification of the optimum design is impossible because of lack of knowledge, experience and size of the problem. Research by Roy et al. only includes optimisation as relating to a mechanical design problem without considering the thermofluid process, manufacturing process, as well as process manufacturing areas [19].

Engineering designs are still optimised mostly through a manual iterative process, where the designer benchmarks a few designs based on a small number of criteria, such as maximum stress or minimum weight and the best design is selected. The initial design is first checked against constraints, such as manufacturability, tools availability and cost, and only feasible designs are considered for optimisation. However, this manual process is often limited to selecting designs that are recognised by the designers, and it fails to identify any unknown but potentially significantly improved design. The engineering design optimisation approaches are shown in Figure 2.8.

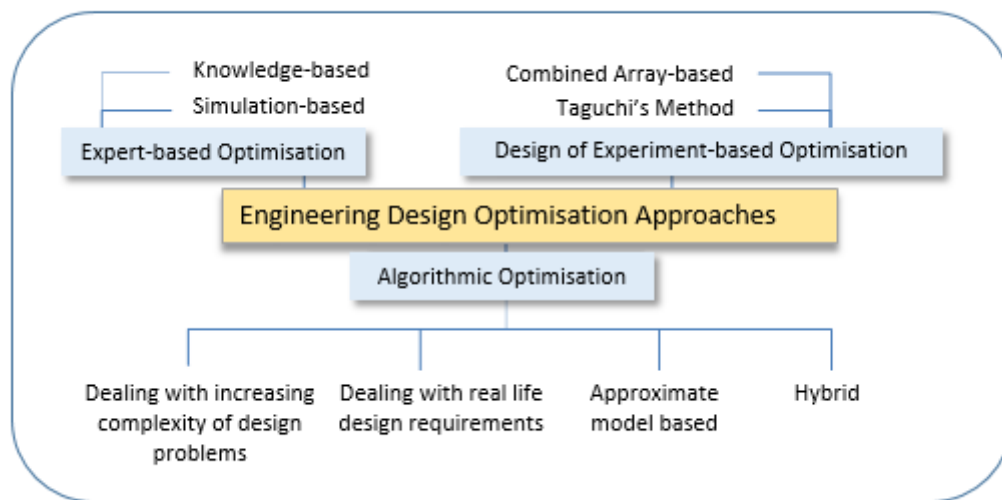


**Figure 2.8 An overview of engineering design optimisation approaches**

### **2.2.5 Expert-Based Optimisation Approach**

Expert-based optimisation approach often uses expert judgment, which involves knowledge-based or simulation techniques such as Finite Element Analysis (FEA) or Computational Fluid Dynamics (CFD) analysis for design optimisation. The advantage of this approach is that designers do not require any additional skill, it may take less time to select a better design, and it gives incremental improvement. However, the challenges of using this method are in the form of dependency on a few experts who could evaluate the designs and find truly novel and significantly better designs.

### **2.2.6 Design of Experiment-Based Optimisation Approach**

A design of the experiment based optimisation approach is a structured, organised method for determining the relationship between factors (X's) affecting a design and the performance of that design (Y) such as maximum stress, minimum weight or cost. Once the contributions of the design variables on the performance are identified, the information is used to identify an ideal set of design variable values that is expected to yield the best result. This approach can optimise development time by reducing the design time, and can often find better performing designs that are outside the 'comfort zone' of designers. The uniqueness of this approach is it provides a structure to the optimisation, but at the same time it can still be a very manual process. The advantage of the experiment based approach is it works fairly well with design variables that are independent from each other. On the other hand, in real life situations this is often not the case. Real life engineering design requires designs that are robust, reliable and can operate with inherent uncertainties associated with engineering systems.

### **2.2.7 Algorithmic Optimisation Approach**

The algorithmic approach deals with real life design requirements and complexity of design problems. Reliability-based design optimisation looks for optimal solutions, considering probabilistic constraints. This optimisation approach is also used in structural design optimisation. Real life design requires robust optimum design that is not sensitive to design tolerances, production parameter drifts during operation, and model sensitivities. Robust optimisation approaches search for solutions that are in robust regions within a design space and locate the optimum among the robust solution.

Boothroyd [18] in his paper stated that the changes in product design can lead to delays in final product completion. The later the product development cycle, the more expensive the part will be. This situation must be prevented at the early design stage, where manufacture and part assembly in production must be taken into account during the design stage. Yuan-Li [31] studied constrained-based modelling for product design and manufacturing. A doll-house model is created to study the possible constraints in a product design. The model is developed to achieve the minimum design time and prototype testing time and simplifies the manufacturing process to attain the mistake-free operation.

Roy et al. [19] found that the biggest challenge to optimise the design technique is scalability, where the large-scale optimisation must involve the efficient algorithm such as swarm intelligence. Nguyen et al. [32] studied the Multidisciplinary Design Optimisation (MDO) by implementing the Multi-Fidelity Model (MFM) for weight analysis of Unmanned Combat Air Vehicle (UCAV) and decomposition of coupling variables during the UCAV mission. The MFM integrates low fidelity codes together with high-fidelity analysis. The codes are developed from empirical equations.

### **2.3 Optimisation of Composite Wing Structure**

Composite material is a very interesting option in design. Different methods are suitable for different purposes and it is the designer's call to choose which method is appropriate to meet the desired properties, as long as it is within the safety envelope. Various methods for composite laminate optimisation have been reported in the literature. Genetic Algorithm (GA) for example is used to reach the optimal stacking sequence, while using little computational cost [33–38]. From basic GA method, An et al. [39] came out with a new optimisation method, where two levels of optimisation are involved. The first level uses the classic GA method, which combines the variables involving sizing variables and stacking sequence, while for the second level, both variables are presented separately using numerical equations. The various variables constrained in composite laminate result in more complex analysis. The most important step is to define the crucial keys for the optimisation. Jing et al. [40] investigated the variation search algorithm, Permutation Search (PS) to reach stacking sequence optimisation by reducing the evaluation. The PS method is then compared with the GA method and Jing discovered that sequence stacking optimisation result is enhanced by using PS.

Wang et al. [41] investigated the different number of T-shape stiffeners employed in symmetric and balanced composite layup structure to reach the maximum buckling load without any weight penalty. In their research, Ant Colony Algorithm (ACA) method has been applied to optimise the objective function, and the finite strip method is used to run the buckling analysis for the stiffened panels. In this paper, the ACA has been extended to Multi City-Layer Ant Colony Algorithm (MCLACA). MCLACA is used to optimise the stacking sequence of the laminates. The example of MCLACA flow chart is shown in Figure 2.9.

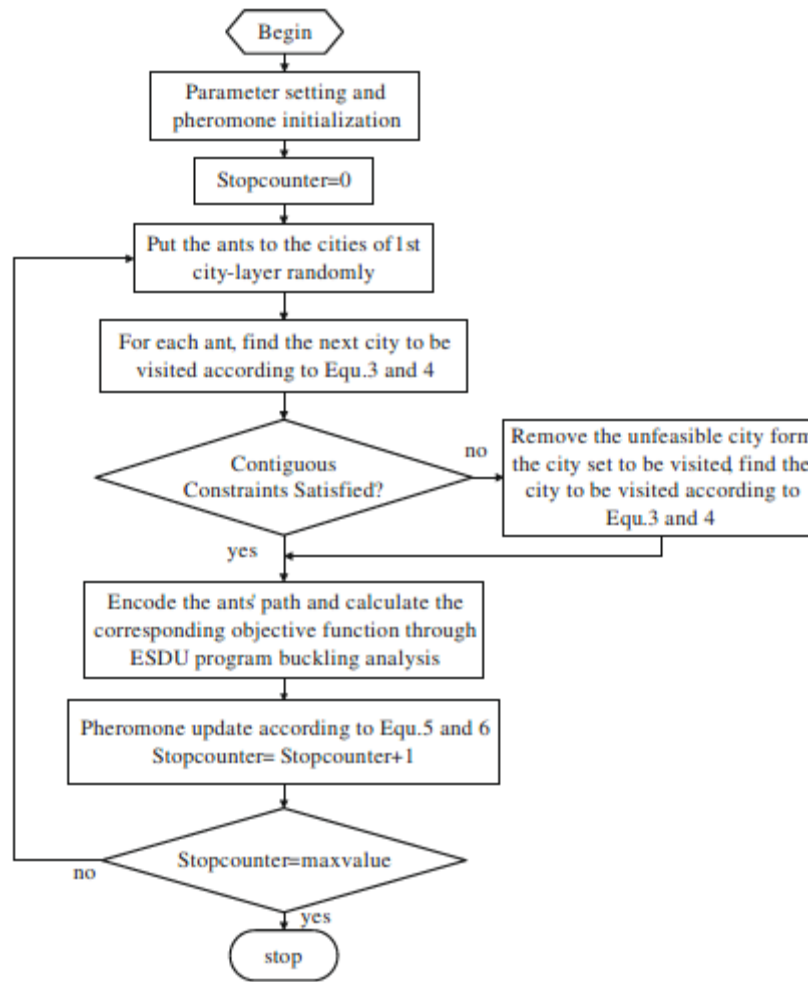


**Figure 2.9 MCLACA flowchart [41]**

Results show that at first the buckling load increases proportionally with the number of stiffeners. After it reached certain value, only a small increment was recorded. This method can be applied to run analysis of any stiffener design but must be of similar loading condition. Research has been continued by Wang et al. [42] by combining two optimisation methods; ant colony and gradient based. These two methods have been carried out simultaneously to reach minimum structural weight of two design variables. Methods and process have been presented to optimise structure layout and structural component size simultaneously. This design optimisation has been carried out using the topology method and Multi City-Layer Ant Colony Optimisation (MCLACO).

Zhao et al. [43] proposed the application of a two-level layout optimisation for large composite wing structures. By targeting efficiency as the objective function, the design

requirements are positioned at the system level and layout is optimised at subsystem level, which must fulfil the constraints from the system level. The stiffened panels are modelled as orthotropic plates. A neural network model has been used to approximate the stringers elasticity on wing skin. Results show that the method presented is feasible.

Hao et al. [44] present a methodology to optimise a composite advanced grid-stiffened cylinder using the Approximation-Based Optimisation (ABO) method. Multi-Island Genetic Algorithm (MIGA) method is applied for global optimum search. The preliminary design tool of a composite advanced grid-stiffened cylinder has been developed using iSIGHT and finite element code MSC.MARC. Based on the Vector Evaluated Artificial Bee Colony (VEABC) algorithm, Omkar et al. [45] introduced design optimisation using Artificial Bee Colony (ABC) which has been performed on the composite structures. Hansen and Horst [46] demonstrate a multilevel optimisation for generic framework structure and aircraft fuselage structure. The top level used topology parameters and the second level incorporated the Gradient-Based (GB) method to optimise the cross-section and thickness of the model. The process has been carried out with respect to different design constraints.

## **2.4 Aeroelastic Tailoring**

Carbon fibre reinforced composite has great potential to improve the aircraft structure efficiency due to the high specific modulus and variable directional stiffness characteristics. The aeroelastic tailoring technique has been applied to optimise composite wing structures. It may also be applied to design a composite wing of high aspect ratio for large aircraft to achieve maximum aerodynamic and structural efficiency [47].

Koji [48] used the direct search method to conduct a feasibility study to prevent the potential interruption of the common optimisation method, which might be caused by discontinuity of the objective function, for example, flutter velocity. This method does not depend on constraint or the objective function.

Guo [49] applied the gradient-based deterministic optimisation method to aeroelastic tailoring of an aerobatic wing structure. With flutter speed and minimum weight as the objective function, the wing skin and spar web fibre orientation laminates have been optimised. It was ascertained that the results of optimised fibre orientation have reduced the wing structure weight and increased by 30% flutter speed compared to the initial design. The final optimised layup was trimmed and reinforced, subject to manufacturing constraints and strength requirement. In another paper, Guo presented a study on the effects of wing geometry and mass distribution on aeroelastic tailoring [50] by combining both gradient based deterministic and genetic algorithm optimisation methods. Wing box laminate layups were optimised for six cases and results show that a uniform non-swept box turned out to be the most effective tailoring for optimum flutter speed.

Mastroddi et al. [51] employed the Multidisciplinary-Design-Optimisation (MDO) method using geometric design variables subject to aeroelastic constraints. In the MDO process, three different types of optimiser have been utilized. For structure, aerodynamics and flight mechanics, a finite element, panel method and longitudinal trim analyser have been applied respectively. The wing structure model has been integrated with structures, aeroelasticity, aerodynamics and flight mechanics and based on result for this model, the benchmark of optimised wing using this approach has been presented. Williams and Banerjee introduced dynamic stiffness matrix method to determine the free vibration of composite wing [52]. Lillico et al. [53] use dynamic stiffness method for aeroelastic optimisation of composite wings. Butler et al. [54] modelled an unsteady aerodynamics by the dynamic stiffness method based on strip theory.

Guo et al. [55] investigated the optimisation of composite wing structure for maximum flutter speed and minimum weight at subsonic speed with the effect to bending, torsion and bending-torsional coupling stiffness at the first stage. At the second stage, the effect of laminate strength and weight resulted from the optimised result at the first stage was studied. Guo et al. in another paper [56] ran MDO of a large composite wing aircraft, subject to multi constraints. The MDO process has been modelled to show the possibility of replacing the conventional iteration in finite element analysis. Two stages of optimisation steps have been proposed, while at the first stage, fibre orientation and

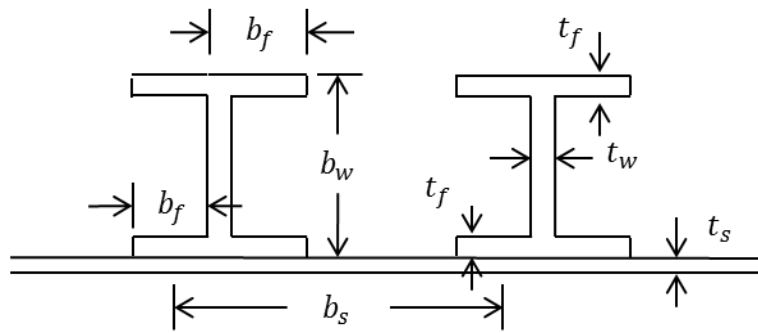


laminated ply thickness were taken as design variables. The objective of this stage is to reach the minimum weight optimization, subject to strength and damage tolerance. In the second stage, aeroelasticity has been taken as a constraint to reduce the wing gust response to the same level as the initial design. The method proposed in this paper allowed the designers to make decisions at the early design stage. The optimisation process was performed using NASTRAN software.

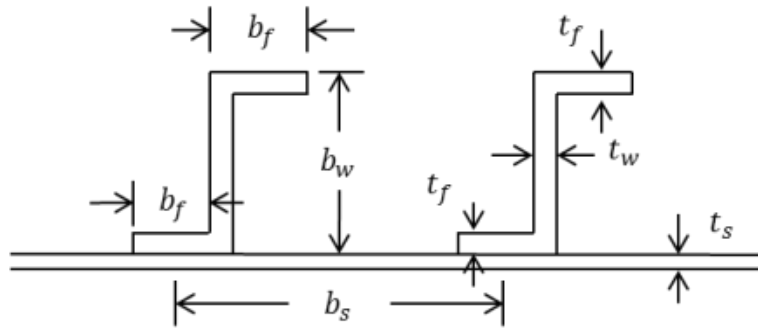
## **2.5 Manufacture Constraint in Composite Structure Optimisation**

Conventionally the optimised fibre orientation layup will suffer penalties when the manufacturing constraint is involved. Nevertheless, the manufacturing constraint must be taken into account to ensure the final design is practically feasible and doable.

Fu [57] explained practical design constraints introduced by Niu [58] with the examples of varying sizes of stringers, subject to buckling load. Figure 2.10 shows the example of a geometry definition for I section and Z section of the stringers.  $b_f$  and  $t_f$  are the length and width of the flange,  $b_w$  is the web height,  $t_w$  is the web.  $t_s$  and  $b_s$  are the skin thickness and width, respectively.



i) I section stringer



ii) Z section stringer

**Figure 2.10 Example of section geometry definition of stringers**

The practical design guideline given by Niu is shown in Table 2.1.  $A_{st}$ , and  $A_{sk}$  are the stringer's section area and skin, respectively.

**Table 2.1 Niu practical design guideline**

$\frac{t_f}{t_w}$	$\frac{b_w}{t_w}$	$\frac{b_f}{t_f}$	$\frac{A_{st}}{A_{sk}}$	$\frac{b_f}{b_w}$
1.0	18 - 22	6 - 8	0.5	0.4

Philips in his thesis [59] explained in detail the multidisciplinary optimisation of a carbon fibre reinforce plastic (CFRP) aircraft wing cover. The optimisation is based on the manufacturing method, material, process, tooling, assembly, damage tolerance, repair and maintenance of the CFRP wing.

Liu and Butler [60] present a bi-level design method to deliver the practical design constraints of composite wing cover panels. Genetic Algorithm and tabular methods have been applied to this bi-level design method where the cross-sectional panel and optimised stacking sequence have been achieved. In order to expedite the optimisation process, a

very powerful optimisation package called VICONOPT is used to run the buckling analysis. All the manufacturing constraints, which include the allowable thickness percentage for each ply orientation, the maximum number of consecutive ply layers in the same orientation,  $\pm 45^\circ$  outer plies for skin and stiffener and the allowable rate of ply drop-off have been taken into account within the method. By using the special layer of 3D finite element analysis, Vidyashankar and Murti [61] reported the effect of tapered and resin pocket laminated with tapered shape by examining its tensile behaviour. High stress concentration exists at the ply drop zone. The delamination propagation was also reported at the ply drop area. Kradinov et al. [62] carried out an experiment of bolted patch repair on the flat composite panel by analysing two types of patch repair among various types of bolt pattern, with the addition of a cut out on the panel. With the presence of an elliptical cut-out shape on the panel, the efficiency patch geometry and bolt pattern in the repair technique have been inspected. The same patch was examined and analysed under several complex loading conditions.

Wang and Costin [63] presented mathematical expressions to apply manufacture constraints and use laminate thickness as design variables in the optimisation. The shape function matrix was introduced in the formula. The matrix was applied for a single finite element. To meet the manufacturing constraint, the percentage of each ply angle is controlled by setting up the upper and lower bound in the formula. Each ply orientation must be between 10% and 70% of total ply thickness for manufacturing constraints. In another paper, Wang and Costin [64] discussed three types of manufacturing constraints in composite structure optimisation, which include the ply orientation percentage, ply drop-off rate and interleaving. The ability of a composite panel to be tailored to meet the desired requirement has given the flexibility and allowed the designer to vary the laminate thickness and ply orientation. The large variations however have created a drawback in manufacturing process where there is a possibility to produce an uneven surface, which will make it difficult to assemble with the adjacent part. The complexity of the laminate design will also cause stress concentration occurrence on the panel and increase the manufacturing cost.

Henderson et al. [65] carried out an optimisation of a blade-stiffened composite panel by combining the structural design and manufacturing constraints using a mixture of analysis and optimisation methods, including the application of a general algorithm. Different

material properties and various cross-sectional geometry have been selected as design variables for structural design. For manufacturing constraint, structural performance, temperature and pressure have been chosen as the design variables and the minimum resin infiltration time has been set as the objective function. Yin and Yu [66] developed the multi-objective optimisation method to integrate the manufacturing cost model into the optimised structural layout by using the trade-off method. The parato optimal set has been used to meet the objective function. The integrated model has been verified by adopting the method into the unmanned aerial vehicle to represent the composite wing structural design.

### **3 KNOWLEDGE-BASED OPTIMISATION ANALYSIS TOOL (K-BOAT)**

Knowledge-Based Optimisation Analysis Tool or K-BOAT is a tool to improve efficiencies and enhance the design effectiveness during the product development or design stage. Maulana et al. [67] have successfully improved the surface jet pump by using one of a knowledge management tools called Set-based Concurrent Engineering (SBCE). By using the basic of business framework, Maulana et al. applied the knowledge-based method to create a well-structured process model in the oil and gas industry. The same SBCE process model has been improved by Zehra et al. [68] by introducing a trade-off curves application. Maulana et al. [69] also outlined that the SBCE approach which provides an atmosphere in which the design space is explored thoroughly and significantly which in turn improves the innovation. Khan et al. [70] developed a framework which includes methods, tools and technique based on Toyota Product Development. Robinson [71] in his paper has explained the framework structure and uses a three stages approach called Improving Management Performance Through Knowledge Transformation or IMPaKT to validate his business case. The three stages in the IMPaKT approach consist of developing business strategy, developing a knowledge-management and developing a knowledge management evaluation strategy. The principle used in IMPaKT has been applied by author to develop K-BOAT.

K-BOAT is a novel technique or tool for the optimal design of composite structures. In this research, it is developed for aircraft composite wing skin optimisation, subject to multi constraints. It includes three levels of design procedure which are:

- Level 1: Initial analysis of the composite wing by using a low fidelity model based on the thin-walled structural analysis method
- Level 2: Focused on an optimal design of the wing skin adopting the analytical method and validation using high fidelity finite element (FE) method
- Level 3: Creates an FE model to present a baseline structure to perform further detailed analysis and optimisation

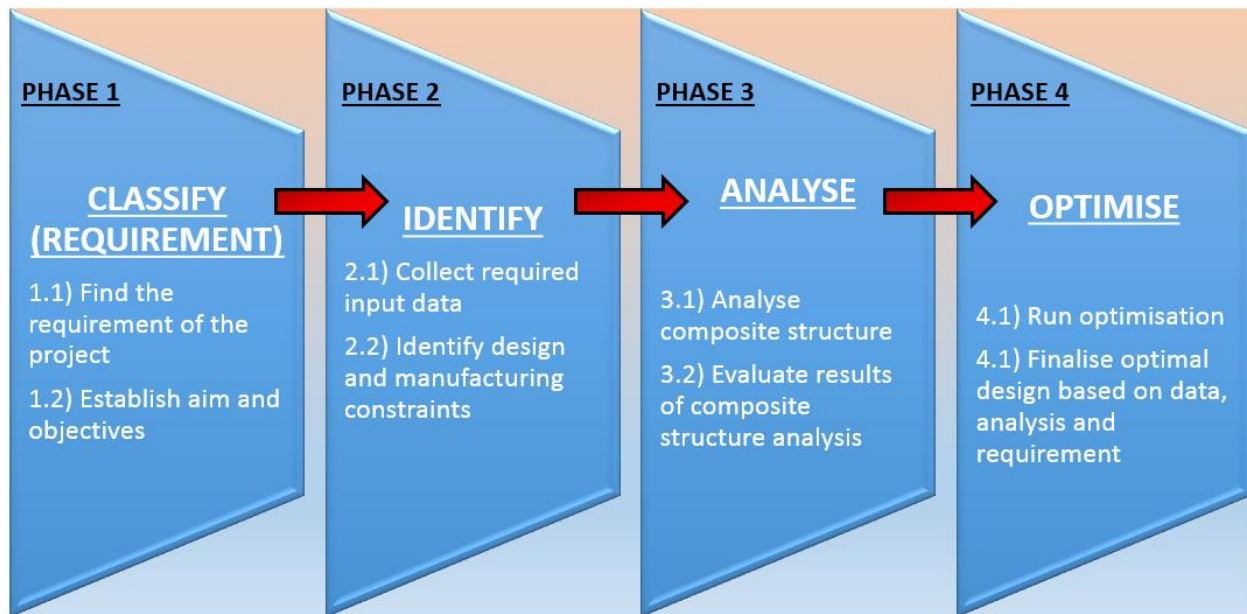


**Figure 3.1 K-BOAT Framework**

“CLASSIFY-IDENTIFY-ANALYSE-OPTIMISE” or CIAO are the four basic keywords in K-BOAT, which represent four phases in K-BOAT, as shown in Figure 3.1. This well-structured framework acts as a guideline for the engineers and designers to understand and expect the optimal solution of composite structures at the early design stage.

### **3.1 Phase 1: Classify (Requirement)**

In Phase 1 “Classify”, the requirement, aim and objectives of the project are classified. A clear understanding of the final product or deliverable is fixed at this phase. The aim of the project is to create an optimal design of the composite wing structure, subject to multi design and manufacturing constraints. The required tool and computational software package are identified at this phase. A low fidelity model based on the thin-walled structure method and in-house FORTRAN based program were first used. Then NASTRAN software for high fidelity finite element method is selected for results validation. This phase helps engineers and designers to identify the right target for the project. Table 3.1 illustrates Phase 1 of the K-BOAT.

**Table 3.1 K-BOAT Phase 1: Classify (Requirement)**

Phase 1: CLASSIFY (REQUIREMENT)	METHOD
1.1) Aim: To create an optimal design of composite aircraft wing structure  1.2) Requirement: Subject to multi design and manufacturing constraint	1.1) Theory and mixture of analytical and numerical methods. Involve computational analysis for validation

### 3.2 Phase 2: Identify

In Phase 2 “Identify”, all the required input data for analysis are gathered and collected. A low-fidelity model based on the thin-walled structure analysis method is used to investigate the macromechanics of fibre reinforced ply, composite laminate and FRP sections. Stiffness analysis is carried out on a generally orthotropic ply, laminate and closed section thin-walled beam. Moreover, the effect of bending stiffness, torsional stiffness and bending-coupling stiffness were identified when the laminate layup is extended to a box structure.

Design and manufacturing constraints were also identified at this phase. The K-BOAT will build a set of parameters in the initial design, based on the knowledge from theoretical and practical constraints, such as damage tolerance and manufacturing. Those parameters include the requirement of minimum percentage of each laminate thickness (minimum 10%), numbers of successive plies in each orientation, rate of ply drop-off and the outer plies  $\pm 45^\circ$ . These constraints must be obeyed to ensure the laminates to have sufficient aeroelastic stiffness, improve the damage tolerance impact, reduce stress concentration and transverse shear stress, increase bolted joint strength, minimise edge splitting and simplify the manufacturing process to reduce the cost. This phase will allow the maximum knowledge input and interface between users (design engineers) with the design tool, rather than leave it to the optimiser for a solution. Table 3.2 shows the K-BOAT Phase 2.

**Table 3.2 Phase 2 K-BOAT: Identify**

Phase 2: <u>IDENTIFY</u>	METHOD
2.1) Develop full understanding of mechanics of composite material and structure	2.1) From theory and extensive literature review
2.3) Identify design and manufacturing constraint	2.3) Based on design rules and practical design constraints

### 3.3 Phase 3: Analyse

In Phase 3 “Analyse”, the composite structure is analysed. Analysis of stress, stiffness, buckling, free vibration and aeroelastic is carried out on a future transport composite wing baseline model. The composite skin properties, layup orientation and stacking sequence, which are all required for the baseline wing have been pre-determined in an initial design. The low-fidelity method, which used the FORTRAN based program is applied to perform the stiffness and aeroelastic analysis. These results are then compared with NASTRAN results for validation processes. Low-fidelity method, ABD Matrix Program is also used to generate equivalent laminate properties to provide input for the high-fidelity analysis, and detailed analysis of stress, buckling, free vibration and aeroelastic are run in NASTRAN. The analysis and methods in Phase 3 are shown in Table 3.3.

**Table 3.3 Phase 3 K-BOAT: Analyse**

Phase 3: <u>ANALYSE</u>	METHOD
3.1) Low fidelity analysis	3.1.1) <u>Stiffness analysis</u> Use FORTRAN based program:
3.2) High fidelity analysis	a) ABD Matrix program for laminate analysis b) BOXMX program for box beam analysis
	3.1.2) <u>Aeroelastic analysis</u> Use FORTRAN based program:
	a) COMFLUT program for flutter speed, natural frequency and mode shape
	3.2) Use CATIA for modelling and NASTRAN to run stress, stiffness, buckling, free vibration and aeroelastic analysis



### 3.4 Phase 4: Optimise

Phase 4 “Optimise” is the final stage of K-BOAT framework. At this phase, results from Phase 3 are finalised and the optimisation process is performed. The objective function of the optimisation is to increase the flutter speed. The design variable is the laminate layup. No design constraint has been set up in this analysis. A NASTRAN-MATLAB-FORTRAN based aeroelastic tailoring program has been developed as a tool for this purpose. The optimisation is run in NASTRAN. “fmincon” in MATLAB is used as an optimiser, where the Gradient-Based Method and the mathematical equation and function are involved in this optimisation. To expedite the optimisation process, the FORTRAN based program is employed, the ABD Matrix Program is used to generate the equivalent laminate properties for NASTRAN input. After achieving the optimal design, a FE model was created to represent this result. Stringers were added to reinforce the thin wing skin. The Phase 4 K-BOAT is shown in Table 3.4.

**Table 3.4 Phase 4 K-BOAT: Optimise**

Phase 4: OPTIMISE	METHOD
4.1) Run optimisation on the wing skin panel a) Objective function: to increase flutter speed b) Design variable: laminate layup c) Design constraint: no design constraint	4.1) Optimisation uses NASTRAN and fmincon in MATLAB as optimiser (Gradient-Based Method). ABD Matrix Program is used to expedite the input data generation for NASTRAN
4.2) Finalised optimal design based on data and analysis	4.2) Create FE model of optimal composite wing cover panel subject to multi design and manufacture constraint

## **4 THEORETICAL STUDY**

### **4.1 Mechanics of Composite Plate**

The classical laminate theory (CLT) is a theory to predict and calculate the behaviour of composite laminate from the material properties of individual layup and the geometry of the laminate [72]. CLT is almost identical to the classical plate theory as proposed by Kirchhoff [73–75], except for the material properties in the stress-strain relationship. By following the simplified engineering assumptions, several assumptions have been made in CLT:

1. Each layer in the laminates are perfectly bonded. There is no gap between layers and no slip between adjacent layers. The bonding between each layer is strong, which makes the laminate act as one single lamina with integrated properties.
2. Each layer is thin and assumed to be a homogeneous layer. Other dimensions, such as width and length must be at least ten times higher than the laminate thickness.
3. Each lamina can either be isotropic, orthotropic or transversely isotropic.
4. Kirchhoff hypothesis is invoked, after deformation the normal to mid-plane remains normal, straight and unstretched. The laminates do not change the thickness and length after deformation.

The key of CLT consist of kinematic, constitutive, force resultant and equilibrium equations [76].

#### **4.1.1 Strain-Displacement Relations of a Composite Plate**

The basis or principle of the strain-displacement field of a composite plate is derived from two approaches. The first approach used deformation of the laminate, where geometry of the laminate before and after the plate deformation (deformed and undeformed plate) is analysed to develop the displacement field. Kirchhoff's assumption for bending and stretching as stated in the CLT assumption in a previous paragraph is used in this approach. For the second approach, the transverse strain components were calculated and the relation for strain-displacement is obtained using the mathematical definition of the strain component [77].

**4.1.1.1 First Approach**

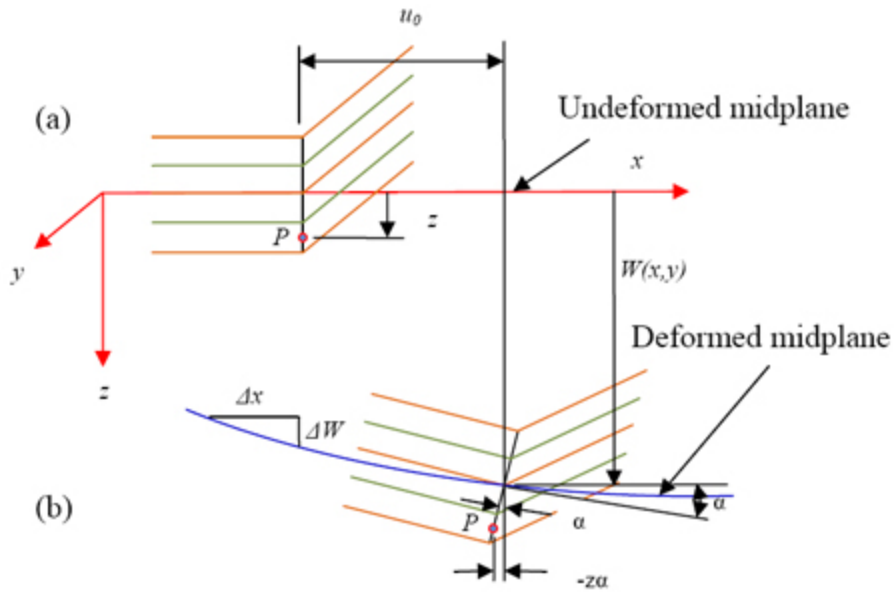


**Figure 4.1 Undeformed (a) and deformed (b) geometry of laminate**

Figure 4.1 illustrates the undeformed (a) and deformed (b) of laminate geometry in  $xz$  plane. According to Kirchhoff, in composite plate theory, it is assumed that the mid-plane after deformation remains normal as the undeformed mid-plane. This condition produced a zero-transverse shear strain. The laminate stretching, however, has moved the intersection point of mid-plane and normal along  $x$ -direction. Due to the bending action, the same point also moved along in  $z$ -direction. The second assumption according to Kirchhoff is that the normal to the mid-plane remains unstretched. As the length remains unchanged after the deformation, this condition has resulted in the transverse normal strain. Any transverse deflection of any point in the laminate is independent of the  $z$ -direction. Therefore, only  $x$  and  $y$  function are involved and the equation can be written as:

$$W(x, y, z) = W_0(x, y) \tag{4.1}$$

where  $W_0$  is a function of  $x$  and  $y$  only and a constant for a given  $x$  and  $y$  location.

The deflection angle  $\alpha$  can be calculated from the slope of the mid-plane.

$$\tan \alpha = \frac{\Delta W}{\Delta x} \quad (4.2)$$

In this theory, the deformation is considered very small, thus Equation (4.2) can be rewritten as:

$$\tan \alpha \approx \alpha = \frac{\partial W}{\partial x} \quad (4.3)$$

Point  $P$  in Figure 4.1 is a point located on the mid-plane of the laminate geometry. This point is positioned on the mid-plane at a distance in  $z$  direction from the mid-plane. After deformation, the displacement of point  $P$  along  $x$  direction became:

$$\begin{aligned} u(x, y, z) &= u_0(x, y) - z \tan \alpha \\ &= u_0(x, y) - z \alpha \\ &= u_0(x, y) - z \frac{\partial W}{\partial x} \end{aligned} \quad (4.4)$$

$u$  and  $u_0$  is a displacement before and after deformation respectively in  $x$  direction.

The displacement of point  $P$  in  $y$  direction is given by:

$$v(x, y, z) = v_0(x, y) - z \frac{\partial W}{\partial y} \quad (4.5)$$

where  $v$  and  $v_0$  are displacement before and after deformation respectively in  $y$  direction.

Based on CLT, the displacement field for a generic point in  $x, y$  and  $z$  direction is given as:

$$\begin{aligned} u(x, y, z) &= u_0(x, y) - z \frac{\partial W}{\partial x} \\ v(x, y, z) &= v_0(x, y) - z \frac{\partial W}{\partial y} \\ W(x, y, z) &= W_0(x, y) \end{aligned} \quad (4.6)$$

In this approach,  $u_0(x, y)$ ,  $v_0(x, y)$  and  $W_0(x, y)$  correspond to the mid-plane linear displacements in  $x, y$  and  $z$  direction respectively.

#### 4.1.1.2 Second Approach

In the second approach, the second assumption of the Kirchhoff's composite plate theory is used. After deformation, the length of normal to the mid-plane remains the same, which results zero transverse normal strains. Therefore:

$$\epsilon_{zz} = \frac{\partial W}{\partial z} = 0 \quad (4.7)$$

From Equation (4.7), no transverse shear strain exists, so only  $x$  and  $y$  coordinates are involved for displacement in  $z$  direction, which gives the  $W$  function:

$$W(x, y, z) = W_0(x, y) \quad (4.8)$$

From the first approach, using Kirchhoff's assumption, after deformation the normal generic point at the mid-plane remains normal and straight, hence induces zero transverse shear strain. Therefore:

$$\gamma_{xz} = \gamma_{yz} = 0$$

From Figure 4.1 it is assumed that the strain is small, thus Equation (4.7) can be rewritten as:

$$\gamma_{xz} = \frac{\partial u}{\partial z} + \frac{\partial W}{\partial x} = 0 \quad (4.9)$$

$$\gamma_{yz} = \frac{\partial v}{\partial z} + \frac{\partial W}{\partial y} = 0 \quad (4.10)$$

where  $\gamma_{xz}$  and  $\gamma_{yz}$  are transverse, shear strain in normal to  $x$  and  $y$  direction, respectively.

Rearrange Equation (4.9):

$$\frac{\partial u}{\partial z} = -\frac{\partial W}{\partial x} \quad (4.11)$$

Integrate Equation (4.11) with respect to  $z$ , the equation becomes:

$$u(x, y, z) = -z \frac{\partial W}{\partial x} + u_0(x, y) \quad (4.12)$$

Using the similar theory, rearrange Equation (4.10) and integrate with respect to  $z$  direction, thus:

$$v(x, y, z) = -z \frac{\partial W}{\partial y} + v_0(x, y) \quad (4.13)$$

From the derived equations, the displacement in  $x, y$  and  $z$  direction can be summed up as:

$$u(x, y, z) = u_0(x, y) - z \frac{\partial W}{\partial x}$$

$$v(x, y, z) = v_0(x, y) - z \frac{\partial W}{\partial y}$$

$$W(x, y, z) = W_0(x, y) \quad (4.14)$$

Displacement field in Equation (4.14) is identical to Equation (4.6) derived from the first approach.

From Equation (4.6), for the infinitesimal strains, the strain displacement relations can be written as:

$$\epsilon_{xx} = \frac{\partial u}{\partial x} = \frac{\partial u_0}{\partial x} - z \frac{\partial^2 W}{\partial x^2}$$

$$\epsilon_{yy} = \frac{\partial v}{\partial y} = \frac{\partial v_0}{\partial y} - z \frac{\partial^2 W}{\partial y^2}$$

$$\gamma_{xy} = \frac{\partial u}{\partial y} + \frac{\partial v}{\partial x} = \frac{\partial u_0}{\partial y} + \frac{\partial v_0}{\partial x} - 2z \frac{\partial^2 W}{\partial x \partial y} \quad (4.15)$$

Rewrite Equation (4.15) into matrix form:

$$\begin{Bmatrix} \epsilon_{xx} \\ \epsilon_{yy} \\ \gamma_{xy} \end{Bmatrix} = \begin{Bmatrix} \epsilon_{xx}^{(0)} \\ \epsilon_{yy}^{(0)} \\ \gamma_{xy}^{(0)} \end{Bmatrix} + z \begin{Bmatrix} k_{xx} \\ k_{yy} \\ k_{xy} \end{Bmatrix} \quad (4.16)$$

or simplify the equation and becomes:

$$\{\epsilon\}_{xy} = \{\epsilon^{(0)}\}_{xy} + z\{k\}_{xy} \quad (4.17)$$

where:

$$\{\epsilon^{(0)}\}_{xy} = \left\{ \epsilon_{xx}^{(0)} \quad \epsilon_{yy}^{(0)} \quad \gamma_{xy}^{(0)} \right\}^T = \left\{ \frac{\partial u_0}{\partial x} \quad \frac{\partial v_0}{\partial y} \quad \frac{\partial u_0}{\partial y} + \frac{\partial v_0}{\partial x} \right\}^T \quad (4.18)$$

Equation (4.18) consists of mid-plane strains.

$$\{k\}_{xy} = \{k_{xx} \ k_{yy} \ k_{xy}\}^T = \left\{ \frac{-\partial^2 W}{\partial x^2} - \frac{-\partial^2 W}{\partial y^2} - 2 \frac{\partial^2 W}{\partial x \partial y} \right\}^T \quad (4.19)$$

Equation (4.19) shows the mid-plane curvatures element.  $k_{xx}$  and  $k_{yy}$  are the bending moment curvature in  $x$  and  $y$  direction respectively while  $k_{xy}$  represents the twisting moment curvature of the plate.

#### 4.1.2 Stress-Strain Relations

Composite materials by nature are anisotropic. Stresses at any point on the composite plate can be calculated from the strains and lamina constitutive relations. From lamina properties, the constitutive equation can be identified, thus the stresses of the  $k^{th}$  lamina of the stressed can be calculated from the reduced stiffness matrix shown below.

$$\begin{Bmatrix} \sigma_{xx} \\ \sigma_{yy} \\ \tau_{xy} \end{Bmatrix} = \begin{bmatrix} \bar{Q}_{11} & \bar{Q}_{12} & \bar{Q}_{16} \\ \bar{Q}_{12} & \bar{Q}_{22} & \bar{Q}_{26} \\ \bar{Q}_{16} & \bar{Q}_{26} & \bar{Q}_{66} \end{bmatrix} \begin{Bmatrix} \epsilon_{xx} \\ \epsilon_{yy} \\ \gamma_{xy} \end{Bmatrix} \quad \text{or} \quad \{\sigma\}_{xy}^k = \{\bar{Q}\}^k \{\epsilon\}_{xy}^k \quad (4.20)$$

The reduced transformed stiffness matrix,  $[\bar{Q}]$  is

$$\begin{Bmatrix} \bar{Q}_{11} \\ \bar{Q}_{22} \\ \bar{Q}_{33} \\ \bar{Q}_{12} \\ \bar{Q}_{13} \\ \bar{Q}_{23} \end{Bmatrix} = \begin{bmatrix} m^4 & n^4 & 2m^2n^2 & 4m^2n^2 & & \\ n^4 & m^4 & 2m^2n^2 & 4m^2n^2 & & \\ m^2n^2 & m^2n^2 & -2m^2n^2 & (m^2 - n^2)^2 & & \\ m^2n^2 & m^2n^2 & m^4 + n^4 & -4m^2n^2 & & \\ m^3n & -mn^3 & mn^3 - m^3n & 2(mn^3 - m^3n) & & \\ mn^3 & -m^3n & m^3n - mn^3 & 2(m^3n - mn^3) & & \end{bmatrix} \begin{Bmatrix} Q_{11} \\ Q_{22} \\ Q_{12} \\ Q_{33} \end{Bmatrix}$$

$$m = \cos \theta \quad n = \sin \theta$$

$$Q_{11} = \frac{E_1}{1 - \nu_{12}\nu_{21}} \quad Q_{22} = \frac{E_2}{1 - \nu_{12}\nu_{21}} \quad Q_{12} = \frac{\nu_{21}E_1}{1 - \nu_{12}\nu_{21}} \quad Q_{33} = G_{12} \quad \frac{\nu_{12}}{\nu_{21}} = \frac{E_1}{E_2} \quad (4.21)$$

$E_1$ ,  $E_2$  and  $G_{12}$  are the longitudinal modulus, transverse modulus and in-plane shear modulus respectively.  $\nu_{12}$  and  $\nu_{21}$  are the Poisson's ratio in fibre and off-fibre direction.  $\sigma_{xx}$  and  $\sigma_{yy}$  are the normal stress, respectively in  $x$  and  $y$  direction and  $\tau_{xy}$  is a shear stress.

By adopting Equation (4.17) into Equation (4.20), the stress formula can be rewritten as

$$\{\sigma\}_{xy}^k = \{\bar{Q}\}^k \{\epsilon^{(0)}\}_{xy} + \{\bar{Q}\}^k z \{k\}_{xy} \quad (4.22)$$

From derivation of strain from Kirchhoff's assumption, it is observed that strains are constant through the laminate thickness. It also varies linearly. Meanwhile, for stresses, conversely the stress values vary in different thickness because each laminae has different stiffness in the thickness direction. However, both strain and stress vary linearly through the thickness.

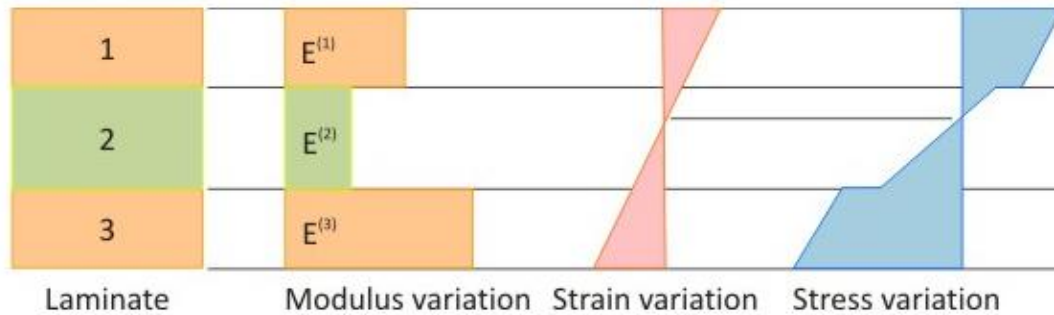


**Figure 4.2 Modulus, strain and stress variation through the laminate thickness [64]**

From Figure 4.2, the different slope for strain and stress depend on the moduli's of each laminae property. Kirchhoff theory also applied to stress-strain relationship where the transverse normal strain is used in Equation (4.20).

In three dimensions, the states of deformation for stress and strain in composites are denoted in matrix form:

$$[\sigma_{xx} \ \sigma_{yy} \ \sigma_{zz} \ \tau_{yz} \ \tau_{xz} \ \tau_{xy}] \quad (4.23)$$

$$[\epsilon_{xx} \ \epsilon_{yy} \ \epsilon_{zz} \ \gamma_{yz} \ \gamma_{xz} \ \gamma_{xy}] \quad (4.24)$$

where:

$\sigma$  = normal stress

$\tau$  = shear stress

$\epsilon$  = normal strain

$\gamma$  = shear strain

in  $x, y$  and  $z$  direction.



According to Hooke's Law, the stress-strain relations:

$$\begin{Bmatrix} \sigma_{xx} \\ \sigma_{yy} \\ \sigma_{zz} \\ \tau_{yz} \\ \tau_{xz} \\ \tau_{xy} \end{Bmatrix} = \begin{bmatrix} E_{11} & E_{12} & E_{13} & E_{14} & E_{15} & E_{16} \\ E_{21} & E_{22} & E_{23} & E_{24} & E_{25} & E_{26} \\ E_{31} & E_{32} & E_{33} & E_{34} & E_{35} & E_{36} \\ E_{41} & E_{42} & E_{43} & E_{44} & E_{45} & E_{46} \\ E_{51} & E_{52} & E_{53} & E_{54} & E_{55} & E_{56} \\ E_{61} & E_{62} & E_{63} & E_{64} & E_{65} & E_{66} \end{bmatrix} \begin{Bmatrix} \varepsilon_{xx} \\ \varepsilon_{yy} \\ \varepsilon_{zz} \\ \gamma_{yz} \\ \gamma_{xz} \\ \gamma_{xy} \end{Bmatrix} \quad (4.25)$$

For orthotropic materials, two planes of these materials are symmetric. This causes some of the coupling to become zero.

$$E_{14} = E_{15} = E_{16} = E_{24} = E_{25} = E_{26} = E_{34} = E_{35} = E_{36} = 0 \quad (4.26)$$

The shear stress in one plane does not cause shear strain with each other in orthotropic body. So,

$$E_{45} = E_{46} = E_{56} = 0 \quad (4.27)$$

The stress-strain relations for orthotropic material become:

$$\begin{Bmatrix} \sigma_{xx} \\ \sigma_{yy} \\ \sigma_{zz} \\ \tau_{yz} \\ \tau_{xz} \\ \tau_{xy} \end{Bmatrix} = \begin{bmatrix} E_{11} & E_{12} & E_{13} & 0 & 0 & 0 \\ E_{21} & E_{22} & E_{23} & 0 & 0 & 0 \\ E_{31} & E_{32} & E_{33} & 0 & 0 & 0 \\ 0 & 0 & 0 & E_{44} & 0 & 0 \\ 0 & 0 & 0 & 0 & E_{55} & 0 \\ 0 & 0 & 0 & 0 & 0 & E_{66} \end{bmatrix} \begin{Bmatrix} \varepsilon_{xx} \\ \varepsilon_{yy} \\ \varepsilon_{zz} \\ \gamma_{yz} \\ \gamma_{xz} \\ \gamma_{xy} \end{Bmatrix} \quad (4.28)$$

However, if in the laminate coordinate system, the plies stacked together are not  $0^\circ$ ,  $90^\circ$  or  $[0/90]$ , the two planes are no longer symmetrical and some of the couplings in Equation (4.28) are no longer zero. The stress-strain relation for this laminate is as follows. Note that the values of  $E_{ij}$  are no longer ply quantities, but are now laminate.

$$\begin{Bmatrix} \sigma_{xx} \\ \sigma_{yy} \\ \sigma_{zz} \\ \tau_{yz} \\ \tau_{xz} \\ \tau_{xy} \end{Bmatrix} = \begin{bmatrix} E_{11} & E_{12} & E_{13} & 0 & 0 & E_{16} \\ E_{21} & E_{22} & E_{23} & 0 & 0 & E_{26} \\ E_{31} & E_{32} & E_{33} & 0 & 0 & E_{36} \\ 0 & 0 & 0 & E_{44} & E_{45} & 0 \\ 0 & 0 & 0 & E_{45} & E_{55} & 0 \\ E_{16} & E_{26} & E_{36} & 0 & 0 & E_{66} \end{bmatrix} \begin{Bmatrix} \varepsilon_{xx} \\ \varepsilon_{yy} \\ \varepsilon_{zz} \\ \gamma_{yz} \\ \gamma_{xz} \\ \gamma_{xy} \end{Bmatrix} \quad (4.29)$$

Compliance matrix is the inverse of the stiffness matrix:

$$[S] = [E]^{-1} \quad (4.30)$$

The stress-strain relation for compliance tensor,  $S_{ij}$  is:

$$\begin{Bmatrix} \varepsilon_{xx} \\ \varepsilon_{yy} \\ \varepsilon_{zz} \\ \gamma_{yz} \\ \gamma_{xz} \\ \gamma_{xy} \end{Bmatrix} = \begin{bmatrix} S_{11} & S_{12} & S_{13} & 0 & 0 & E_{16} \\ S_{21} & E_{22} & E_{23} & 0 & 0 & E_{26} \\ E_{31} & E_{32} & E_{33} & 0 & 0 & E_{36} \\ 0 & 0 & 0 & E_{44} & E_{45} & 0 \\ 0 & 0 & 0 & E_{45} & E_{55} & 0 \\ E_{16} & E_{26} & E_{36} & 0 & 0 & E_{66} \end{bmatrix} \begin{Bmatrix} \sigma_{xx} \\ \sigma_{yy} \\ \sigma_{zz} \\ \tau_{yz} \\ \tau_{xz} \\ \tau_{xy} \end{Bmatrix} \quad (4.31)$$

In classical laminate theory, the ply coordinate system (local coordinate system) is transferred to the laminate coordinate system (global coordinate system) according to the angle between them. A laminate is formed by stacking and bonding plies of the same or different angles in the x-y coordinate. There are several types of laminates usually used, based on the design requirement and part application.

- Symmetric Laminate:  
Layup is symmetrical with respect to the mid-plane.  
Example:  $[-45_2/0_2]_s$ ,  $[\pm 45_2/0_2/90_2]_s$
- Balanced Laminate:  
For every  $+\theta$  ply, there is a  $-\theta$  ply (not necessarily symmetrical)  
Example:  $[45_2/30_2/-30_2/-45_2]_s$ ,  $[\pm 30/\pm 45]_s$
- Angle-ply Laminate:  
Laminate consists of plies in  $+\theta$  and  $-\theta$  oriented fibres  
Example:  $[30_3/-30_3/30_3]$ ,  $[-45_2/45_2]$
- Cross-ply Laminate:  
Fibre orientation only in  $0^\circ$  and  $90^\circ$   
Example:  $[0_2/90_2]_s$ ,  $[0_3/90_3/0_3]$
- Quasi-isotropic Laminate:  
Laminate has the same stiffness in any direction of the plane. Layup is symmetrical and balance. The number of plies in  $0^\circ$ ,  $+45^\circ$ ,  $-45^\circ$  and  $90^\circ$  are same.  
Example:  $[45/-45/90/0]_s$ ,  $[45/0/90/-45]_s$

The classic composite laminate theory is based on a ply coordinate system (local coordinate system) and laminate coordinate system (global coordinate system). Ply stiffness of each ply in the ply coordinate system is transferred into laminate coordinate

stiffness according to the angle  $\theta$  between the ply coordinate system and the laminate coordinate system. By a specific stacking sequence of a laminate and ply thickness, the stiffness of the laminate can be determined.

### 4.1.3 In-plane Resultant Forces

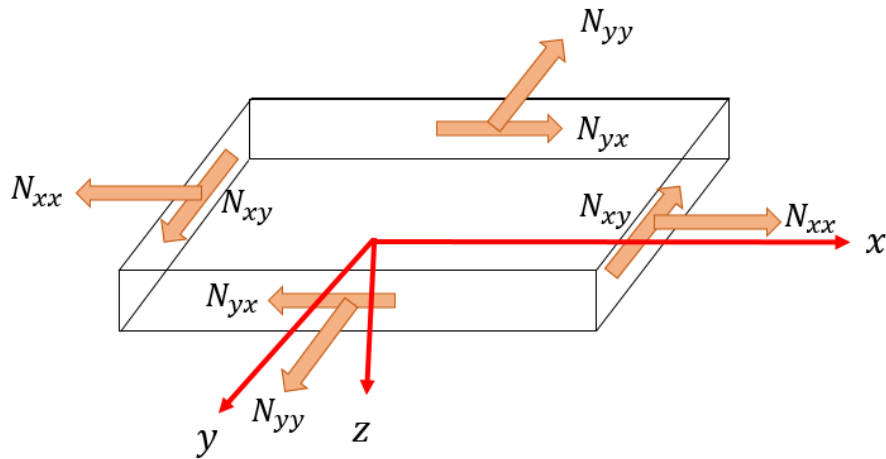


**Figure 4.3 Force intensity on a composite plate**

From the definition, the in-plane forces per unit length formula ( $N/m$ ) in  $x$  and  $y$  directions are

$$N_{xx} = \int_{-H}^H \sigma_{xx} dz, \quad N_{yy} = \int_{-H}^H \sigma_{yy} dz, \quad N_{xy} = \int_{-H}^H \tau_{xy} dz \quad (4.32)$$

Equation (4.32) can be simplified as

$$\{N\}_{xy} = \int_{-H}^H \{\sigma\}_{xy} dz \quad (4.33)$$

By applying Equation (4.22), the in-plane resultant force formula can be rewritten as

$$\{N\}_{xy} = \int_{-H}^H [\bar{Q}]^k \{\epsilon^{(0)}\}_{xy} dz + \int_{-H}^H [\bar{Q}]^k \{k\}_{xy} z dz \quad (4.34)$$

In the previous section, it has been shown that the mid-plane strain and curvatures,  $\{\epsilon^{(0)}\}_{xy}$  and  $\{k\}_{xy}$  respectively are independent of location in  $z$  direction.  $[\bar{Q}]$ , the reduced stiffness matrix in addition is a function of plate thickness and the material properties of each laminae. Thus,

$$\{N\}_{xy} = \sum_{k=1}^{N_{Layer}} \int_{-z_{k-1}}^{z_k} [\bar{Q}]^k \{\epsilon^{(0)}\}_{xy} dz + \sum_{k=1}^{N_{Layer}} \int_{-z_{k-1}}^{z_k} [\bar{Q}]^k \{k\}_{xy} z dz \quad (4.35)$$

Rearrange and simplified Equation (4.35), the new in-plane resultant force equation becomes:

$$\{N\}_{xy} = [A]\{\epsilon^{(0)}\}_{xy} + [B]\{k\}_{xy} \quad (4.36)$$

where

$$[A] = \sum_{k=1}^{N_{Layer}} [\bar{Q}]^k (z_k - z_{k-1}) \quad \text{and} \quad [B] = \frac{1}{2} \sum_{k=1}^{N_{Layer}} [\bar{Q}]^k (z_k^2 - z_{k-1}^2) \quad (4.37)$$

[A] is an in-plane stiffness matrix and matrix [B] is a bending coupling stiffness. The in-plane stiffness matrix relates the in-plane forces  $N_{xx}$ ,  $N_{yy}$  and  $N_{xy}$  with the mid-plane strains while the coupling stiffness relate the in-plane forces with the mid-plane curvatures.

The in-plane forces relationships with a stiffness matrix for the composite laminate can be written as

$$\begin{Bmatrix} N_{xx} \\ N_{yy} \\ N_{xy} \end{Bmatrix} = [A] \begin{Bmatrix} \epsilon_{xx}^0 \\ \epsilon_{yy}^0 \\ \epsilon_{xy}^0 \end{Bmatrix} + [B] \begin{Bmatrix} k_{xx} \\ k_{yy} \\ k_{xy} \end{Bmatrix} \quad (4.38)$$

The compliance relationship for a composite laminate is:

$$\begin{Bmatrix} \epsilon_{xx}^0 \\ \epsilon_{yy}^0 \\ \epsilon_{xy}^0 \end{Bmatrix} = [a] \begin{Bmatrix} N_{xx} \\ N_{yy} \\ N_{xy} \end{Bmatrix} + [b] \begin{Bmatrix} k_{xx} \\ k_{yy} \\ k_{xy} \end{Bmatrix} \quad (4.39)$$

It is noted that matrix [A], [B] and  $[\bar{Q}]$  are symmetric.

#### 4.1.4 Resultant Moments

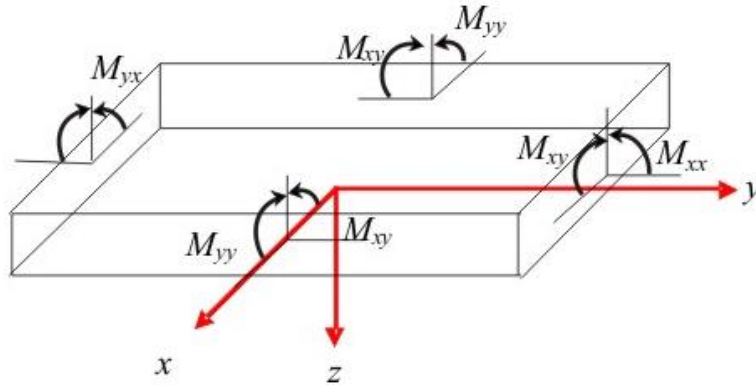


**Figure 4.4 Moment intensity on a composite pate**

From the definition, the resultant moments or moment intensity per unit length formula ( $N/m$ ) are

$$M_{xx} = \int_{-H}^H \sigma_{xx} z dz, \quad M_{yy} = \int_{-H}^H \sigma_{yy} z dz, \quad M_{xy} = \int_{-H}^H \tau_{xy} z dz \quad (4.40)$$

Equation (4.40) can be simplified as

$$\{M\}_{xy} = \int_{-H}^H \{\sigma\}_{xy} z dz \quad (4.41)$$

Recall Equation (4.22), the resultant moment formula can be rewritten as

$$\{M\}_{xy} = \int_{-H}^H [\bar{Q}]^k \{\epsilon^{(0)}\}_{xy} z dz + \int_{-H}^H [\bar{Q}]^k \{k\}_{xy} z^2 dz$$

Using the same Kirchhoff assumption and justification as in Equation (4.32),

$$\{M\}_{xy} = \sum_{k=1}^{N_{Layer}} \int_{-z_{k-1}}^{z_k} [\bar{Q}]^k \{\epsilon^{(0)}\}_{xy} dz + \sum_{k=1}^{N_{Lay}} \int_{-z_{k-1}}^{z_k} [\bar{Q}]^k \{k\}_{xy} z dz$$

This formula can be simplified as

$$\{M\}_{xy} = [B] \{\epsilon^{(0)}\}_{xy} + [D] \{k\}_{xy} \quad (4.42)$$

where

$$[D] = \frac{1}{3} \sum_{k=1}^{N_{Layer}} [\bar{Q}]^k (z_k^3 - z_{k-1}^3) \quad (4.43)$$

and recall from Equation (4.37),  $[B] = \frac{1}{2} \sum_{k=1}^{N_{Layer}} [\bar{Q}]^k (z_k^2 - z_{k-1}^2)$

Matrix  $[D]$  illustrates the bending stiffness. Matrix  $[B]$  in this equation represents the membrane coupling stiffness. Matrix  $[D]$  and  $[B]$  are symmetric.

The resultant moment relationships with a stiffness matrix for the composite laminate can be written as

$$\begin{Bmatrix} M_{xx} \\ M_{yy} \\ M_{xy} \end{Bmatrix} = [B] \begin{Bmatrix} \epsilon_{xx}^0 \\ \epsilon_{yy}^0 \\ \epsilon_{xy}^0 \end{Bmatrix} + [D] \begin{Bmatrix} k_{xx} \\ k_{yy} \\ k_{xy} \end{Bmatrix} \quad (4.44)$$

The compliance relationship for a composite laminate is:

$$\begin{Bmatrix} k_{xx} \\ k_{yy} \\ k_{xy} \end{Bmatrix} = [b] \begin{Bmatrix} N_{xx} \\ N_{yy} \\ N_{xy} \end{Bmatrix} + [d] \begin{Bmatrix} \epsilon_{xx}^0 \\ \epsilon_{yy}^0 \\ \epsilon_{xy}^0 \end{Bmatrix} \quad (4.45)$$

The relationship between resultant in-plane forces, resultant moments, the resulting mid-plane strains and curvatures and laminate stiffness matrices  $[A, ] [B], [D]$  can be written as

$$\begin{Bmatrix} N_{xx} \\ N_{yy} \\ N_{xy} \\ M_{xx} \\ M_{yy} \\ M_{xy} \end{Bmatrix} = \begin{bmatrix} A_{11} & A_{12} & A_{13} & B_{11} & B_{12} & B_{13} \\ A_{21} & A_{22} & A_{23} & B_{21} & B_{22} & B_{23} \\ A_{31} & A_{32} & A_{33} & B_{31} & B_{32} & B_{33} \\ B_{11} & B_{12} & B_{13} & D_{11} & D_{12} & D_{13} \\ B_{21} & B_{22} & B_{23} & D_{21} & D_{22} & D_{23} \\ B_{31} & B_{32} & B_{33} & D_{31} & D_{32} & D_{33} \end{bmatrix} \begin{Bmatrix} \epsilon_{xx}^0 \\ \epsilon_{yy}^0 \\ \epsilon_{xy}^0 \\ k_{xx} \\ k_{yy} \\ k_{xy} \end{Bmatrix} \quad (4.46)$$

Equation (4.46) can be simplified and summarize in one single matrix:

$$\begin{Bmatrix} N \\ M \end{Bmatrix} = \begin{bmatrix} A & B \\ B & D \end{bmatrix} \begin{Bmatrix} \epsilon^{(0)} \\ k \end{Bmatrix} \text{ or } \begin{Bmatrix} \epsilon^{(0)} \\ k \end{Bmatrix} = \begin{bmatrix} a & b \\ b & d \end{bmatrix} \begin{Bmatrix} N \\ M \end{Bmatrix} \quad (4.47)$$

[A] is an extensional or in-plane stiffness matrix, [B] is a membrane-bending coupling stiffness matrix and [D] is a bending stiffness matrix of the composite plate.  $\epsilon^o$  denotes the value of strain or plate deformation, while  $k$  is the laminate curvature. If [B] is not equal to zero, laminate will experience the membrane-bending coupling effect where the in-plane loads and out-of-plane loads will cause both in-plane and out-of-plane deformation simultaneously. If the value of [B] is zero, the laminate is uncoupled. No membrane-bending coupling occurs in this condition. This happens to the symmetric laminate.

Laminate is symmetrical when the layup is symmetric with respect to the mid-plane of the laminate. Example of symmetric laminates are [45<sub>2</sub>/90<sub>2</sub>/90<sub>2</sub>/45<sub>2</sub>] and [45<sub>2</sub>/-45<sub>2</sub>/0<sub>2</sub>/90<sub>2</sub>/90<sub>2</sub>/0<sub>2</sub>/-45<sub>2</sub>/45<sub>2</sub>].

#### 4.1.5 Laminate Equivalent Engineering Elastic Constant

Isotropic materials are materials with properties that are uniform and independent of the direction of space, while anisotropic materials are dependent on the direction in space. In other words, the material properties of isotropic materials are uniform or the same in all directions, while for anisotropic, the material properties vary in different directions [78–82]. Composite materials are classified as anisotropic materials. The modulus of fibre depends on the direction of the laminate. For example, for unidirectionally-reinforced fibre composites, the Young's Modulus, in fibre direction,  $E_1$  is different to the off-fibre direction,  $E_2$ .

According to reference [4], the laminate engineering elastic constants of composite materials can be calculated from compliance matrices [a] and [d] by using the formula presented in Table 4.1.

**Table 4.1 [a], [d] compliance matrix elements for a composite laminate**

[a]	[d]
$a_{11} = \frac{A_{22}A_{33} - A_{23}^2}{A}$	$d_{11} = \frac{D_{22}D_{33} - D_{23}^2}{D}$
$a_{22} = \frac{A_{11}A_{33} - A_{13}^2}{A}$	$d_{22} = \frac{D_{11}D_{33} - D_{13}^2}{D}$
$a_{33} = \frac{A_{11}A_{22} - A_{12}^2}{A}$	$d_{33} = \frac{D_{11}D_{22} - D_{12}^2}{D}$
$a_{12} = \frac{A_{13}A_{23} - A_{12}A_{33}}{A}$	$d_{12} = \frac{D_{13}D_{23} - D_{12}D_{33}}{D}$
$a_{13} = \frac{A_{12}A_{23} - A_{22}A_{13}}{A}$	$d_{13} = \frac{D_{12}D_{23} - D_{22}D_{13}}{D}$
$a_{23} = \frac{A_{12}A_{13} - A_{11}A_{23}}{A}$	$d_{23} = \frac{D_{12}D_{13} - D_{11}D_{23}}{D}$
$A = A_{11}A_{22}A_{33} + 2A_{12}A_{23}A_{13} - A_{22}A_{13}^2 - A_{33}A_{12}^2 - A_{11}A_{23}^2$	
$D = D_{11}D_{22}D_{33} + 2D_{12}D_{23}D_{13} - D_{22}D_{13}^2 - D_{33}D_{12}^2 - D_{11}D_{23}^2$	

Table 4.2 shows the formula to calculate the laminate engineering elastic constants.  $E_x$ ,  $E_y$  and  $G_{xy}$  are the equivalent elastic constant in  $x$ ,  $y$  and  $xy$  directions respectively.  $\nu_{xy}$  and  $\nu_{yx}$  are Poisson's ratio while  $m_x$  and  $m_y$  represent the shear coupling coefficient in  $x$  and  $y$  direction respectively.

**Table 4.2 Laminate engineering elastic constants**

	Membrane Mode	Bending Mode
$E_x$	$\frac{1}{t \cdot a_{11}}$	$\frac{12}{t^3 d_{11}}$
$E_y$	$\frac{1}{t \cdot a_{22}}$	$\frac{12}{t^3 d_{22}}$
$G_{xy}$	$\frac{1}{t \cdot a_{33}}$	$\frac{12}{t^3 d_{33}}$
$\nu_{xy}$	$-\frac{a_{12}}{a_{11}}$	$-\frac{d_{12}}{d_{11}}$
$\nu_{yx}$	$-\frac{a_{12}}{a_{22}}$	$-\frac{d_{12}}{d_{22}}$
$m_x$	$-\frac{a_{13}}{a_{11}}$	$-\frac{d_{13}}{d_{11}}$
$m_y$	$-\frac{a_{23}}{a_{22}}$	$-\frac{d_{23}}{d_{22}}$



## 4.2 Thin-walled Composite Beams: Single-Cell and Double-Cell

The application of closed, thin-walled box beams is huge in the aerospace, civil and marine industry. The superior fatigue features and the ability to tailor the composite materials to meet the desire specification has increased the demand of composite in those industries. Due to the high specific stiffness in bending, torsion and the high strength to weight ratio properties, composite thin-walled box beams are now favourable compared to metal counterparts. For example, advanced composite materials have been used to construct helicopter and tilt rotor blades and even wind turbine blades [83]. The closed thin-walled beam can be constructed into single-cell, double-cell or multi-cell, depends on its application. Helicopter rotor blade for example are made of closed multi-cell beams to achieve the optimum performance.

### 4.2.1 Displacement Field of a Composite Box Beam

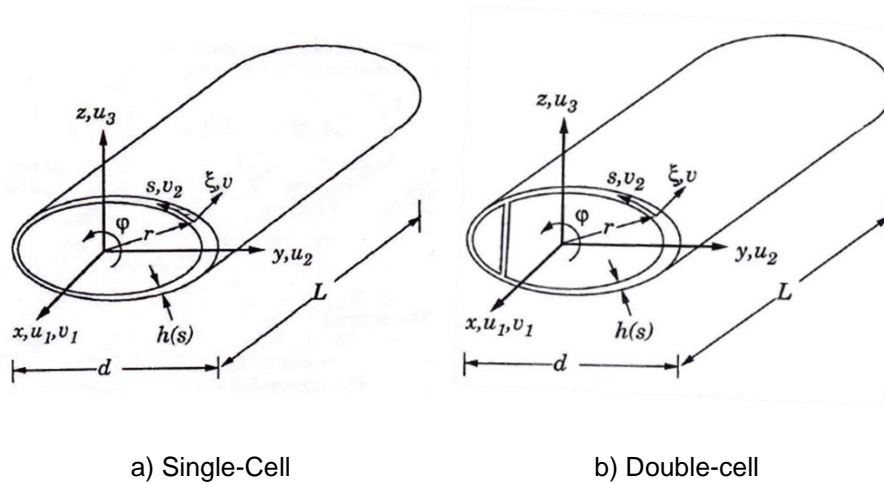


**Figure 4.5 Coordinate systems and kinematic variables for thin-walled shell**

The analysis of the thin-wall beam in Figure 4.5 are derived using Hamilton's principle [12]. The beam is considered as a slender thin-walled elastic shell. The assumptions made in this analysis are:

$$\begin{aligned}
d &<< L \\
h &<< d \\
h &<< R
\end{aligned}
\tag{4.48}$$

Where  $d$  is a cross-section dimension,  $L$  represents the length of the shell,  $h$  is the thickness and  $R$  denotes the curvature radius of the middle wall. The deviation of the properties over distance  $d$  in the axial direction is also assumed to be very small.

The shell material is anisotropic, which means it is dependent on the direction. Its properties can vary in normal and circumference direction. Thickness of the shell is not uniform throughout the length in circumference direction. The circumferential coordinate is denoted as  $s$ , and throughout the length it is measured in anti-clockwise direction, always tangent to the mid-surface.

Referring the coordinate system in Figure 4.5,  $(x, y, z)$ , the closed contour,  $\Gamma$  in  $y$  direction is

$$y = y(s) \tag{4.49}$$

And the closed contour in  $z$  direction is

$$z = z(s) \tag{4.50}$$

From Figure 4.5, the displacement field can be written as

$$\begin{aligned}
u_1(x, y) &= U_1(x) - y(s)U'_2(x) - z(s)U'_3(x) + g(s, x) \\
u_2(x, s) &= U_2(x) - z(s)\varphi(x) \\
u_3(x, s) &= U_3(x) + y(s)\varphi(x)
\end{aligned}
\tag{4.51}$$

$\varphi(x)$  is a twist angle and the prime symbol (') shows the differentiation with respect to the  $x$  direction.

In 2D anisotropic shell, the strain energy density  $\Phi$  is related to membrane characteristic. Thus the equation can be written as

$$2\Phi = A_{11}(\gamma_{11})^2 + A_{22}(\gamma_{22})^2 + 4A_{66}(\gamma_{12})^2 + 2A_{12}\gamma_{11}\gamma_{22} + 4A_{16}\gamma_{11}\gamma_{12} + 4A_{26}\gamma_{22}\gamma_{12} \quad (4.52)$$

From Equation (4.52), the strain energy can be expressed as

$$U = \int_0^L \phi \Phi ds dx \quad (4.53)$$

To find the expression for in-plane strains, it is noted that the axial, tangential and normal displacement,  $u_1, v_2$  and  $v$  respectively are related with the curvilinear coordinate  $x, s, \xi$ .

Refer to Figure 4.5, the in-plane strain can be expressed as

$$\begin{aligned} \gamma_{11} &= \frac{\partial u_1}{\partial x} \\ 2\gamma_{12} &= \frac{\partial u_1}{\partial s} + \frac{\partial v_2}{\partial x} \\ \gamma_{22} &= \frac{\partial v_2}{\partial s} + \frac{v}{R} \end{aligned} \quad (4.54)$$

$v_2$  and  $v$  are associated with the Cartesian displacement components. The equation is shown below

$$\begin{aligned} v_2 &= u_2 \frac{dy}{ds} + u_3 \frac{dz}{ds} \\ v &= u_2 \frac{dz}{ds} - u_3 \frac{dy}{ds} \end{aligned} \quad (4.55)$$

In a case where there is no internal pressure,

$$N_{22} = \frac{\partial \Phi}{\partial \gamma_{22}} = 0 \quad (4.56)$$

Equation (4.56) can also be applied if there is no hoop stress or the hoop stress is too small, hence negligible.

Equation (4.56) is combined with Equation (4.52) and thus the expression  $\gamma_{22}$  can be written as

$$\gamma_{22} = -\frac{1}{A_{22}} (A_{12}\gamma_{11} + 2A_{26}\gamma_{12}) \quad (4.57)$$

Insert Equation (4.57) into Equation (4.52),

$$2\Phi_1 = \min_{\gamma_{12}} 2\Phi_1 = A(s)(\gamma_{11})^2 + 2B(s)\gamma_{11}\gamma_{12} + C(s)(\gamma_{12})^2 \quad (4.58)$$

where

$$\begin{aligned} A(s) &= A_{11} - \frac{(A_{12})^2}{A_{22}} \\ B(s) &= 2 \left[ A_{16} - \frac{A_{12}A_{26}}{A_{22}} \right] \\ C(s) &= 4 \left[ A_{66} - \frac{(A_{26})^2}{A_{22}} \right] \end{aligned} \quad (4.59)$$

$A(s)$ ,  $B(s)$  and  $C(s)$  denotes the reduced axial stiffness, reduced coupling stiffness and reduced shear stiffness, respectively.

The shear flow,  $N_{12}$  can be calculated from formula

$$N_{12} = \frac{\partial \Phi}{\partial (2\gamma_{12})} = \frac{1}{2} (B(s)\gamma_{11} + C(s)\gamma_{12}) \quad (4.60)$$

Rearrange Equation (4.60),

$$\gamma_{12} = \frac{2N_{12}}{C(s)} - \frac{B(s)}{C(s)}\gamma_{11} \quad (4.61)$$

Replace the strain value from Equation (4.61) with Equation (4.51), (4.54) and (4.55)

$$\frac{\partial g}{\partial s} + \frac{2B(s)}{C(s)} g'(s, x) = -r_n(s)\varphi' - \frac{2B(s)}{C(s)} [U'_1 - y(s)U''_2 - z(s)U''_3] + \frac{4N_{12}}{C(s)} \quad (4.62)$$

$r_n$  is a projection of the position vector  $r$  in normal direction of the shell. The formula to calculate  $r_n$  is shown below.

$$r_n = y \frac{dz}{ds} - z \frac{dy}{ds} \quad (4.63)$$

### 4.2.2 Force-Deformation Relationships

In kinematic, the strain energy can be calculated by substituting the values of  $\gamma_{11}$  and  $\gamma_{12}$  from Equation (4.54) into Equation (4.53) and (4.58). Thus the strain energy equations of kinematic becomes

$$U = \frac{1}{2} \int_0^L \{\delta\}^T [C]_{4 \times 4} \{\delta\} dx \quad (4.64)$$

$\{\delta\}$  is a 4 x 1 column matrix of kinematic variables.

$$\{\delta\}^T = \{U'_1 \quad \varphi' \quad U''_3 \quad U''_2\} \quad (4.65)$$

$[C]$  is a stiffness matrix. It is a 4 x 4 symmetric matrix.

$$[C] = \begin{bmatrix} C_{11} & C_{12} & C_{13} & C_{14} \\ C_{12} & C_{22} & C_{23} & C_{24} \\ C_{13} & C_{23} & C_{33} & C_{34} \\ C_{14} & C_{24} & C_{34} & C_{44} \end{bmatrix} \quad (4.66)$$

$$C_{11} = \oint \left( A - \frac{B^2}{c} \right) ds + \frac{[\oint (B/C) ds]^2}{\oint (1/C) ds}$$

$$C_{12} = \frac{\oint (B/C) ds}{\oint (1/C) ds} A_e$$

$$C_{13} = -\oint \left( A - \frac{B^2}{c} \right) z ds - \frac{\oint (B/C) ds \oint (B/C) z ds}{\oint (1/C) ds}$$

$$C_{14} = -\oint \left( A - \frac{B^2}{c} \right) y ds - \frac{\oint (B/C) ds \oint (B/C) y ds}{\oint (1/C) ds}$$

$$C_{22} = \frac{1}{\oint (1/C) ds} A_e^2$$

$$C_{23} = -\frac{\oint (B/C) z ds}{\oint (1/C) ds} A_e$$

$$C_{24} = -\frac{\oint (B/C) y ds}{\oint (1/C) ds} A_e$$

$$C_{33} = \oint \left( A - \frac{B^2}{c} \right) z^2 ds + \frac{[\oint (B/C) z ds]^2}{\oint (1/C) ds}$$

$$C_{34} = \oint \left( A - \frac{B^2}{c} \right) yz ds + \frac{\oint (B/C) y ds \oint (B/C) z ds}{\oint (1/C) ds}$$

$$C_{44} = \oint \left( A - \frac{B^2}{c} \right) y^2 ds + \frac{[\oint (B/C) y ds]^2}{\oint (1/C) ds} \quad (4.67)$$

$A_e$  is the enclosed area of the cross section where

$$A_e = \frac{1}{2} \oint r_n ds = \frac{l}{2} \bar{r}_n \quad (4.68)$$

From [12], bending stiffness, torsional stiffness and coupling stiffness of the thin-walled shell are represented from elements in matrix  $[C]$  where

Bending stiffness,  $EI = C_{33}$

Torsional stiffness,  $GJ = C_{22}$

Coupling stiffness,  $CK = C_{23}$

### 4.3 Optimisation Method

Optimum design methods for composite structure have been applied and investigated by researchers using different methods. Today, the researchers' prowess and technologies have made the optimisation routines and numerical analysis tools utilised with improved accuracy. Through employing the optimisation techniques, the design space now can be explored more rigorously, with greater trade-offs to be carried out between different designs.

The purpose of optimisation is to make or produce the most effective design or product subject to requirement and resources [84–90]. Philips [59] has divided the optimisation tools into two categories; computational based and knowledge base. There are several advantages and disadvantages associated with both tools.

For computational based, the approach can be sub-categorised into analytical methods and numerical methods. Analytical methods are based on the mathematical theory whilst numerical methods involve mathematical programming. Numerical methods generate the optimal design in an iterative manner. It relies on a predetermined set of the existing computational tools and geometric models to generate data and information that is interpreted by computer and to a lesser extent by the engineers.

Fu [91] has classified the optimisation methods into four categories; Gradient-based Methods, Direct Search Methods, Specialised Algorithm and Hybrid methods. The examples of optimisation methods classification are shown in Table 4.3. Hybrid methods combine two or more optimisation methods.

**Table 4.3 Example of optimisation methods [91,92]**

<b>Gradient-based methods</b>	
• Vanishing the function's first gradient	• Quasi-Newton method
• Steepest descent	• Method of feasible directions
• Conjugate gradient	• Approximation schemes
<b>Direct search methods</b>	
• Partitioning methods	• Genetic algorithm
• Enumeration search	• Tabu search
• Simplex method	• Scatter search
• Random and greedy search	• Particle swarm
• Simulated annealing	• Ant colony
<b>Special algorithm</b>	
• Design with lamination parameters	• Discrete material optimization
• Layer-wise optimisation	• Fractal branch-and-bound method
• Problem partitioning	• Knowledge-based methods

The objective of wing structure optimisation is to find the optimum structural configuration to meet the specified structural task or requirement [93]. The example on how to define the objective function, design variables and constraints on one case is shown below.

*Example:*

Objective function: to reduce the structure mass

Design variables: the cross-sectional area of the beam

Constraints: stress, aeroelastic effects (flutter and divergence)

Structural optimisation involves the mathematical equation and function. Example:

$$\text{Minimize } W(X) \tag{4.69}$$

$$\text{Subject to } G_n(X) \leq; n = 1, 2, \dots, n_c \tag{4.70}$$

$$\text{and } \{X_L\} \leq \{X\} \{X_U\} \quad (4.71)$$

where  $W(X) = \text{objective function}$

$G_n(X) = \text{a set of } n_c \text{ constraint}$

$\{X\} = \text{set of } n_{Dv} \text{ variables for upper and lower bound}$

$\{X_U\} = \text{upper bound}$

$\{X_L\} = \text{lower bound}$

$$\text{For } G_n(X) = \left[ \frac{F_n(X)}{F_n} \right] - 1 \quad (4.72)$$

$F_n = \text{upper limit on a quantity}$

$F_n(X) = \text{behaviour of current design e. g. stress}$

$$\text{For } G_n(X) = 1 - \left[ \frac{F_n(X)}{F_n} \right] \quad (4.73)$$

$F_n = \text{lower limit on behaviour, e. g. flutter speed}$



## 5 ANALYSIS OF COMPOSITE PLATES AND THIN-WALLED COMPOSITE BEAMS

The properties of composite plate or laminate can be calculated by using two methods:

- i. Measurement in experiment.
- ii. Calculation based on the study of micro-mechanics of composite ply. The relative amount of fibres and matrix are calculated by using the strength of materials or the theory of elasticity approach.

For this research, analysis for composite laminate and box is carried out, based on option (ii), where detail calculation and mathematical solutions involved in the analysis.

### 5.1 Composite Laminate Analysis

#### 5.1.1 Equivalent Elastic Constant-Stiffness Relationship

The development of optimisation theory for composite laminate in this study is associated with the theory of elasticity. The material properties of composite laminate used in the analysis are listed in Table 5.1.

**Table 5.1: Material properties and dimension**

<b>Material type</b>	Carbon fibre, fibre/epoxy resin (120°C Cure, std CF UD)
<b>Material properties</b>	Young's Modulus, $E_1 = 135 \text{ GPa}$ , $E_2 = 10 \text{ GPa}$ Poisson's ratio, $\nu_{12} = 0.3$ Shear Modulus, $G_{12} = 5 \text{ GPa}$
<b>Dimension</b>	Total thickness of laminate, $t = 0.001\text{m}$ Laminate width, $b = 1\text{m}$ Number of layers = 8 layers

The final formula for calculating equivalent elastic constants  $E_x, E_y, G_{xy}$  and bending stiffness, torsional stiffness and coupling stiffness  $EI, GJ, CK$  respectively, for laminate, are presented in Equations (5.1) to (5.5).

### Equivalent elastic constants for membrane mode

$$\text{Membrane Mode: } E_x = \frac{1}{t.a_{11}}, E_y = \frac{1}{t.a_{22}}, G_{xy} = \frac{1}{t.a_{33}} \quad (5.1)$$

### Equivalent elastic constants for bending mode

$$\text{Bending Mode: } E_x = \frac{12}{t^3 d_{11}}, E_y = \frac{12}{t^3 d_{22}}, G_{xy} = \frac{12}{t^3 d_{33}} \quad (5.2)$$

where  $[a]$  and  $[d]$  is a compliance matrix element for a composite laminate.

Bending stiffness, torsional stiffness and coupling stiffness values have also been analysed to investigate the equivalent engineering elastic constant-stiffness correlation for symmetrical and balance layup,  $L_B$  and symmetrical and unbalance layup,  $L_U$  by using formula from [94].

### Bending stiffness of laminate, $EI$

$$EI = b \left( D_{11} - \frac{D_{12}^2}{D_{22}} \right) \quad (5.3)$$

### Torsional stiffness of laminate, $GJ$

$$GJ = 4b \left( D_{33} - \frac{D_{23}^2}{D_{22}} \right) \quad (5.4)$$

### Coupling stiffness of laminate, $CK$

$$CK = 2b \left( D_{13} - \frac{D_{12}D_{23}}{D_{22}} \right) \quad (5.5)$$

where  $b$  = laminate width

$D_{11}, D_{12}, D_{22}, D_{23}, D_{33}$  = bending stiffness element in  $[D]$  matrix of a laminate

Details for each element in  $[a]$  and  $[d]$  as shown in Table 4.1 in previous chapter.

### 5.1.1.1 Results

Figure 5.1 shows the results of  $E_x$  at different ply angle for  $L_U$  and  $L_B$  in membrane and bending mode. The details of  $E_x$  values are given in Table 5.2.

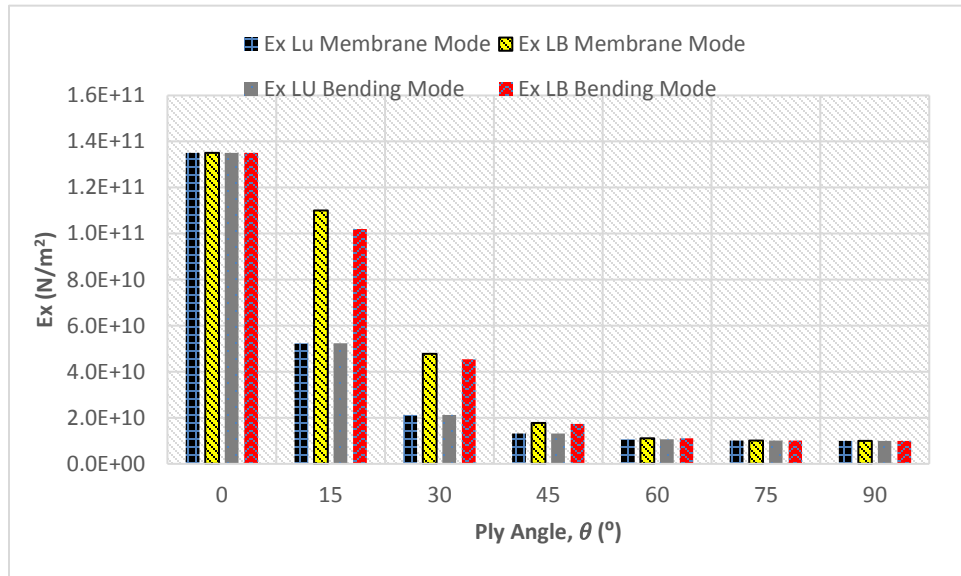


Figure 5.1  $E_x$  for  $L_U$  and  $L_B$  membrane and bending mode at different ply angle

Table 5.2  $E_x$  membrane and bending mode

Ply Angle (°)	$E_x$ Membrane Mode (N/m <sup>2</sup> )		$E_x$ Bending Mode (N/m <sup>2</sup> )	
	$L_U$	$L_B$	$L_U$	$L_B$
0	1.35E+11	1.35E+11	1.35E+11	1.35E+11
15	5.23E+10	1.10E+11	5.23E+10	1.02E+11
30	2.12E+10	4.78E+10	2.12E+10	4.54E+10
45	1.32E+10	1.77E+10	1.32E+10	1.74E+10
60	1.07E+10	1.11E+10	1.07E+10	1.11E+10
75	1.01E+10	1.01E+10	1.01E+10	1.01E+10
90	1.00E+10	1.00E+10	1.00E+10	1.00E+10

The theory and constitutive equation of macromechanics of a laminate are applied in this analysis. The results were obtained using the analytical method as the basis. The appearing result in Figure 5.1 shows that the values of  $E_x$  for  $L_U$  and  $L_B$  coincide at  $0^0$ ,  $60^0$ ,  $75^0$  and  $90^0$ . The in-plane and out-of-plane direction, membrane and bending mode, respectively did not affect the graph pattern at this angle.  $E_x$  values for  $L_U$  are perfectly

matched between the two modes.  $L_B$  conversely appear to have slightly different values between  $15^\circ$  and  $45^\circ$ , which range from 1% to 7% difference. For the two types of mode variation, plotted graphs showed that the extension-shear coupling from element  $A_{13}$  and  $A_{23}$  have a significant influence on the stiffness laminate in the membrane and bending mode. The extension shear coupling proved that the uncoupled laminate provided improved the strength in the fibre direction.

In order to illustrate the influenced of extension shear coupling in off-fibre or transverse direction  $E_y$ , data were analysed and plotted for  $L_U$  and  $L_B$  laminate against ply angle  $\theta$  as shown in Figure 5.2. Again, with the presence of extension shear coupling, the  $E_y$  values for membrane mode and bending mode are equal at every angle. Without  $A_{13}$  and  $A_{23}$  terms,  $L_B$  the values did not match when fibres are orientated at  $45^\circ$  to  $75^\circ$ .  $E_y$  values plotted with angle variation for  $L_B$  showed that laminate without extension shear coupling develops higher modulus in transverse plate direction for in-plane and out-of-plane direction. The details of  $E_y$  values are given in Table 5.3.

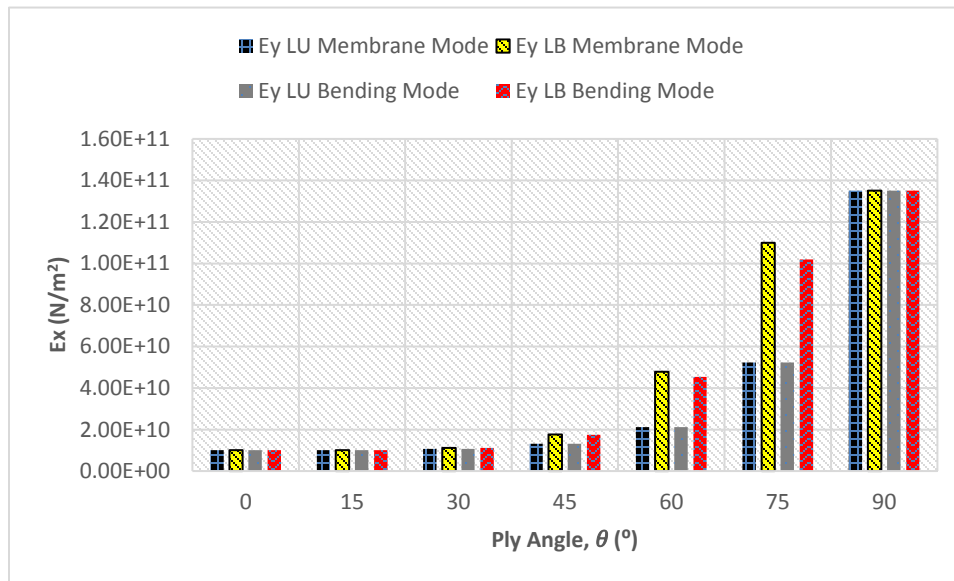


Figure 5.2  $E_y$  for  $L_U$  and  $L_B$  membrane and bending mode at different ply angle

**Table 5.3  $E_y$  membrane and bending mode**

Ply Angle (°)	$E_y$ Membrane Mode (N/m <sup>2</sup> )		$E_y$ Bending Mode (N/m <sup>2</sup> )	
	$L_U$	$L_B$	$L_U$	$L_B$
0	1.00E+10	1.00E+10	1.00E+10	1.00E+10
15	1.01E+10	1.01E+10	1.01E+10	1.01E+10
30	1.07E+10	1.11E+10	1.07E+10	1.11E+10
45	1.32E+10	1.77E+10	1.32E+10	1.74E+10
60	2.12E+10	4.78E+10	2.12E+10	4.54E+10
75	5.23E+10	1.10E+11	5.23E+10	1.02E+11
90	1.35E+11	1.35E+11	1.35E+11	1.35E+11

The variation of shear modulus,  $G_{xy}$  with ply angle  $\theta$  showed a mirror image at a  $45^\circ$  angle, as illustrated in Figure 5.3. The details of  $G_{xy}$  values are presented in

Table 5.4. Extension shear coupling, obviously affects the integrity of laminate in shear. Both mode variations to this point significantly impact on this coupled and uncoupled plate.  $L_B$ , which denotes that the uncoupled extension shear laminate has a greater shear modulus compared to laminate with this coupled term except at  $0^\circ$  and  $90^\circ$ . This suggests that such dissimilarity does not exist in  $0^\circ$  and  $90^\circ$  for orthotropic and especially orthotropic laminate; while in this study, neither Young's Modulus nor shear modulus have distinct value at membrane and bending mode.

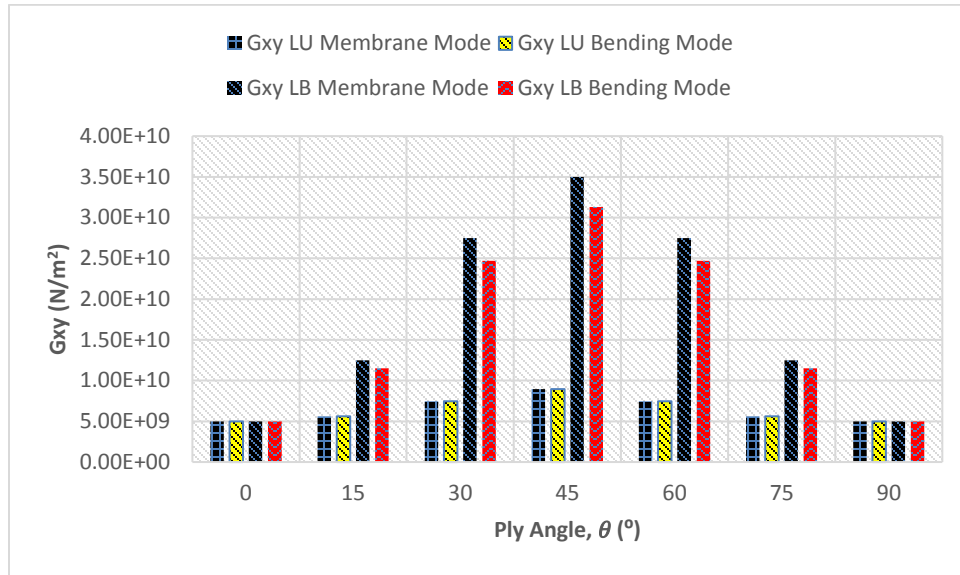
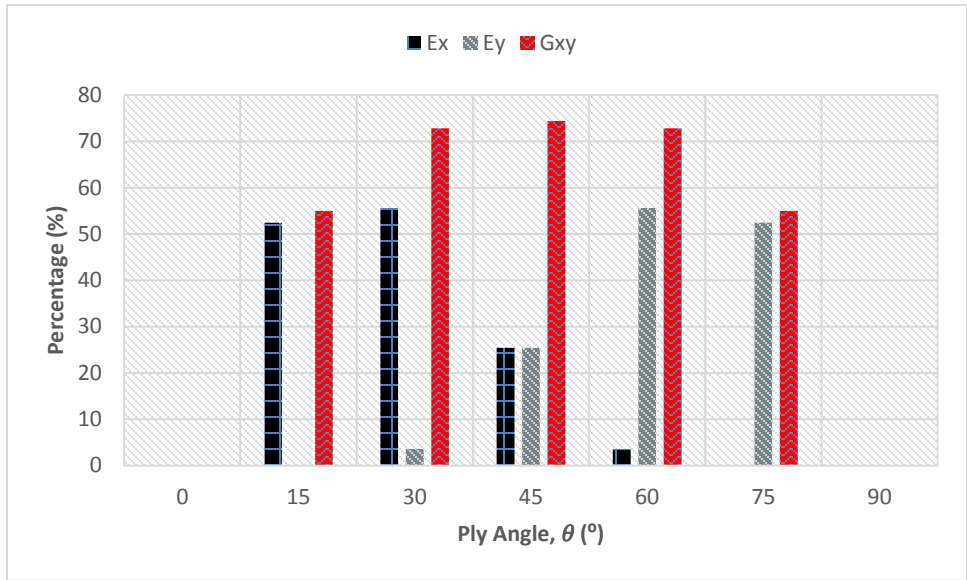


Figure 5.3  $G_{xy}$  for  $L_U$  and  $L_B$  membrane mode and bending mode at different ply angle

Table 5.4  $G_{xy}$  membrane mode and bending mode

Ply Angle (°)	$G_{xy}$ Mode I (N/m <sup>2</sup> )		$G_{xy}$ Mode II (N/m <sup>2</sup> )	
	$L_U$	$L_B$	$L_U$	$L_B$
0	5.00E+09	5.00E+09	5.00E+09	5.00E+09
15	5.62E+09	1.25E+10	5.62E+09	1.15E+10
30	7.47E+09	2.75E+10	7.47E+09	2.47E+10
45	8.94E+09	3.50E+10	8.94E+09	3.13E+10
60	7.47E+09	2.75E+10	7.47E+09	2.47E+10
75	5.62E+09	1.25E+10	5.62E+09	1.15E+10
90	5.00E+09	5.00E+09	5.00E+09	5.00E+09

The assessment effects of extension shear coupling in terms of percentage difference for  $E_x$ ,  $E_y$  and  $G_{xy}$  between symmetrical balance and symmetrical unbalance layup are presented in Figure 5.4 and Figure 5.5. No difference occurs in any modulus or mode at  $0^\circ$  and  $90^\circ$ . The highest effect, however, is clearly seen at shear modulus. Theory and findings from this section are then used in the analysis of bending or flexural stiffness,  $EI$  and torsional stiffness,  $GJ$  where these parameters are required in the composite structure analysis.



**Figure 5.4 Percentage different  $L_U$  and  $L_B$  for  $E_x$ ,  $E_y$  and  $G_{xy}$  membrane mode**

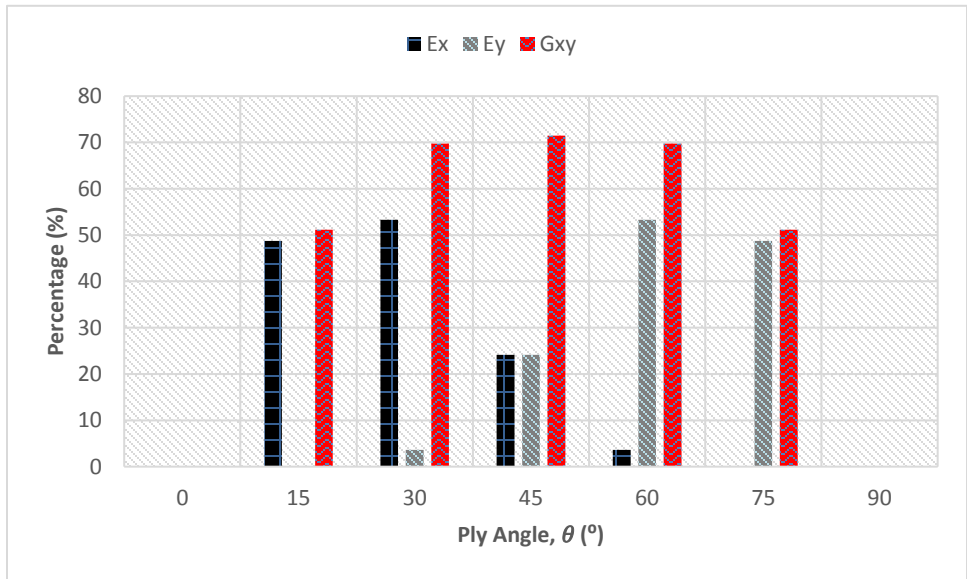


**Figure 5.5 Percentage different  $L_U$  and  $L_B$  for  $E_x$ ,  $E_y$  and  $G_{xy}$  bending mode**

Based on the formula, mathematically  $EI$  and  $GJ$  is a direct equation to compute bending stiffness and torsional stiffness of the plate respectively.  $EI$  is a product of Young's Modulus and area moment of inertia,  $E_x$  and  $I$  respectively, while  $GJ$  is a product of shear modulus,  $G_{xy}$  and polar moment of inertia of the plate,  $J$ .

$EI$  and  $GJ$  data are illustrated in Figure 5.6, and Figure 5.7 as predicted follows the similar pattern as  $E_x$  and  $G_{xy}$  presented previously in Figure 5.1 to Figure 5.3. This confirms that for the fixed dimension of composite laminate or box structure, either the wing box or fuselage, the optimisation of the structure can be achieved by optimising the value of laminate modulus. The uncoupled laminate offers higher flexural and torsional stiffness compared to coupled laminate. Modulus is expressed as a linear variable in the stiffness analysis.

$EI$  values were calculated from Equation 5.2 and  $GJ$  values were obtained from Equation 5.3. Results for  $EI$  and  $GJ$  are plotted and illustrated in Figure 5.6 and 5.7, respectively.

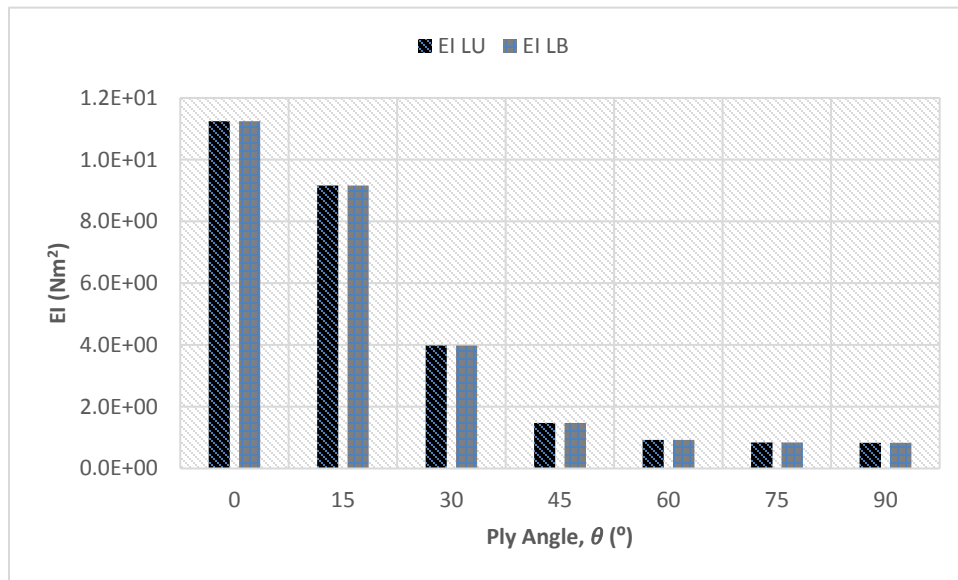


**Figure 5.6  $EI$  for  $L_U$  and  $L_B$**



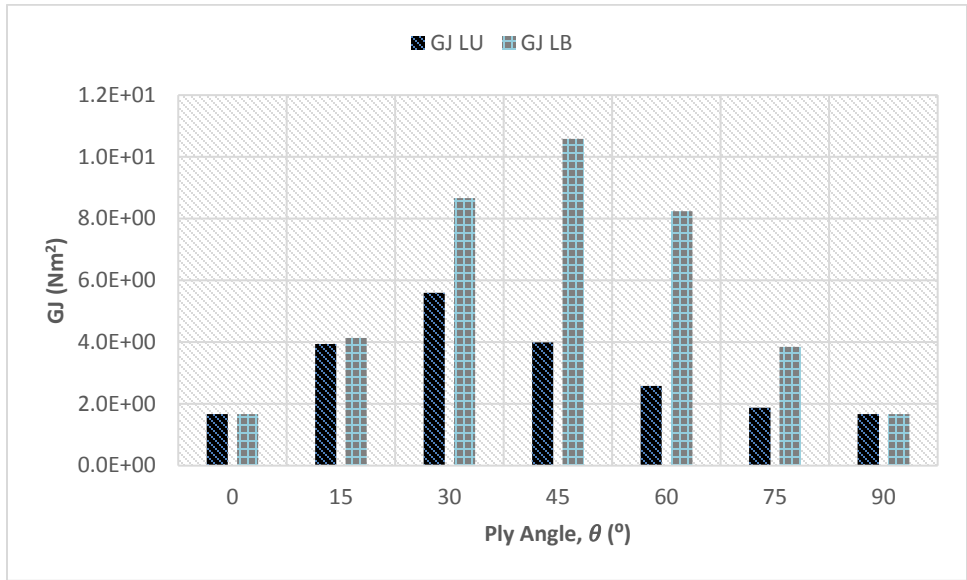


**Figure 5.7  $GJ$  for  $L_U$  and  $L_B$**

Coupling stiffness data were analysed to find out how it associates and relates to bending stiffness and torsional stiffness. Composite coupling constant represents the strength of interaction between the plies. At any angle if the coupling constant presents, the stiffness and strength of laminate will deteriorate. Referring Figure 5.8, the data plotted confirmed the theory.

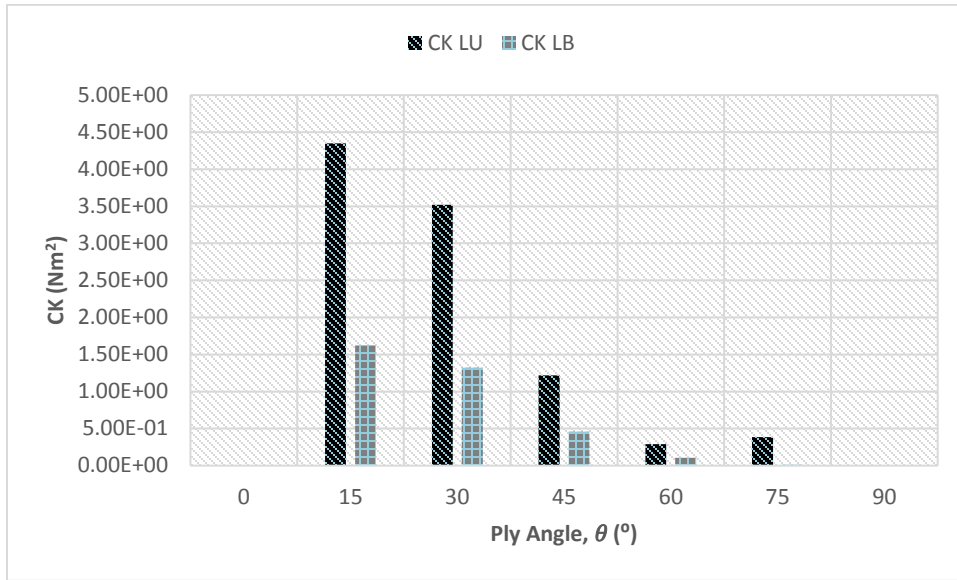


**Figure 5.8 CK for  $L_U$  and  $L_B$**

It is well understood that bending stiffness and torsional stiffness depend on the value of laminate equivalent engineering elastic constants,  $E_x$  and  $G_{xy}$  respectively. From classical laminate theory, the symmetric laminate produces zero coupling and gives the results of membrane-bending coupling stiffness matrix,  $[B]$  zero. From this theory, detailed analysis has been carried out to find out which element in the extensional and bending matrix actually contribute to the bending and torsional stiffness. Results indicate that both  $EI$  and  $GJ$  values are higher in symmetrical and balance layup compared to symmetrical and unbalance layup, but the reason behind this result is still unclear. Therefore, further analysis has been done where the stiffness matrix has been dug deeper. Each element in  $[A]$  and  $[D]$  has been analysed individually and the results are shown in Figure 5.9 and Figure 5.10.

Equations (5.6) and (5.7) present the elements in  $[A]$  and  $[D]$ .

$$[A] \text{ matrix, } [A] = \begin{bmatrix} A_{11} & A_{12} & A_{13} \\ & A_{22} & A_{23} \\ & & A_{33} \end{bmatrix} \quad (5.6)$$

Each  $[A]$  element for  $L_U$  and  $L_B$  is plotted in Figure 5.9.

$$[D] \text{ matrix, } [D] = \begin{bmatrix} D_{11} & D_{12} & D_{13} \\ & D_{22} & D_{23} \\ & & D_{33} \end{bmatrix} \quad (5.7)$$

Each  $[D]$  element for  $L_U$  and  $L_B$  is plotted in Figure 5.10

The membrane-bending coupling matrix,  $[B]$  matrix is zero for  $L_U$  and  $L_B$  since both laminates are symmetric, hence only  $[A]$  and  $[D]$  elements are plotted in the following figures.

$[A] =$

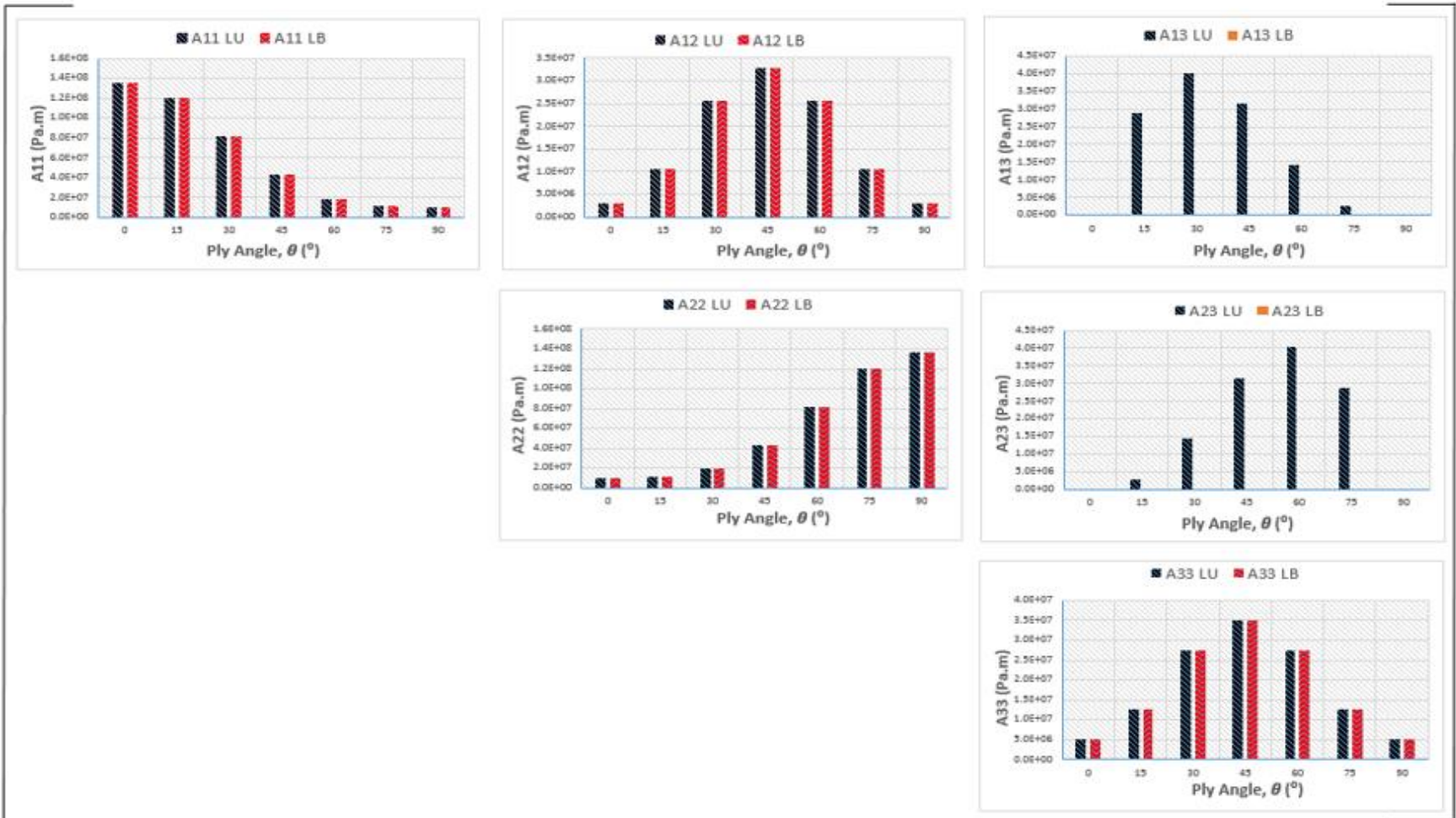


Figure 5.9 Individual element for  $[A] L_U$  and  $L_B$

$[D] =$

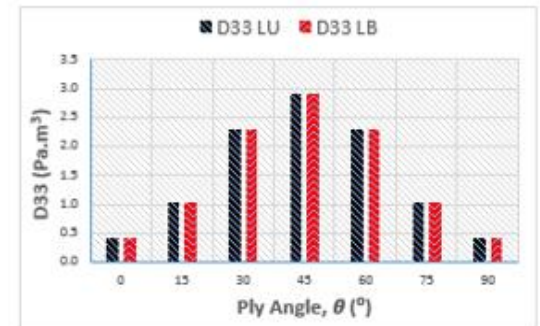
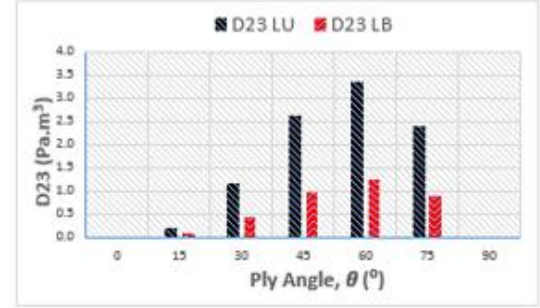
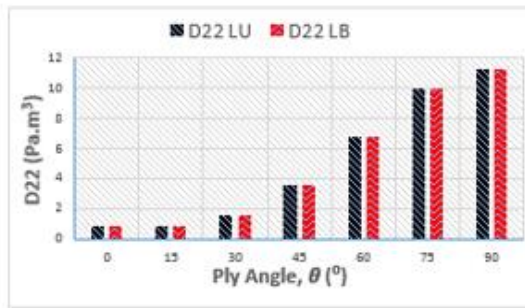
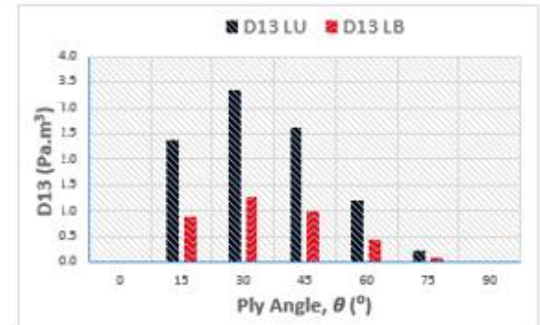
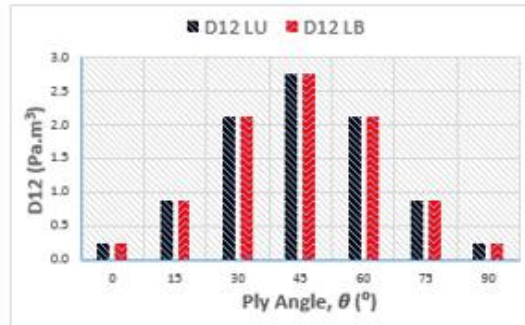
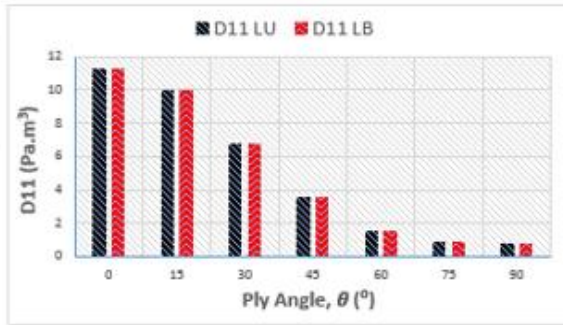


Figure 5.10 Individual element for  $[D]$   $L_U$  and  $L_B$

From Figure 5.9, all elements are identical for  $L_U$  and  $L_B$  except for  $A_{13}$  and  $A_{23}$ .  $A_{13}$  and  $A_{23}$  are zero for  $L_B$ . This result shows that at the same ply angle, symmetrical balance and unbalance layup have similar value in  $[A]$  except for the extension-shear stiffness. For bending stiffness  $[D]$ , as shown in Figure 5.10, the same pattern has been observed. The element which are dissimilar values being only at  $D_{13}$  and  $D_{23}$ , the bending-twist stiffness. All other elements in  $[D]$  are identical for  $L_U$  and  $L_B$ .

### 5.1.2 Mathematical Equation: $E_x$ , $E_y$ and $G_{xy}$ Membrane Mode and Bending Mode

The purpose of this section is to find the maximum values of equivalent engineering elastic constants in composite laminate,  $E_x$ ,  $E_y$ ,  $G_{xy}$  in symmetrical laminate. It is proved that symmetrical laminate produced higher stiffness compared to unsymmetrical laminate, because in symmetrical laminate, no coupling exist. Analysis has been carried out at a different angle orientation on two types of laminate layups; symmetrical and unbalance layup,  $L_U$  and symmetrical and balance layup,  $L_B$ . Effects of coupling in both layups were analysed and identified for a solid understanding of laminate analysis.

- Symmetrical and unbalance layup,  $L_U = [\alpha / \alpha / \alpha / \alpha]_s$
- Symmetrical and balance layup,  $L_B = [\alpha / -\alpha / \alpha / -\alpha]_s$

where  $\alpha$  is a ply angle.

#### 5.1.2.1 : $E_x$ Mathematical Equation Membrane Mode and Bending Mode

Recall previous section,  $E_x \text{ Membrane Mode} = \frac{1}{t \cdot a_{11}}$  and  $E_x \text{ Bending Mode} = \frac{12}{t^3 \cdot d_{11}}$ .

The formula has been looked at in detail to identify which elements in the in-plane stiffness matrix are associated with and has influenced on the laminate stiffness values in fibre direction or  $x$  direction. The detail formula for membrane mode and bending mode are presented in

Table 5.5 and Table 5.6, respectively.

**Table 5.5:  $E_x$  membrane mode for  $L_U$  and  $L_B$**

	$L_U$	$L_B$
<b>[A]</b>	$\begin{bmatrix} A_{11} & A_{12} & A_{13} \\ A_{12} & A_{22} & A_{23} \\ A_{13} & A_{23} & A_{33} \end{bmatrix}$	$\begin{bmatrix} A_{11} & A_{12} & 0 \\ A_{12} & A_{22} & 0 \\ 0 & 0 & A_{33} \end{bmatrix}$
$E_x$ from formula	$\frac{1}{t \cdot a_{11}}$	$\frac{1}{t \cdot a_{11}}$
$a_{11}$	$\frac{A_{22}A_{33} - A_{23}^2}{A}$	$\frac{A_{22}A_{33}}{A}$
$A$	$A_{11}A_{22}A_{33} + 2A_{12}A_{23}A_{13} - A_{22}A_{13}^2 - A_{33}A_{12}^2 - A_{11}A_{23}^2$	$A_{11}A_{22}A_{33} - A_{33}A_{12}^2$
$E_x$	$\frac{1}{t \frac{A_{22}A_{33} - A_{23}^2}{A_{11}A_{22}A_{33} + 2A_{12}A_{23}A_{13} - A_{22}A_{13}^2 - A_{33}A_{12}^2 - A_{11}A_{23}^2}}$	$\frac{1}{t \frac{A_{22}A_{33}}{A_{11}A_{22}A_{33} - A_{33}A_{12}^2}}$

**Table 5.6:  $E_x$  bending mode for  $L_U$  and  $L_B$**

	$L_U$	$L_B$
<b>[D]</b>	$\begin{bmatrix} D_{11} & D_{12} & D_{13} \\ D_{12} & D_{22} & D_{23} \\ D_{12} & D_{23} & D_{33} \end{bmatrix}$	$\begin{bmatrix} D_{11} & D_{12} & D_{13} \\ D_{12} & D_{22} & D_{23} \\ D_{12} & D_{23} & D_{33} \end{bmatrix}$
$E_x$ from formula	$\frac{12}{t^3 \cdot d_{11}}$	$\frac{12}{t^3 \cdot d_{11}}$
$d_{11}$	$\frac{D_{22}D_{33} - D_{23}^2}{D}$	$\frac{D_{22}D_{33} - D_{23}^2}{D}$
$D$	$D_{11}D_{22}D_{33} + 2D_{12}D_{23}D_{13} - D_{22}D_{13}^2 - D_{33}D_{12}^2 - D_{11}D_{23}^2$	$D_{11}D_{22}D_{33} + 2D_{12}D_{23}D_{13} - D_{22}D_{13}^2 - D_{33}D_{12}^2 - D_{11}D_{23}^2$
$E_x$	$\frac{12}{t \frac{D_{22}D_{33} - D_{23}^2}{D_{11}D_{22}D_{33} + 2D_{12}D_{23}D_{13} - D_{22}D_{13}^2 - D_{33}D_{12}^2 - D_{11}D_{23}^2}}$	$\frac{12}{t \frac{D_{22}D_{33} - D_{23}^2}{D_{11}D_{22}D_{33} + 2D_{12}D_{23}D_{13} - D_{22}D_{13}^2 - D_{33}D_{12}^2 - D_{11}D_{23}^2}}$

### 5.1.2.2 : $E_y$ Mathematical Equation Membrane Mode and Bending Mode

Formula for  $E_y$  Membrane Mode and  $E_y$  Bending Mode:

$$E_{y \text{ Membrane Mode}} = \frac{1}{t.a_{22}}, E_{y \text{ Bending Mode}} = \frac{12}{t^3.d_{22}}$$

A similar method has been applied to stiffness in off-fibre direction or  $y$  direction. A mathematical equation is used to demonstrate the influenced of elements in  $[A]$  and  $[D]$  matrices that contribute to laminate stiffness, which then are illustrated in the following graphs. Table 5.7 and Table 5.8 show the detail formula for  $E_y$  membrane and bending mode, respectively.

**Table 5.7  $E_y$  membrane mode from  $L_U$  and  $L_B$**

	$L_U$	$L_B$
<b>[A]</b>	$\begin{bmatrix} A_{11} & A_{12} & A_{13} \\ A_{12} & A_{22} & A_{23} \\ A_{13} & A_{23} & A_{33} \end{bmatrix}$	$\begin{bmatrix} A_{11} & A_{12} & 0 \\ A_{12} & A_{22} & 0 \\ 0 & 0 & A_{33} \end{bmatrix}$
<b><math>E_y</math> from formula</b>	$\frac{1}{t.a_{22}}$	$\frac{1}{t.a_{22}}$
<b><math>a_{22}</math></b>	$\frac{A_{11}A_{33} - A_{13}^2}{A}$	$\frac{A_{11}A_{33}}{A}$
<b>A</b>	$A_{11}A_{22}A_{33} + 2A_{12}A_{23}A_{13} - A_{22}A_{13}^2 - A_{33}A_{12}^2 - A_{11}A_{23}^2$	$A_{11}A_{22}A_{33} - A_{33}A_{12}^2$
<b><math>E_y</math></b>	$\frac{1}{t \frac{A_{11}A_{33} - A_{13}^2}{A_{11}A_{22}A_{33} + 2A_{12}A_{23}A_{13} - A_{22}A_{13}^2 - A_{33}A_{12}^2 - A_{11}A_{23}^2}}$	$\frac{1}{t \frac{A_{11}A_{33}}{A_{11}A_{22}A_{33} - A_{33}A_{12}^2}}$



**Table 5.8:  $E_y$  bending mode for  $L_U$  and  $L_B$**

	$L_U$	$L_B$
<b>[D]</b>	$\begin{bmatrix} D_{11} & D_{12} & D_{13} \\ D_{12} & D_{22} & D_{23} \\ D_{12} & D_{23} & D_{33} \end{bmatrix}$	$\begin{bmatrix} D_{11} & D_{12} & D_{13} \\ D_{12} & D_{22} & D_{23} \\ D_{12} & D_{23} & D_{33} \end{bmatrix}$
<b><math>E_y</math> from formula</b>	$\frac{12}{t^3 \cdot d_{22}}$	$\frac{12}{t^3 \cdot d_{22}}$
<b><math>d_{22}</math></b>	$\frac{D_{11}D_{33} - D_{13}^2}{D}$	$\frac{D_{11}D_{33} - D_{13}^2}{D}$
<b>D</b>	$D_{11}D_{22}D_{33} + 2D_{12}D_{23}D_{13} - D_{22}D_{13}^2 - D_{33}D_{12}^2 - D_{11}D_{23}^2$	$D_{11}D_{22}D_{33} + 2D_{12}D_{23}D_{13} - D_{22}D_{13}^2 - D_{33}D_{12}^2 - D_{11}D_{23}^2$
<b><math>E_y</math></b>	$\frac{12}{t^3 \frac{D_{11}D_{33} - D_{13}^2}{D_{11}D_{22}D_{33} + 2D_{12}D_{23}D_{13} - D_{22}D_{13}^2 - D_{33}D_{12}^2 - D_{11}D_{23}^2}}$	$\frac{12}{t^3 \frac{D_{11}D_{33} - D_{13}^2}{D_{11}D_{22}D_{33} + 2D_{12}D_{23}D_{13} - D_{22}D_{13}^2 - D_{33}D_{12}^2 - D_{11}D_{23}^2}}$

### 5.1.2.3 Laminate Analysis: $G_{xy}$ Mathematical Equation

In the previous section, formula for shear modulus,  $G_{xy}$  for membrane mode and bending mode were derived as:

$$G_{xy \text{ Membrane Mode}} = \frac{1}{t \cdot a_{33}}, \quad G_{xy \text{ Bending Mode}} = \frac{12}{t^3 \cdot d_{33}}$$

These formulas are derived from [A] and [D] matrices. The following tables, Table 5.9 and Table 5.10 show the detailed terms involved in [A] and [D] matrices for  $L_U$  and  $L_B$  laminates for membrane and bending mode.

**Table 5.9:  $G_{xy}$  membrane mode for  $L_U$  and  $L_B$**

	$L_U$	$L_B$
<b>[A]</b>	$\begin{bmatrix} A_{11} & A_{12} & A_{13} \\ A_{12} & A_{22} & A_{23} \\ A_{13} & A_{23} & A_{33} \end{bmatrix}$	$\begin{bmatrix} A_{11} & A_{12} & 0 \\ A_{12} & A_{22} & 0 \\ 0 & 0 & A_{33} \end{bmatrix}$
<b><math>G_{xy}</math> from formula</b>	$\frac{1}{t \cdot a_{33}}$	$\frac{1}{t \cdot a_{33}}$
<b><math>a_{33}</math></b>	$\frac{A_{11}A_{22} - A_{12}^2}{A}$	$\frac{A_{11}A_{22} - A_{12}^2}{A}$
<b>A</b>	$A_{11}A_{22}A_{33} + 2A_{12}A_{23}A_{13} - A_{22}A_{13}^2 - A_{33}A_{12}^2 - A_{11}A_{23}^2$	$A_{11}A_{22}A_{33} - A_{33}A_{12}^2$
<b><math>G_{xy}</math></b>	$\frac{1}{t \frac{A_{11}A_{22} - A_{12}^2}{A_{11}A_{22}A_{33} + 2A_{12}A_{23}A_{13} - A_{22}A_{13}^2 - A_{33}A_{12}^2 - A_{11}A_{23}^2}}$	$\frac{1}{t \frac{A_{11}A_{22} - A_{12}^2}{A_{11}A_{22}A_{33} - A_{33}A_{12}^2}}$

**Table 5.10:  $G_{xy}$  bending mode for  $L_U$  and  $L_B$**

	$L_U$	$L_B$
<b>[D]</b>	$\begin{bmatrix} D_{11} & D_{12} & D_{13} \\ D_{12} & D_{22} & D_{23} \\ D_{12} & D_{23} & D_{33} \end{bmatrix}$	$\begin{bmatrix} D_{11} & D_{12} & D_{13} \\ D_{12} & D_{22} & D_{23} \\ D_{12} & D_{23} & D_{33} \end{bmatrix}$
<b><math>G_{xy}</math> from formula</b>	$\frac{12}{t^3 \cdot d_{33}}$	$\frac{12}{t^3 \cdot d_{33}}$
<b><math>d_{33}</math></b>	$\frac{D_{11}D_{22} - D_{12}^2}{D}$	$\frac{D_{11}D_{22} - D_{12}^2}{D}$
<b>D</b>	$D_{11}D_{22}D_{33} + 2D_{12}D_{23}D_{13} - D_{22}D_{13}^2 - D_{33}D_{12}^2 - D_{11}D_{23}^2$	$D_{11}D_{22}D_{33} + 2D_{12}D_{23}D_{13} - D_{22}D_{13}^2 - D_{33}D_{12}^2 - D_{11}D_{23}^2$
<b><math>G_{xy}</math></b>	$\frac{12}{t^3 \frac{D_{11}D_{22} - D_{12}^2}{D_{11}D_{22}D_{33} + 2D_{12}D_{23}D_{13} - D_{22}D_{13}^2 - D_{33}D_{12}^2 - D_{11}D_{23}^2}}$	$\frac{12}{t^3 \frac{D_{11}D_{22} - D_{12}^2}{D_{11}D_{22}D_{33} + 2D_{12}D_{23}D_{13} - D_{22}D_{13}^2 - D_{33}D_{12}^2 - D_{11}D_{23}^2}}$

## 5.2 Composite Box Analysis

Armanios' formula from [12] has been used thoroughly in this section to calculate the values of  $EI$ ,  $GJ$  and  $CK$  for  $L_U$  and  $L_B$ . Refer Equation (4.67) for details of the formula.

Recall that for thin-walled composite beam structure, the bending, torsion and coupling stiffness can be calculated by using these formula:

### Bending Stiffness, $EI$

$$EI = \oint \left( A - \frac{B^2}{C} \right) z^2 ds + \frac{[\oint (B/C)z ds]^2}{\oint (1/C)ds} \quad (5.8)$$

### Torsional Stiffness, $GJ$

$$GJ = \frac{1}{\oint (1/C)ds} A_e^2 \quad (5.9)$$

### Coupling Stiffness, $CK$

$$CK = -\frac{\oint (B/C)z ds}{\oint (1/C)ds} A_e \quad (5.10)$$

where  $A(s)$ ,  $B(s)$  and  $C(s)$  denotes the reduced axial stiffness, reduced coupling stiffness and reduced shear stiffness, respectively and  $A_e$  is the enclosed area of the cross section. Refer Equations (4.59) and (4.68) for formula  $A(s)$ ,  $B(s)$ ,  $C(s)$  and  $A_e$ .

Torsional stiffness and the bending stiffness formula for laminate, single-cell box and double-cell box are used later in this research to find the optimum value of structure rigidity for each case. The result then will be analysed and the factors effecting structural strength and rigidity subjected to laminate stacking sequence; laminate ply orientation and composite structure type will be gained and concluded. The results obtained will be added to the design optimisation guideline to provide the design engineer with a starting point quick assessment of the structural rigidity at early design process.

The composite box analysis is more perplex compared to laminate analysis. Structural rigidity analysis,  $EI$ ,  $GJ$  and  $CK$  are carried out for the composite closed single-cell and double-cell box beam for  $L_U$  and  $L_B$ . Results are illustrated in Figure 5.11, 5.12 and 5.13.

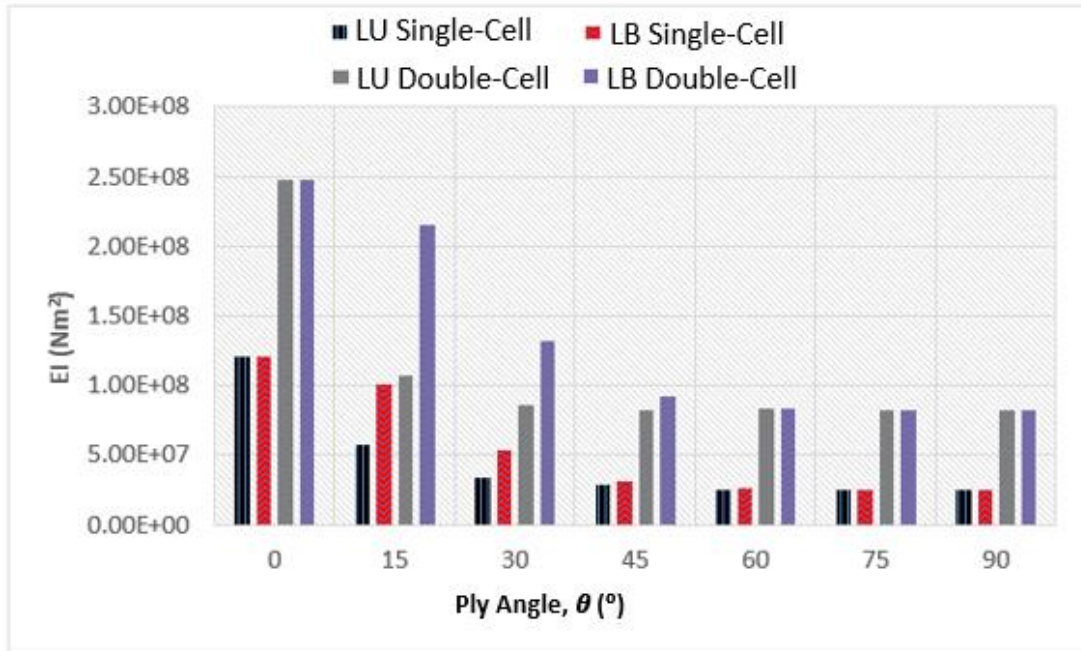


**Figure 5.11**  $EI_{L_U}$  and  $L_B$  for single-cell and double-cell box

Bending rigidity was unaffected at  $0^\circ$ ,  $75^\circ$ , and  $90^\circ$  if the same type of box structure, with the same ply angle but different sequence stacking is constructed. Figure 5.13 is plotted to confirm the presence of coupling at this fibre orientation. Double-cell obviously offer better shear flow distribution compared to single cell. In torsion however, bending twisting coupling only influenced the box torsional stiffness at  $0^\circ$  and  $90^\circ$  fibre angle. Looking at the graph in Figure 5.12, the shear flow distribution also improved with the addition of extra wall in a double-cell box.

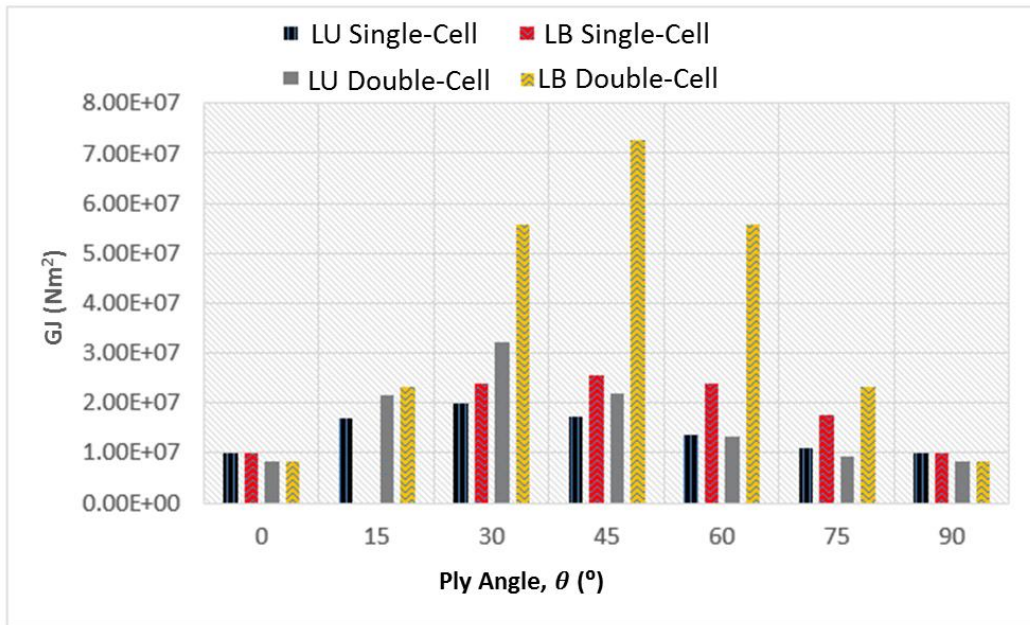


Figure 5.12  $GJ L_U$  and  $L_B$  for single-cell and double-cell

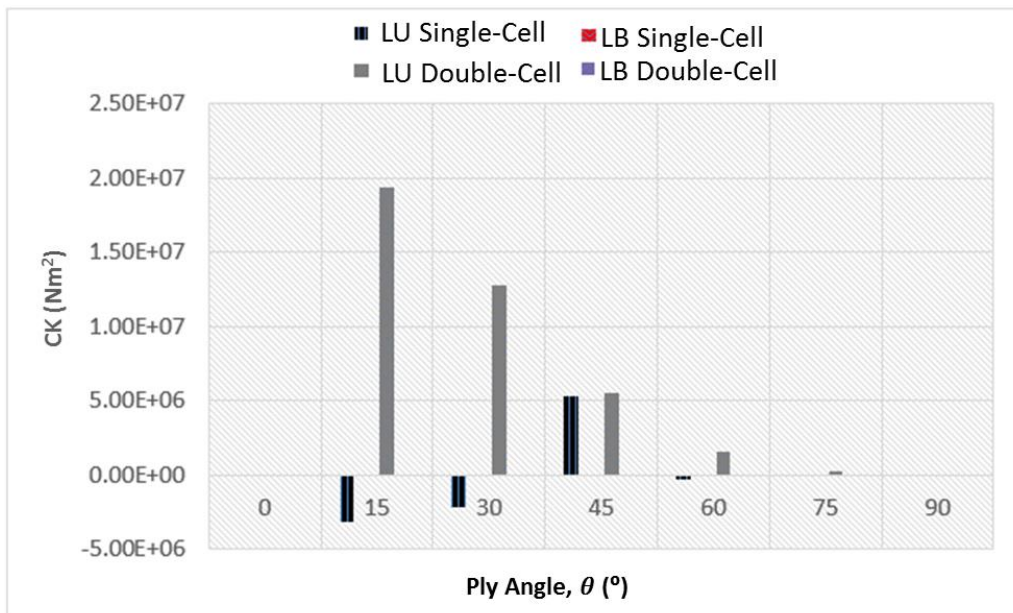
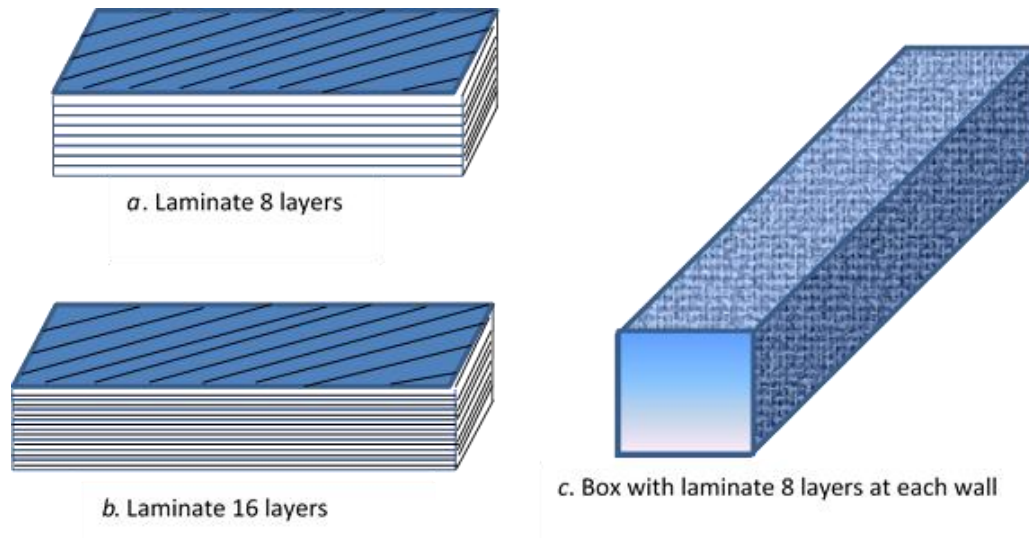


Figure 5.13  $CK L_U$  and  $L_B$  for single-cell and double-cell

### 5.2.1 Composite Laminate and Box Relation

This parametric study aims to find the key factors that can relate strength and stiffness of ply laminate to the composite box. Results for the laminate and the box will be compared numerically. If no difference is identified, then the theory for laminate can be applied to the box. Figure 5.14 shows the laminates and composite box used in this analysis.



**Figure 5.14 Laminates and composite box used in this analysis**

The classical laminate theory was applied in this analysis. A FORTRAN based in-house program, *ABD* program [94] is used in laminate analysis to generate values for  $a_{11}$  and  $a_{33}$  stiffness matrix, where the particular values are required for  $E_x$  and  $G_{xy}$  calculations. From these values,  $EI$  and  $GJ$  of laminates can be calculated directly using formula as presented previously. Another FORTRAN based in-house program, *BOXMX* program [95] is used in this case study to generate values for  $EI$  and  $GJ$  for the composite box, therefore  $E_x$  and  $G_{xy}$  value can be calculated as long as the area moment of inertia and polar moment of inertia are known. Table 5.11 and Table 5.12 present results from the *BOXMX* Program while Table 5.13 show results obtained from formula.

Table 5.11: Bending Stiffness for Laminate 8 Layers, Laminate 16 Layers and Box

Material type	Carbon fibre, fibre/epoxy resin (120°C Cure, std CF UD)		
Material properties	Young's Modulus, $E_1 = 135 \text{ GPa}$ , $E_2 = 10 \text{ GPa}$ Poisson's Ratio, $\nu_{12} = 0.3$ Shear Modulus, $G_{12} = 5 \text{ GPa}$		
	Laminate: 8 Layers	Laminate: 16 Layers	Composite Box
<b>Case 1:</b> Symmetry & Unbalance Layup	Ply orientation: [45/45/45/45]s	Ply orientation: [45/45/45/45/45/45/45/45]s	Ply orientation: Upper wall : [45/45/45/45]s Side wall left : [45/45/45/45]s Lower wall : [45/45/45/45]s Side wall right : [45/45/45/45]s
	width, $w = 1\text{m}$ Thickness, $t = 0.001\text{m}$	width = 1m thickness = 0.002m	width=1m thickness=0.001m (each laminate)
	$E_x = 1.32 \times 10^{10} \text{ N/m}^2$ $I = 8.333 \times 10^{-11} \text{ m}^4$ $EI = 1.1 \text{ Nm}^2$	$E_x = 1.32 \times 10^{10} \text{ N/m}^2$ $I = 6.667 \times 10^{-10} \text{ m}^4$ $EI = 8.8 \text{ Nm}^2$	$E_x = 1.32 \times 10^{10} \text{ N/m}^2$ $I = 6.647 \times 10^{-4} \text{ m}^4$ $EI = 0.88 \times 10^7 \text{ Nm}^2$
<b>Case 2:</b> Symmetry & Balance Layup	Ply orientation: [45/-45/45/-45]s	Ply orientation: [45/-45/45/-45/45/-45/45/-45]s	Ply orientation: Upper wall : [45/-45/45/-45]s Side wall left : [45/-45/45/-45]s Lower wall : [45/-45/45/-45]s Side wall right : [45/-45/45/-45]s
	width, $w = 1\text{m}$ Thickness, $t = 0.001\text{m}$	width = 1m thickness = 0.002m	width=1m thickness=0.001m (each laminate)
	$E_x = 1.77 \times 10^{10} \text{ N/m}^2$ $I = 8.333 \times 10^{-11} \text{ m}^4$ $EI = 1.47 \text{ Nm}^2$	$E_x = 1.77 \times 10^{10} \text{ N/m}^2$ $I = 6.667 \times 10^{-10} \text{ m}^4$ $EI = 11.8 \text{ Nm}^2$	$E_x = 1.77 \times 10^{10} \text{ N/m}^2$ $I = 6.647 \times 10^{-4} \text{ m}^4$ $EI = 0.118 \times 10^8 \text{ Nm}^2$

Table 5.12: Torsional Stiffness for Laminate 8 Layers, Laminate 16 Layers and Box

Material type	Carbon fibre, fibre/epoxy resin (120°C Cure, std CF UD)		
Material properties	Young's Modulus, $E_1 = 135 \text{ GPa}$ , $E_2 = 10 \text{ GPa}$ Poisson's Ratio, $\nu_{12} = 0.3$ Shear Modulus, $G_{12} = 5 \text{ GPa}$		
	Laminate: 8 Layers	Laminate: 16 Layers	Composite Box
<b>Case 1:</b> Symmetry & Unbalance Layup	Ply orientation: [45/45/45/45]s	Ply orientation: [45/45/45/45/45/45/45/45]s	Ply orientation: Upper wall : [45/45/45/45]s Side wall left : [45/45/45/45]s Lower wall : [45/45/45/45]s Side wall right : [45/45/45/45]s
	width, $w = 1\text{m}$ Thickness, $t = 0.001\text{m}$	width = 1m thickness = 0.002m	width=1m thickness=0.001m (each laminate)
	<b><math>G_{xy} = 8.94 \times 10^9 \text{ N/m}^2</math></b> <b><math>J = 3.333 \times 10^{-10} \text{ m}^4</math></b> <b><math>GJ = 2.98 \text{ Nm}^2</math></b>	<b><math>G_{xy} = 8.94 \times 10^9 \text{ N/m}^2</math></b> <b><math>J = 2.667 \times 10^{-9} \text{ m}^4</math></b> <b><math>GJ = 23.84 \text{ Nm}^2</math></b>	<b><math>G_{xy} = 8.998 \times 10^9 \text{ N/m}^2</math></b> <b><math>J = 1.33 \times 10^{-3} \text{ m}^4</math></b> <b><math>GJ = 0.11968 \times 10^8 \text{ Nm}^2</math></b>
<b>Case 2:</b> Symmetry & Balance Layup	Ply orientation: [45/-45/45/-45]s	Ply orientation: [45/-45/45/-45/45/-45/45/-45]s	Ply orientation: 0.34983E+08 Upper wall : [45/-45/45/-45]s Side wall left : [45/-45/45/-45]s Lower wall : [45/-45/45/-45]s Side wall right : [45/-45/45/-45]s
	width, $w = 1\text{m}$ Thickness, $t = 0.001\text{m}$	width = 1m thickness = 0.002m	width=1m thickness=0.001m (each laminate)
	<b><math>G_{xy} = 3.5 \times 10^{10} \text{ N/m}^2</math></b> <b><math>J = 3.333 \times 10^{-10} \text{ m}^4</math></b> <b><math>GJ = 11.7 \text{ Nm}^2</math></b>	<b><math>G_{xy} = 3.5 \times 10^{10} \text{ N/m}^2</math></b> <b><math>J = 2.667 \times 10^{-9} \text{ m}^4</math></b> <b><math>GJ = 93.3 \text{ Nm}^2</math></b>	<b><math>G_{xy} = 2.6 \times 10^{10} \text{ N/m}^2</math></b> <b><math>J = 1.33 \times 10^{-3} \text{ m}^4</math></b> <b><math>GJ = 0.34983 \times 10^8 \text{ Nm}^2</math></b>



**Table 5.13: Value of  $E_x$  membrane,  $E_x$  Bending and  $E_x$  from EI for Laminate**

		From formula: ( $E_x=1/t.a_{11}$ )		From formula: ( $E_x=12/t^3.d_{11}$ )		From ABD Program: ( $E_x=EI/I$ )	
		Ex Membrane		Ex Bending		Ex from EI	
		8 Layers	16 Layers	8 Layers	16 Layers	8 Layers	16 Layers
45°	Case 1	1.77E+10	1.77E+10	1.74E+10	1.76E+10	1.77E+10	1.77E+10
	Case 2	1.32E+10	1.32E+10	1.32E+10	1.32E+10	1.32E+10	1.32E+10

$E_x$  is not affected by the number of layers for the same fibre orientation. This has been proved by hand calculation using equation  $1/ta_{11}$  for  $E_x$  membrane and  $12/t^3d_{11}$  for  $E_x$  bending. The values of  $a_{11}$  were obtained first and then applied to the formula. As the values of  $E_x$  are same for 8 layers and 16 layers in similar angle ply orientation, the values for  $EI$  are also identical.  $I$ ; the second moment area is fixed for both laminates. The laminate dimension is shown in Table 5.11. Refer Table 5.13, the calculation result matched with results obtained from the *ABD* program. It can be concluded that for the symmetrical layup, for the same total dimension, different thickness in each ply does not affect the bending rigidity, as long as the total laminate thickness of the plate is the same. This characteristic also applied to the box. The values for  $E_x$  are the same for laminate 8 layers, laminate 16 layers and the box with 8 layers of laminate. The value of the bending rigidity however, is greater in the box ( Table 5.11) compared to laminate. Looking at the formula, mathematically bending stiffness is a product of modulus and area at the moment of inertia. Thus, the bigger area at the moment of inertia of the beam produces a significant factor that contributes to the structural rigidity.

For torsional stiffness, the same values of shear stiffness between the laminate and the box were achieved in symmetrical and unbalanced laminate only. For symmetrical and balance, shear stiffness values are identical for 8 layer and 16 layer laminates. The box constructed, using this laminate, has caused the torsional rigidity to deteriorate. This study can be beneficial to aircraft structure engineers and designers where the initial idea of optimised laminate selection can be confirmed at the early design stage.

## 5.2.2 Laminate, Single-Cell Box and Double-Cell Box Relationship

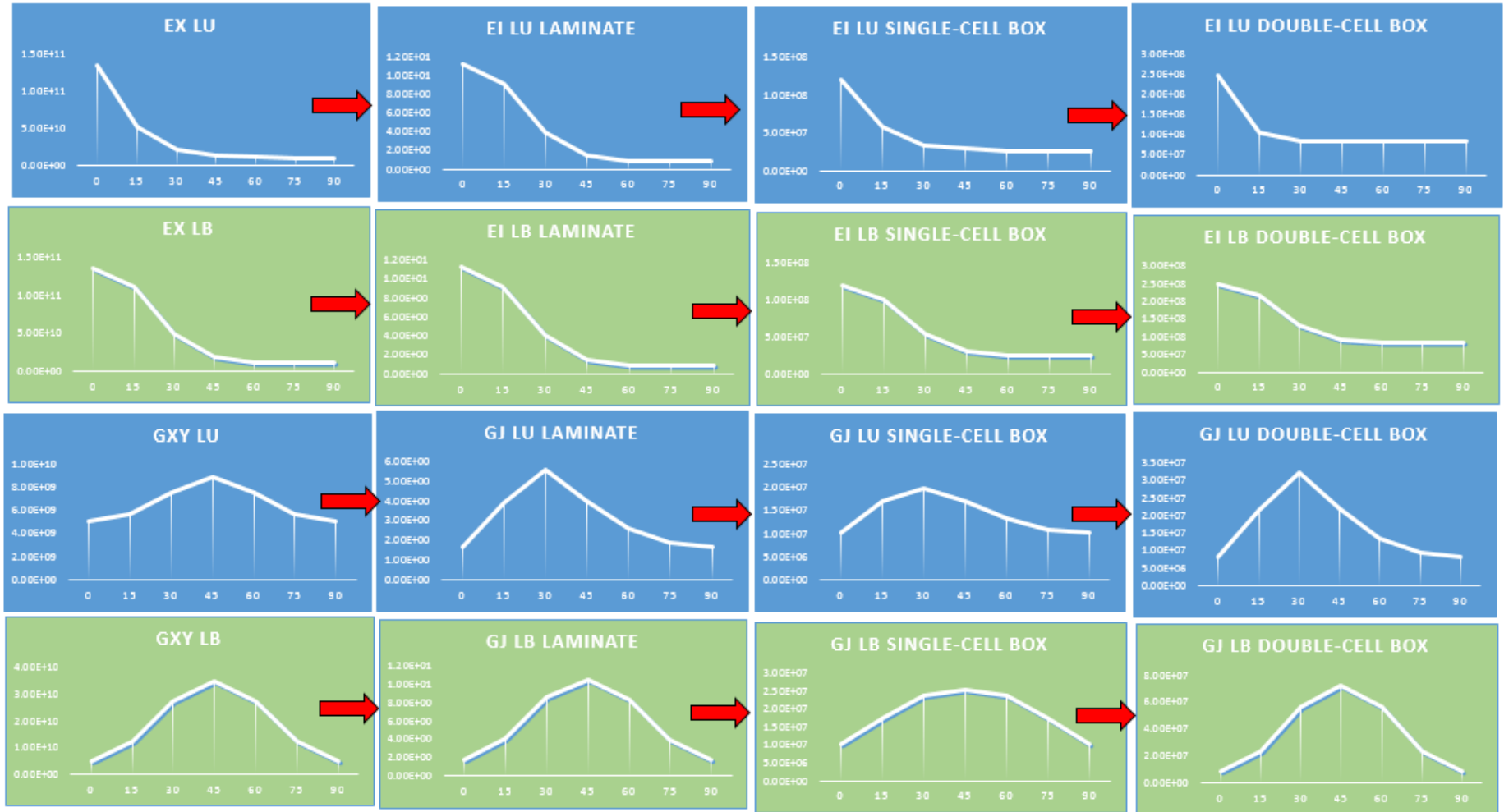


Figure 5.15 The relationship between laminate equivalent engineering elastic constants, single-cell and double-cell box

It is important for the design engineers to understand the fundamentals of how the stiffness of the structure turn when the same laminate with identical equivalent engineering elastic constants was constructed into the different structure type. Graphs in Figure 5.15 demonstrate how the values of bending stiffness and torsional stiffness vary when the same composite laminate was constructed into the single-cell box and then into double-cell box structure at a different ply angle. The results of the graphs show that for the symmetrical and balance layup,  $L_B$  the pattern of the graphs for bending stiffness are similar for all geometries. The values are different because the second moment area,  $I$  value for each geometry is different. For  $L_B$ , the maximum value for bending stiffness at  $0^\circ$  for laminate, single-cell and double-cell. The pattern also follows the laminate equivalent engineering constant in  $x$  direction,  $E_x$ . For torsional stiffness,  $GJ$  laminate and double-cell box follow exactly the same pattern with  $G_{xy}$ . The single-cell slope at peak point is not as steep as  $G_{xy}$ ,  $GJ$  laminate and  $GJ$  double-cell, but the maximum value is still at  $45^\circ$ . For symmetrical and unbalance layup, the bending stiffness,  $EI$  for single-cell and double-cell follow  $E_x$  trend, but  $EI$  laminate is different until the angle increases to  $30^\circ$  degrees. For torsional stiffness, the maximum value of  $G_{xy}$  is at  $45^\circ$  however, when it is constructed into the laminate and box single-cell and double-cell, the maximum value is at  $30^\circ$ . This might be caused by the bending-torsion coupling, which has been produced by this unbalanced layup.

This result has produced a very useful key parameter that relates a single laminate to single-cell and double-cell box structure. By understanding the fundamental concept, this parameter will be a guideline for a design engineer to find a starting point when designing a composite product. The final outcome of the product can be predicted at the early design stage. For example, if the requirement needs a high torsional stiffness value, the design engineer can start the design by using symmetrical and balance layup and later can tailor the laminate subject to the requirement and constraint.

### 5.3 A Matrix Element Analysis

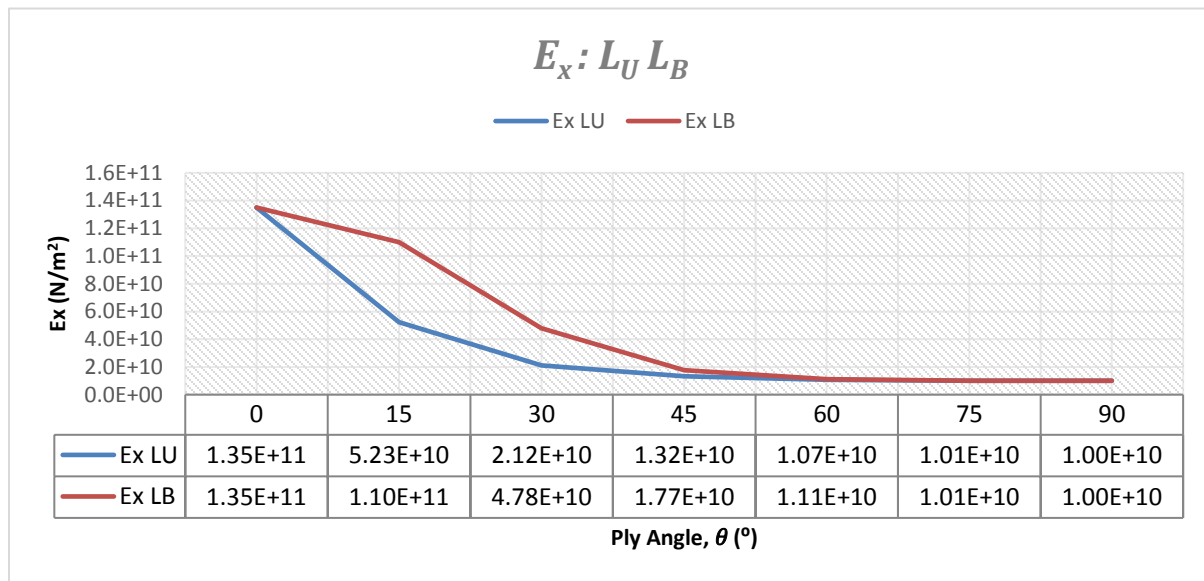


Figure 5.16 Graph  $E_x$  for  $L_U$  and  $L_B$

From formula in

Table 5.5, graph  $E_x$  were generated for  $L_U$  and  $L_B$ .

From Figure 5.16, the big difference of  $E_x$  for  $L_U$  and  $L_B$  occurs before  $45^\circ$ . After  $45^\circ$ , the difference rapidly decreased and finally became similar towards  $90^\circ$ . To identify what causes this result, a detailed mathematical equation was carried out and analysed.

From Equation 5.1,  $E_x = \frac{1}{t.a_{11}}$ . Graph of  $a_{11}$  was plotted to find the pattern for  $L_U$  and  $L_B$  and compare with  $E_x$  from Figure 5.16.

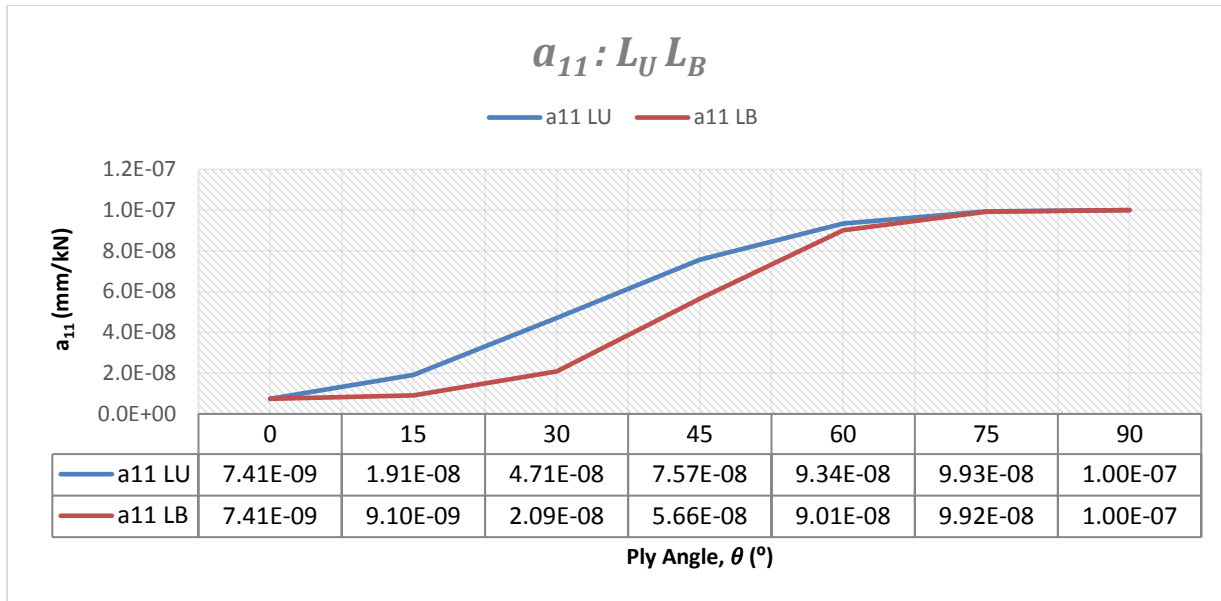


**Figure 5.17  $a_{11}$  for  $L_U$  and  $L_B$**

Using Equation 5.1, since the thickness,  $t$  for the laminate is constant for every ply angle,  $E_x$  values are inversely proportional with  $a_{11}$ .  $a_{11}$  values are calculated and the results are plotted in Figure 5.17. A significant difference was observed in Figure 5.17 before  $45^\circ$  and conversely kept decreasing towards  $90^\circ$ . This pattern has led to a detailed analysis as the same formula is used for both types of laminates but the effect was only spotted at ply angle before  $45^\circ$ . After  $45^\circ$ , symmetrical balance and unbalance laminates produce almost the same stiffness value towards  $90^\circ$ . To verify this, detailed of each element in  $a_{11}$  were analysed.

Recall  $a_{11}$  in Table 4.1,

$$a_{11} = \frac{A_{22}A_{33} - A_{23}^2}{A} = \frac{A_{22}A_{33} - A_{23}^2}{A_{11}A_{22}A_{33} + 2A_{12}A_{23}A_{13} - A_{22}A_{13}^2 - A_{33}A_{12}^2 - A_{11}A_{23}^2}$$

Each element in  $a_{11}$  was plotted for both cases and results are illustrated in the following figures. Figure 5.18, Figure 5.19, Figure 5.20, Figure 5.21, Figure 5.23 and Figure 5.24 show element  $A_{11}$ ,  $A_{12}$ ,  $A_{13}$ ,  $A_{22}$ ,  $A_{23}$  and  $A_{33}$ , respectively.

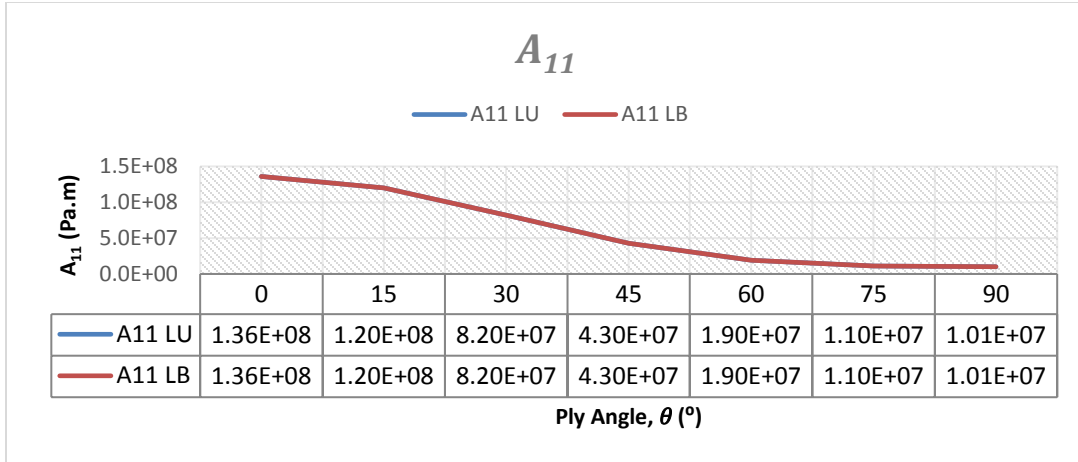


Figure 5.18 Element  $A_{11}$  of  $A$  Matrix for  $L_U$  and  $L_B$

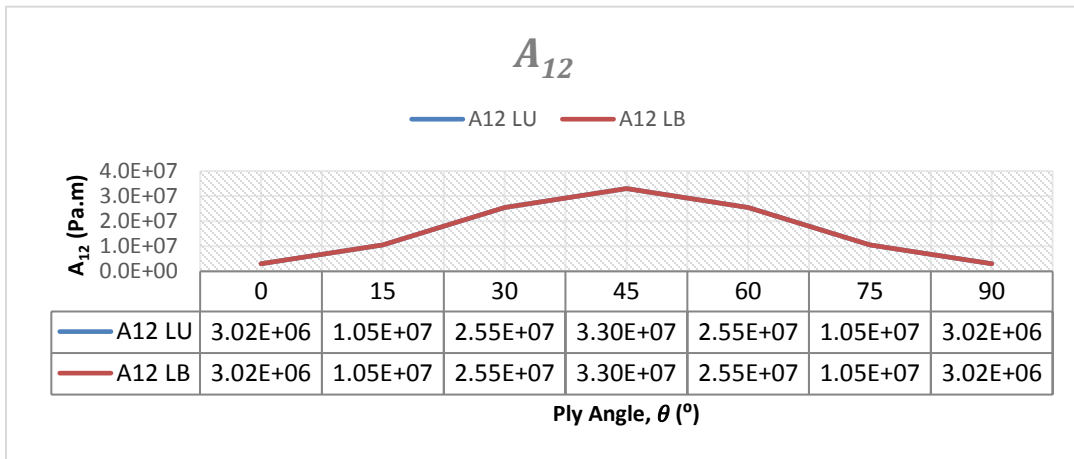


Figure 5.19 Element  $A_{12}$  of  $A$  Matrix for  $L_U$  and  $L_B$

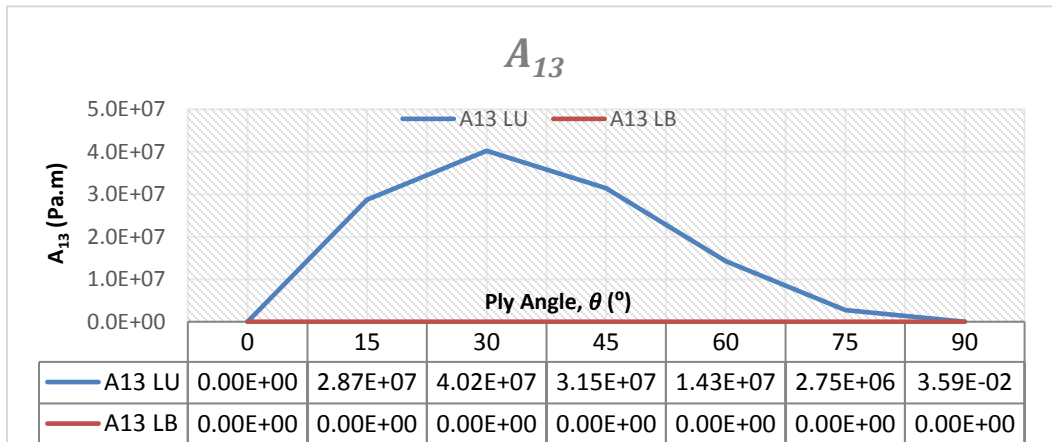


Figure 5.20 Element  $A_{13}$  of  $A$  Matrix for  $L_U$  and  $L_B$

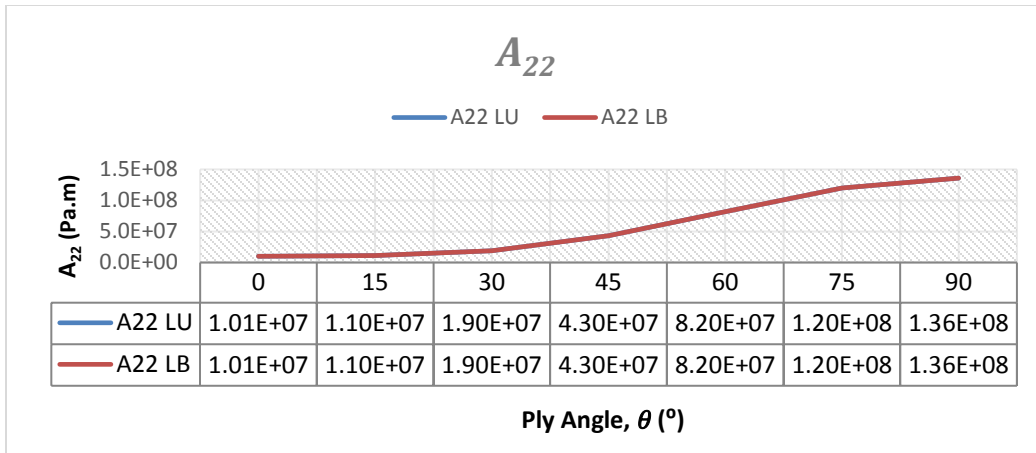


Figure 5.21 Element  $A_{22}$  of  $A$  Matrix for  $L_U$  and  $L_B$

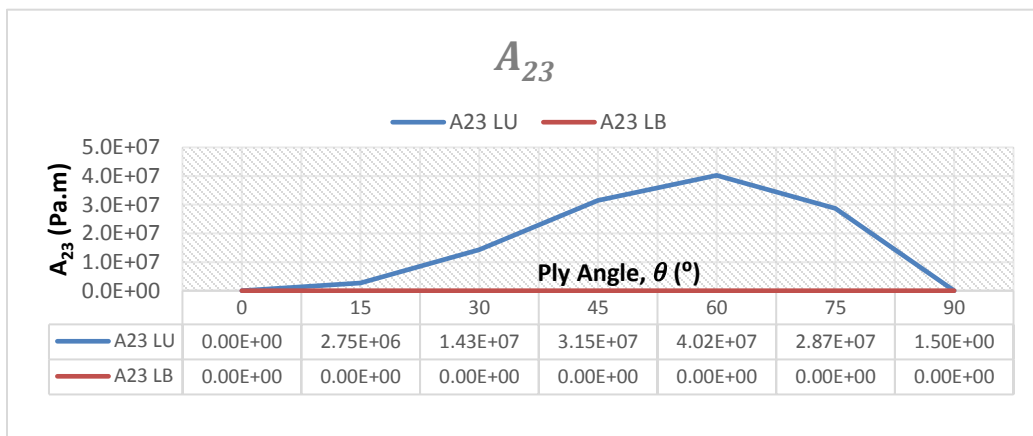


Figure 5.22 Element  $A_{23}$  of  $A$  Matrix for  $L_U$  and  $L_B$

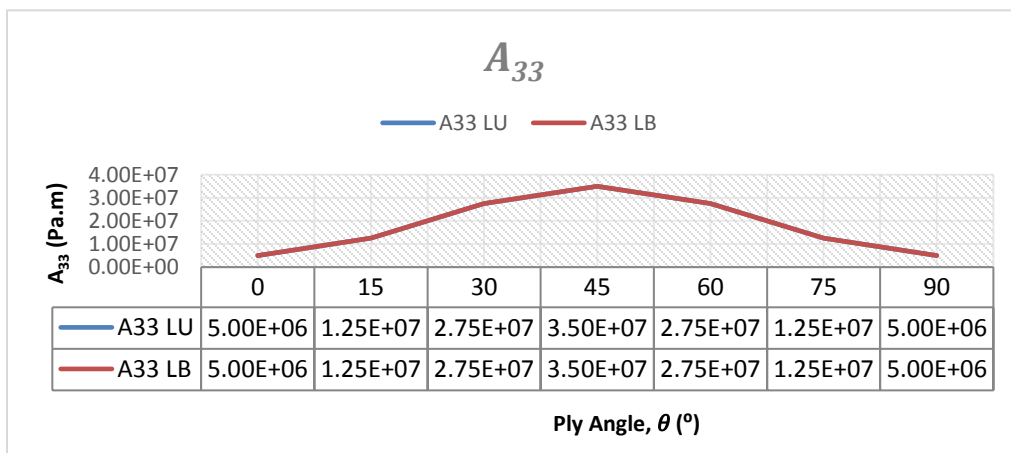
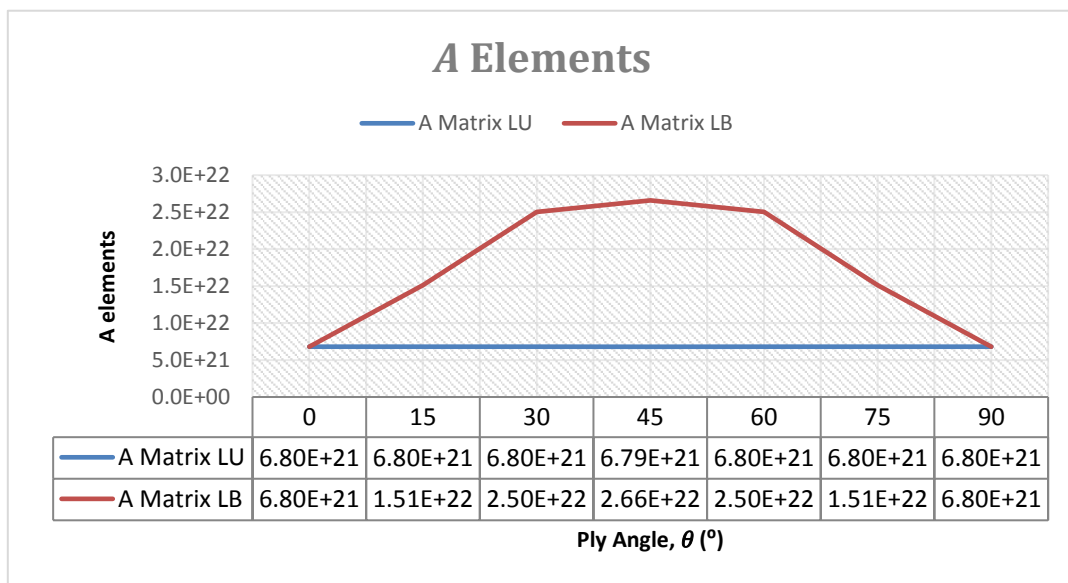


Figure 5.23 Element  $A_{33}$  of  $A$  Matrix for  $L_U$  and  $L_B$

From Figure 5.18 to Figure 5.23, the only difference between  $L_U$  and  $L_B$  are elements  $A_{13}$  and  $A_{23}$ . Unlike  $L_U$ ,  $L_B$  has zero value for  $A_{13}$  and  $A_{23}$  shows no shear coupling occurring in  $L_U$ . Refer Table 4.1,

$$A = A_{11}A_{22}A_{33} + 2A_{12}A_{23}A_{13} - A_{22}A_{13}^2 - A_{33}A_{12}^2 - A_{11}A_{23}^2$$

To see the effect of these elements, a graph of  $A$  elements was plotted in Figure 5.24 for  $L_U$  and  $L_B$ .



**Figure 5.24 Graph of  $A$  elements**

$A$  elements are consistent for  $L_U$  from  $0^\circ$  to  $90^\circ$  ply angles, but  $L_B$  has a mirror image with peak value at  $45^\circ$ . This result nevertheless does not reflect on the results of  $E_x$ .

Recall  $a_{11} = \frac{A_{22}A_{33} - A_{23}^2}{A}$ ,

As  $A$  elements did not reflect the  $E_x$  result, the analysis has narrowed down to the equation  $A_{22}A_{33} - A_{23}^2$  in  $a_{11}$  formula. Graphs for  $A_{22}A_{33}$ ,  $A_{23}^2$  and  $A_{22}A_{33} - A_{23}^2$  were plotted in the following graphs.



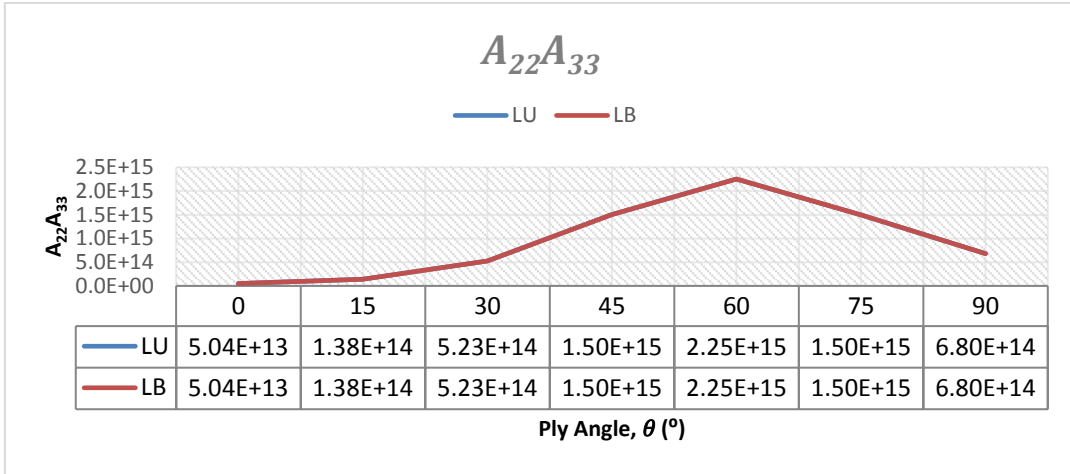


Figure 5.25 Graph  $A_{22} A_{33}$

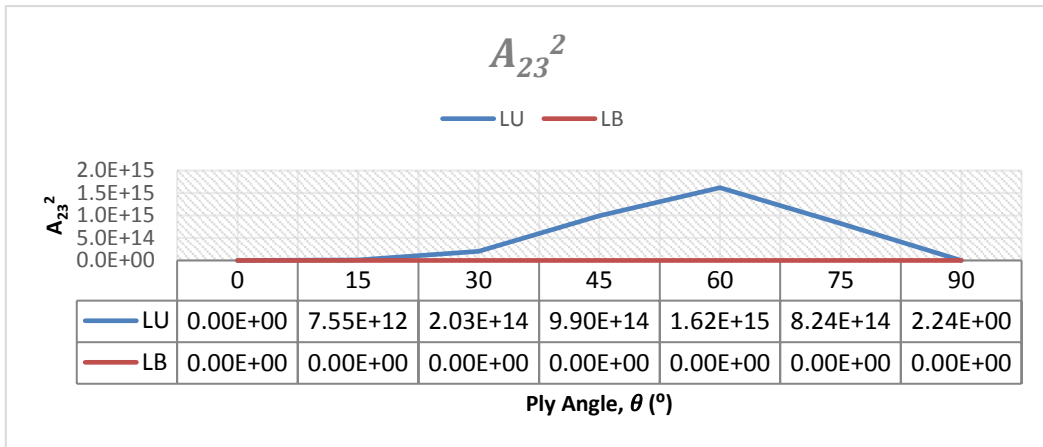


Figure 5.26 Graph  $A_{23}^2$

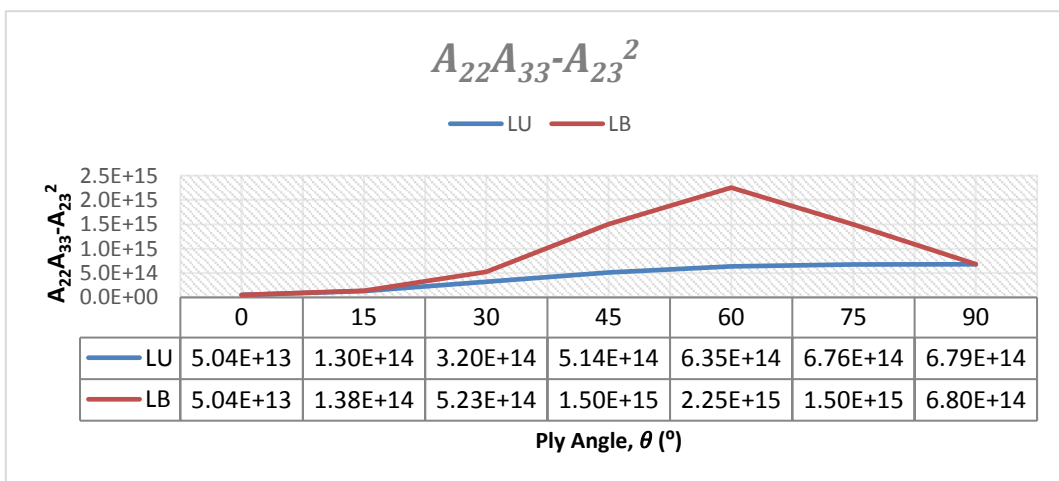


Figure 5.27: Graph  $A_{22}A_{33} - A_{23}^2$

Figure 5.25 shows the  $A_{22}A_{33}$  graph. Result reveals that the values of  $A_{22}A_{33}$  for  $L_U$  and  $L_B$  are identical. For  $A_{23}^2$ ,  $L_U$  follows the  $A_{22}A_{33}$  pattern while  $L_B$  is constantly zero for every ply angle.  $A_{23}^2$  graphs are presented in Figure 5.26. Then graphs for  $A_{22}A_{33} - A_{23}^2$  are plotted in Figure 5.27.  $L_U$  follows the  $A_{22}A_{33}$  graph pattern while  $L_B$  increases linearly with the ply angle. For  $L_U$ , results show that  $A_{22}A_{33}$  pattern is the same as  $A_{23}$ . It means that when coupled term combined with coupled term, the trend is same as the uncoupled term.

Next, graph for each term in  $A$  are plotted in the following figures.

$$\text{Recall } A = A_{11}A_{22}A_{33} + 2A_{12}A_{23}A_{13} - A_{22}A_{13}^2 - A_{33}A_{12}^2 - A_{11}A_{23}^2$$

Graph for  $A_{11}A_{22}A_{33}$ ,  $2A_{12}A_{23}A_{13}$ ,  $-A_{22}A_{13}^2$ ,  $-A_{33}A_{12}^2$  and  $-A_{11}A_{23}^2$  are illustrated in **Error! Reference source not found.**, Figure 5.29, **Error! Reference source not found.**, **Error! Reference source not found.** and **Error! Reference source not found.**, respectively.

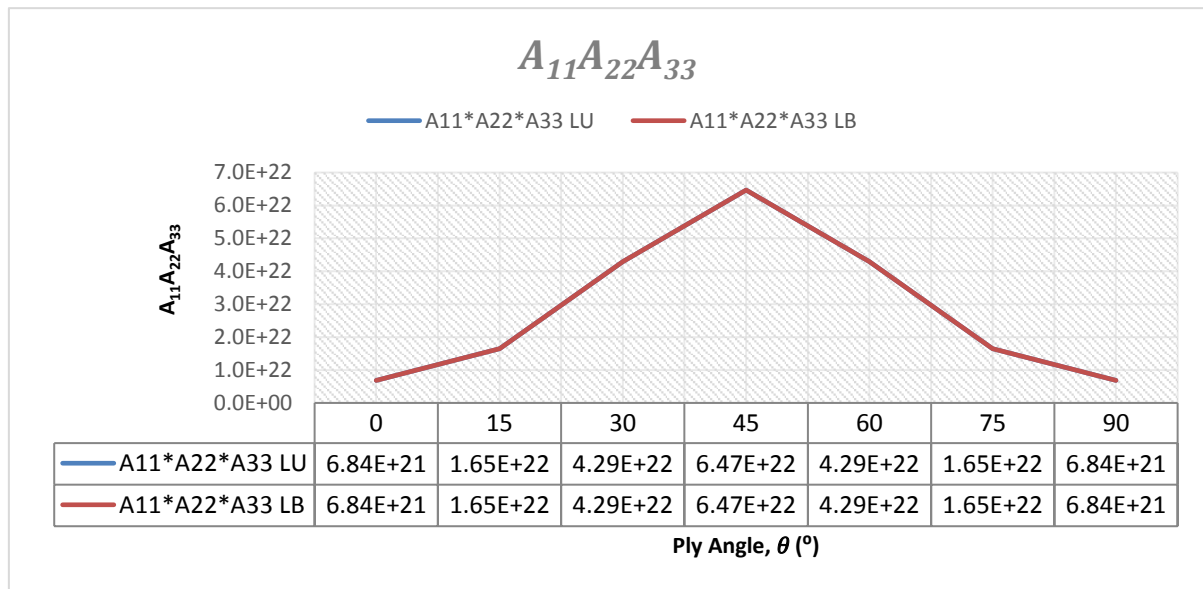
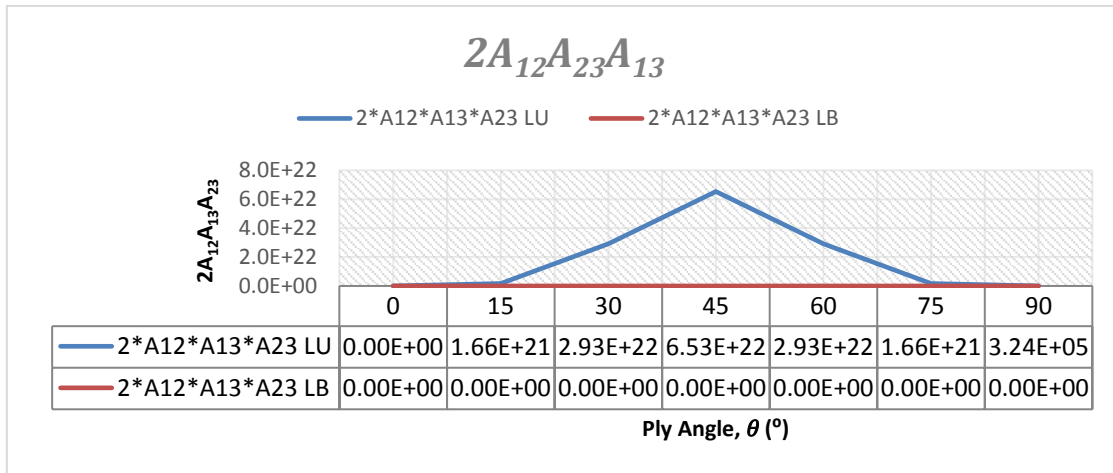
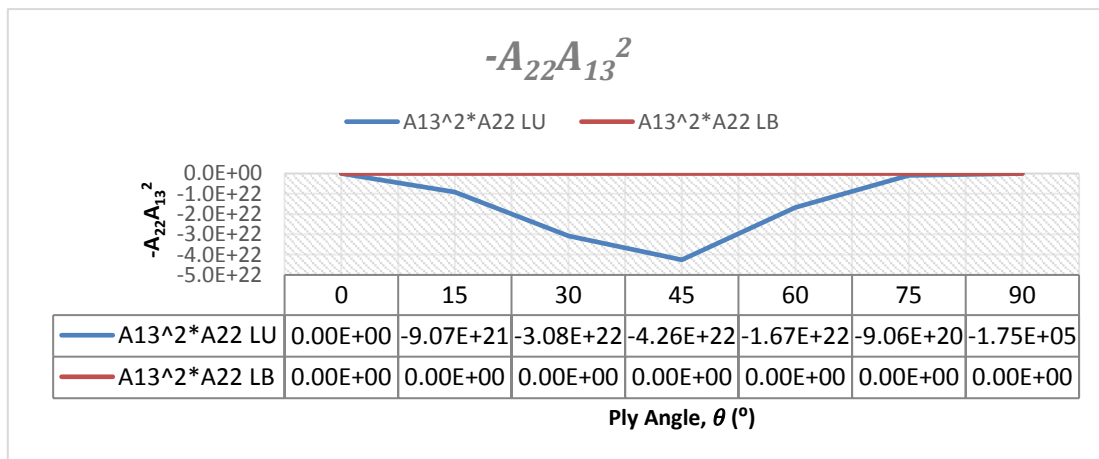


Figure 5.28 Graph  $A_{11}A_{22}A_{33}$



**Figure 5.29 Graph  $2A_{12}A_{23}A_{13}$**



**Figure 5.30 Graph  $-A_{22}A_{13}^2$**

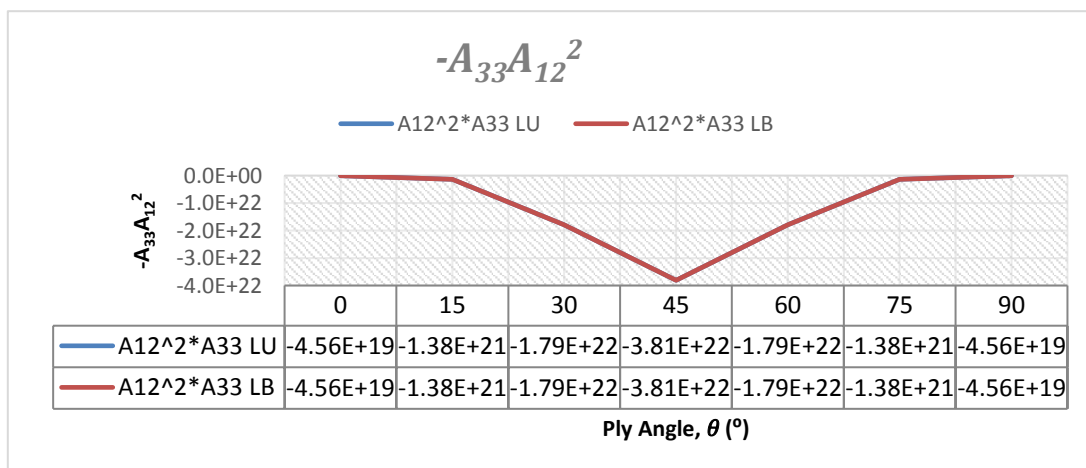


**Figure 5.31 Graph  $-A_{33}A_{12}^2$**

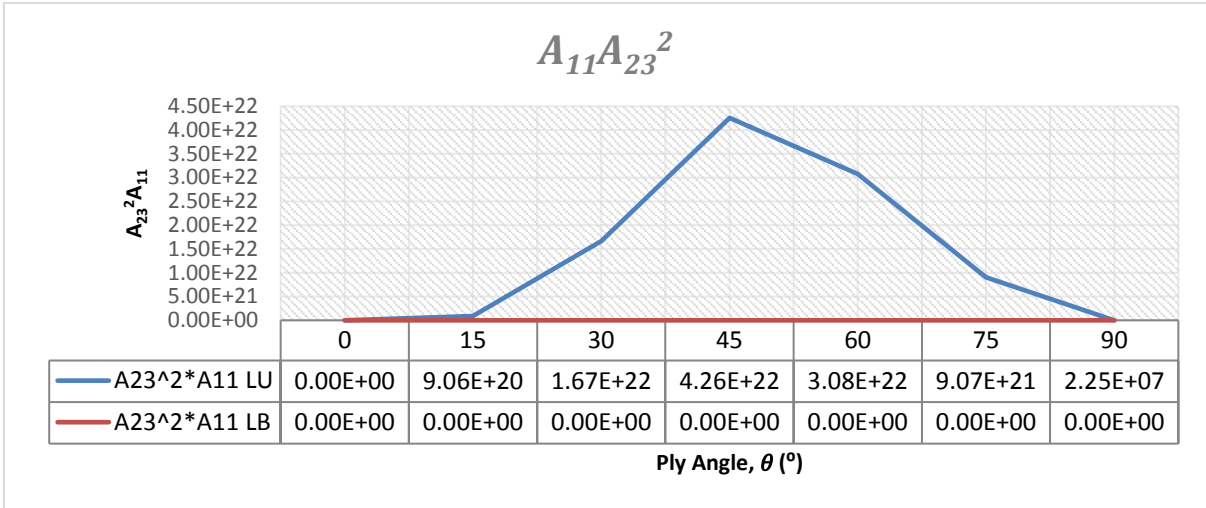


Figure 5.32 Graph  $A_{11}A_{23}^2$

The breakdown of  $A$  matrix elements for  $L_U$  are shown in Figure 5.33. For  $L_B$ , the details of each element are presented in **Error! Reference source not found.**

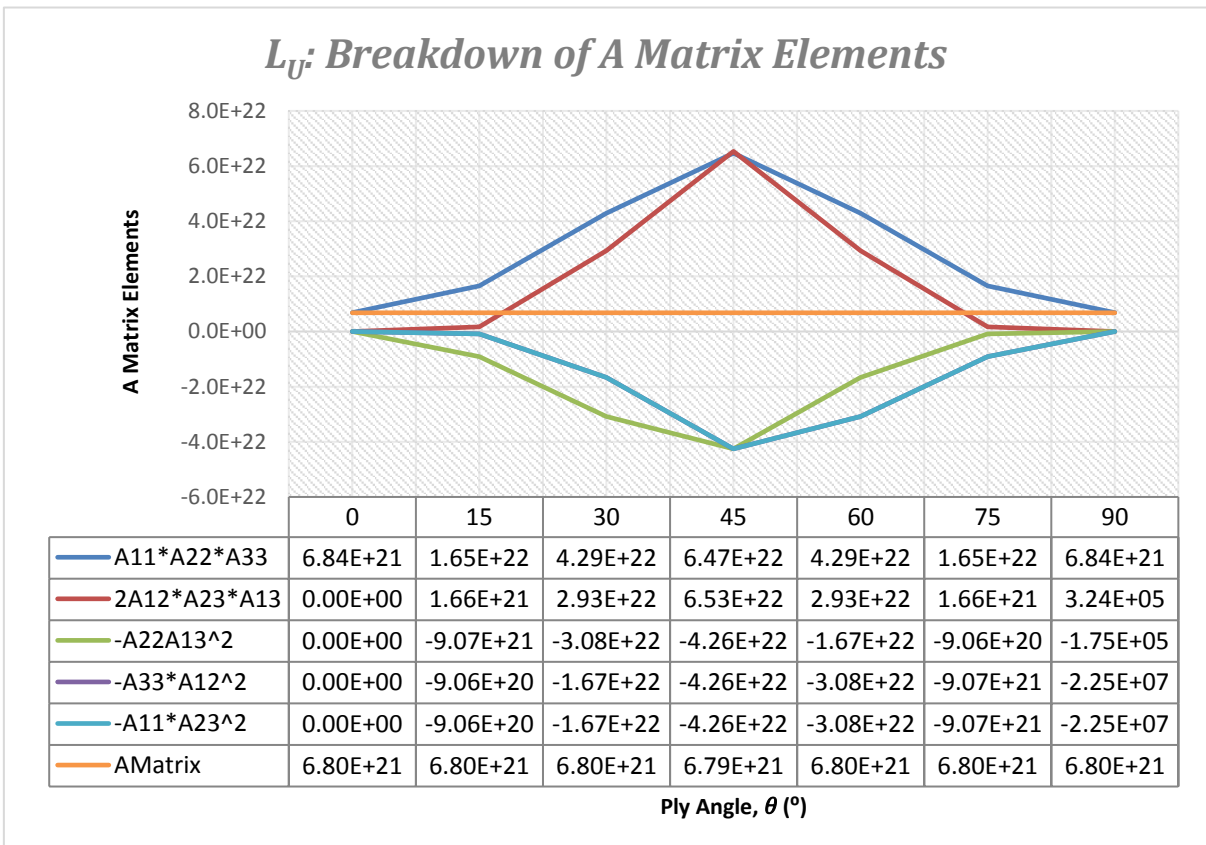
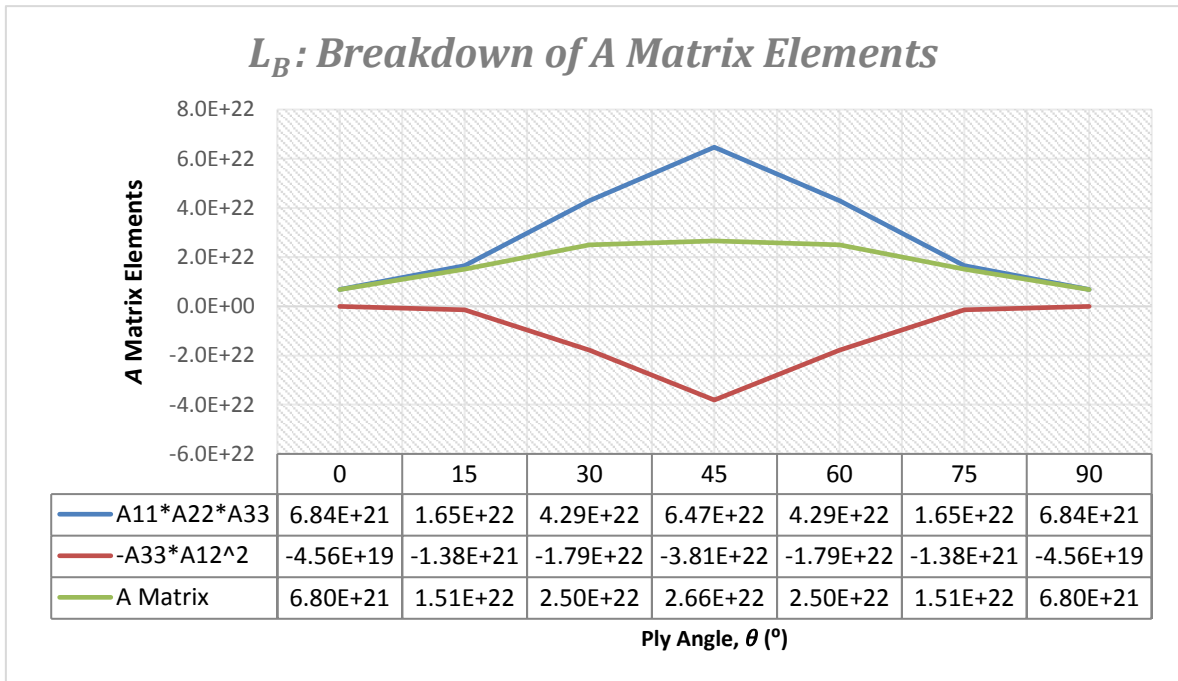


Figure 5.33 Breakdown of  $A$  Matrix elements for  $L_U$



**Figure 5.34 Breakdown of A Matrix elements for  $L_B$**

The A matrix trend is dominated by  $A_{33}$  element.  $A_{33}$  values for  $L_U$  and  $L_B$  are identical at every ply angle. However,  $a_{11}$  for  $L_U$  is higher than  $L_B$  because  $A_{13}$  and  $A_{23}$  for  $L_B$  are zero and thus, result in higher  $a_{11}$ . The result is summarised in a figure form, presented in Figure 5.35 to show how the elements in  $a_{11}$  contribute to the  $E_x$  values. This study is important in order to understand the contribution of each element in a A matrix so that during the material selection process and laminate design stage, design engineers will be able to tailor the laminate as desired.

Result Summary:

Formula:

$$E_x = \frac{1}{t \cdot a_{11}} = \frac{1}{t \frac{A_{22}A_{33} - A_{23}^2}{A_{11}A_{22}A_{33} + 2A_{12}A_{23}A_{13} - A_{22}A_{13}^2 - A_{33}A_{12}^2 - A_{11}A_{23}^2}} = \frac{1}{t \frac{A_{22}A_{33} - A_{23}^2}{A}}$$

Graph:

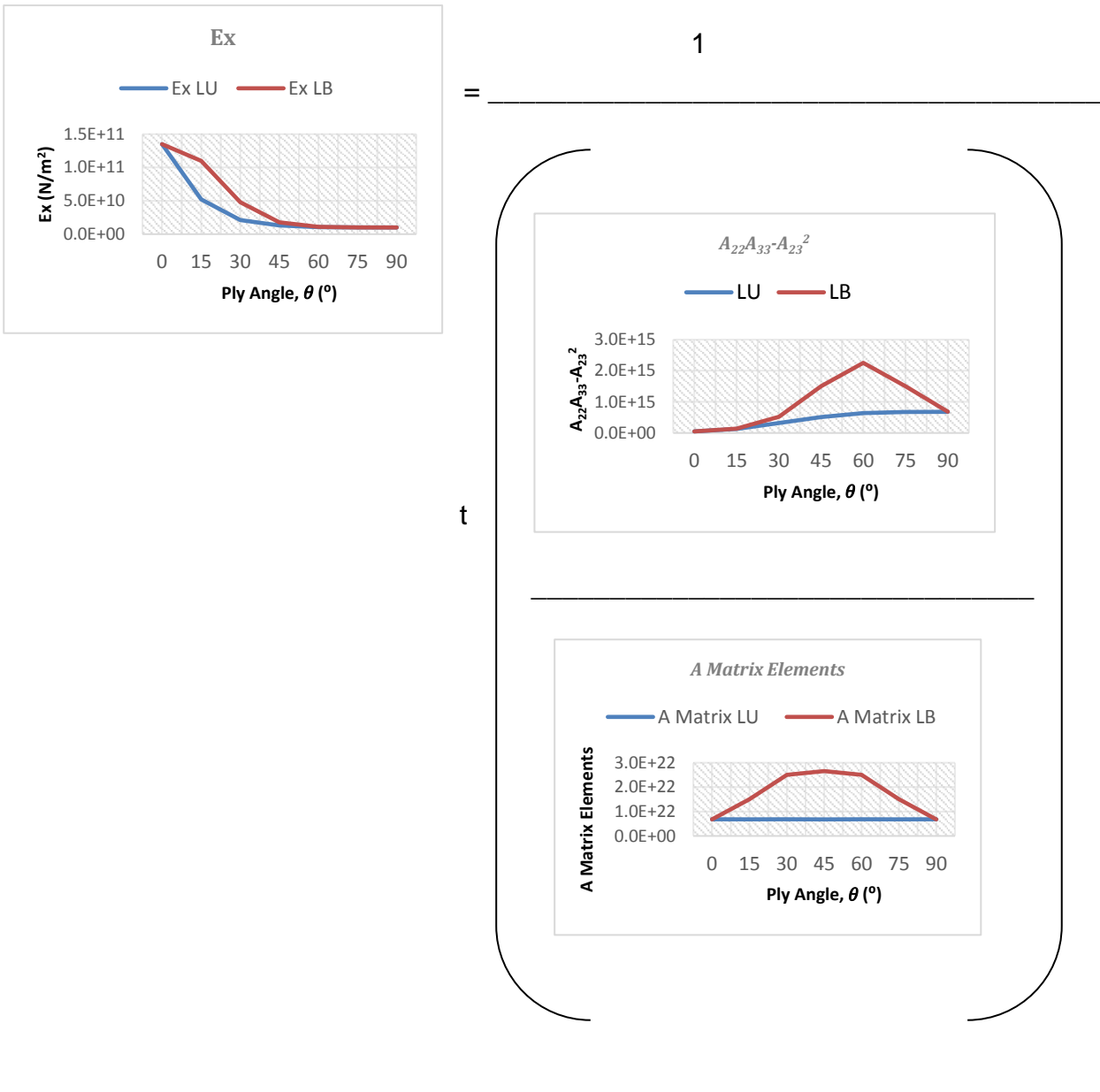
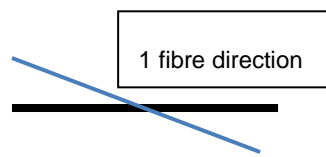


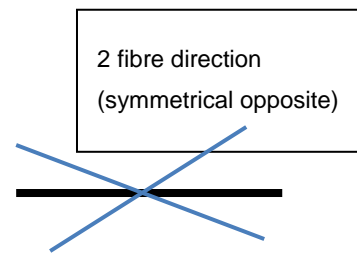
Figure 5.35  $E_x$  and  $a_{11}$  correlation in a figure form

### 5.3.1 Principal Findings

1. Analysis for the factors effecting coupling and uncoupling terms for symmetrical laminate is developed.
2. Symmetrical and balance layup results in no extension-shear coupling and reduce bending-twist coupling.
3. If the same laminate is used to construct the box, the stiffness graph of the box follows the laminate pattern, however, the stiffness value is higher in the box.
4. When coupled terms combine with coupled terms, the trend is the same as an uncoupled term. Eg;  $A_{22}A_{33}$  has the same trend as  $A_{23}$ . However, for symmetrical and balance layup,  $A_{23}$  and  $A_{13}$  are zero because the opposite fibre direction in balance layup cancelled each other. The shear strain cancels each other hence the extension-shear coupling,  $A_{13}$  and  $A_{23}$  are zero.



Symmetrical Unbalance, LU:  
Normal + shear strain



Symmetrical Balance, LB:  
Normal strain only. Shear strain cancel each other

5. When all coupled terms combined,  $A_{33}$  will dominate the trend.
6. For stiffness in fibre direction, after  $45^\circ$  ply angle, the symmetrical balance and unbalance laminate values are almost identical, starting to get similar towards  $90^\circ$  ply angle. The shear coupling coefficient in  $x$  direction only give larger different below  $45^\circ$ . After  $45^\circ$ , the fibre starting to get into  $y$  direction and it becomes independent to the ply stacking sequence in  $x$  direction.

## 5.4 Coupling Stiffness Analysis

### 5.4.1 Coupling Stiffness Formula

From [96], coupling stiffness,  $CK$  for a thin-walled beam with a single-cell cross section can be calculated using formula:

$$CK = \frac{2A_e}{c} \oint \left( A_{16} - \frac{A_{12} A_{26}}{A_{22}} \right) z ds \quad (5.11)$$

where:

$CK$  = coupling stiffness

$A_e$  = enclosed area of the cross section

$c$  = circumference

$A_{16}, A_{12}, A_{22}, A_{26}$  = laminate stiffness of matrix  $A$

$z$  =  $z$  coordinate from reference axis.

The reference axis and the  $x$ ,  $y$  and  $z$  coordinates directions are shown in Figure 5.36.

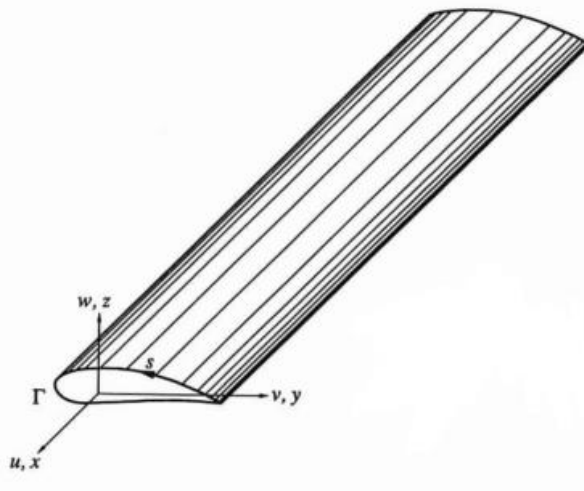


Figure 5.36 Reference axis. Coordinate for  $x$ ,  $y$  and  $z$  direction



### 5.4.1.1 Case Study

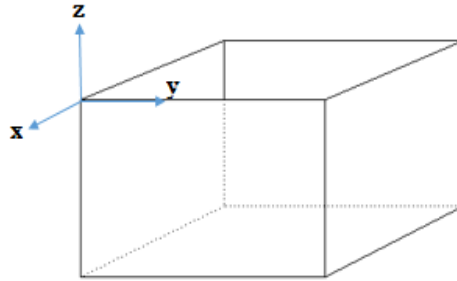


Figure 5.37 Closed, single-cell cross section box beam

Box measurement:

Width: 0.5m, depth: 0.2m, length: 1m

Ply thickness: 0.183E-03m

Material properties:

$E_1$	$E_2$	$G_{12}$	$G_{13}$	$G_{23}$	$\nu_{12}$
1.48E13Pa	1.03E10Pa	5.93E09Pa	5.93E09Pa	5.90E09Pa	0.27

The box beam cross section is shown in Figure 5.37.

Coupling values were calculated for 4 cases of different layup stacking sequences. Table 5.14 shows the layup for each case. All cases are then analysed using the thin-walled beam formula, BOXMX Program and NASTRAN.

**Table 5.14 Layup for coupling study**

Case 1: Upper and lower wall 45° plies	
Upper wall:	[45/45/45/45/45/45/45/45/45/45]s
Lower wall:	[45/45/45/45/45/45/45/45/45/45]s
Front wall	[0/0/0/0/0/0/0/0/0/0/0/0/0/0/0/0/0]s
Rear wall:	[0/0/0/0/0/0/0/0/0/0/0/0/0/0/0/0/0]s
Case 2: Upper and lower wall -45° plies	
Upper wall:	[-45/-45/-45/-45/-45/-45/-45/-45/-45/-45]s
Lower wall:	[-45/-45/-45/-45/-45/-45/-45/-45/-45/-45]s
Front wall	[0/0/0/0/0/0/0/0/0/0/0/0/0/0/0/0/0]s
Rear wall:	[0/0/0/0/0/0/0/0/0/0/0/0/0/0/0/0/0]s
Case 3: Upper wall 45° plies, lower wall -45° plies	
Upper wall:	[45/45/45/45/45/45/45/45/45/45]s
Lower wall:	[-45/-45/-45/-45/-45/-45/-45/-45/-45/-45]s
Front wall	[0/0/0/0/0/0/0/0/0/0/0/0/0/0/0/0/0]s
Rear wall:	[0/0/0/0/0/0/0/0/0/0/0/0/0/0/0/0/0]s
Case 4: Upper wall -45° plies, lower wall 45° plies	
Upper wall:	[-45/-45/-45/-45/-45/-45/-45/-45/-45/-45]s
Lower wall:	[45/45/45/45/45/45/45/45/45/45]s
Front wall	[0/0/0/0/0/0/0/0/0/0/0/0/0/0/0/0/0]s
Rear wall:	[0/0/0/0/0/0/0/0/0/0/0/0/0/0/0/0/0]s

### 5.4.2 BOXMX Program

Another method to calculate the coupling value is by using a FORTRAN based Box Program called BOXMX [95]. Using the same material properties and box dimensions, the same cases were analysed. Coupling results and the percentage difference obtained from the formula and BOXMX Program are presented in Table 5.15. For Case 1 and Case 2, no coupling occurs hence the percentage difference is 0%. For Case 3 and Case 4, a small percentage difference calculated, which is merely 1.28%. Since the percentage difference between formula and BOXMX Program is very small, therefore, both methods can be applied to measure coupling.

**Table 5.15 Result comparison between formula and BOXMX Program**

Case:	Coupling, $CK$ (Nm <sup>2</sup> )		Percentage Difference (%)
	Formula	Box Program	
Case 1	0	0	0
Case 2	0	0	0
Case 3	6.26E+05	6.18E+05	1.28
Case 4	-6.26E+05	-6.18E+05	1.28

### 5.4.3 FE Analysis

Analysis were run in NASTRAN to verify results obtained from formula and BOXMX Program.

#### 5.4.3.1 FE Box Analysis

Using the same material properties and box dimensions, 10kN load is applied in FE analysis. In NASTRAN, box analysis were carried out using 2 methods:

**Method 1:** Use layup as input. Input example as shown in Figure 5.38.

**Method 2:** Use equivalent stiffness as input. Input example as illustrated in Figure 5.39. The equivalent stiffness values were obtained from ABD Matrix Program. The example of ABD Matrix Program input and output are shown in Appendix A.

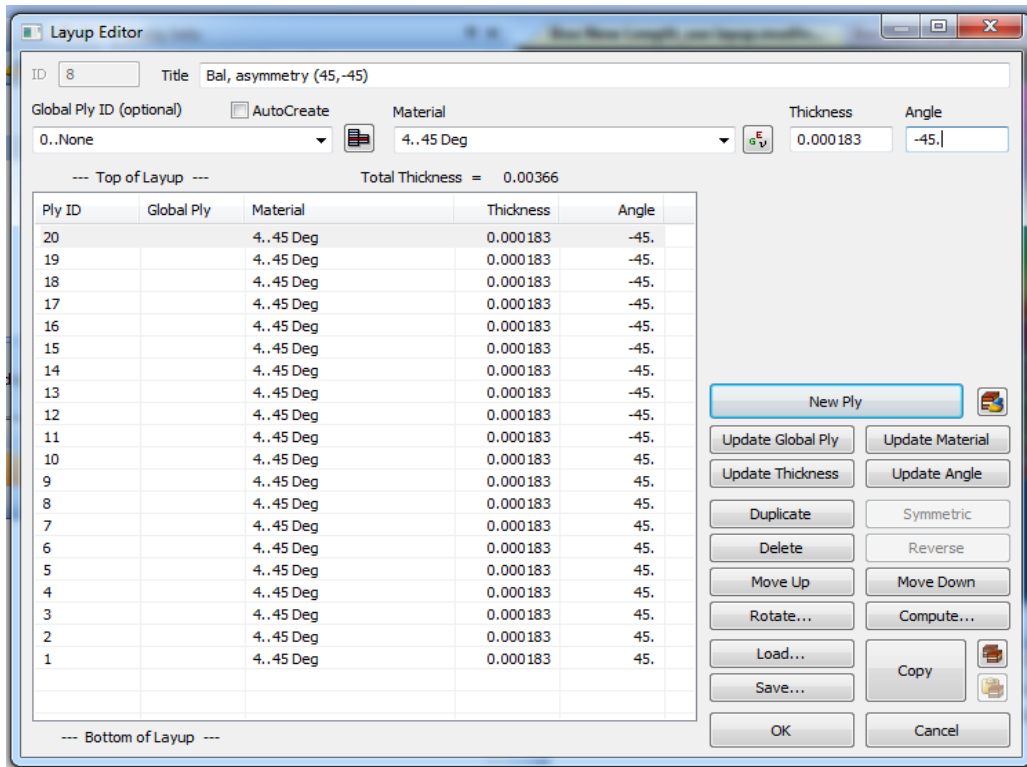


Figure 5.38 Method 1. Input example using layup properties

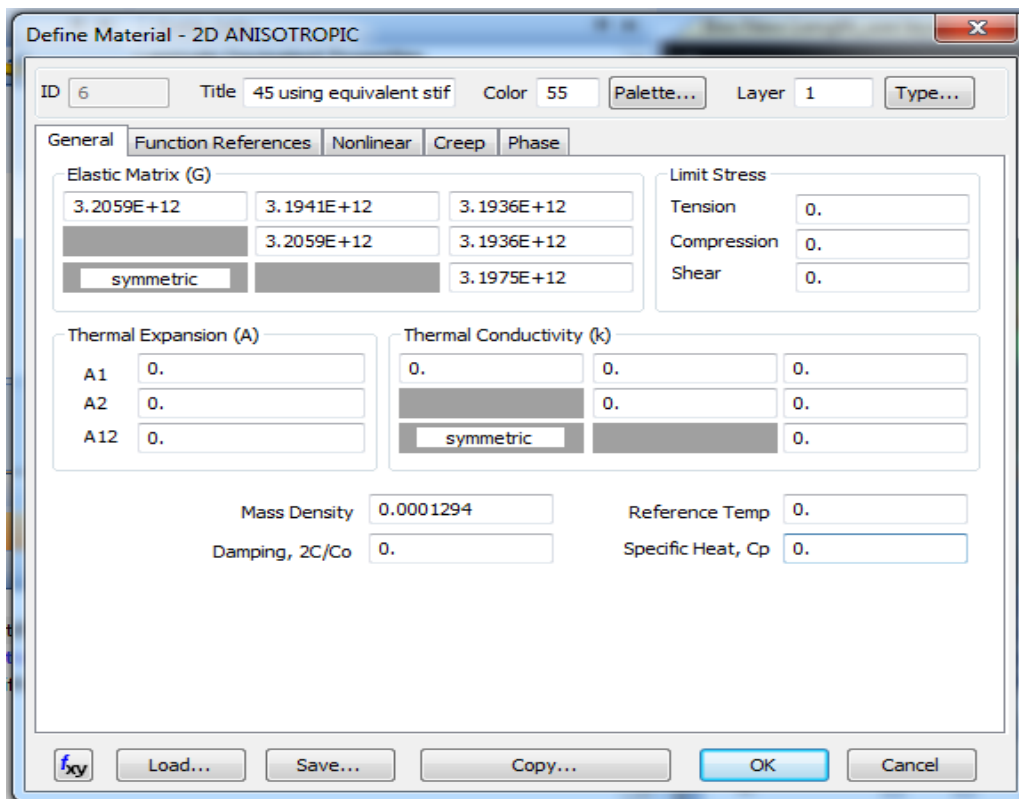


Figure 5.39 Method 2. Input example using equivalent stiffness

### 5.4.3.2 Result

Results for Case 1, Case 2, Case 3 and Case 4 are presented in Figure 5.40, Figure 5.41, Figure 5.42 and Figure 5.43, respectively.

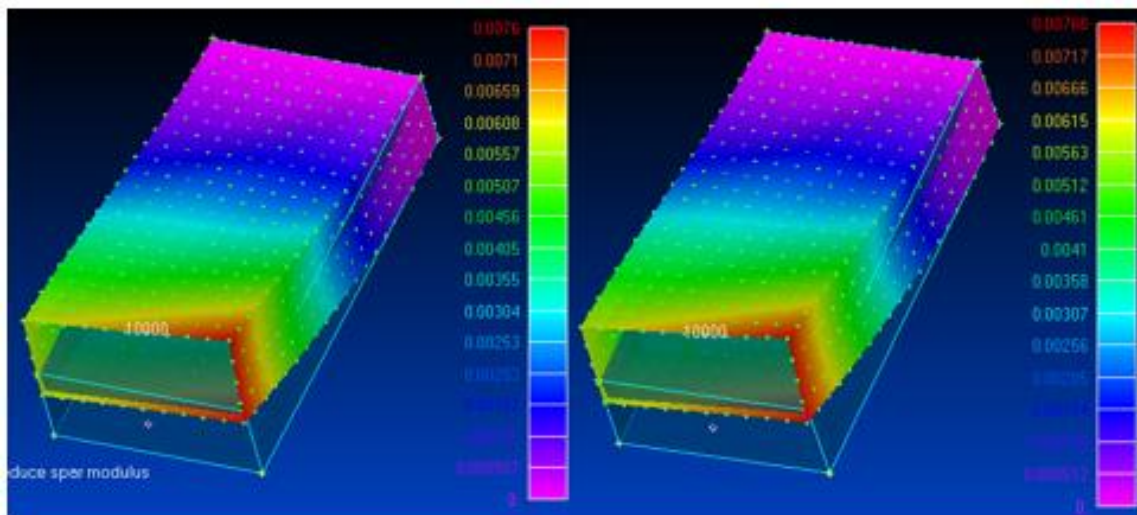
#### 5.4.3.2.1 *Case 1: Upper and lower wall 45° plies*

Upper skin: [45/45/45/45/45/45/45/45/45/45]s

Lower skin: [45/45/45/45/45/45/45/45/45/45]s

Front spar: [0/0/0/0/0/0/0/0/0/0/0/0/0/0/0/0]s

Rear spar: [0/0/0/0/0/0/0/0/0/0/0/0/0/0/0/0]s



a) Method 1

b) Method 2

Figure 5.40 Result for Case 1

#### Maximum displacement result

Method 1: 7.6E-03m

Method 2: 7.68E-03m

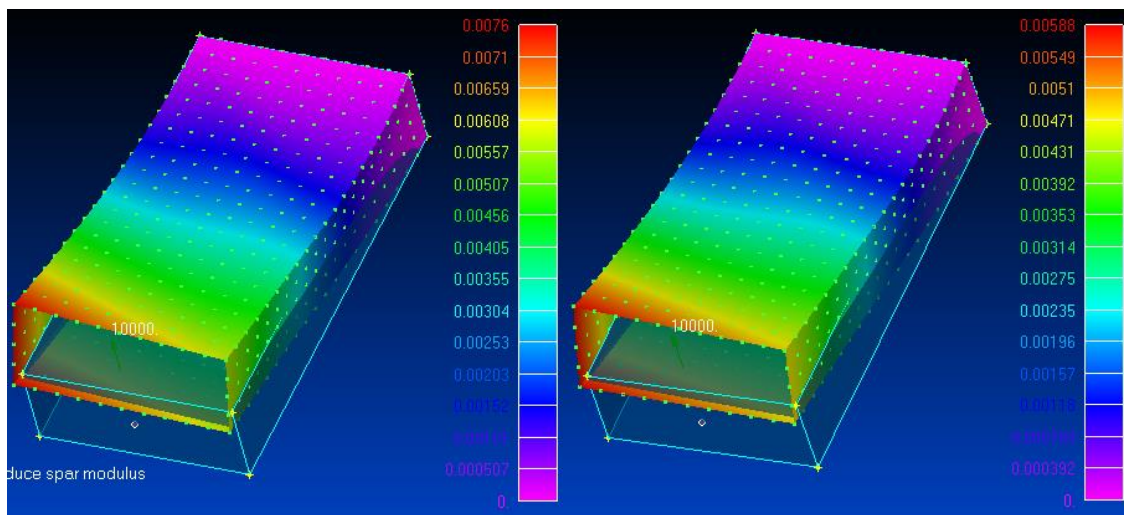
**5.4.3.2.2 Case 2: Upper and lower wall -45° plies**

Upper skin: [-45/-45/-45/-45/-45/-45/-45/-45/-45/-45]s

Lower skin: [-45/-45/-45/-45/-45/-45/-45/-45/-45/-45]s

Front spar: [0/0/0/0/0/0/0/0/0/0/0/0/0/0/0/0/0]s

Rear spar: [0/0/0/0/0/0/0/0/0/0/0/0/0/0/0/0/0]s



a) Method 1

b) Method 2

Figure 5.41 Result for Case 2

Maximum displacement result

Method 1: 7.6E-03m

Method 2: 7.68E-03m

**5.4.3.2.3 Case 3: Upper wall 45° plies, lower wall -45° plies**

Upper skin: [45/45/45/45/45/45/45/45/45/45]s

Lower skin: [-45/-45/-45/-45/-45/-45/-45/-45/-45/-45]s

Front spar: [0/0/0/0/0/0/0/0/0/0/0/0/0/0/0/0]s

Rear spar: [0/0/0/0/0/0/0/0/0/0/0/0/0/0/0/0]s

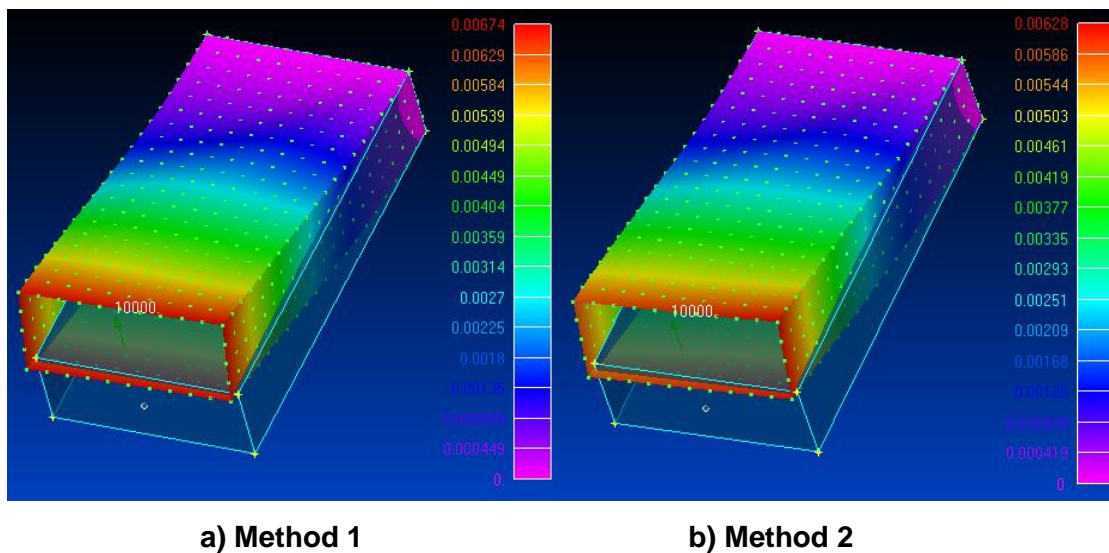


**Figure 5.42 Result for Case 3**

Max displacement result

Method 1: 6.74E-03m

Method 2: 6.28E-03m

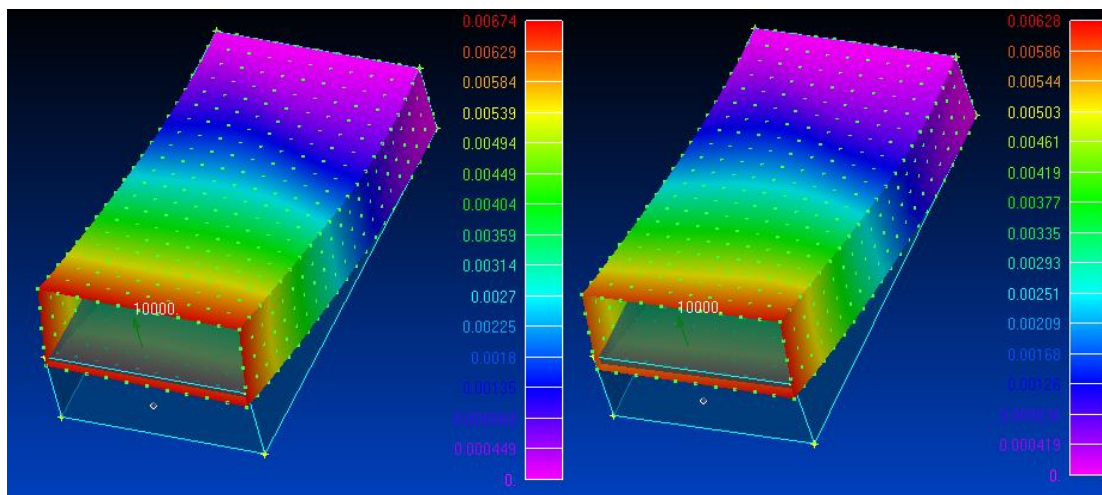
**5.4.3.2.4 Case 4: Upper wall -45° plies, lower wall 45° plies**

Upper skin: [-45/-45/-45/-45/-45/-45/-45/-45/-45/-45]s

Lower skin: [45/45/45/45/45/45/45/45/45/45]s

Front spar: [0/0/0/0/0/0/0/0/0/0/0/0/0/0/0/0/0]s

Rear spar: [0/0/0/0/0/0/0/0/0/0/0/0/0/0/0/0/0]s



**a) Method 1**

**b) Method 2**

**Figure 5.43 Result for Case 4**

Max displacement result

Method 1: 6.74E-03m

Method 2: 6.28E-03m



The maximum displacement results for all cases are presented in Table 5.16

**Table 5.16 Maximum displacement results for Method 1 and Method 2**

	Maximum displacement (m)	
	Method 1	Method 2
Case 1	7.6E-03	7.68E-03
Case 2	7.6E-03	5.88E-03
Case 3	6.74E-03	6.28E-03
Case 4	6.74E-03	6.28E-03

#### 5.4.4 Discussion

Result in Table 5.15 shows that the unbalance and symmetric layup calculated using formula and BOXMX Program (Example of BOXMX Program input is shown in Appendix B) has zero coupling while balance and asymmetric layup produced coupling. These results are opposed to our current understanding, where the balance layup supposed to cancel each other and eliminate coupling.

Further research is done in NASTRAN to confirm this theory. Since the coupling stiffness cannot be measured directly in NASTRAN, the maximum displacement is measured in each case. In NASTRAN, results produced show that the unbalance and symmetric layup in Case 1 and Case 2 have a higher displacement compared to balance and asymmetric layup in Case 3 and Case 4. The unbalance contour results in Figure 5.40 and **Error! Reference source not found.** also show that coupling exist in Case 1 and Case 2. These results are totally contra with formula and the BOXMX Program result.

According to reference [12], the in-plane stiffness  $A$  matrix is constant throughout the cross-section. It means that in box beam, the circumferentially uniform stiffness (CUS) has a constant throughout in-plane stiffness. The ply layups of opposite sides of a box beam shall be in reversed orientation to make the stiffness uniform. This configuration is antisymmetric between the opposite walls and produces extension-twist and bending-transverse shear couplings. In this case

study, Case 1 and Case 2 are CUS configuration for formula and BOXMX Program analysis but Case 3 and Case 4 for FE analysis in NASTRAN.

For circumferentially asymmetric stiffness (CAS), the ply layups along the horizontal members are mirror image. The beam box has symmetric configuration between the opposite walls and produces bending-twist and extension-transverse shear coupling. In this case study, Case 3 and Case 4 are CAS configuration for formula and BOXMX Program analysis but Case 1 and Case 2 in FE analysis.

#### 5.4.5 Conclusion

1. For box beam, the CUS layup of opposite side must be in reversed orientation while for CAS configuration, the layup of opposite side must be symmetric. In paper, CUS configuration is the balance and asymmetric layup while for CAS it is the unbalance and symmetric layup. It is noted that no clear explanation about CUS and CAS layup arrangement for box. For example in Figure 5.44 below, Berdichevsky et al. [13], Rehfield et al. [96], Hodges et al. [97] only denote  $[\theta]_T$  for the composite layup but did not mention anywhere in the papers what does 'T' means. There is no explanation regarding this term. In this analysis BOXMX Program is used to represent theory and NASTRAN analysis has been conducted for result comparison and validation.

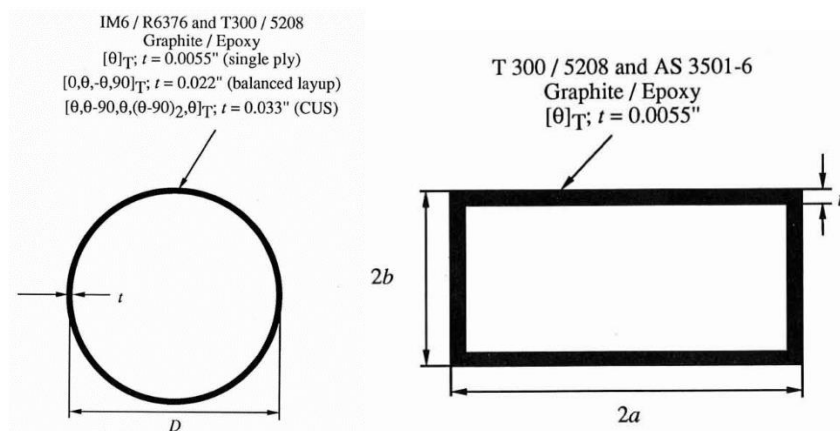


Figure 5.44 Example of CUS layup for circular tube and box beam cross section

2. Layup configuration in NASTRAN agree with definition stated in paper. In contra, layup configuration in BOXMX Program produced opposite results. The definition of ply orientation while using formula and BOXMX Program must be changed to align with FE and theory in paper. The lower skin angle must be in the opposite direction from current input. The example of input for the formula and BOXMX Program are shown in Table 5.17.

**Table 5.17 Example of input for formula and BOXMX Program**

Case 1: Upper 45° Lower 45° (Unbalance and symmetry: CAS)				
		Layup	K from formula (Nm <sup>2</sup> )	K from BOXMX Program (Nm <sup>2</sup> )
Input	Upper Skin 45°	All 45°	6.26E+05	6.18E+05
	Front Spar 0°	All 0°		
	Lower Skin -45°	All -45°		
	Rear Spar 0°	All 0		
Case 2: Upper -45° Lower -45° (Unbalance and symmetry: CAS)				
		Layup	K from formula (Nm <sup>2</sup> )	K from BOXMX Program (Nm <sup>2</sup> )
Input	Upper Skin -45°	All -45°	-6.26E+05	-6.18E+05
	Front Spar 0°	All 0°		
	Lower Skin 45°	All 45°		
	Rear Spar 0°	All 0°		
Case 3: Upper 45° Lower -45° (Balance and asymmetry: CUS)				
		Layup	K from formula (Nm <sup>2</sup> )	K from BOXMX Program (Nm <sup>2</sup> )
Input	Upper Skin 45°	All 45°	0	0
	Front Spar 0°	All 0°		
	Lower Skin 45°	All 45°		
	Rear Spar 0°	All 0°		
Case 4: Upper -45° Lower 45° (Balance and asymmetry: CUS)				
		Layup	K from formula (Nm <sup>2</sup> )	K from BOXMX Program (Nm <sup>2</sup> )
Input	Upper Skin -45°	All -45°	0	0
	Front Spar 0°	All 0°		
	Lower Skin -45°	All -45°		
	Rear Spar 0°	All 0°		

## 5.5 Cut-out Analysis of Aluminium and Composite Box

4 idealized uniform box models have been created in Femap for cut-out study. All boxes have the same dimension: Width = 0.5m, Depth = 0.2m, Length = 1m

The cut-out keeps almost the same area = 0.097 ~ 0.098 m<sup>2</sup>;

Box 1: No cut-out. Use for reference (baseline).

Box 2: Circular shape cut-out at box centre. R=0.176m (D/W=0.704); Area = 0.097m<sup>2</sup>

Box 3: Elliptical shape cut-out, 0.2m eccentric from the centre. Rb=0.125 (D/W=0.5); Area = 0.098m<sup>2</sup>

Box 4: Same elliptical shape cut-out, at the box centre. Area = 0.098m<sup>2</sup>

Figure 5.45 shows the cut-out location and dimension for Box 1-Box 4.

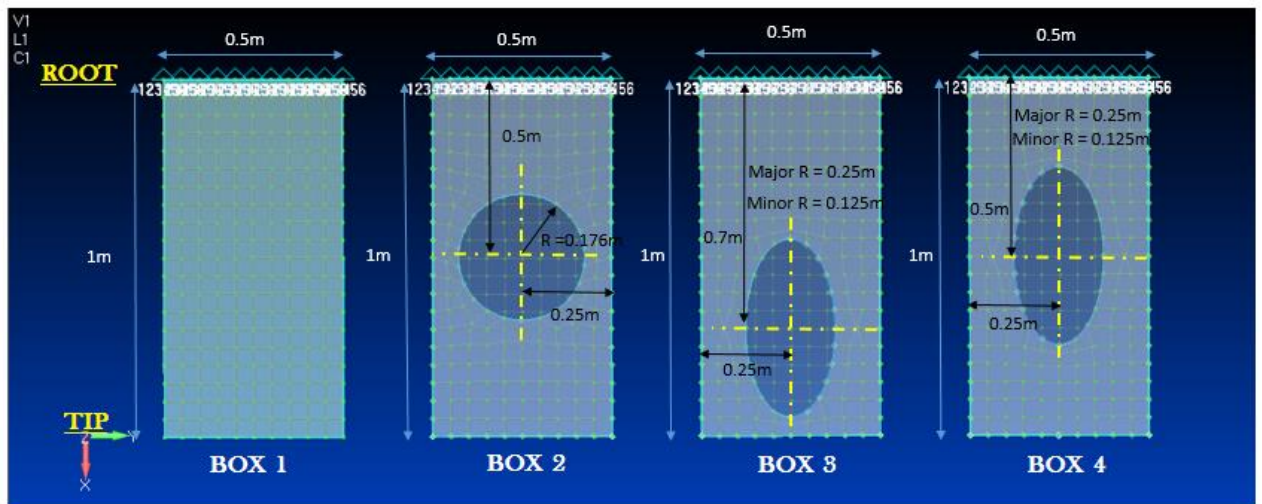


Figure 5.45 Cut-out location and dimension. R = radius

The isometric view and box mesh in NASTRAN are shown in Figure 5.46 and Figure 5.47, respectively.

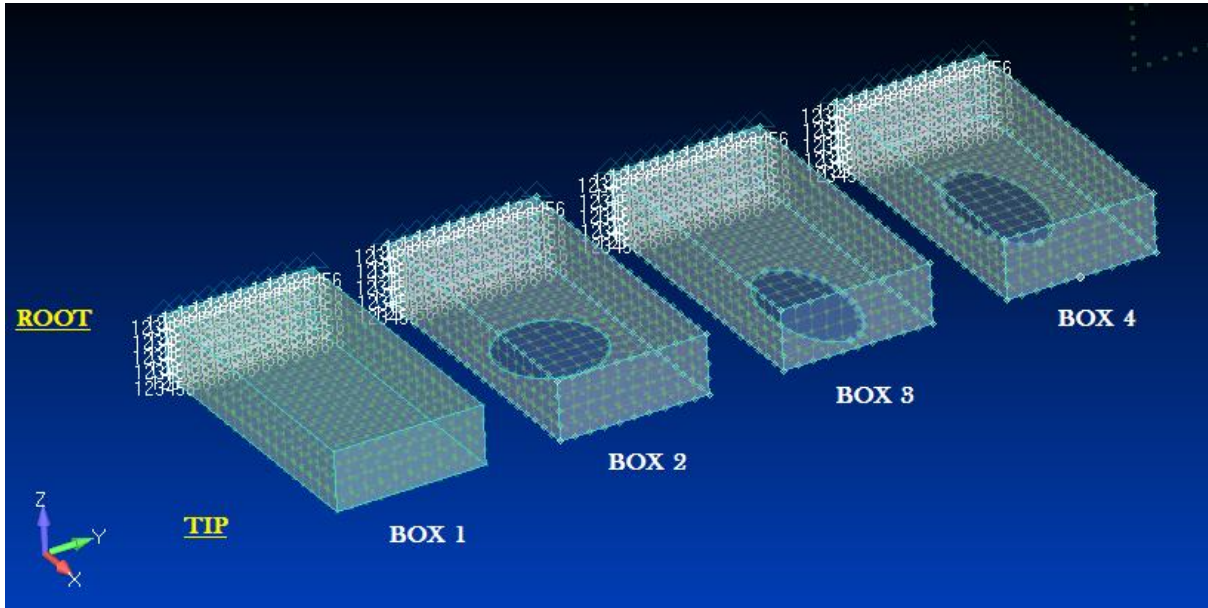


Figure 5.46 Isometric view

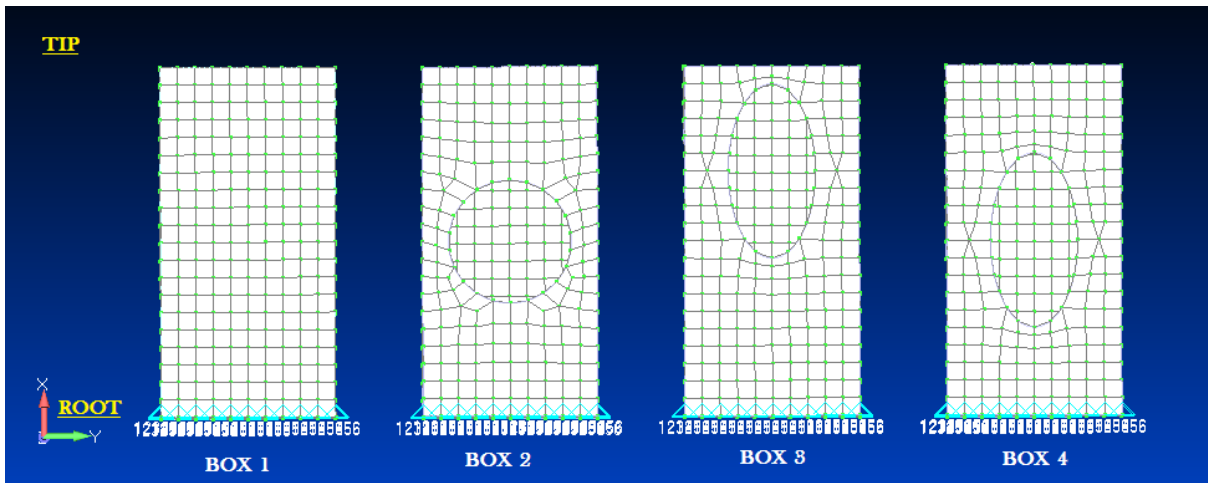
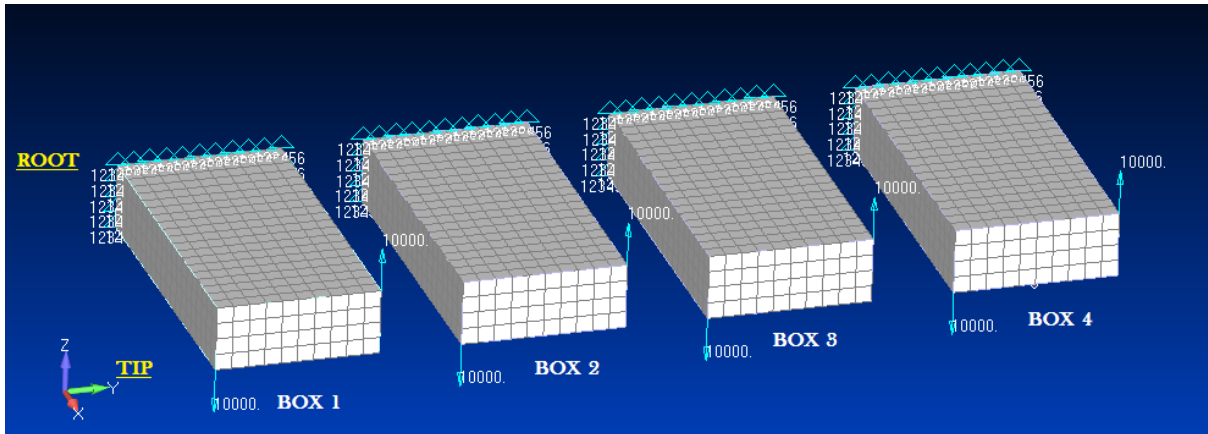


Figure 5.47 Bottom view. Box with mesh



**Figure 5.48 Loads applied at each box**

The torsional loads applied on the box are shown in Figure 5.48. The objective of this analysis is to find out the effect of cut-out to torsional stiffness of the box. Analysis was carried out using 2 types of materials:

1. Aluminium.

Material properties;  $E = 7E10$ ,  $G = 2.7E10$ ,  $\nu = 0.27$ , *Thickness = 7mm*

2. Composite

Material properties;  $E_1 = 1.43E11$ ,  $E_2 = 1.03E10$ ,  $G_{12} = 5.3E09$ ,  $G_{13} = 5.3E09$ ,  
 $G_{23} = 5.3E09$ ,  $\nu_{12} = 0.27$

The laminate layup for composite material used in this study are presented in Table 5.18. The layup used are based on the real industry case study, which is applied on the aircraft wing.

**Table 5.18 Laminate layup of baseline wing model used in case study**

Laminate layup	
Upper skin	[45/45/45/0/45/45/0/0/-45/-45/90/0/-45/-45/90/90/90/-45/90]s
Lower skin	[45/45/45/0/0/45/45/-45/0/45/0/0/90/-45/45/90/90/90/-45]s
Front spar (right)	[45/0/45/45/45/-45/45/0/0/0/-45/90/-45/90/-45/90/90/-45/90]s
Rear spar (left)	[45/45/45/0/45/45/0/45/0/0/-45/0/-45/-45/90/90/90/-45/90]s

Single layup thickness: 0.183 mm

Total laminate thickness for each skin: 6.954 mm

## Results

### 1. Aluminium

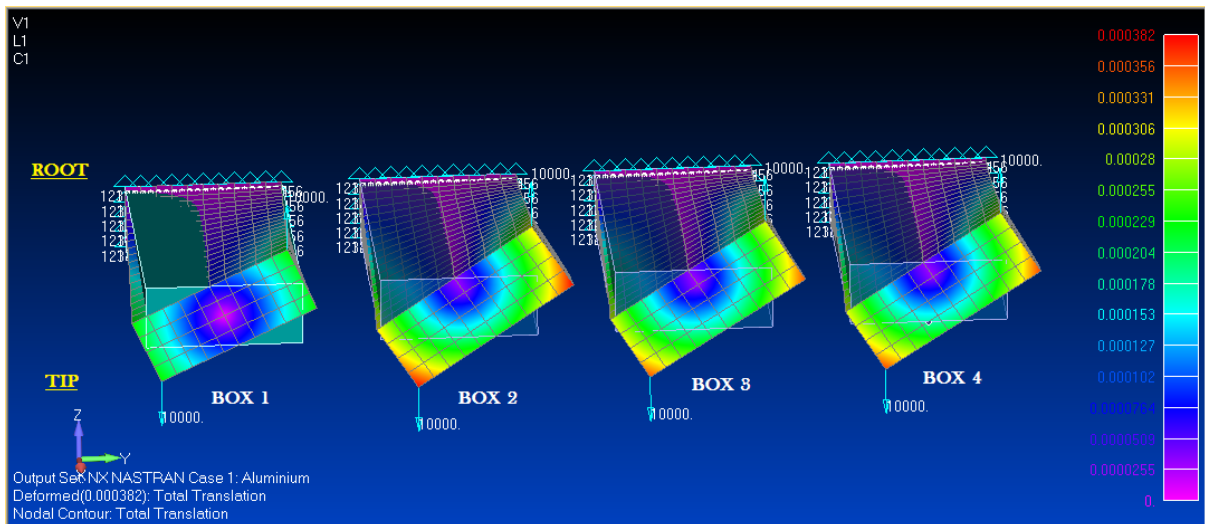


**Figure 5.49 Torsion results using aluminium**

The results of torsional stiffness,  $GJ$  reduction due to cut-out obtained from NASTRAN are shown in

Table 5.19 and graphs are illustrated in Figure 5.50.

**Table 5.19 Torsional stiffness and  $GJ$  reduction percentage due to cut-out (aluminium)**

Case	Torsional Stiffness, $GJ$ (Nm <sup>2</sup> )	$GJ$ reduction due to cut-out (%)
Box 1	5.74E+06	<i>No cut-out</i>
Box 2	4.02E+06	29.97
Box 3	4.23E+06	26.31
Box 4	4.19E+06	27.00

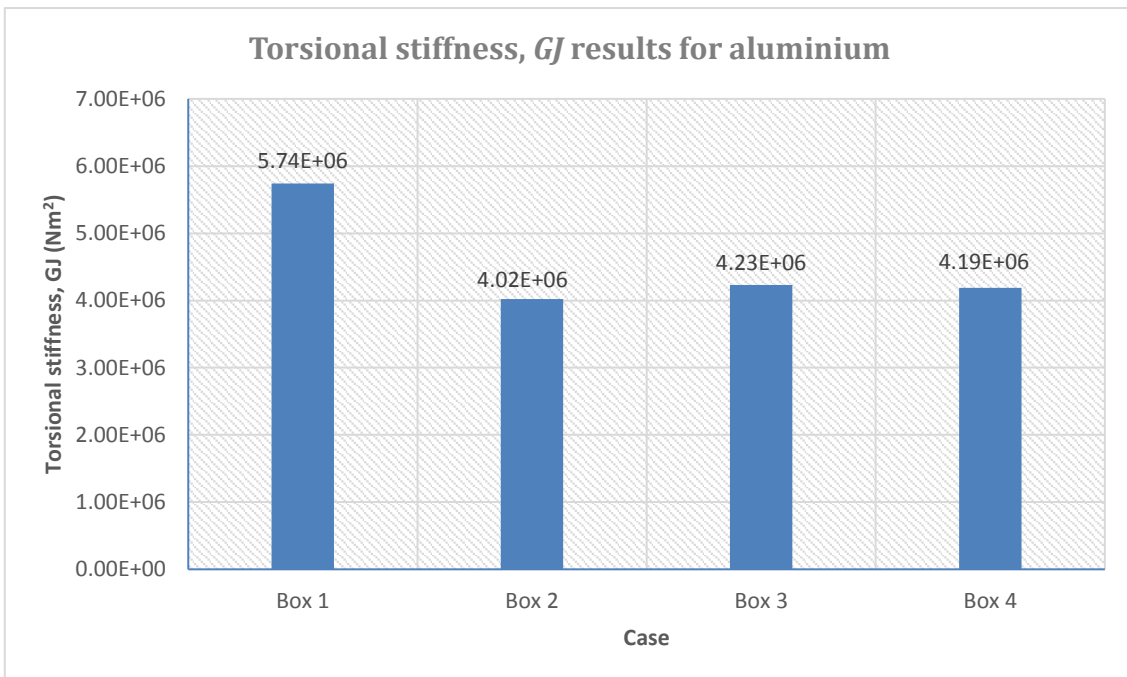


**Figure 5.50 Graph of torsional stiffness for each case**



## 2. Composite

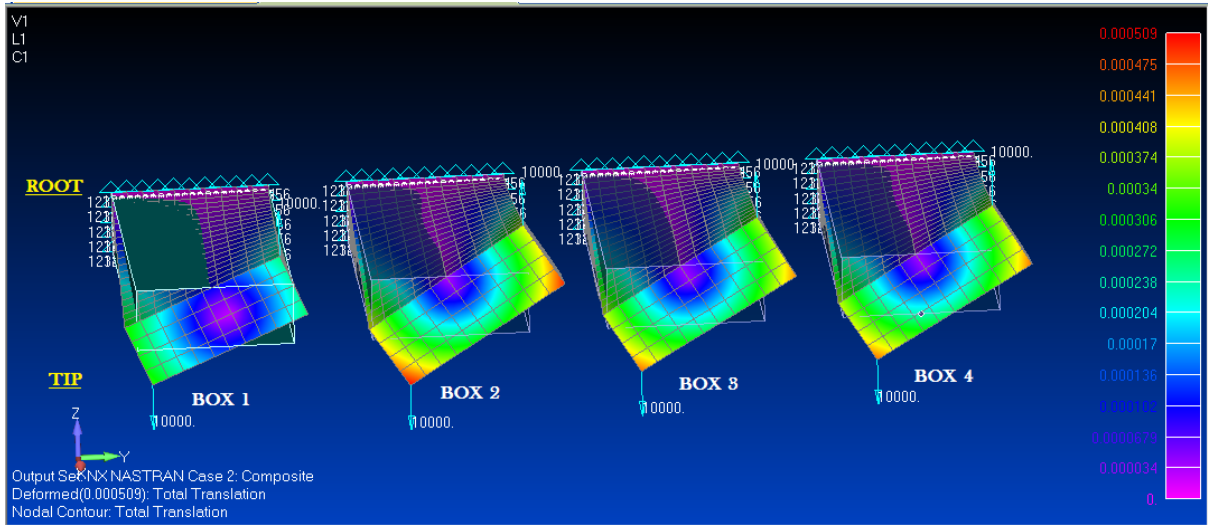
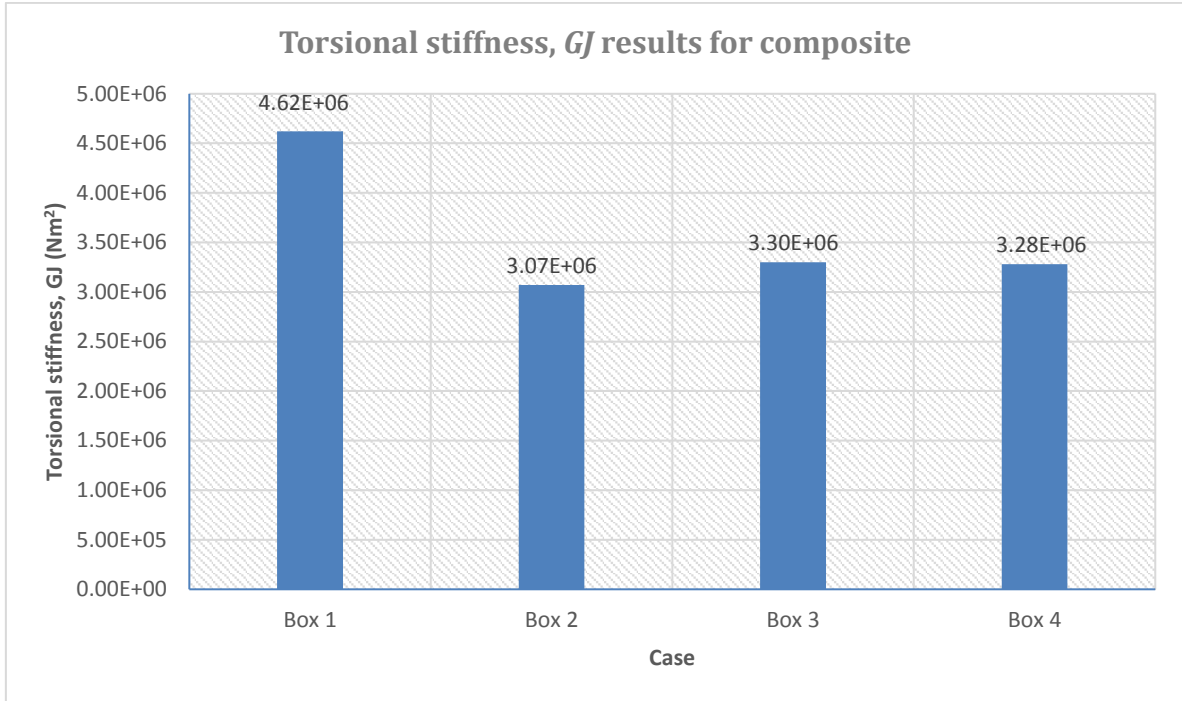


Figure 5.51 Torsion results for composite boxes

Torsional stiffness,  $GJ$  for composite obtained from NASTRAN are shown in Table 5.20 and illustrated in Figure 5.52.

Table 5.20 Torsional stiffness and  $GJ$  reduction percentage due to cut-out (composite)

Case	Torsional Stiffness, $GJ$ ( $\text{Nm}^2$ )	$GJ$ reduction due to cut-out (%)
Box 1	4.62E+06	No cut-out
Box 2	3.07E+06	33.55
Box 3	3.30E+06	28.57
Box 4	3.28E+06	29.00



**Figure 5.52 Graph of torsional stiffness for each case**

Percentage difference between box with cut-out and without cut-out for aluminium and composite for all cases are presented in Table 5.21.

**Table 5.21 GJ reduction percentage due to cut-out for aluminium and composite**

Case	GJ reduction due to cut-out for aluminium (%)	GJ reduction due to cut-out for composite (%)
Box 1	<i>No cut-out</i>	<i>No cut-out</i>
Box 2	29.97	33.55
Box 3	26.31	28.57
Box 4	27.00	29.00

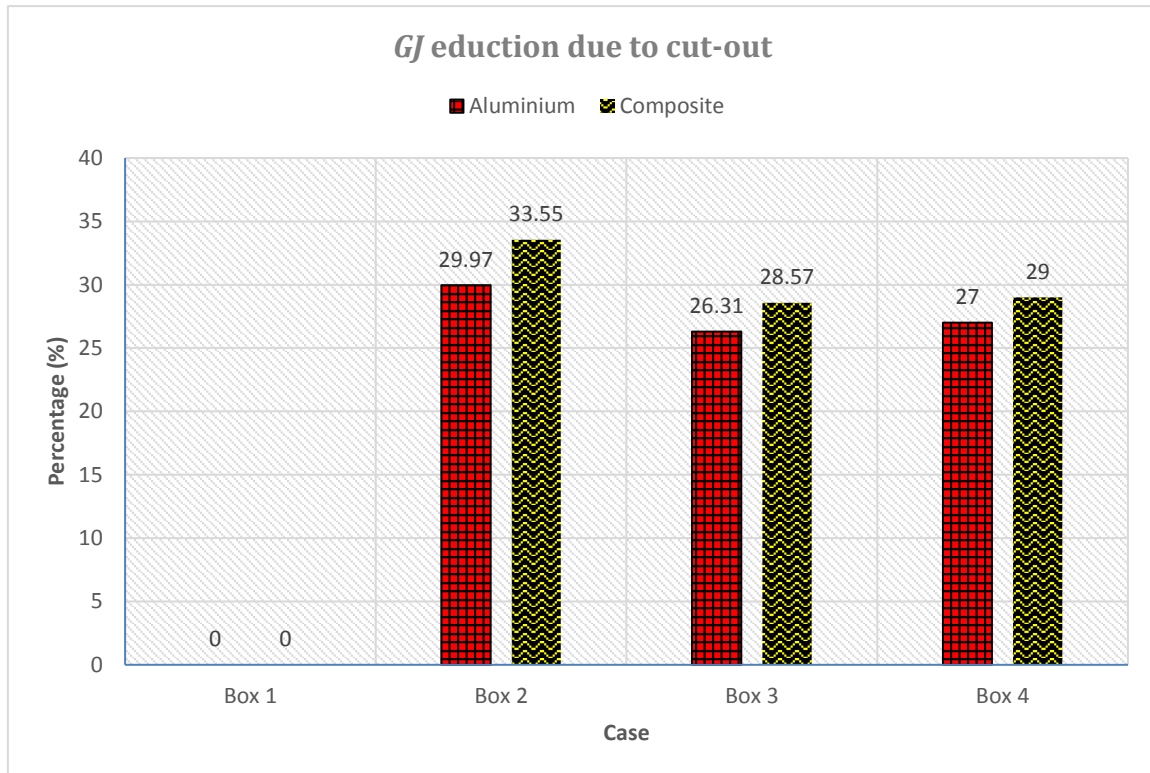


**Figure 5.53  $GJ$  reduction due to cut-out for aluminium and composite**

Figure 5.53 illustrates the percentage of torsional stiffness reduction due to cut-out for aluminium and composite box. From Figure 5.50, Figure 5.52 and Figure 5.53, results show that Box 2, which contains the circular shape cut-out has the biggest torsional stiffness percentage reduction, which is 29.97% for aluminium and 33.55% for composite. For elliptical shape cut-out, Box 3, which is 0.2m eccentric from the centre has less torsional stiffness reduction compared to elliptical shape cut-out at the box centre (Box 4). Having the same box dimension and the same cut-out area, the elliptical cut-out shape gives better torsional stiffness compared to the circular shape. The location of the cut-out also influences the torsional stiffness of the box where in this study, the cut-out which the location is 0.2m eccentric from the box centre gives better torsional stiffness than the cut-out at the box centre.

## 5.6 Design Composite Box in Laminate Level

The inevitable iterative design and repetitive validation process during the design stage undoubtedly will increase the development time and cost. These processes, however, can be reduced by adapting the following guidelines. Three methods can be used to design composite box in laminate level where the stiffness of the wing box structure can be predicted during the material selection process and laminate design stage. The first method is the simplest method which used the Ten-Percent Rule as a guideline. The second method uses framework which has been developed in this research using the Classical Lamination Theory and composite thin-walled beam theory. This method correlates 1-dimensional and 2-dimensional beam structure. The third method is the most complex method, which involves the correlation between 2-dimensional and 3-dimensional beam structure. FE model is required in this method. The third method represents the real case and hence more details were taken into account in this method.

### 5.6.1 Method 1: Use Ten-Percent Rule

The Ten-Percent Rule is the simplest and reliable method for the preliminary sizing of composite structures, by using a simple rule of mixtures. The rule stated that the primary fibres for each uniaxial load condition are considered to develop hundred percent of the reference strength of the composite material for each environment, while the secondary fibres (transverse fibres) are attributed with only ten percent of this strength and stiffness [98]. Each  $45^\circ$  or  $90^\circ$  ply has ten percent tensile stiffness and strength of  $0^\circ$  ply, while each  $0^\circ$  or  $90^\circ$  ply has ten percent shear stiffness and strength of  $\pm 45^\circ$  ply. This procedure is applied to uniaxial loads, to biaxial loads of the same sign, and to biaxial loads of opposite signs, which is equivalent to in-plane shear with respect to the rotated axis [98].

In order to find the stiffness correlations between laminate and composite box using the Ten-Percent Rule, bending stiffness,  $EI$  and torsional stiffness,  $GJ$  for laminates, box CUS and box CAS at different ply angle combinations were calculated and plotted in Figure 5.54 and Figure 5.55. Details of the ply angle combinations for each case are shown in Table 5.22.

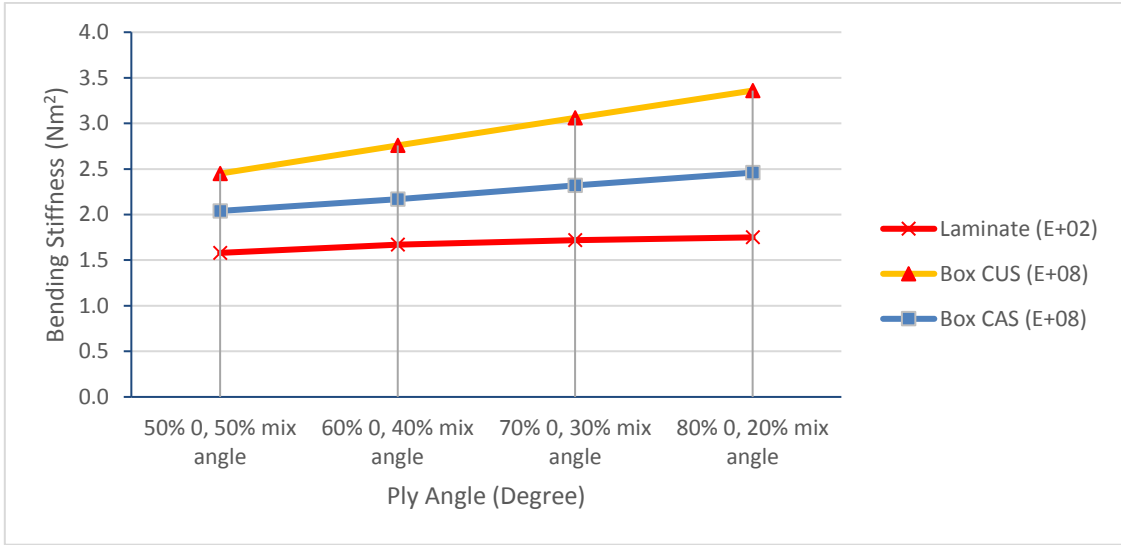


**Figure 5.54 Bending stiffness for laminate, box CUS and box CAS at different ply angle mixtures**

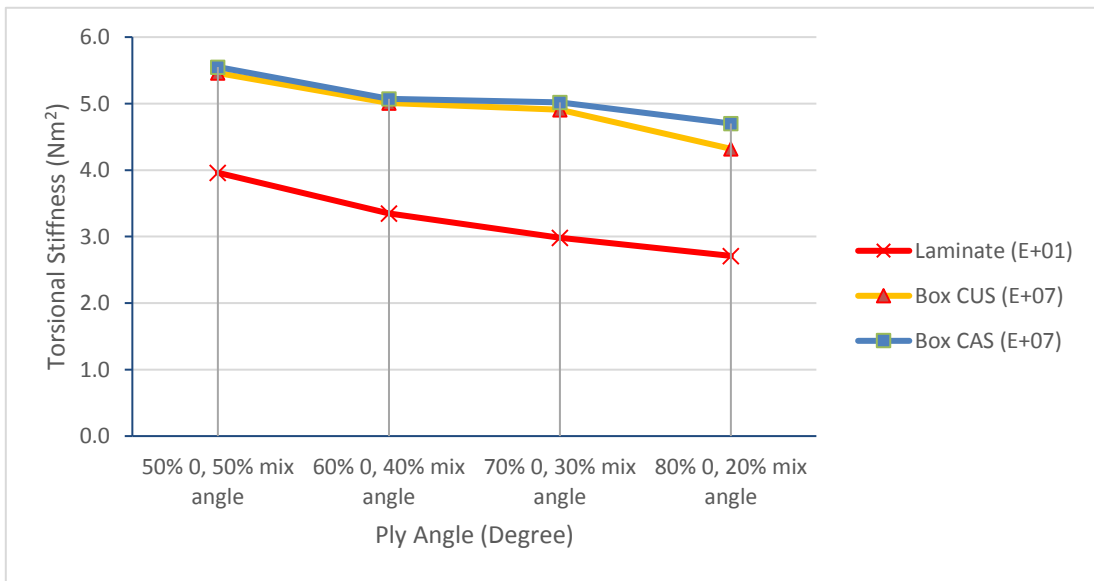


**Figure 5.55 Torsional stiffness for laminate, box CUS and box CAS at different ply angle mixtures**

**Table 5.22 Ply angle mixtures**

Case	Ply angle mixture (%)		
	0°	45°	90°
1. 50% 0°, 50% mix angle	50	30	20
2. 60% 0°, 40% mix angle	60	20	20
3. 70% 0°, 30% mix angle	70	20	10
4. 80% 0°, 20% mix angle	80	10	10

Result from Figure 5.54 shows that the bending stiffness graphs for laminate, box CUS layup and box CAS layup are linear. For torsional stiffness, refer Figure 5.55, the graph results are not linear. It is because the 45° ply percentage for case 2 and 3, 60% 0°, 40% mix angle and 70% 0°, 30% mix angle, respectively, have the same value. The 45° ply angle dominates the in-plane shear modulus  $G_{xy}$ , where it directly contributes to the torsional stiffness calculation, by definition. The result, however shows that the graph patterns for laminates, box CUS and box CAS layup are similar.

Based on these results, the stiffness correlation between laminate and composite box was developed by using this simple method. The Ten-Percent Rule can be applied to predict the laminate stiffness during the preliminary sizing of composite structures. From Figure 5.54 and Figure 5.55, it is shown that the bending stiffness and torsional stiffness for laminate and boxes are directly proportional. Therefore, from this correlation, when designing a composite box, the final outcome of the product can predicted during the laminate design stage.

### **5.6.2 Method 2: Use Laminate and Thin-Walled Beam Theory (1-dimensional to 2-dimensional box)**

In this method, the existing methodology is used to calculate the bending stiffness, the torsional stiffness and coupling stiffness of the laminate and composite box. The laminate theory, ABD Matrix is used for laminate analysis whilst for box analysis, thin-walled composite beam theory is applied.

#### **5.6.2.1 Bending Stiffness, $EI$ formula from laminate and beam theory**

From laminate theory,

$$EI = E_x \cdot I \quad (5.12)$$

where

$$E_x = \frac{1}{t \cdot a_{11}} \quad (5.13)$$

and

$I$  = second moment of area

From laminate theory,

$$E_x = \frac{1}{t} \left( \frac{A_{11}A_{22}A_{33} + 2A_{12}A_{23}A_{13} - A_{22}A_{13}^2 - A_{33}A_{12}^2 - A_{11}A_{23}^2}{A_{22}A_{33} - A_{23}^2} \right) \quad (5.14)$$

For symmetrical and balance layup,  $A_{13}$  and  $A_{23} = 0$

Therefore

$$\begin{aligned} E_x &= \frac{1}{t} \left( \frac{A_{11}A_{22}A_{33} - A_{33}A_{12}^2}{A_{22}A_{33}} \right) \\ &= \frac{1}{t} \left( \frac{A_{11}A_{22} - A_{12}^2}{A_{22}} \right) \\ &= \frac{1}{t} \left( A_{11} - \frac{A_{12}^2}{A_{22}} \right) \end{aligned} \quad (5.15)$$

Bending stiffness,

$$E_x \cdot I = \frac{1}{t} \left( A_{11} - \frac{A_{12}^2}{A_{22}} \right) \cdot I \quad (5.16)$$

$E_x$  value is calculated from the material properties while  $I$  is from the geometrical properties.

For composite box, to calculate bending stiffness, Armanios formula for thin-walled composite beam theory is applied. From Armanios formula

$$EI = \oint \left( A(s) - \frac{B(s)^2}{C(s)} \right) z^2 ds + \frac{[\oint (B(s)/C(s))z ds]^2}{\oint (1/C(s))ds} \quad (5.17)$$

where

$$A(s) = A_{11} - \frac{A_{12}^2}{A_{22}} \quad (5.18)$$

$$B(s) = 2 \left[ A_{13} - \frac{A_{12}A_{23}}{A_{22}} \right] \quad (5.19)$$

$$C(s) = 4 \left[ A_{33} - \frac{(A_{23})^2}{A_{22}} \right] \quad (5.20)$$

$A(s)$ ,  $B(s)$  and  $C(s)$  define the reduced axial stiffness, reduced coupling stiffness and reduced torsion stiffness respectively.  $z$  is the  $z$  coordinate and  $ds$  is the distance or changes in the circumference coordinate.

For symmetrical and balance layup,  $A_{13}$  and  $A_{23} = 0$

Therefore, bending stiffness of a box

$$EI = \oint A(s) z^2 ds$$

$$= \oint \left( A_{11} - \frac{A_{12}^2}{A_{22}} \right) z^2 ds \quad (5.21)$$

$A(s)$  value comes from the material properties while  $z^2$  and  $ds$  are from the box geometry.

Table 5.23 shows the bending stiffness formula from laminate theory and thin-walled beam theory.

**Table 5.23 Bending stiffness formula from laminate and beam theory**

	From laminate theory	From thin-walled beam theory (Armanios formula)
Bending stiffness formula	$E_x \cdot I = \frac{1}{t} \left( A_{11} - \frac{A_{12}^2}{A_{22}} \right) \cdot I$	$EI = \oint \left( A_{11} - \frac{A_{12}^2}{A_{22}} \right) z^2 ds$

### 5.6.2.2 Torsional stiffness, $GJ$ formula from laminate and beam theory

From laminate theory,

$$GJ = G_{xy} \cdot J \quad (5.22)$$

where

$$G_{xy} = \frac{1}{t \cdot a_{13}} \quad (5.23)$$

and



$J$  = polar moment of inertia

Shear modulus,

$$G_{xy} = \frac{1}{t} \left( \frac{A_{11}A_{22}A_{33} + 2A_{12}A_{23}A_{13} - A_{22}A_{13}^2 - A_{33}A_{12}^2 - A_{11}A_{23}^2}{A_{11}A_{22} - A_{12}^2} \right) \quad (5.24)$$

For symmetrical and balance layup,  $A_{13}$  and  $A_{23} = 0$

Therefore

$$\begin{aligned} G_{xy} &= \frac{1}{t} \left( \frac{A_{11}A_{22}A_{33} - A_{33}A_{12}^2}{A_{11}A_{22} - A_{12}^2} \right) \\ &= \frac{1}{t} \left( A_{33} \left( \frac{A_{11}A_{22} - A_{12}^2}{A_{11}A_{22} - A_{12}^2} \right) \right) \\ &= \frac{1}{t} (A_{33}) \end{aligned} \quad (5.25)$$

Torsional stiffness

$$G_{xy} \cdot J = \frac{1}{t} (A_{33}) \cdot J \quad (5.26)$$

$G_{xy}$  value is obtained from material properties while  $J$  is from the geometrical properties.

For composite box, to calculate the torsional stiffness, Armanios formula for thin-walled composite beam theory is applied. From Armanios formula

$$GJ = \frac{1}{\oint (1/C(s)) ds} A_e^2 \quad (5.27)$$

From Equation (5.20)

$$C(s) = 4 \left[ A_{33} - \frac{(A_{23})^2}{A_{22}} \right]$$

Recall Equation (5.20),  $C(s)$  defines the reduced torsion stiffness,  $ds$  is the distance changes in the circumference coordinate and  $A_e^2$  is the enclosed area of the cross section.

For symmetrical and balance layup,  $A_{13}$  and  $A_{23} = 0$

Therefore, torsional stiffness of a box

$$\begin{aligned}
 GJ &= \frac{1}{\oint (1/C(s)) ds} A_e^2 \\
 &= \oint \frac{1}{\oint (1/4(A_{33})) ds} A_e^2 \quad (5.28)
 \end{aligned}$$

$A_{33}$  value is obtained from material properties while  $A_e^2$  and  $ds$  are from the geometrical properties.

Table 5.24 shows the torsional stiffness formula from laminate theory and thin-walled beam theory.

**Table 5.24 Torsional stiffness formula from laminate and beam theory**

	From laminate theory	From thin-walled beam theory (Armanios formula)
Torsional stiffness formula	$G_{xy} \cdot J = \frac{1}{t} (A_{33}) \cdot J$	$GJ = \oint \frac{1}{\oint (1/4(A_{33})) ds} A_e^2$

### 5.6.2.3 Coupling coefficient ( $m$ ) and coupling stiffness ( $CK$ ) formula from laminate and beam theory

From laminate theory, coupling coefficient

$$\begin{aligned}
 m_x &= - \frac{a_{13}}{a_{11}} \\
 &= - \frac{A_{13}A_{22} - A_{12}A_{23}}{A_{22}A_{33} - A_{23}^2} \quad (5.29)
 \end{aligned}$$

For composite box, from Armanios formula, coupling stiffness

$$CK = -\frac{\oint (B(s)/C(s))z ds}{\oint (1/C(s))ds} A_e \quad (5.30)$$

$$CK = -\frac{\oint \frac{A_{13}A_{22}-A_{12}A_{23}}{2(A_{22}A_{33}-A_{23}^2)}z ds}{\oint \left( \frac{A_{22}}{4(A_{22}A_{33}-A_{23}^2)} \right) ds} A_e \quad (5.31)$$

From Equation (5.29)

$$-\frac{B(s)}{C(s)} = -\frac{a_{13}}{a_{11}} = m_x \quad (5.32)$$

From composite laminate theory,

$$\begin{aligned} G_{xy} &= \frac{1}{t.a_{33}} \\ a_{33} &= \frac{A_{11}A_{22}-A_{12}^2}{A} \\ &= \frac{1}{A} \left( A_{22} \left( A_{11} - \frac{A_{12}^2}{A_{22}} \right) \right) \end{aligned} \quad (5.33)$$

From Equation (5.18)

$$A(s) = A_{11} - \frac{A_{12}^2}{A_{22}}$$

Therefore

$$\begin{aligned} G_{xy} &= \frac{1}{t.a_{33}} \\ &= \frac{1}{t \cdot \left( \frac{1}{A} \left( A_{22} \left( A_{11} - \frac{A_{12}^2}{A_{22}} \right) \right) \right)} \\ &= \frac{1}{t \cdot \left( \frac{1}{A} (A_{22} \cdot A(s)) \right)} \\ &= \frac{A}{t \cdot A_{22} \cdot A(s)} \end{aligned} \quad (5.34)$$

Insert Equations (5.32) and (5.34) inside Equation (5.31)

$$\begin{aligned}
CK &= -\frac{\oint \frac{1}{2} \left( \frac{a_{13}}{a_{11}} \right) z ds}{\oint 4 a_{11} \frac{A}{A_{22}} ds} A_e \\
&= \frac{\frac{1}{2} \oint (m_x) z ds}{-4 \oint a_{11} \frac{A}{A_{22}} ds} A_e \\
&= \frac{\frac{1}{2} \oint (m_x) z ds}{-4 \oint \frac{G_{xy}}{E_x} A(s) ds} A_e \tag{5.35}
\end{aligned}$$

Table 5.25 shows the torsional stiffness formula from laminate theory and thin-walled beam theory.

**Table 5.25 Coupling stiffness formula from laminate and beam theory**

	From laminate theory (Coupling coefficient, $m_x$ )	From thin-walled beam theory (Armanios formula) (Coupling stiffness, $CK$ )
Coupling formula	$m_x = -\frac{A_{13}A_{22} - A_{12}A_{23}}{A_{22}A_{33} - A_{23}^2}$ $m_x = -\frac{a_{13}}{a_{11}}$	$CK = -\frac{\oint \frac{A_{13}A_{22} - A_{12}A_{23}}{2(A_{22}A_{33} - A_{23}^2)} z ds}{\oint \left( \frac{A_{22}}{4(A_{22}A_{33} - A_{23}^2)} \right) ds} A_e$ $= -\frac{\oint \frac{1}{2} \left( \frac{a_{13}}{a_{11}} \right) z ds}{\oint 4 a_{11} \frac{A}{A_{22}} ds} A_e$ $= \frac{\frac{1}{2} \oint (m_x) z ds}{-4 \oint \frac{G_{xy}}{E_x} A(s) ds} A_e$

The  $m_x$  value is obtained from the material properties while  $z$ ,  $ds$  and  $A_e$  are from the geometrical properties. In  $CK$  formula, the  $\frac{G_{xy}}{E_x}$  term shows the ratio magnitude of shear and in-plane elastic constant, respectively.  $A(s)$  in the formula is the reduced axial stiffness term.

### 5.6.2.4 Design tool

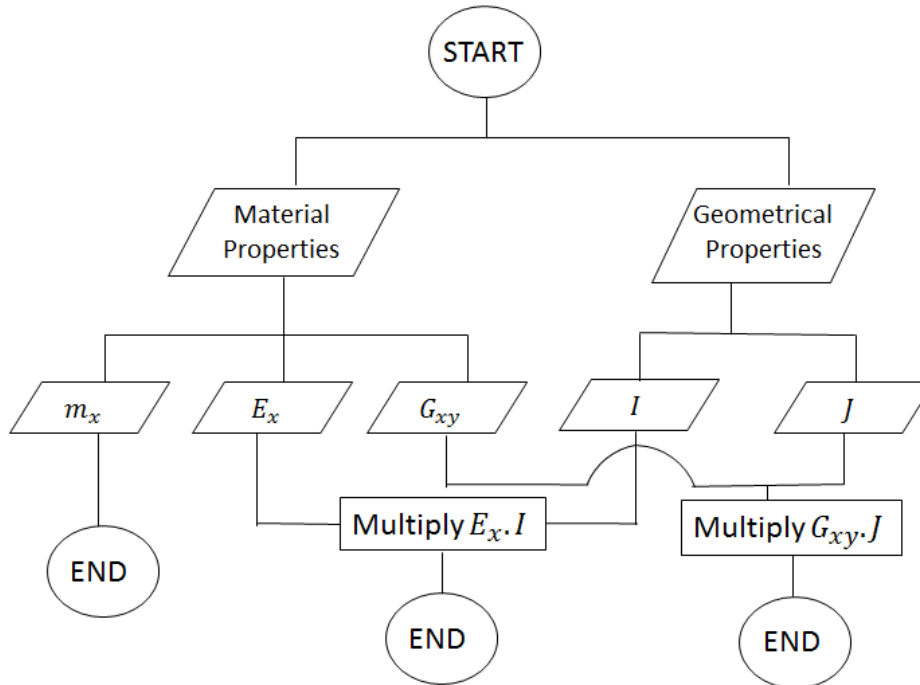


**Figure 5.56 New conceptual framework for design tool to calculate bending stiffness,  $EI$ , torsional stiffness,  $GJ$  and coupling coefficient,  $m_x$**

From the bending stiffness, torsional stiffness and coupling stiffness formula in Table 5.23, Table 5.24 and Table 5.25, respectively, a simple but very useful design tool has been developed to predict the stiffness of the structure during the material selection process and laminate design stage. From the material properties and geometrical properties, bending stiffness, torsional stiffness and coupling stiffness can be computed easily by following the framework in Figure 5.56. In order to calculate the results of bending stiffness, value of  $E_x$  from material properties to be multiplied with the  $I$  value from the geometrical properties. Same goes to calculate torsional stiffness, value of  $G_{xy}$  from material properties has to be multiplied with the value of  $J$  taken from the geometrical properties. The pattern of coupling coefficient,  $m_x$  can be predicted by referring Figure 5.57.

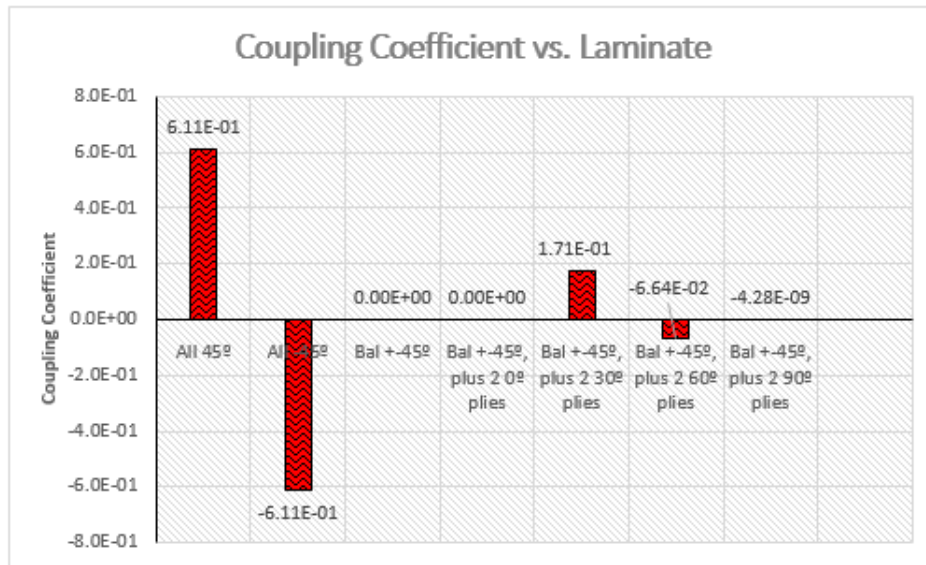


**Figure 5.57 Coupling coefficient against laminate for different ply orientation**

The correlation between laminate and composite box developed in Table 5.23, Table 5.24 and Table 5.25 can be used to correlate the stiffness of 1-dimensional to 2-dimensional beam structure.

### 5.6.3 Method 3: Use Thin-Walled Beam Theory and FE Model (2-dimensional to 3-dimensional box)

This method is used to correlate the 2-dimensional box to 3-dimensional box. The existing methodology is applied in this method to calculate box stiffness where for 2-dimensional box beam, the thin-walled composite beam theory using the Armanios formula is applied. For 3-dimensional box beam, FE model was created and analysis was carried out by using the Euler-Bernoulli beam theory.

#### 5.6.3.1 Bending Stiffness

For 2-dimensional box, recall Equation 6, bending stiffness

$$EI = \oint \left( A(s) - \frac{B(s)^2}{C(s)} \right) z^2 ds + \frac{[\oint (B(s)/C(s))z ds]^2}{\oint (1/C(s))ds}$$

For 3-dimensional box (FE model), from Euler-Bernoulli beam theory, bending stiffness

$$EI = \frac{ML}{\theta(L)} \quad (5.36)$$

where  $M$  is the applied bending moment,  $L$  is the length of the box and  $\theta(L)$  is the angle of rotation in radian.

Figure 5.58 illustrates the example of bending moment loads and the boundary condition applied on the FE model.

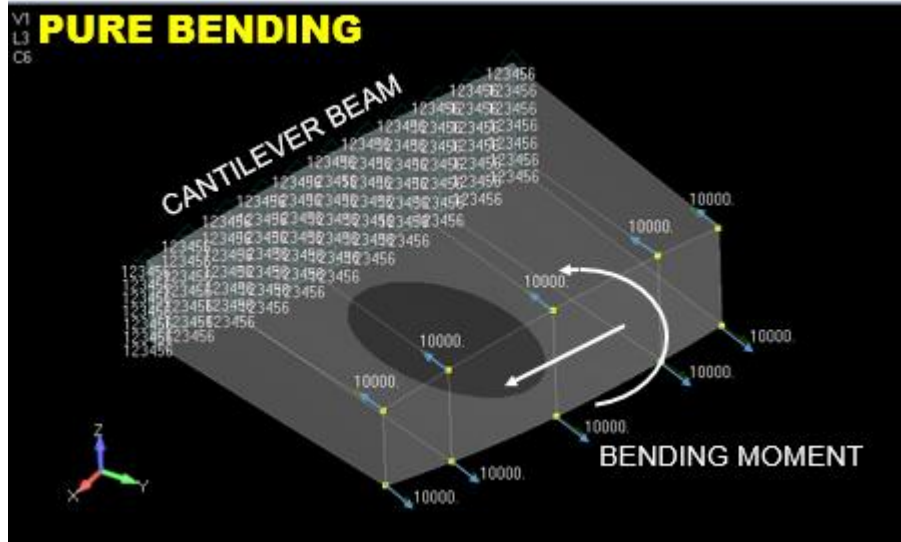


Figure 5.58 Example of bending moment load and boundary condition

### 5.6.3.2 Torsional Stiffness

For 2-dimensional box, recall Equation (5.26), torsional stiffness

$$GJ = \frac{1}{\oint (1/C(s)) ds} A_e^2$$

For 3-dimensional box (FE model), from Euler-Bernoulli beam theory, torsional stiffness

$$GJ = \frac{TL}{\psi(L)} \quad (5.37)$$

where  $T$  is the applied torque,  $L$  is the length of the box and  $\psi(L)$  is the twist angle of the cross section in radian.

Figure 5.59 illustrates the example of torsional loads and the boundary condition applied on the FE model.

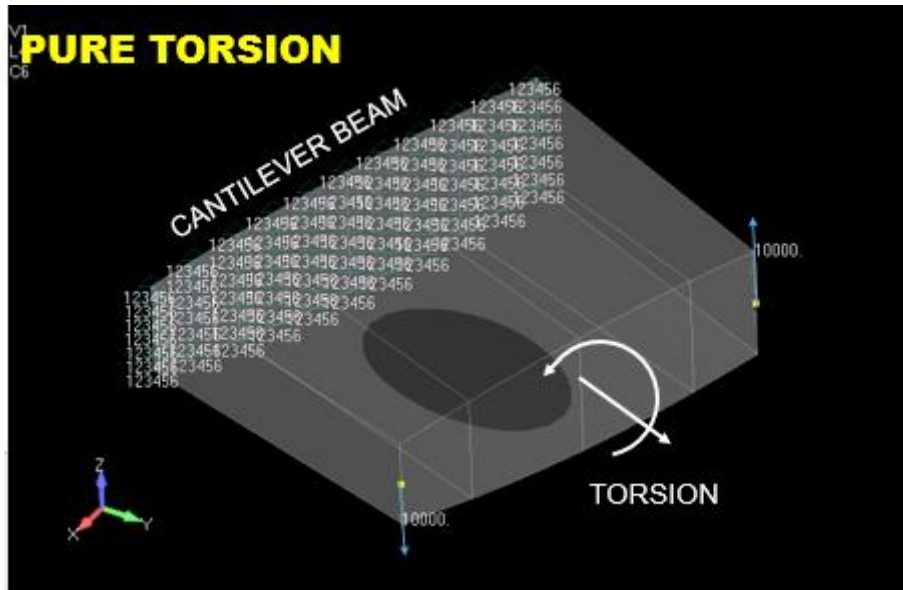


**Figure 5.59 Example of applied torque and boundary condition**

The 3-dimensional box in FE model represents the real case. There are some parameters that 2-dimensional model does not take into account which include:

1. Manhole
2. Width to length ratio
3. Taper ratio

On the other hand, for coupling, the 2-dimensional box can be calculated using thin-walled beam theory, but for 3-dimensional model, the Euler-Bernoulli beam theory is for pure bending and pure torsion only. There is no formula available to calculate coupling coefficient for FE model.

To correlate the parameters between 2-dimensional and 3-dimensional box, the cut-out, width to length ratio and taper ratio study have been carried out and analysed.

### **5.6.3.3 Manhole study**

Wing box sections with manhole and without manhole have been created in Femap for this study. The cut-out is located on the lower skin of the wing box section. The box sections are illustrated in Figure 5.60.



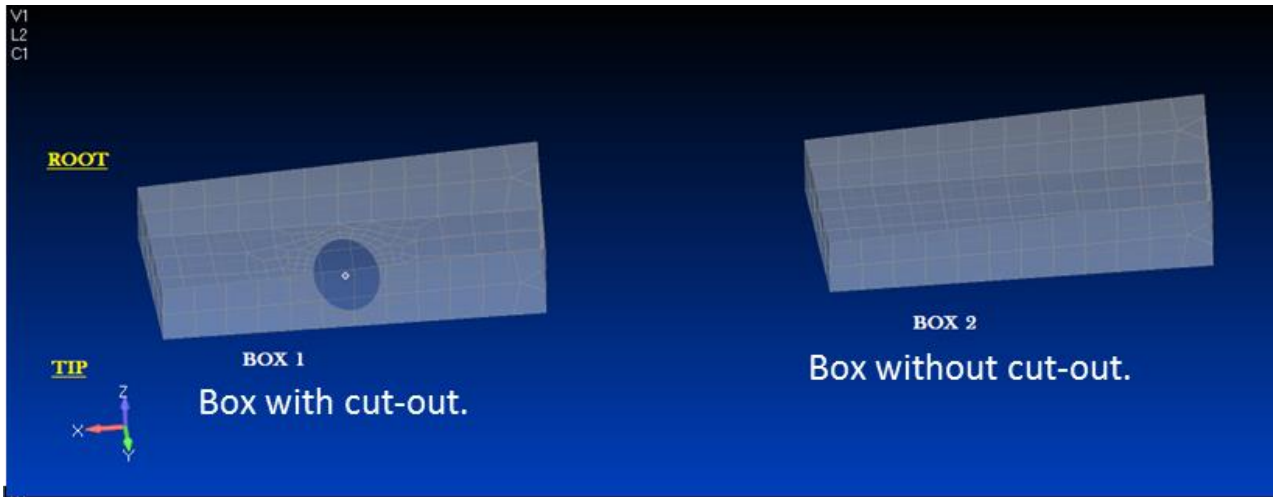


**Figure 5.60 Box section with cut-out (left) and without cut-out (right)**

Both boxes have similar length and width as shown in Figure 5.61. The box width is 1.4m and the length is 0.6m. Box with manhole has an elliptical shape cut-out. The major radius of the cut-out is 0.2m and the minor radius is 0.1m, which gives the cut-out radius  $0.13\text{m}^2$ .

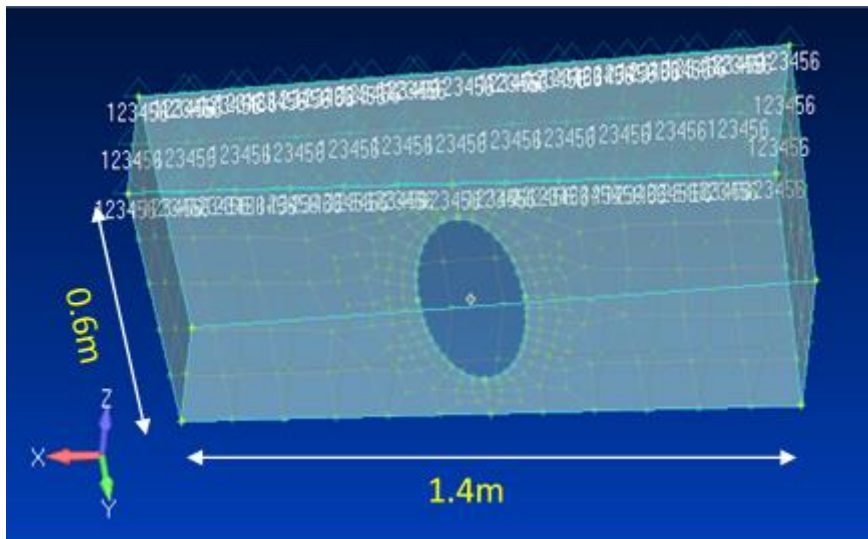


**Figure 5.61 Dimension of box with hole**

The bending and torsional stiffness analyses were carried out on the box model using NASTRAN. Table 5.26 and Table 5.27 shows the material properties for aluminium and composite, respectively.

**Table 5.26 Material properties for aluminium**

Material	Material Properties			
	Young's Modulus, $E$ (Pa)	Shear Modulus, $G$ (Pa)	Poisson's ratio, $\nu_{12}$	Thickness, $t$ (m)
Aluminium	7E10	2.7E10	0.27	0.007

**Table 5.27 Material properties for composite**

Material	Material Properties						
	Young's Modulus, $E_1$ (Pa) $E_2$ (Pa)		Shear Modulus, $G_{12}$ (Pa) $G_{13}$ (Pa) $G_{23}$ (Pa)			Poisson's ratio, $\nu_{12}$	Ply thickness, $t$ (mm)
Composite	1.43E11	1.03E10	5.3E09	5.3E09	5.3E09	0.27	0.183

Bending stiffness and torsional stiffness analysis for box with and without cut-out were performed in NASTRAN. Analysis were carried out for aluminium and composite material. Results for bending stiffness are shown in Figure 5.62 and Figure 5.63 illustrates the graph results. From Figure 5.63, for aluminium, the cut-out has reduced 10.2% bending stiffness. For composite, bending stiffness is decreased by 5.13%.

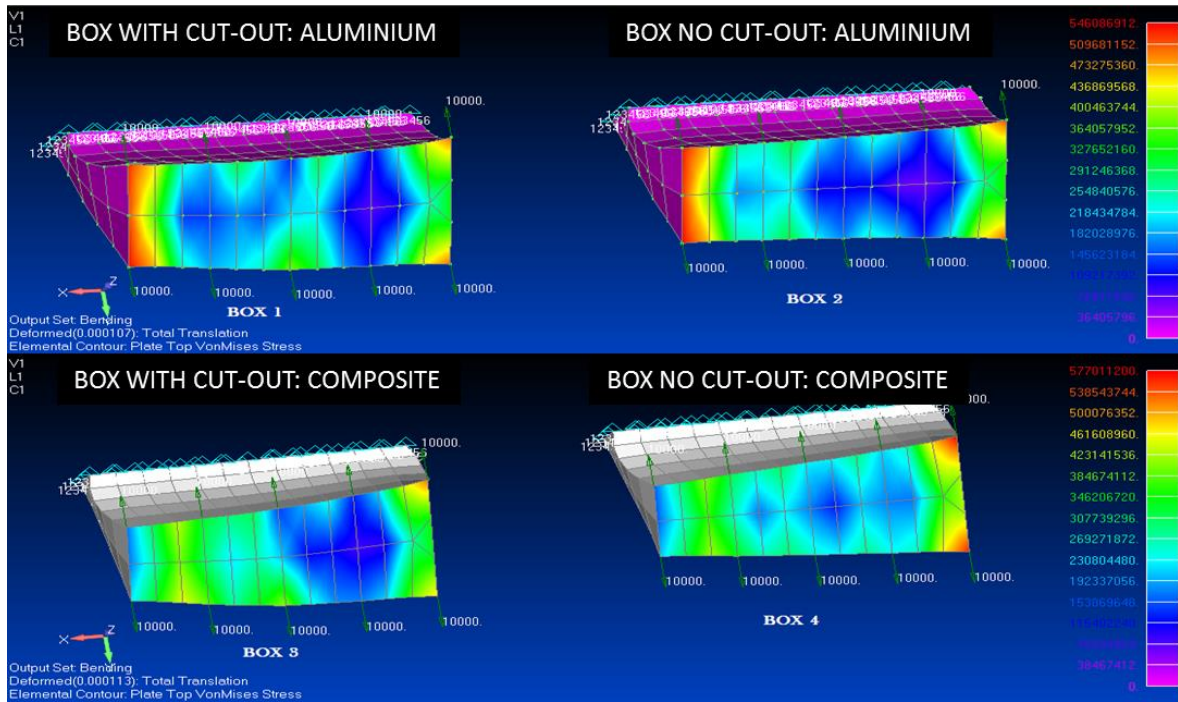


Figure 5.62 Bending stiffness results from NASTRAN

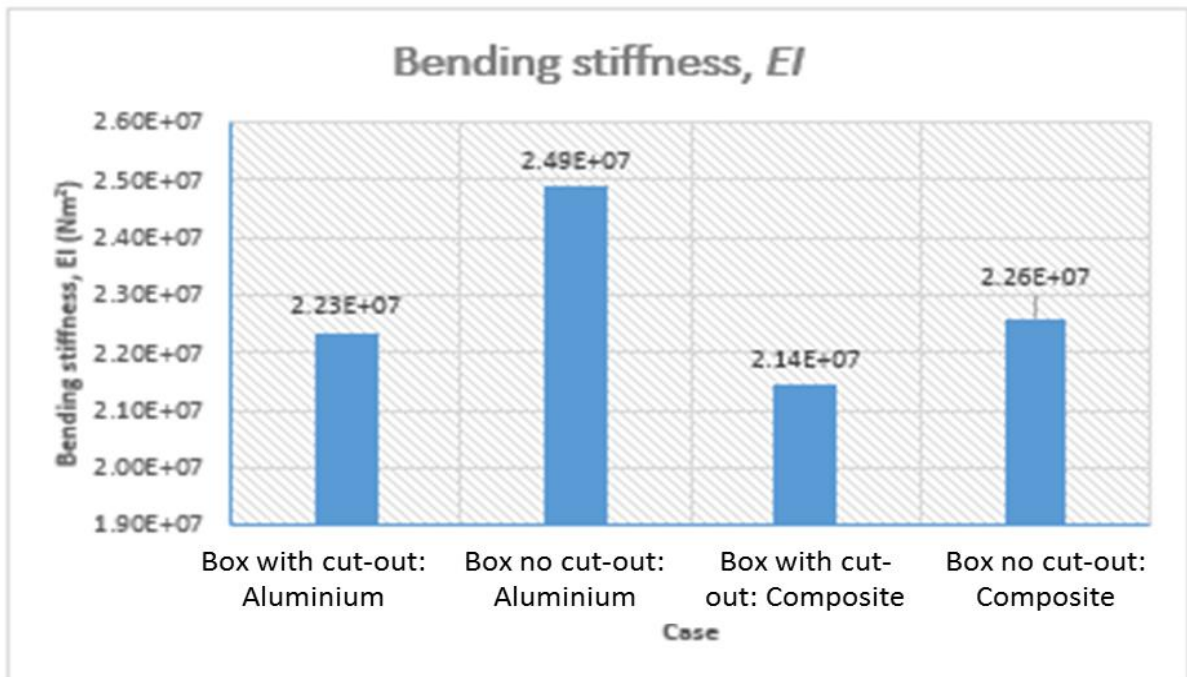


Figure 5.63 Bending stiffness results box with and without cut-out

Torsional stiffness results in NASTRAN are presented in Figure 5.64. Results are then illustrated in Figure 5.65. The reduction of torsional stiffness due to cut-out is 2.99% for aluminium and 1.95% for composite.

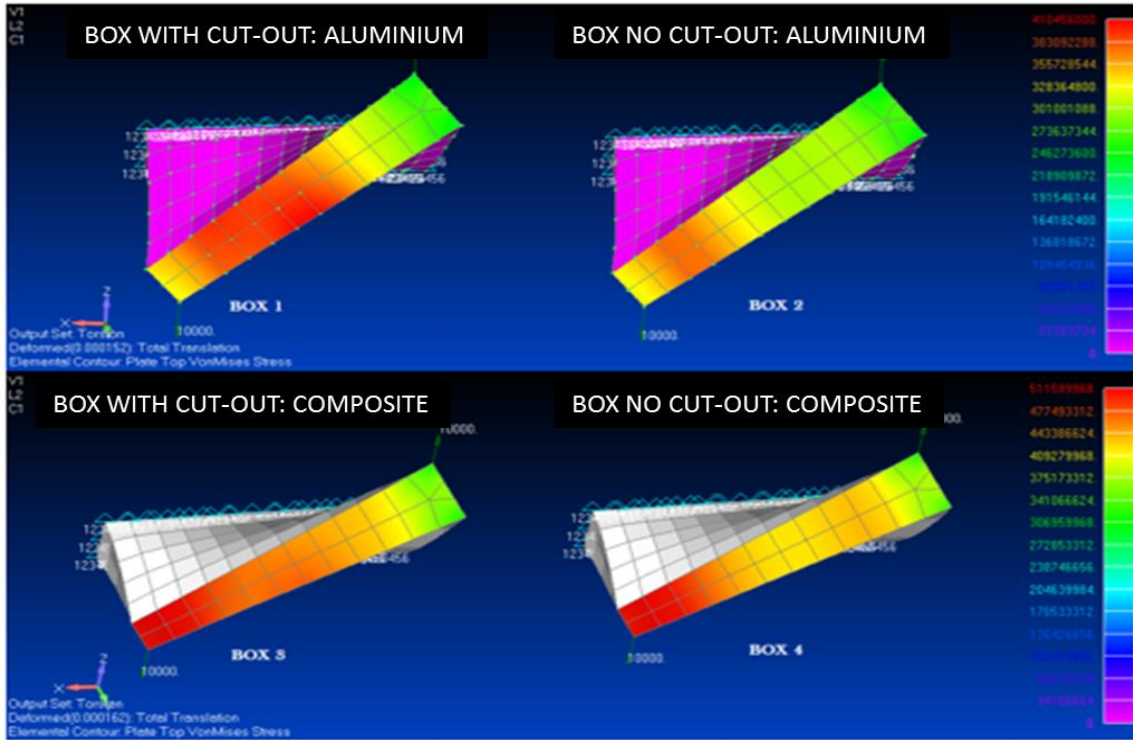


Figure 5.64 Torsional stiffness results from NASTRAN

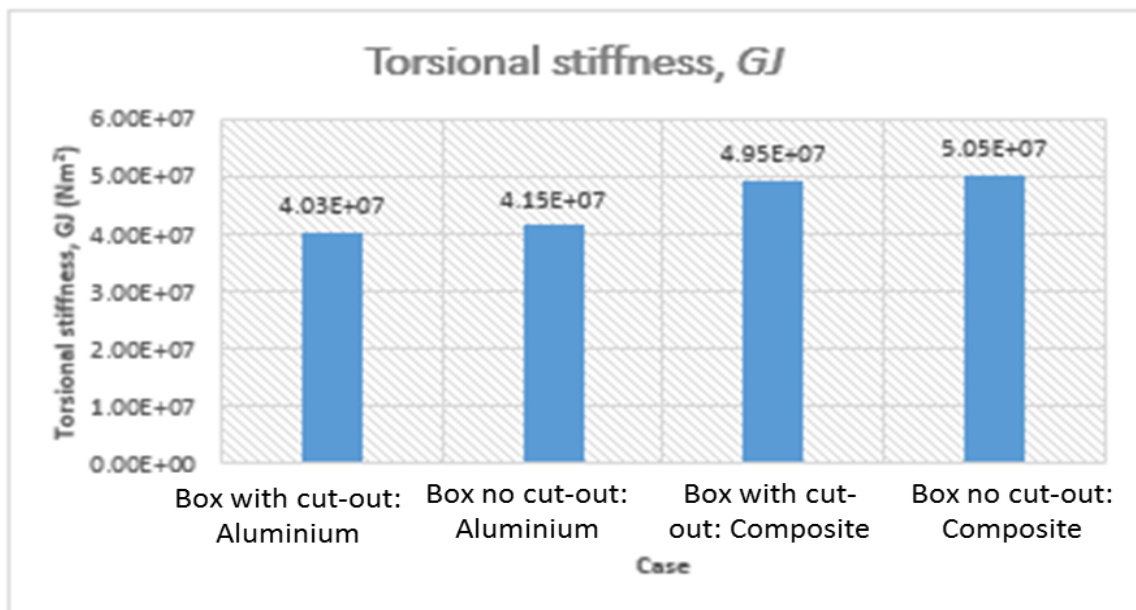


Figure 5.65 Torsional stiffness results for box with and without cut-out

Figure 5.66 and Table 5.28 show the percentage reduction of bending stiffness and torsional stiffness due to cut-out. The cut-out area is 15% of the lower skin panel area. For bending stiffness, aluminium and composite boxes are reduced by 10.2% and 5.13%, respectively. Aluminium box with cut-out has decreased the torsional stiffness by 2.99%, while for composite box, the torsional stiffness are reduced by 1.95%.

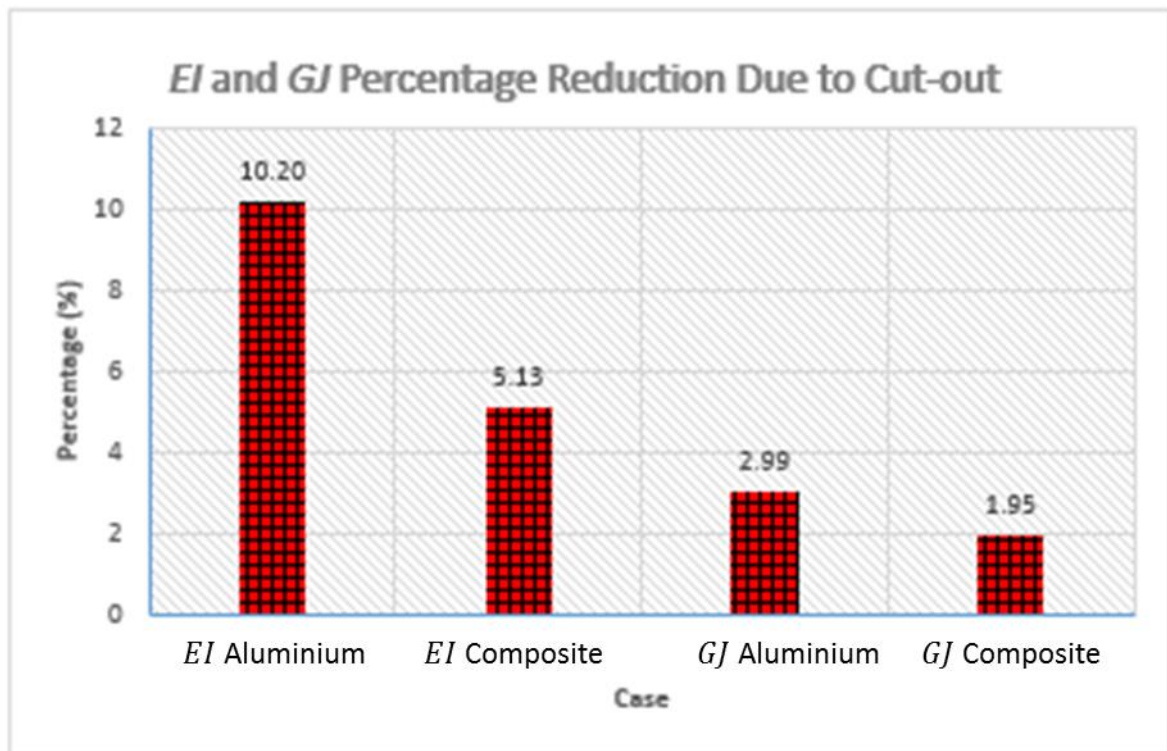


Figure 5.66 *EI* and *GJ* percentage reduction due to cut-out

Table 5.28 The percentage of *EI* and *GJ* reduction due to cut-out

Case	<i>EI</i> and <i>GJ</i> reduction due to cut-out (%)
EI aluminium	10.20
EI composite	5.13
GJ aluminium	2.99
GJ composite	1.95

### 5.6.3.4 Width to length ratio study

The width to length ratio study was carried out to see the cut-out effect of different box length to the bending stiffness. Two box models have been created in Femap for this analysis. Box 1 has 0.6m length while Box 2 has 1.95m length. Both boxes have been fixed to 1.4m width, as shown in Figure 5.67.

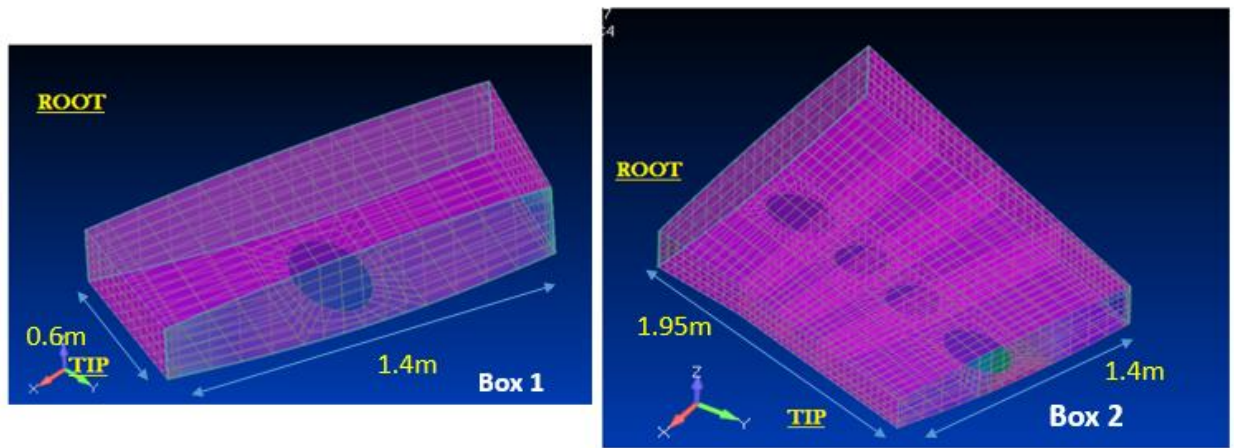


Figure 5.67 Different box dimensions for bending stiffness analysis

The bending stiffness analysis was run in NASTRAN. Refer results in Table 5.29, the bending stiffness increases with the increased of the box length. In this study, the length ratio of Box 1 to Box 2 is 0.6 to 1.95. With the addition of 69% of the box length, bending stiffness is increased by 21%.

Table 5.29 Bending stiffness result for width to length ratio study

Case	Bending stiffness, $EI$ ( $\text{Nm}^2$ )
Box 1	2.51E07
Box 2	3.16E07

### 5.6.3.5 Taper ratio study

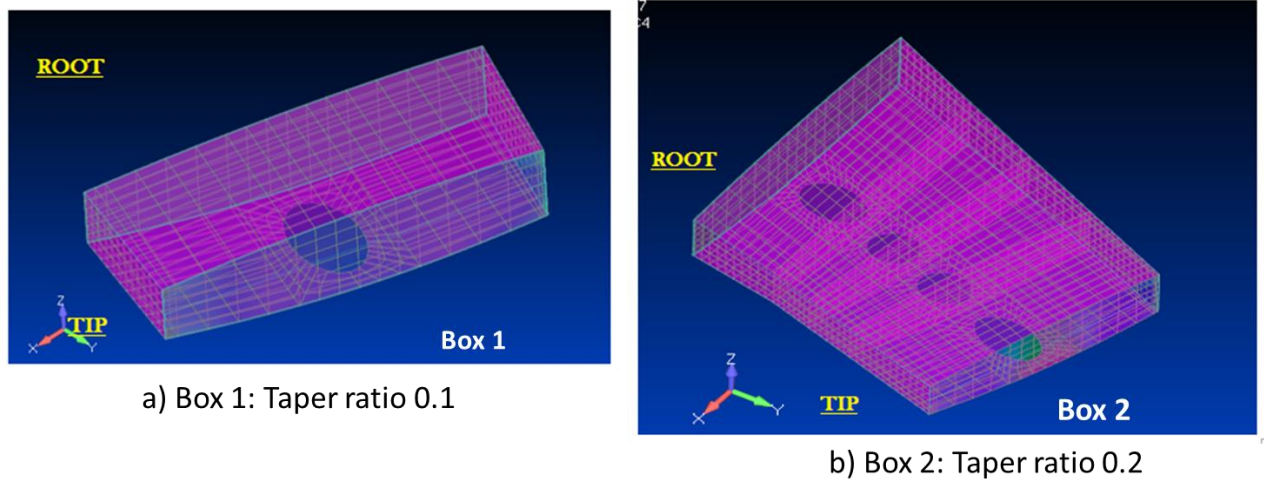


**Figure 5.68 Different taper ratio for torsional stiffness analysis**

Two box models have been created in Femap to see the effect of cut-out of the different taper ratio to the torsional stiffness. As shown in Figure 5.68, Box 1 has 0.1 taper ratio while Box 2 has 0.2 taper ratio. The torsional stiffness analysis is carried out in NASTRAN. The analysis was run for aluminium and composite material. Results of this analysis are presented in Table 5.30.

**Table 5.30 Torsional stiffness results for taper ratio study**

Case	$GJ$ (Nm <sup>2</sup> )
Box 1: Aluminium	5.15E07
Box 1: Composite	4.36E07
Box 2: Aluminium	4.69E07
Box 2: Composite	3.92E07

From Table 5.30, the results show that if the taper ratio is doubled, therefore the cut-out will reduce the torsional stiffness of aluminium box by 8.9% while the torsional stiffness of composite box is reduced by 10%.

## 6 STRESS, BUCKLING, FREE VIBRATION AND AEROELASTIC ANALYSIS OF COMPOSITE WING

Stress, buckling, free vibration and aeroelastic analysis has been carried out on a future transport composite wing in the current case study. The wing model in the form of NASTRAN input file has been extensively used and substantially modified to carry out the work for the project. This wing FE model is hereafter referred to as baseline model.

The baseline model included the finite element idealisation and the critical aerodynamic load based on 2.5g normal acceleration. The composite skin properties, layup orientation and stacking sequence which are all required for the baseline wing have been pre-determined in an initial design. The wing geometry has manholes in the lower skins of the box sections and the landing gear box lower skins have been removed.

To generate equivalent laminate properties, the low fidelity method was first used to provide input for the high fidelity analysis. From the skin properties provided, BOXMX Program [95] was first run to determine the equivalent elastic constants,  $E_x$ ,  $E_y$  and shear modulus  $G_{xy}$  which became the input for FEMAP with NASTRAN to calculate the bending stiffness,  $EI$  and torsional stiffness,  $GJ$  of the wing. These stiffness properties,  $EI$  and  $GJ$  are then used to create the data needed for COMFLUT Program [99] to calculate the free vibrational modes and flutter speed (see Appendix C for COMFLUT Program example). BOXMX and COMFLUT are the FORTRAN based program used extensively throughout the research.

The data from the initial design have been consistently used throughout the investigation. The layout and general geometric data and other parameters for the baseline model are shown in Figure 6.1 and Table 6.1-Table 6.3.



## 6.1 General Information

The current baseline FE model is shown in Figure 6.1. The general information including aerodynamic, geometric, material properties and mass data of the baseline wing are given in Table 6.1-Table 6.3.

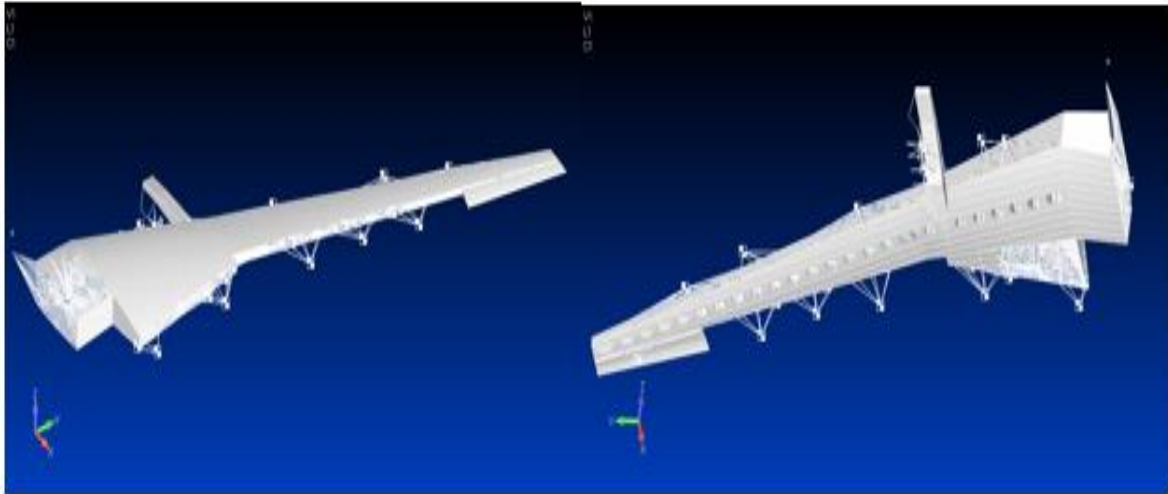


Figure 6.1 FE model of baseline wing

Table 6.1 General parameters of baseline wing

Geometric Parameter	Value
Aspect Ratio	10
Wing Area	92.25 m <sup>2</sup>
Wing Span	30.42 m
Root Chord	5.30 m
Tip Chord	1.34 m
Mean Aerodynamic Chord	3.363 m

**Table 6.2 Material properties of baseline wing**

Location	Material	Material Properties				
Spars, Stringers, Ribs & Web stiffeners	Aluminium	Density (kg/m <sup>3</sup> )	E (Pa)	G (Pa)	$\nu$	
		2700	7.0E10	2.69E10	0.3	
Pylon (Density=0),						
Skins	Composite Laminate		E <sub>1</sub>	E <sub>2</sub>	G <sub>12</sub>	$\nu_{12}$
		1580	1.48E+11	1.03E10	5.93E9	0.27

**Table 6.3 Mass data**

Components	Mass (Kg)
Fuselage (Half)	15000
Wing Structural (Single)	1800
Wing Non-Structural (Leading & Trailing Edge; Landing Gear)	1800
Engine & Pylon	3100
Fuel for Single Wing	7300
<b>Total Mass</b>	<b>29000</b>

## 6.2 Skin Laminate Properties

The skin composite laminate data are from the baseline model initial design. The locations of skin composite laminates from wing root to wingtip are presented in Figure 6.2.

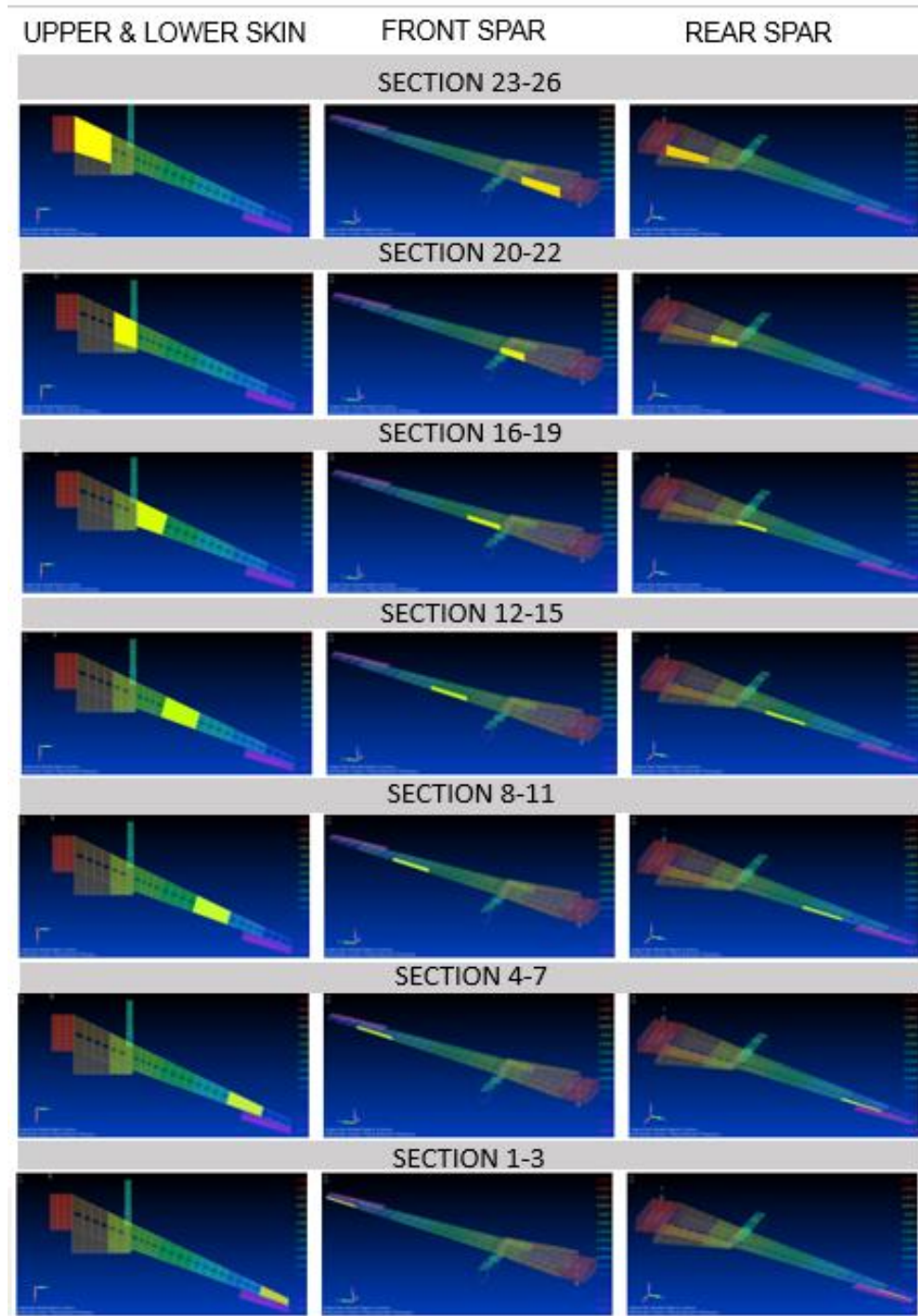
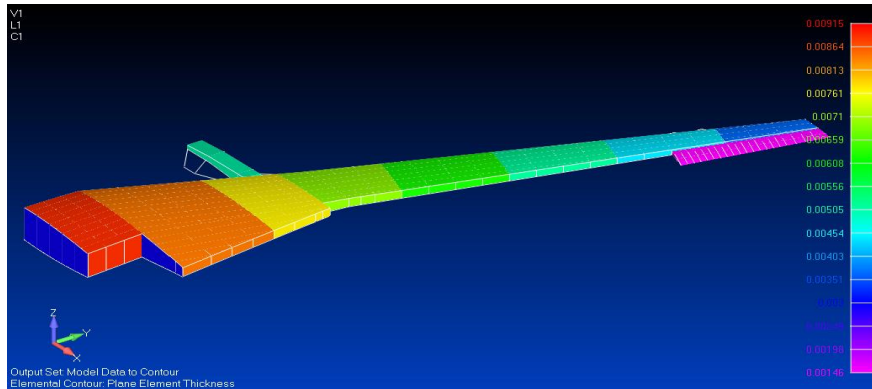


Figure 6.2 Locations of skin composite laminates from root to tip

The skin thickness distribution is shown in Figure 6.3 and the equivalent elastic constants of the laminates at different sections are given in Table 6.4.



**Figure 6.3 Composite wing skin thickness distributions  
(min  $t=1.46\text{mm}$ , max  $t=9.15\text{mm}$ )**

**Table 6.4 Equivalent elastic properties of skin composite laminates**

Section No. & Location	$E_x$	$E_y$	$G_{xy}$
<b>Section 1-3</b>			
Upper Skin, Lower Skin, Rear Spar	0.510E11	0.636E11	0.219E11
Front Spar	0.518E11	0.518E11	0.254E11
<b>Section 4-7</b>			
Upper Skin, Front Spar, Rear Spar	0.576E11	0.576E11	0.222E11
Lower Skin	0.569E11	0.569E11	0.213E11
<b>Section 8-11</b>			
Upper Skin, Lower Skin, Front Spar, Rear Spar	0.620E11	0.529E11	0.220E11
	0.529E11	0.620E11	0.220E11
<b>Section 12-15</b>			
Upper Skin, Front Spar,	0.554E11	0.629E11	0.212E11
	0.572E11	0.572E11	0.217E11
Lower Skin, Rear Spar	0.559E11	0.559E11	0.230E11
<b>Section 16-19</b>			
Upper Skin, Front Spar	0.529E11	0.594E11	0.230E11
Lower Skin, Rear Spar	0.591E11	0.526E11	0.227E11
<b>Section 20-22 (Double Cell)</b>			
Upper Skin, Front Spar, Lower Skin	0.562E11	0.562E11	0.229E11
Rear Spar, Mid Wall	0.621E11	0.502E11	0.229E11
<b>Section 23-26 (Double Cell)</b>			
Upper Skin, Lower Skin, Rear Spar, Mid Wall	0.591E11	0.537E11	0.229E11
Front Spar	0.589E11	0.535E11	0.226E11

## 6.3 Stiffness Analysis

For stiffness analysis, the in-house beam-box program called BOXMX Program is used to calculate the bending and torsional stiffness of the wing box side by side to a numerical FEM approach which uses FEMAP with NASTRAN.

### 6.3.1 Wing Box Sections

For the bending stiffness and torsional stiffness calculation, the wing box was initially divided into 26 span wise sections numbered from tip to root according to the ribs position as shown in Figure 6.4.

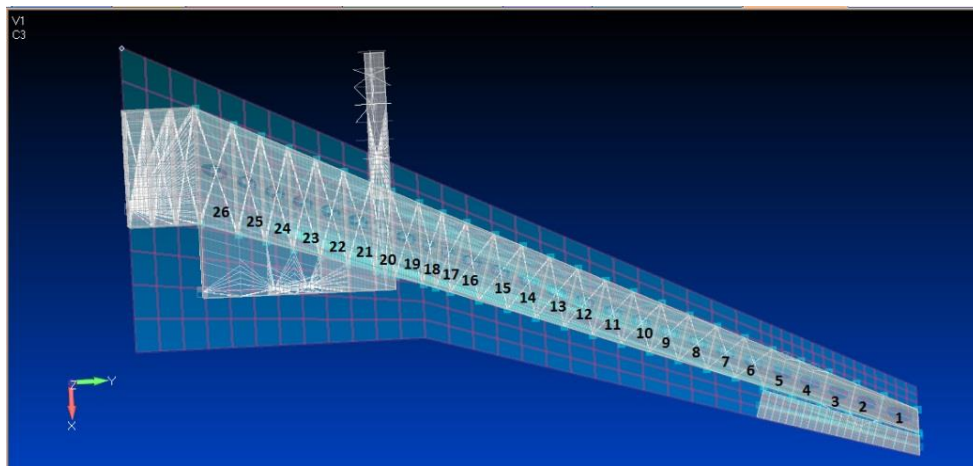


**Figure 6.4 Wing box sections along the span**

Sections 1 to 19 are idealised as single-cell box whereas sections 20 to 26 are considered as double-cell box. It should be noted that section 1 is near the wing tip and section 19 is just before the pylon when viewed from the tip end. For sections 23 to 26, one of the two cells, which is located in the rear of the mid-spar, the lower skin is ignored in the analysis because the corresponding area is effectively empty to accommodate for the landing gears. Bending stiffness and torsional stiffness analysis were carried out at each section using FEM through FEMAP with NASTRAN and the results were compared with those calculated from the analytical approach using BOXMX Program.

Details of laminate layup and stacking sequence used for each section are shown in

Table 6.5. Thickness for each laminate is  $1.83 \times 10^{-4}$  m. All laminate layup, stacking sequence and laminate thickness applied in this analysis are based on the baseline data.

**Table 6.5 Laminate layup and stacking sequences**

SECTION	LAMINATE LAYUP	
SECTIONS 1-3	UPPER SKIN	[45/45/0/45/0/-45/90/-45/90/90]s
	LOWER SKIN	[45/45/0/-45/0/45/90/-45/90/90]s
	FRONT SPAR	[45/0/45/45/-45/0/-45/90/90/-45]s
	REAR SPAR	[45/45/0/45/0/-45/90/90-45/90]s
SECTIONS 4-7	UPPER SKIN	[45/45/0/45/0/0/-45/-45/90/-45/90/90]s
	LOWER SKIN	[45/45/0/45/-45/0/45/0/90/45/90/90]s
	FRONT SPAR	[45/0/45/45/-45/0/0/-45/90/90/-45/90]s
	REAR SPAR	[45/45/0/45/0/-45/0/-45/90/90/-45/90]s
SECTIONS 8-11	UPPER SKIN	[45/45/0/45/45/0/0/-45/-45/90/0/-45/90/90]s
	LOWER SKIN	[45/45/0/45/-45/0/45/0/0/90/-45/-45/90/90]s
	FRONT SPAR	[45/0/45/45/45/-45/0/0/-45/90/90/90/-45/90]s
	REAR SPAR	[45/45/0/45/45/0/-45/0/-45/90/90/90-45/90]s
SECTIONS 12-15	UPPER SKIN	[45/45/0/45/45/0/0/-45/-45/90/0/-45/90/90/90/90/-45/90]s
	LOWER SKIN	[45/45/0/45/45/-45/0/45/0/0/90/-45/-45/90/90/90/-45]s
	FRONT SPAR	[45/0/45/45/45/-45/45/0/0/0/-45/90/90/90/-45/90]s
	REAR SPAR	[45/45/0/45/45/0/45/0/-45/0/-45/-45/90/90/90/-45/90]s
SECTIONS 16-19	UPPER SKIN	[45/45/45/0/45/45/0/0/-45-45/90/0/-45/-45-90/90/90/-45/90/90/90/-45/90]s
	LOWER SKIN	[45/45/45/0/0/45/45/-45/0/45/0/0/90/-45/45/90/90/90-45]s
	FRONT SPAR	[45/0/45/45/45/-45/45/0/0/0/-45/90/-45/90/-45/90/90/-45/90]s
	REAR SPAR	[45/45/45/0/45/45/0/45/0/0/-45/0/-45/-45/90/90/90/-45/90]s
SECTIONS 20-22	UPPER SKIN	
	1. FRONT BOX	[45/45/45/0/45/45/0/0/-45/-45/90/0/-45/0/-45/-45/90/90/90/-45/90]s
	2. REAR BOX	[45/45/45/0/45/45/0/0/-45/-45/90/0/-45/0/-45/-45/90/90/90/-45/90]s
	LOWER SKIN	
	1. FRONT BOX	[45/45/45/0/0/45/45/-45/0/-45/45/0/0/90/-45/-45/90/90/90/90/-45]s
	2. REAR BOX	[45/45/45/0/0/45/45/-45/0/-45/45/0/0/90/-45/45/90/90/90/90/-45]s
	FRONT SPAR	[45/0/45/45/45/-45/45/45/0/0/0/0/-45/90/-45/90/-45/90/90/-45/90]s
REAR SPAR	[45/45/45/45/0/0/45/45/0/0/-45/-45/0/-45/90/-45/90/-45/90/90/90/90/-45]s	
MIDWALL	[45/45/45/0/45/45/0/45/-45/0/0/0/-45/0/-45/-45/90/90/90/-45/90]s	
SECTIONS 23-26	UPPER SKIN	
	1. FRONT BOX	[45/45/45/45/0/45/45/0/0/0/-45/-45/90/0/-45/0/-45/-45/90/90/90/-45/90]s
	2. REAR BOX	[45/45/45/45/0/45/45/0/0/0/-45/-45/90/0/-45/0/-45/-45/90/90/90/-45/90]s
	LOWER SKIN	
	1. FRONT BOX	[45/45/45/0/0/45/45/-45/0/-45/45/0/0/90/0/-45/-45/90/90/90/90/-45/-45]s
2. REAR BOX	[45/45/45/0/0/45/45/-45/0/-45/45/0/0/90/0/-45/-45/90/90/90/90/-45/-45]s	

FRONT SPAR	[45/0/45/45/45/-45/45/45/0/45/0/0/0/0/-45/90/-45/90/-45/90/90/-45/90]s
REAR SPAR	[45/45/45/45/0/0/45/45/0/0/-45/-45/0/-45/-45/90/-45/0/90/90/90/90/-45]s
MIDWALL	[45/45/45/0/45/45/0/45/-45/0/0/0/-45/0/-45/-45/90/90/-45/90/-45/90/90]s

### 6.3.2 Stiffness Evaluation using BOXMX Program

For each of the box sections, the bending, torsion and bending- torsion coupling rigidities  $EI$ ,  $GJ$  and  $CK$  have been obtained based on its geometry, properties and laminate lay-ups using the method from Armanios and Badir [17].

From FE model, the baseline wing was split into 26 sections. Each of the 26 cross sections was at the middle of two successive ribs which cut across the centre line of each manhole. Among these 26 sections, the first 19 sections are made up of single-cell whereas the remaining sections 20-26 are idealised as double-cells. BOXMX Program needs the coordinates of each part divided around the circumference of the box section which is difficult to obtain directly from FEMAP with NASTRAN and furthermore, the BOXMX Program prefers the wing box section to be roughly symmetrical about the horizontal axis. So as an acceptable alternative, the dimensions needed for the 26 wing box sections are found from FEMAP with NASTRAN as distance between two nodes along upper skin, lower skin, front spar, rear spar (for sections 1-19) and middle spar (for sections 20-26). Upper skin and Lower skin were further subdivided between two stringers. AUTOCAD is then used to plot these parts to recreate the 26 cross-sections. By using AUTOCAD, coordinates of each part were identified along the circumference of the wing box sections. Using these coordinates, element properties, material properties, laminate layup and stacking sequence, the input data file for BOXMX program was created. As required, two different input files are created, one for the single-cell and the other is for the double-cell. The output from BOXMX Program gives stiffness properties,  $EI$  and  $GJ$  and elastic constants  $E_x$ ,  $E_y$  and  $G_{xy}$ .

The elastic constants  $E_x$ ,  $E_y$  and  $G_{xy}$  obtained from BOXMX program are then fed into FEMAP with NASTRAN to determine the stiffness properties  $EI$  and  $GJ$ . Note that the BOXMX Program does not take into account the contribution of the

stringers. So by using the parallel axis theorem, effect of the stringer was taken into account.

When comparing the values obtained using BOXMX Program and FEMAP with NASTRAN, there are considerable discrepancies in the results. It was adjudged best to use stiffness properties from NASTRAN for further analysis because BOXMX Program at present is deficient in stiffness calculation of cross-sections with cut-outs.

The following tables and graphs show the results of bending stiffness and torsional stiffness calculated from the BOXMX Program. Table 6.6 presents the bending stiffness and the result is illustrated in Figure 6.5.

Table 6.7 shows the torsional stiffness result and the graph is plotted in Figure 6.6.



**Table 6.6 Bending stiffness of the wing box sections from BOXMX Program**

<b>SECTION</b>	<b>Bending Stiffness (Nm<sup>2</sup>)</b>
1	2.76E+06
2	3.39E+06
3	4.06E+06
4	5.39E+06
5	6.40E+06
6	7.54E+06
7	9.34E+06
8	1.32E+07
9	1.52E+07
10	1.74E+07
11	1.98E+07
12	2.35E+07
13	2.64E+07
14	3.08E+07
15	3.64E+07
16	4.30E+07
17	4.70E+07
18	5.21E+07
19	6.49E+07
20	1.03E+08
21	1.44E+08
22	2.02E+08
23	3.08E+08
24	4.04E+08
25	5.12E+08
26	6.45E+08

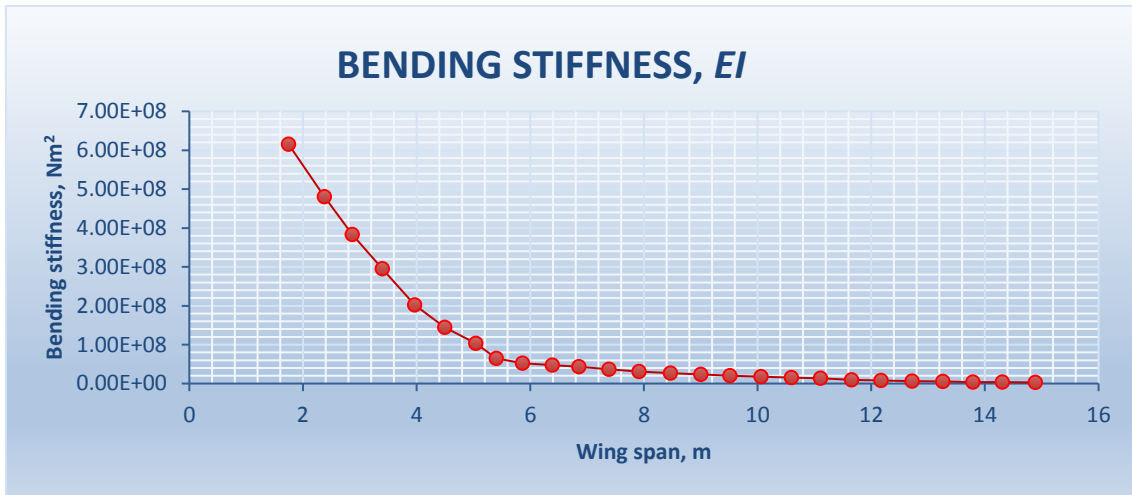


Figure 6.5 Bending stiffness result from BOXMX Program

Table 6.7 Torsional stiffness of the box sections from BOXMX Program

Section	Torsional Stiffness ( $\text{Nm}^2$ )
1	$5.81\text{E}+05$
2	$8.04\text{E}+05$
3	$1.08\text{E}+06$
4	$1.69\text{E}+06$
5	$2.18\text{E}+06$
6	$2.76\text{E}+06$
7	$3.40\text{E}+06$
8	$4.89\text{E}+06$
9	$5.88\text{E}+06$
10	$7.05\text{E}+06$
11	$8.39\text{E}+06$
12	$1.16\text{E}+07$
13	$1.35\text{E}+07$
14	$1.57\text{E}+07$
15	$1.80\text{E}+07$
16	$2.38\text{E}+07$
17	$2.66\text{E}+07$
18	$3.08\text{E}+07$
19	$3.93\text{E}+07$
20	$1.66\text{E}+08$
21	$2.19\text{E}+08$
22	$2.78\text{E}+08$
23	$4.41\text{E}+08$
24	$5.61\text{E}+08$
25	$6.93\text{E}+08$
26	$8.60\text{E}+08$



**Figure 6.6 Torsional stiffness distribution from BOXMX Program**

### 6.3.3 Stiffness Evaluation using NASTRAN

In order to calculate the bending and torsional stiffness, each of the box sections is clamped at the inboard end so as to make it a cantilever beam. Next bending moment and torque are respectively applied at the outboard (free) end and then displacements of the free end section were computed. Illustrative examples of forces and boundary condition applied in this analysis are shown in Figure 6.7.

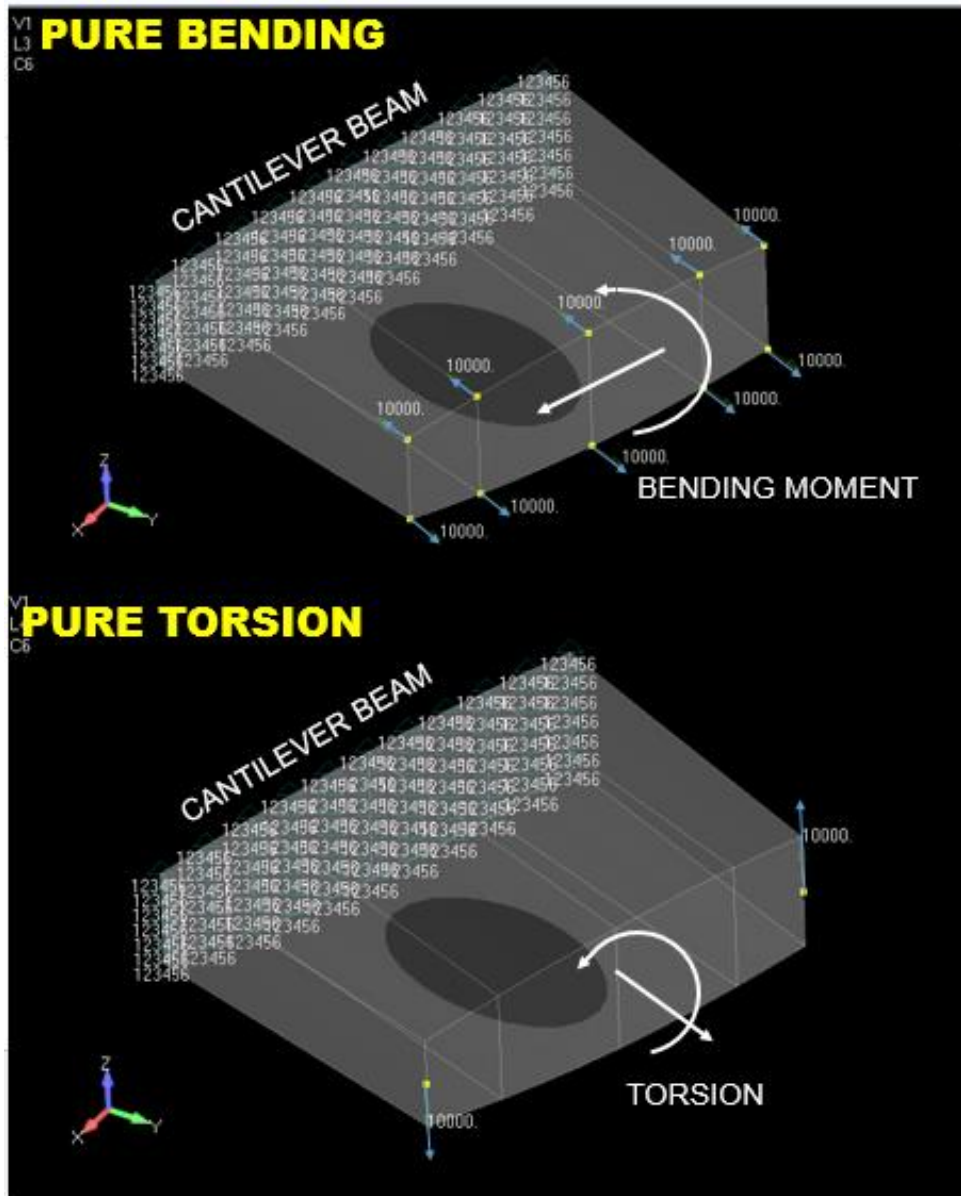


Figure 6.7 End condition and applied bending moment and torque

In order to calculate the wing box bending stiffness, Euler-Bernoulli beam theory is used. Thus the moment-curvature relationship of a beam is

$$M(l) = EI\kappa = EID(l)''$$

The bending moment is assumed constant along the beam. The above equation is integrated to determine the bending stiffness.

$$EI = \frac{ML}{\theta(L)} \quad (6.1)$$

where  $M$  is the applied bending moment,  $L$  is the length of the box and  $\theta(L)$  is the angle of the rotation of the cross section in radian.

The torsional stiffness,  $GJ$  is obtained in a similar manner when a constant torque  $T$  is applied to the outboard section. The cross section is thus twisted by the angle in radian as

$$\psi(L) = \frac{TL}{GJ}$$

In this way, the torsional stiffness  $GJ$  can be calculated from

$$GJ = \frac{TL}{\psi(L)} \quad (6.2)$$

where  $T$  is the applied torque,  $L$  is the box length and  $\psi(L)$  is the twist angle in radian. To calculate the twist angle, the length and displacement of the front spar and rear spar are measured. The twist angle value can be obtained by dividing the front spar and rear spar displacement with the front spar and rear spar length, as shown in Equation 6.3.

$$\psi(L) = \frac{\text{Front spar displacement} - \text{Rear spar displacement}}{\text{Front spar and rear spar length}} \quad (6.3)$$

### 6.3.3.1 Bending Stiffness Results

Figure 6.8 shows the results of bending stiffness for each section obtained from NASTRAN.

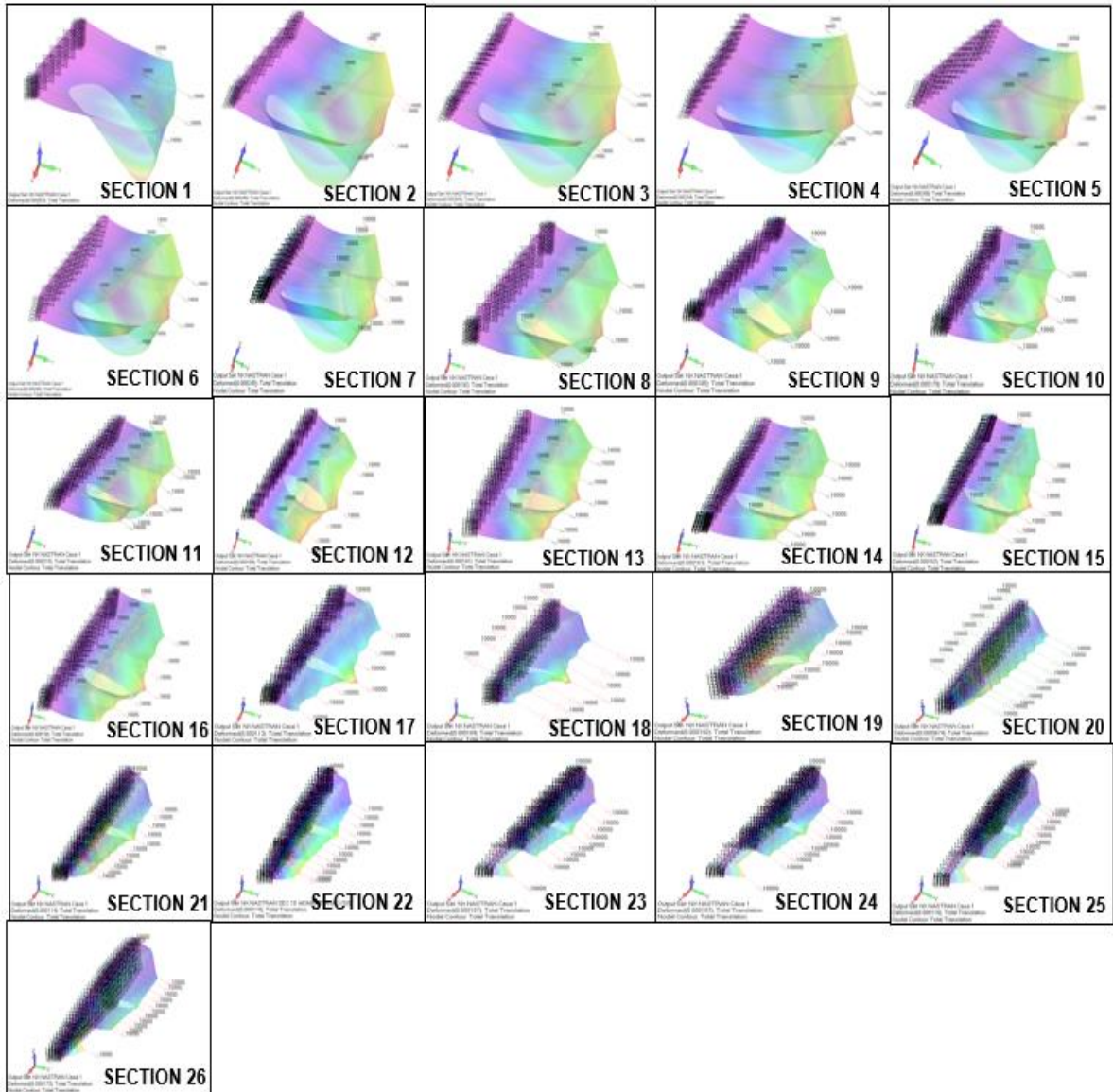


**Figure 6.8 Bending stiffness of the baseline wing sections from NASTRAN**

The applied bending moments and displacements (cross-sectional bending rotation in radian) of each section are given in Table 6.8.

**Table 6.8 Applied bending moment and bending rotation of each section**

Section	Applied Bending Moment (Nm)	Cross-sectional Rotation in Bending (rad)
1	3.83E+03	2.27E-03
2	6.98E+03	1.97E-03
3	7.54E+03	1.76E-03
4	8.11E+03	1.38E-03
5	8.67E+03	1.26E-03
6	9.22E+03	1.16E-03
7	9.78E+03	1.05E-03
8	1.03E+04	8.62E-04
9	1.09E+04	7.88E-04
10	1.15E+04	7.41E-04
11	1.66E+04	7.45E-04
12	1.74E+04	6.44E-04
13	1.83E+04	6.12E-04
14	1.91E+04	5.79E-04
15	1.99E+04	5.51E-04
16	2.07E+04	4.85E-04
17	2.16E+04	4.19E-04
18	2.22E+04	3.87E-04
19	2.86E+04	4.09E-04
20	3.65E+04	1.57E-04
21	4.33E+04	2.95E-04
22	4.74E+04	2.56E-04
23	5.59E+04	2.20E-04
24	5.43E+04	1.92E-04
25	6.90E+04	1.77E-04
26	7.72E+04	1.92E-04

Based on Equation (6.1), the approximate value of bending stiffness,  $EI$  for each section are calculated and the results are presented in Table 6.9 and illustrated in Figure 6.9.

**Table 6.9 Bending stiffness results from NASTRAN**

Section	Bending Stiffness (Nm <sup>2</sup> )
1	1.31E+06
2	2.08E+06
3	2.51E+06
4	3.43E+06
5	4.02E+06
6	4.66E+06
7	5.44E+06
8	7.03E+06
9	8.11E+06
10	9.07E+06
11	1.30E+07
12	1.58E+07
13	1.75E+07
14	1.93E+07
15	2.12E+07
16	2.51E+07
17	2.09E+07
18	2.19E+07
19	4.02E+07
20	9.45E+07
21	8.40E+07
22	1.06E+08
23	1.45E+08
24	1.62E+08
25	2.23E+08
26	3.15E+08



**Figure 6.9 Bending stiffness distribution from NASTRAN**



### 6.3.3.2 Torsional Stiffness Results

Figure 6.10 shows the results of torsional stiffness for each section obtained from NASTRAN.

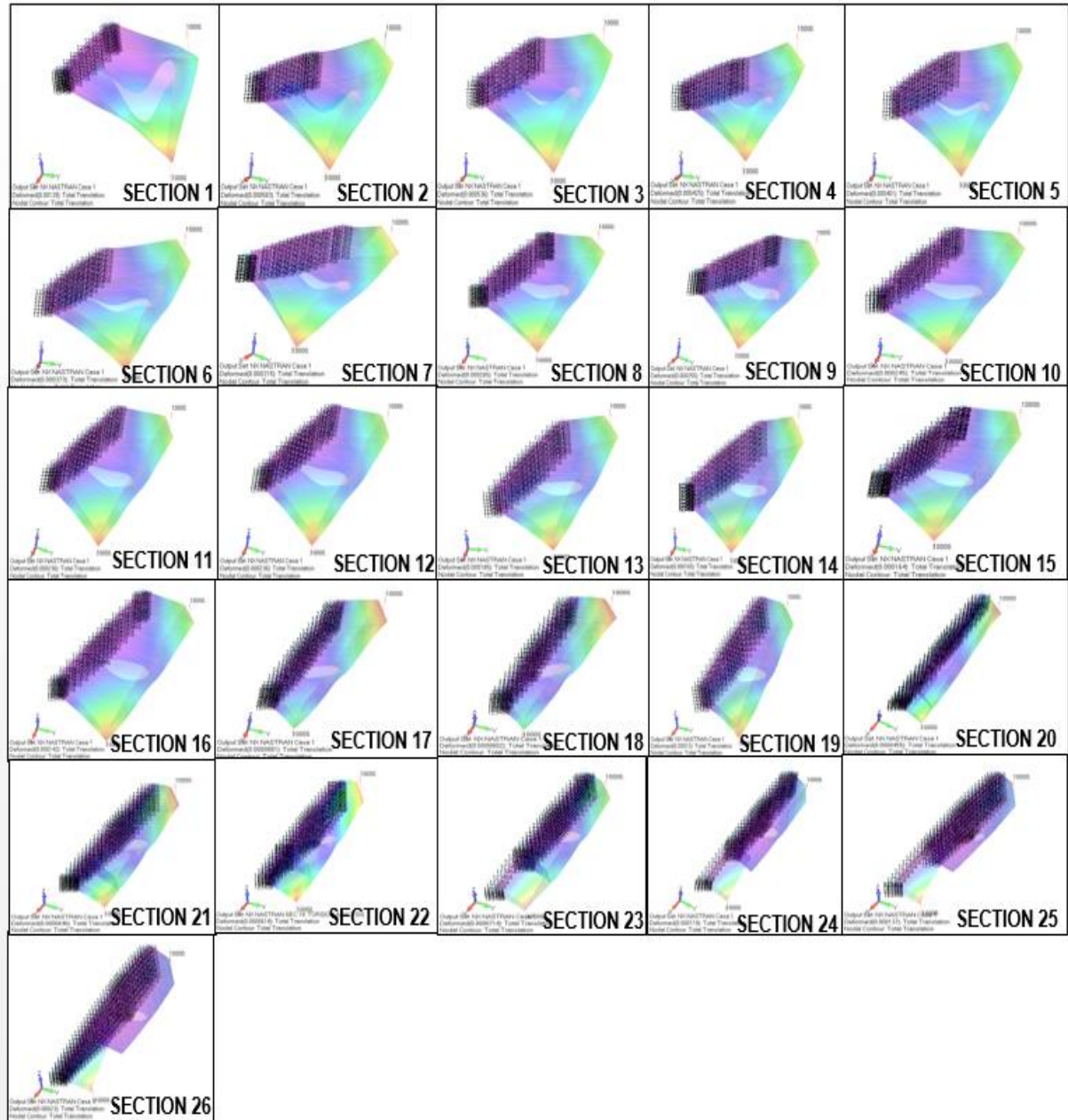


Figure 6.10 Torsional stiffness of the baseline wing sections from NASTRAN

The applied torques and displacements (cross-sectional twist in radian) of the wing box sections are given in Table 6.10.

**Table 6.10 Applied torques and twist of the wing box sections**

<b>Section</b>	<b>Applied Torque (Nm)</b>	<b>Cross Section Twist Angles (rad)</b>
1	4524.72	0.003956
2	4991.11	0.001930
3	5588.99	0.001548
4	6186.92	0.001141
5	6784.92	0.000983
6	7383.78	0.000848
7	7981.13	0.000709
8	8579.26	0.000531
9	9177.42	0.000475
10	9775.63	0.000429
11	10373.85	0.000390
12	10972.09	0.000298
13	11570.34	0.000272
14	12168.61	0.000241
15	12766.88	0.000220
16	13365.16	0.000179
17	13963.47	0.000102
18	14761.07	0.000085
19	15914.49	0.000119
20	19305.14	0.000044
21	21112.71	0.000059
22	23669.77	0.000049
23	26229.54	0.000046
24	28791.83	0.000055
25	31356.53	0.000054
26	33923.45	0.000079

Using Equation (6.2) the approximate value of torsional stiffness,  $GJ$  of the wing boxes are obtained and listed in Table 6.11 and the distribution of torsional stiffness from wing root to tip is shown in Figure 6.11.

**Table 6.11 Torsional stiffness results**

Section	Torsional Stiffness (Nm <sup>2</sup> )
1	8.87E+05
2	1.52E+06
3	2.12E+06
4	3.18E+06
5	4.04E+06
6	5.10E+06
7	6.60E+06
8	9.48E+06
9	1.13E+07
10	1.33E+07
11	1.56E+07
12	2.16E+07
13	2.49E+07
14	2.96E+07
15	3.41E+07
16	4.38E+07
17	5.57E+07
18	6.63E+07
19	7.68E+07
20	1.79E+08
21	2.04E+08
22	2.75E+08
23	3.29E+08
24	3.02E+08
25	3.33E+08
26	3.36E+08

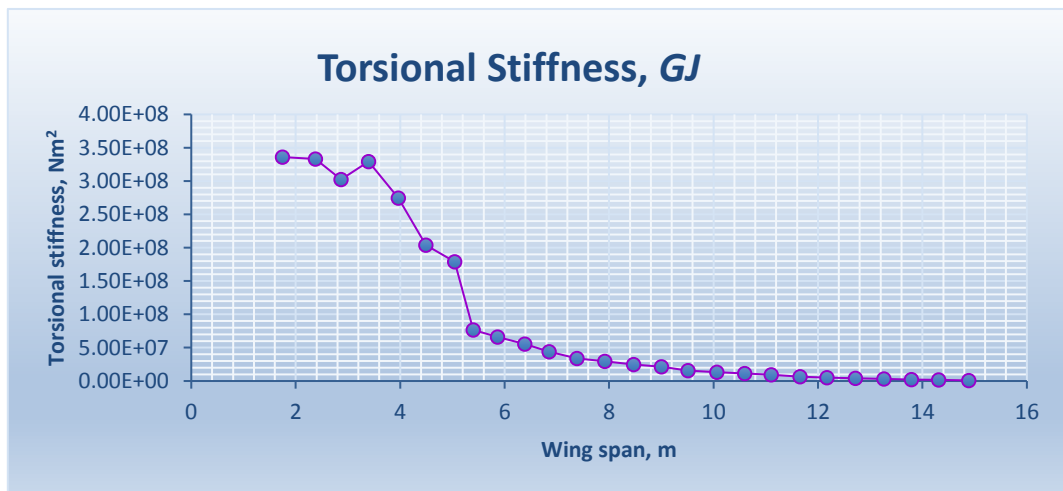


**Figure 6.11 Torsional stiffness distribution from NASTRAN**

### 6.3.4 Comparison of Results Using BOXMX Program and NASTRAN

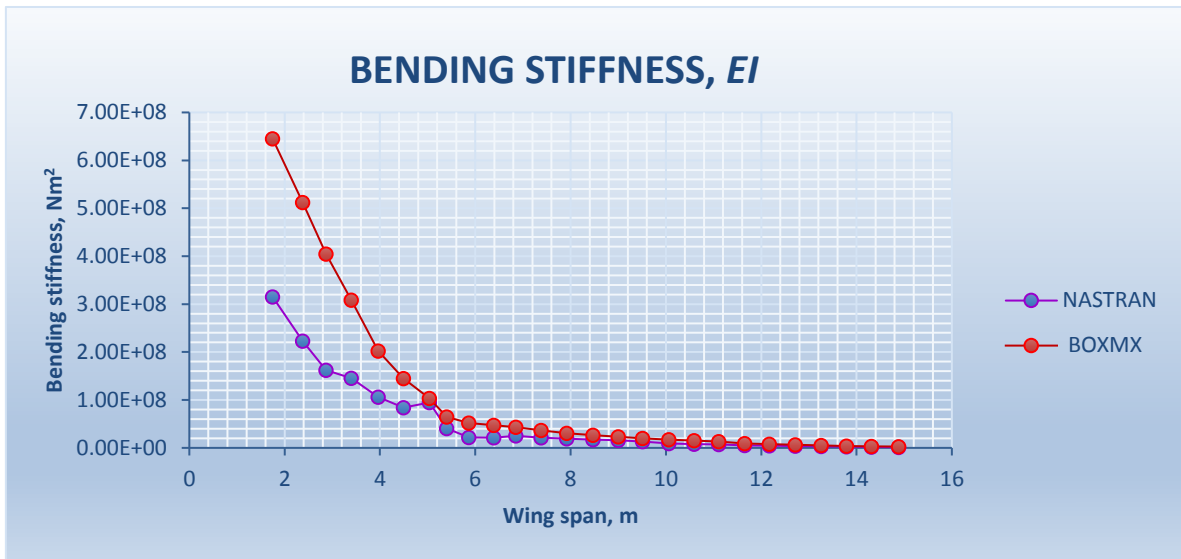


**Figure 6.12 Bending stiffness result BOXMX Program vs NASTRAN**

Bending stiffness for BOXMX Program and NASTRAN are compared in Figure 6.12. From the graph, the values of bending stiffness for BOXMX Program for the inboard wing are much higher than NASTRAN. The difference in results in terms of percentage is plotted in Figure 6.13.

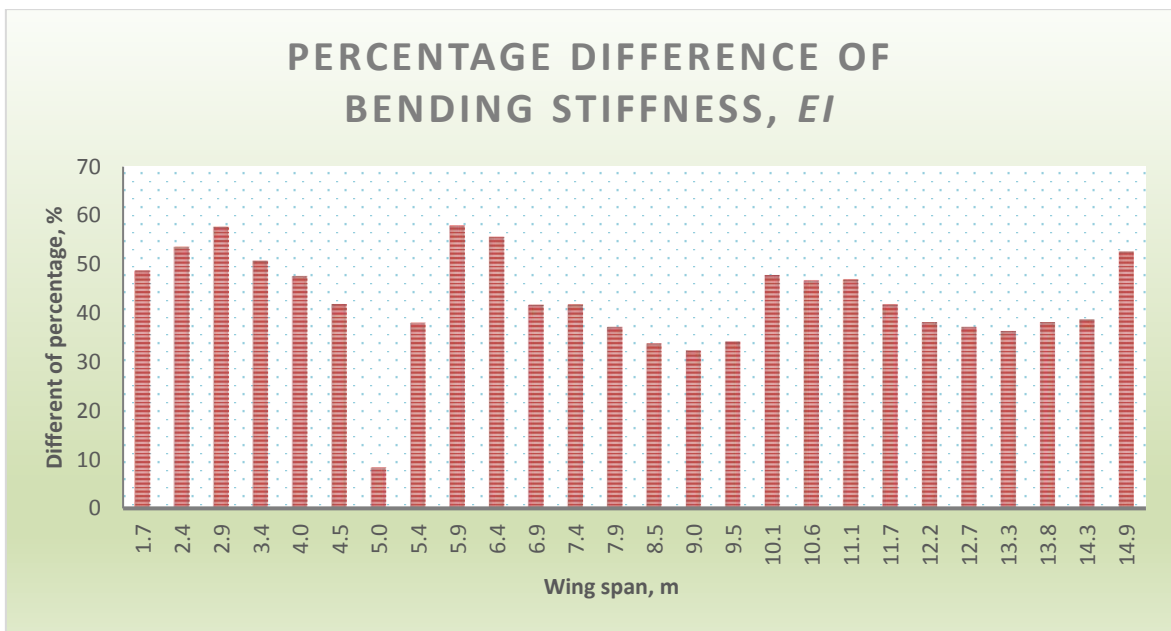


**Figure 6.13 Percentage difference of EI between NASTRAN and BOXMX Program**

The torsional stiffness,  $GJ$  of the inboard wing calculated from BOXMX Program is much higher than the one obtained from NASTRAN as was the case with the bending stiffness,  $EI$  calculation. The discrepancy is being further investigated. The  $GJ$  results are illustrated in Figure 6.14 and the percentage difference is shown in Figure 6.15.

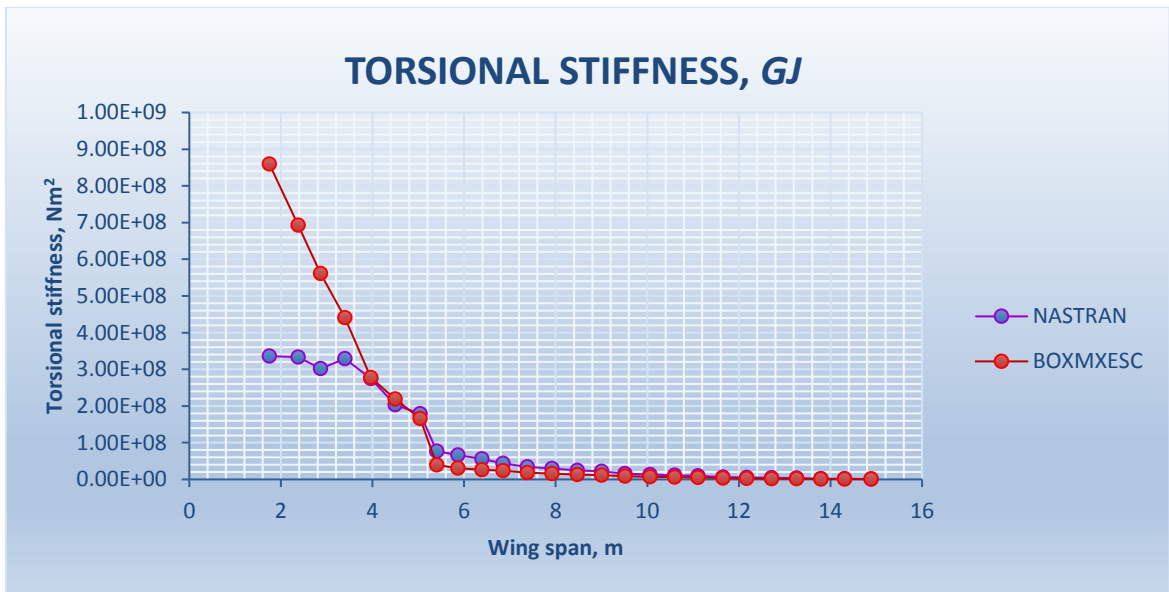


Figure 6.14 Torsional stiffness distribution BOXMX vs NASTRAN

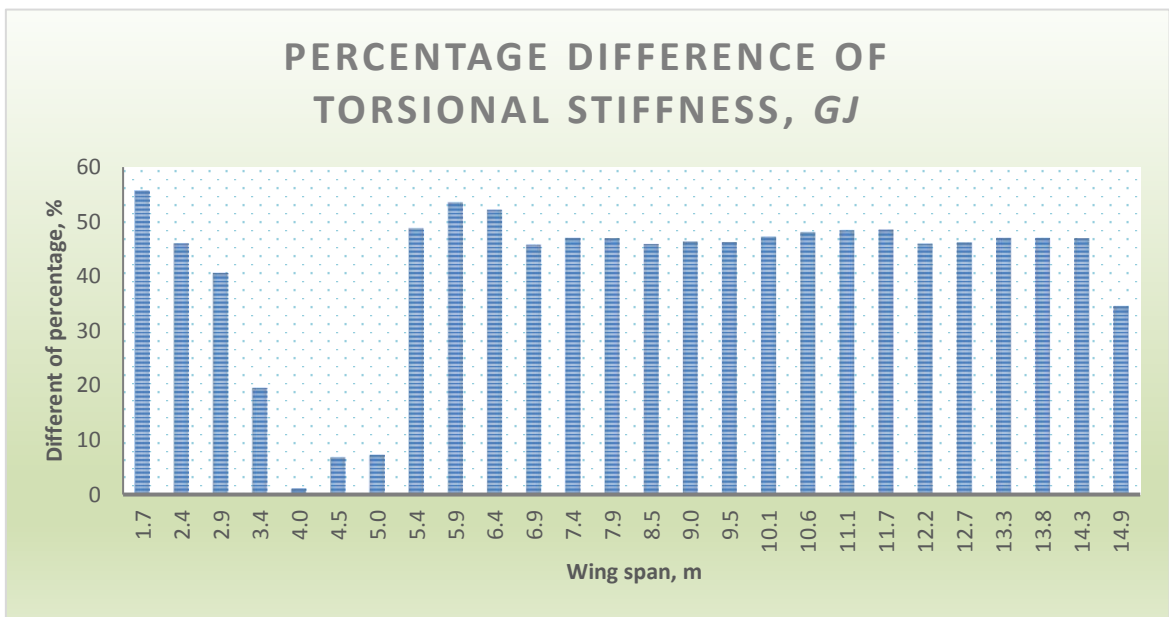


Figure 6.15 Percentage difference of  $GJ$  between NASTRAN and BOXMX Program

Understandably the in-house program BOXMX works well for estimating the stiffness of closed box sections without any manhole, but for a closed section with cut-out (such as the presence of a manhole), the program needs considerable enhancement. Currently there is no theory available to calculate bending stiffness and torsional stiffness for box with cut-out. It is proved that this theory is needful in structural analysis and shall be developed in the near future.

## 6.4 FE Modelling and NASTRAN Analysis

### 6.4.1 Stress and Strain

The baseline wing model is fixed at the root so as to make it a cantilever. The static analysis is then performed under load factor 2.5. The distributed aerodynamic load along the span has a total value of 710000N, and the inertia relief load is set at -2.5g. The aerodynamic load distribution is shown in Figure 6.16. The deflection, stress and strain results of the wing are shown in Figure 6.17- Figure 6.21.

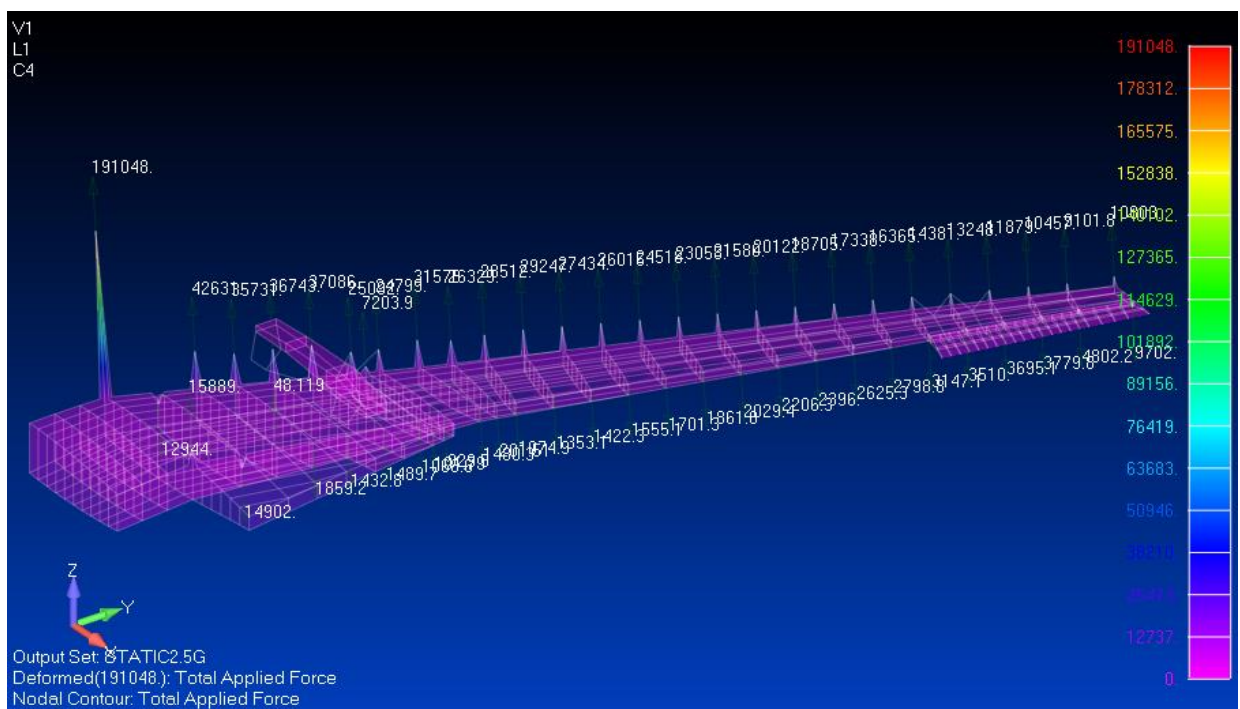


**Figure 6.16 Aerodynamic load distribution under 2.5 load factor  
(total aerodynamic force=710000N)**

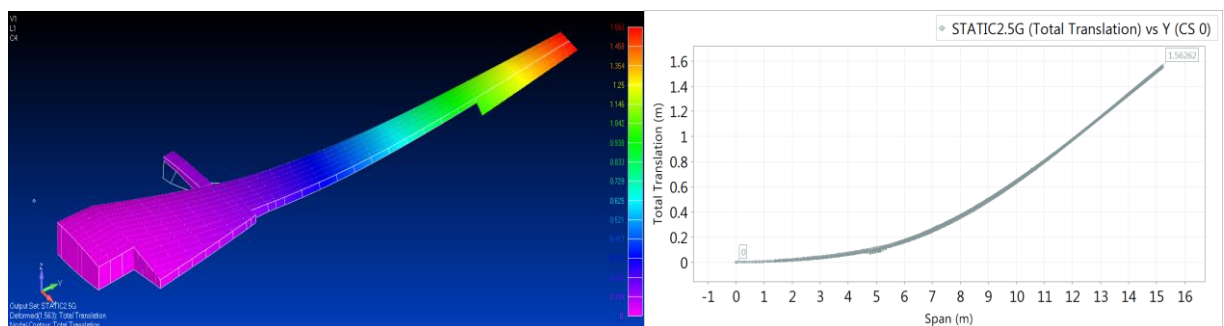


**Figure 6.17 Deflection along span (Max. 1.56m)**

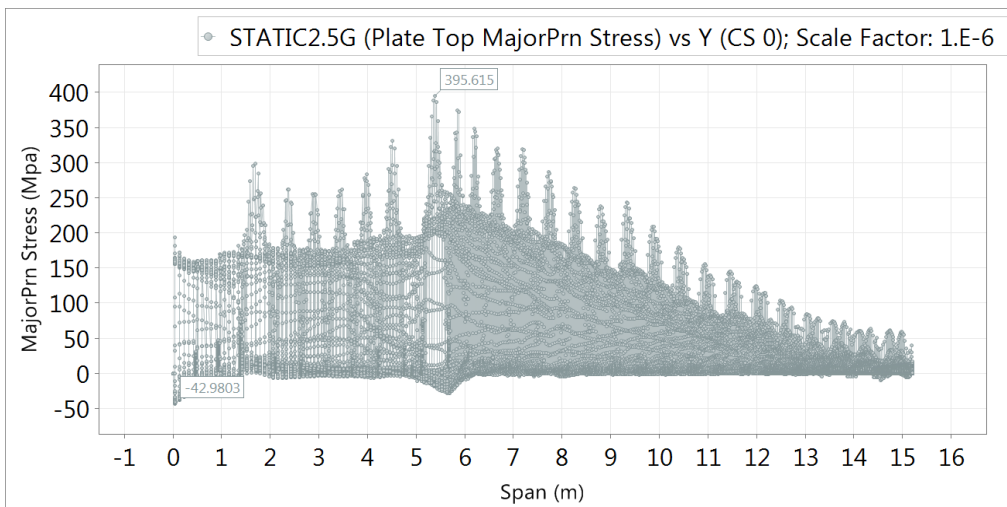
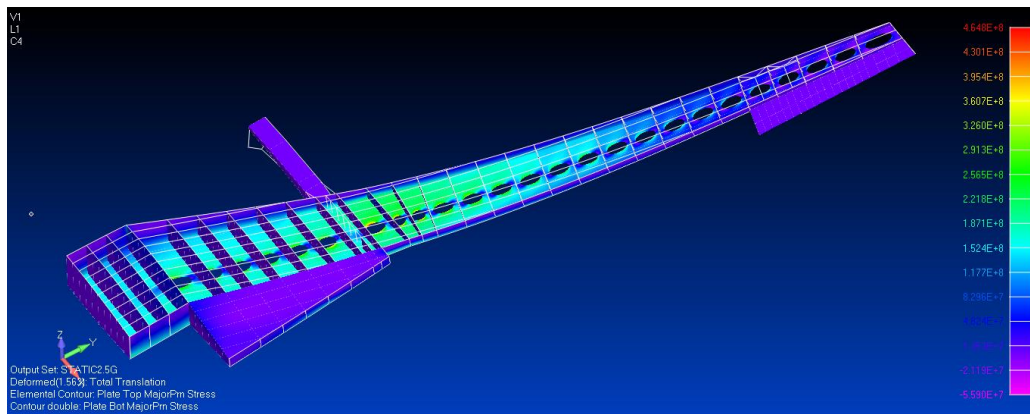
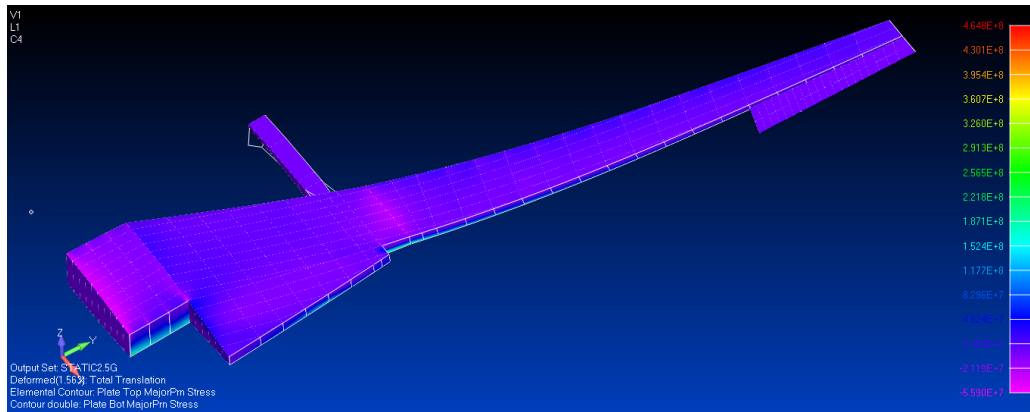


**Figure 6.18 Maximum principal stresses in the upper and lower skins, and spars along the span (Max. 396 MPa)**



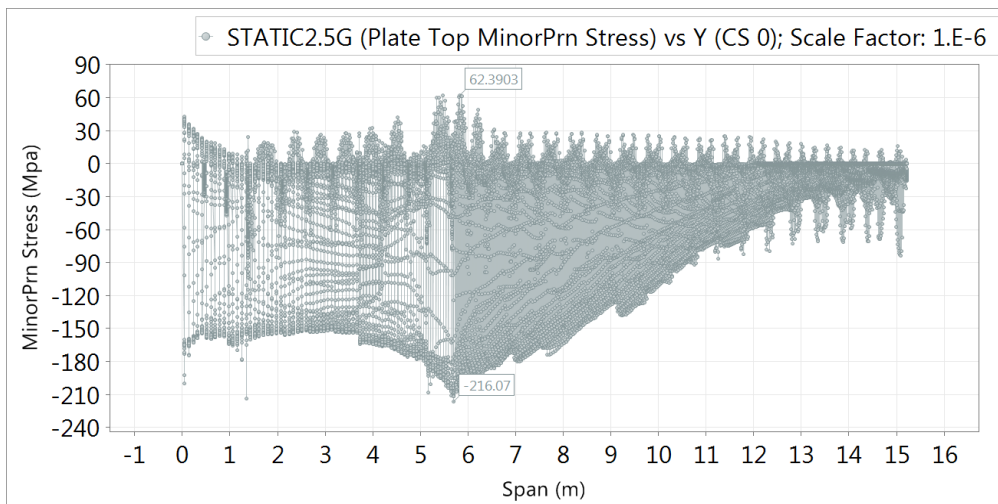
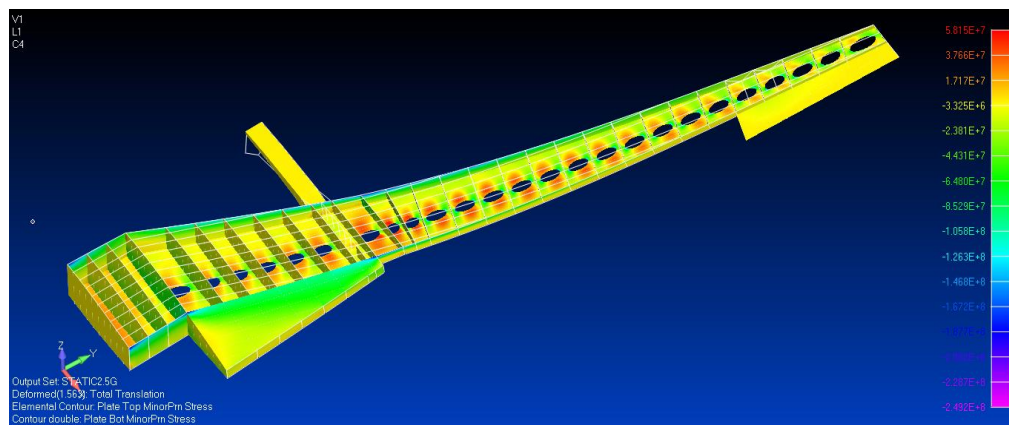
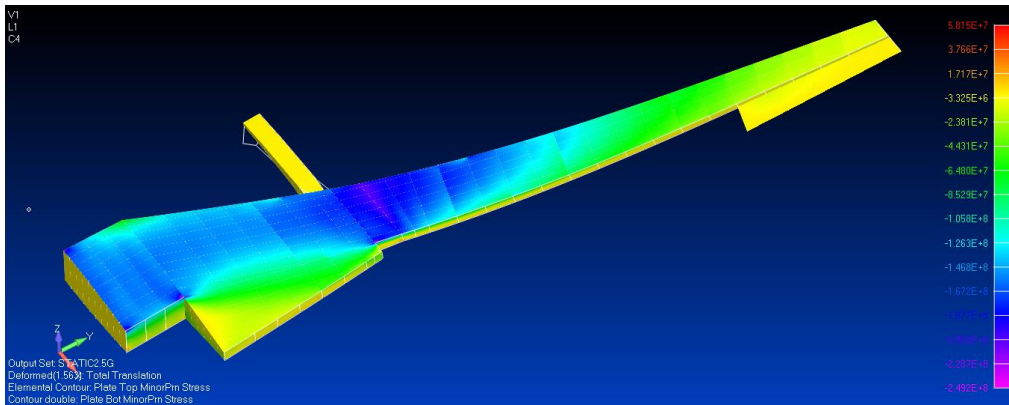


**Figure 6.19 Minimum principal stresses of upper and lower skins, and spars along the span (Max. -216MPa)**

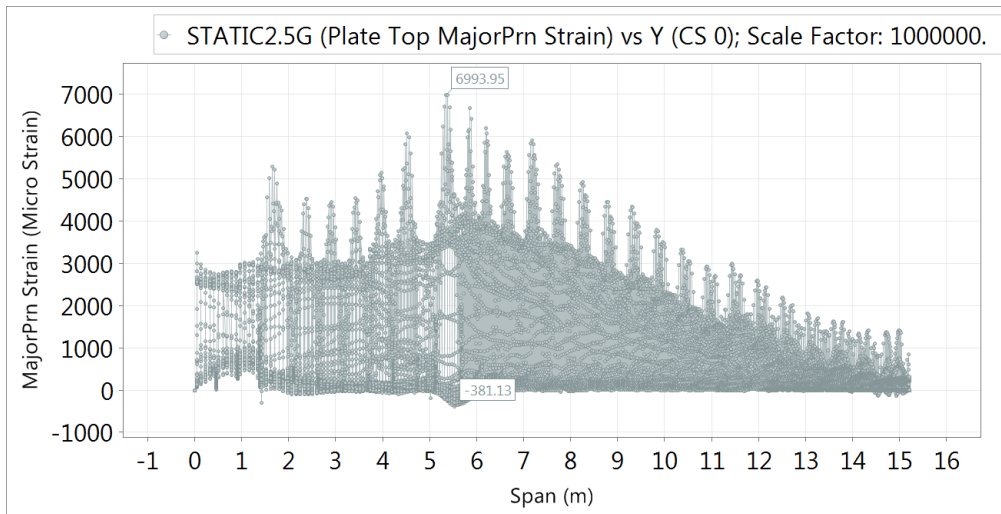
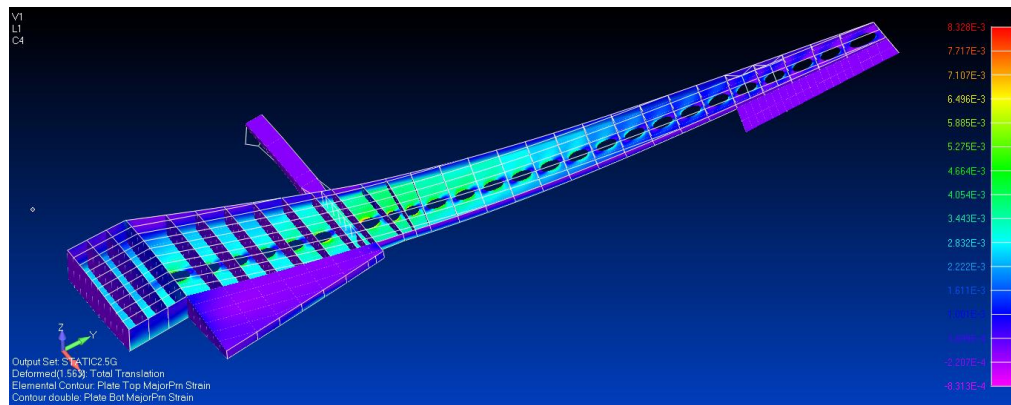
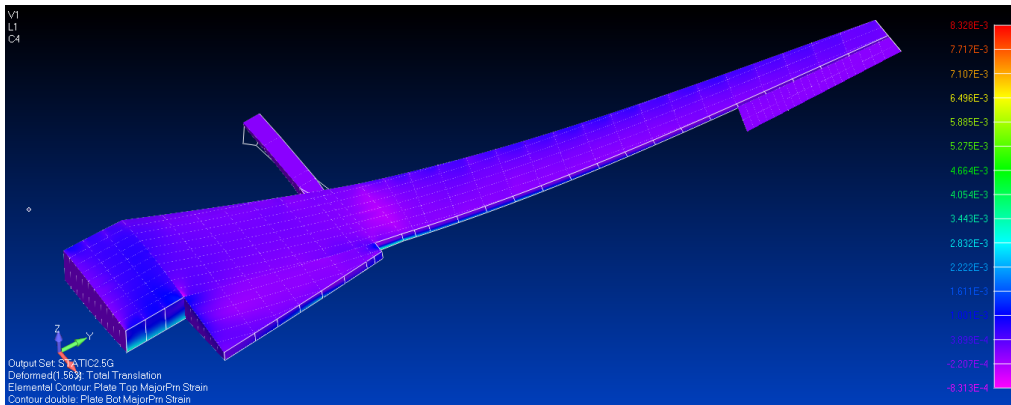


**Figure 6.20 Maximum principal strains of upper and lower skins, and spars along the span (Max. 6994  $\mu\epsilon$ )**

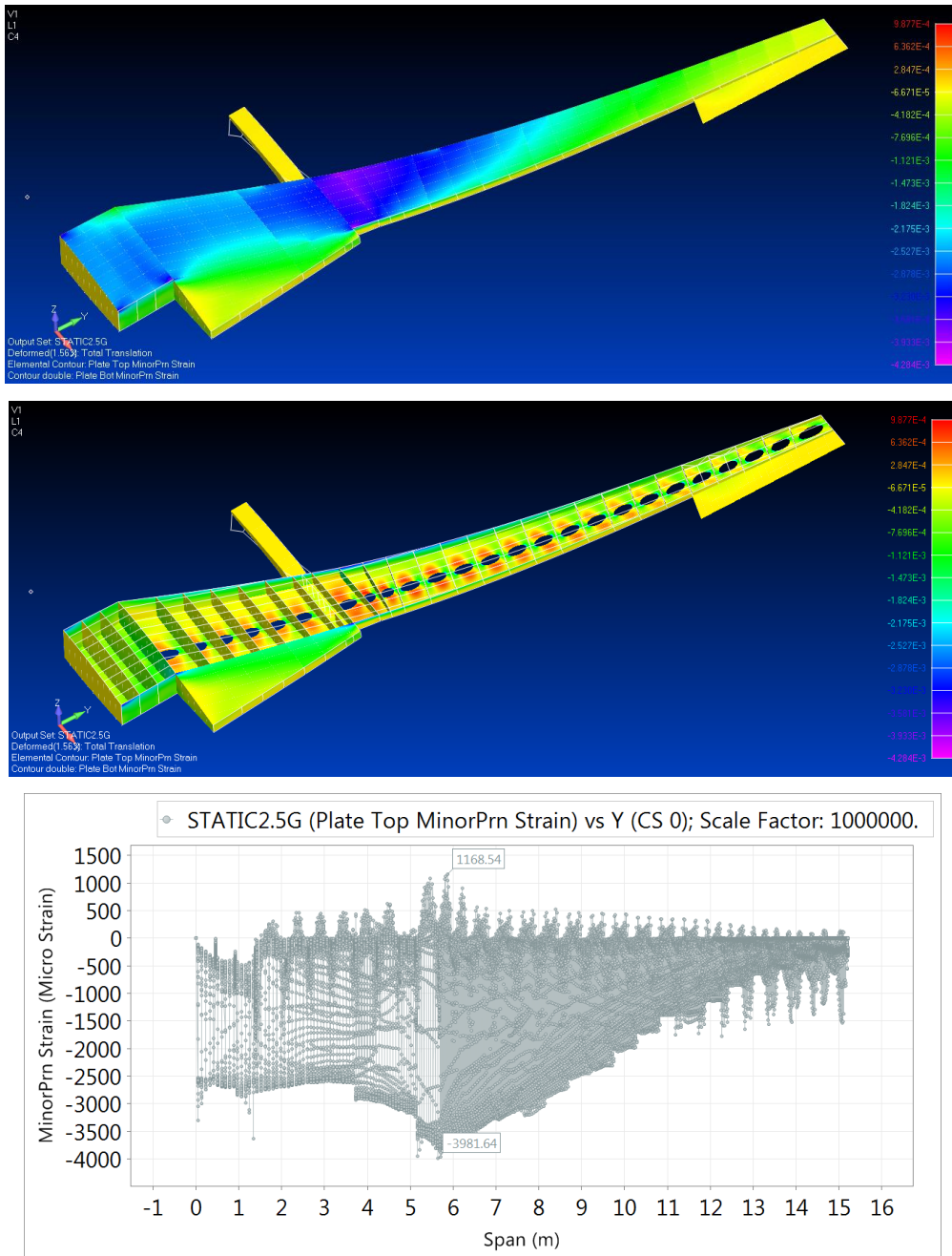


**Figure 6.21 Minimum principal strains of upper and lower skins, and spars along the span (Max. -3982  $\mu\epsilon$ )**

The current model yields large stress and strain under 2.5 load factor. The maximum principal stress is 396MPa and maximum principal strain is 6994 micro strain at the kink position.

## 6.4.2 Buckling Analysis

Buckling is induced by the sudden failure of a mechanical component, which is caused by the material failure and structural instability [100]. Buckling failure is mainly characterised by a loss of structural stiffness. The load at which buckling occurs depends on the stiffness of a component, not upon the strength of its materials. Buckling critical load is the maximum load which the column can remain straight. The critical load puts the column in a state of unstable equilibrium. A load beyond the critical load will cause the column to buckle. The 18<sup>th</sup> century Swiss Mathematician, Leonhard Euler, has derived the critical buckling load formula as:

$$P_{cr} = \frac{\pi^2 EI}{L^2} \quad (6.4)$$

where

$P_{cr}$  = critical buckling load

$E$  = Elastic or Young's Modulus

$I$  = Moment of inertia

$L$  = Length

The buckling factor ( $BF$ ), is a ratio of the buckling loads to the applied load. It is an indicator of the factor of safety against buckling. The formula for  $BF$  is

$$BF = \frac{P_{cr}}{P_{app}} \quad (6.5)$$

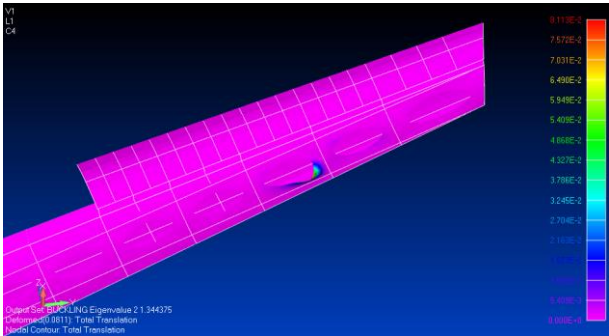
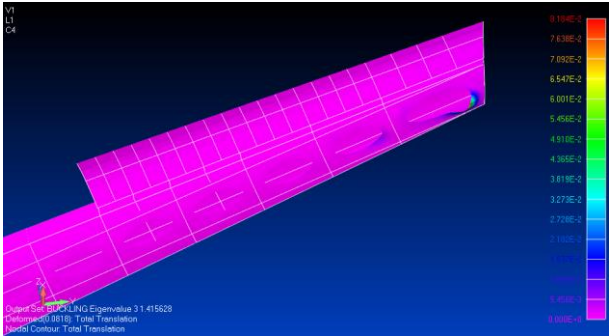
where  $P_{app}$  = applied load

Table 6.12 illustrates  $BF$  and the buckling status of the column. Buckling will occur if  $BF$  is equal or less than 1 because in this condition, the applied loads are equal or exceed the critical loads, respectively.

**Table 6.12 Buckling factor ( $BF$ ) and buckling status**

$BF$ Value	Buckling Status
>1	Buckling does not occur. The applied loads are less than the estimated critical loads
1	Buckling is expected. The applied loads are exactly equal to the critical loads.
<1	Buckling occur. The applied loads exceed the estimated critical loads.

In this research, buckling analysis is performed under the same loading and boundary condition as the static analysis as shown in Figure 6.16. The wing model is fixed at the root and analysis is performed under load factor 2.5. Buckling results from NASTRAN are presented in Figure 6.22.

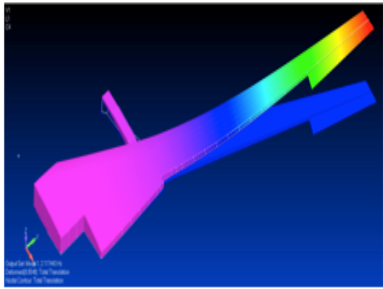
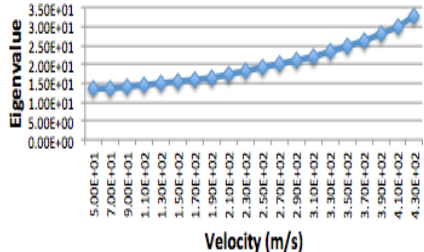
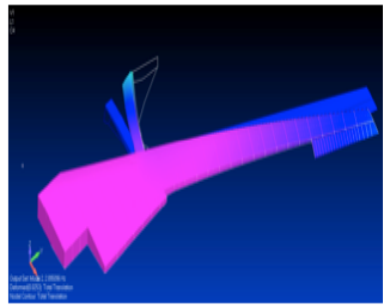
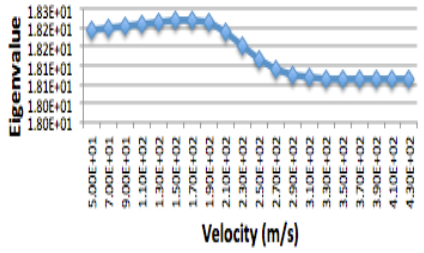
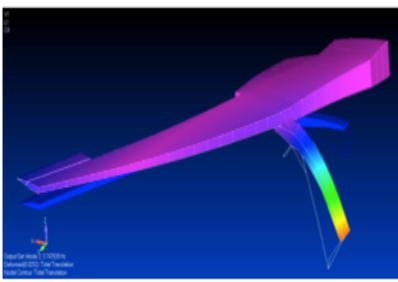
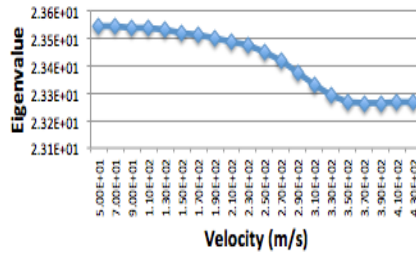
Buckling Factor	Mode Shape
<p>1<sup>st</sup> Buckling is located at the 3<sup>rd</sup> wing box from tip Buckling factor=1.34</p>	
<p>2<sup>nd</sup> Buckling is located at the 1<sup>st</sup> wing box from tip Buckling factor=1.41</p>	

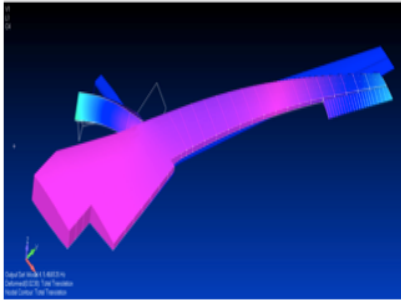
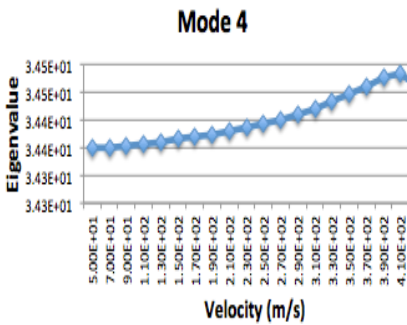
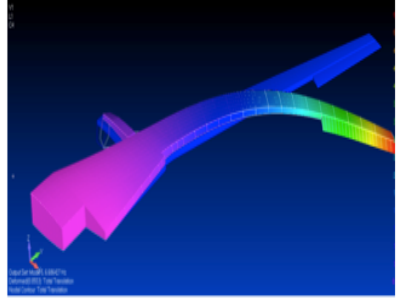
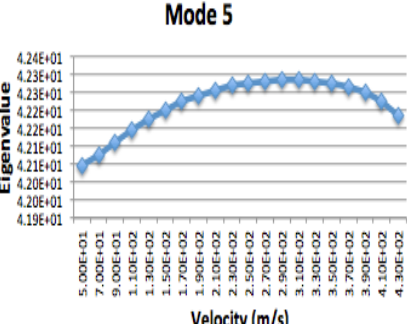
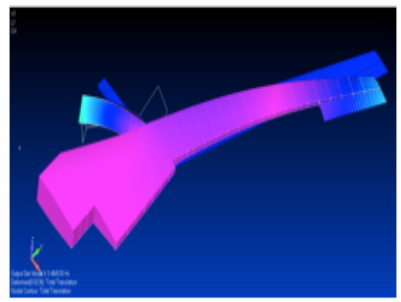
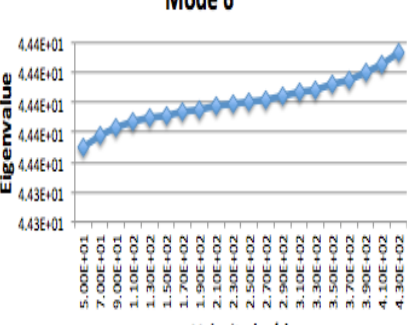
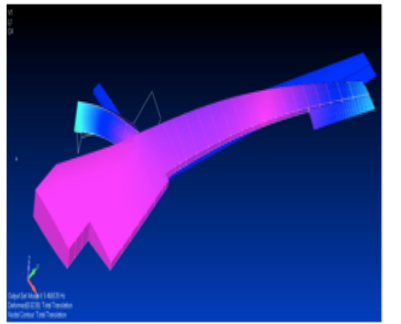
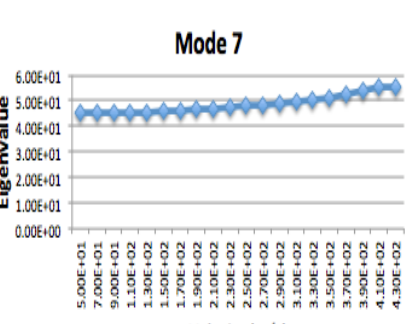
**Figure 6.22 Buckling analysis results under 2.5 load factor**

From the buckling analysis, the first and second buckling modes are discovered at the third and first wing box from the tip, respectively. The first buckling factor is 1.34 and the second buckling factor is 1.41. Since both buckling factors are greater than 1, therefore the wing skin does not buckle. The critical load is larger than the applied load and hence the wing box is capable of taking the buckling load under the 2.5 load factor.

### 6.4.3 Modal Analysis

Modal analysis is a method to determine the dynamic characteristics of engineering structures and its components. It is a process by which the natural frequencies, mode shapes and damping factor of structures to be determined by a relative case. The numerical modal analysis method using FE modelling enables engineers to get a better understanding of dynamic properties of structures. In this research, the modal analysis is performed for the wing structure by clamping the wing at the root section. The first ten natural frequencies and mode shapes results are illustrated in Figure 6.23.

Natural frequency	Mode shape
<p>1<sup>st</sup> Mode: 1<sup>st</sup> Bending Frequency=2.11Hz</p>	 <p style="text-align: center;"><b>Mode 1</b></p> 
<p>2<sup>nd</sup> Mode: Pylon Swing Frequency=2.89Hz</p>	 <p style="text-align: center;"><b>Mode 2</b></p> 
<p>3<sup>rd</sup> Mode: Pylon Pitching Frequency=3.73Hz</p>	 <p style="text-align: center;"><b>Mode 3</b></p> 

<p>4<sup>th</sup> Mode: 1<sup>st</sup> Bending &amp; Swing Frequency=5.45Hz</p>		<p><b>Mode 4</b></p> 
<p>5<sup>th</sup> Mode: 2<sup>nd</sup> Bending &amp; Swing Frequency=6.67Hz</p>		<p><b>Mode 5</b></p> 
<p>6<sup>th</sup> Mode: 3<sup>rd</sup> Bending &amp; Swing Frequency=7.05Hz</p>		<p><b>Mode 6</b></p> 
<p>7<sup>th</sup> Mode: 2<sup>nd</sup> Bending Frequency=7.10Hz</p>		<p><b>Mode 7</b></p> 

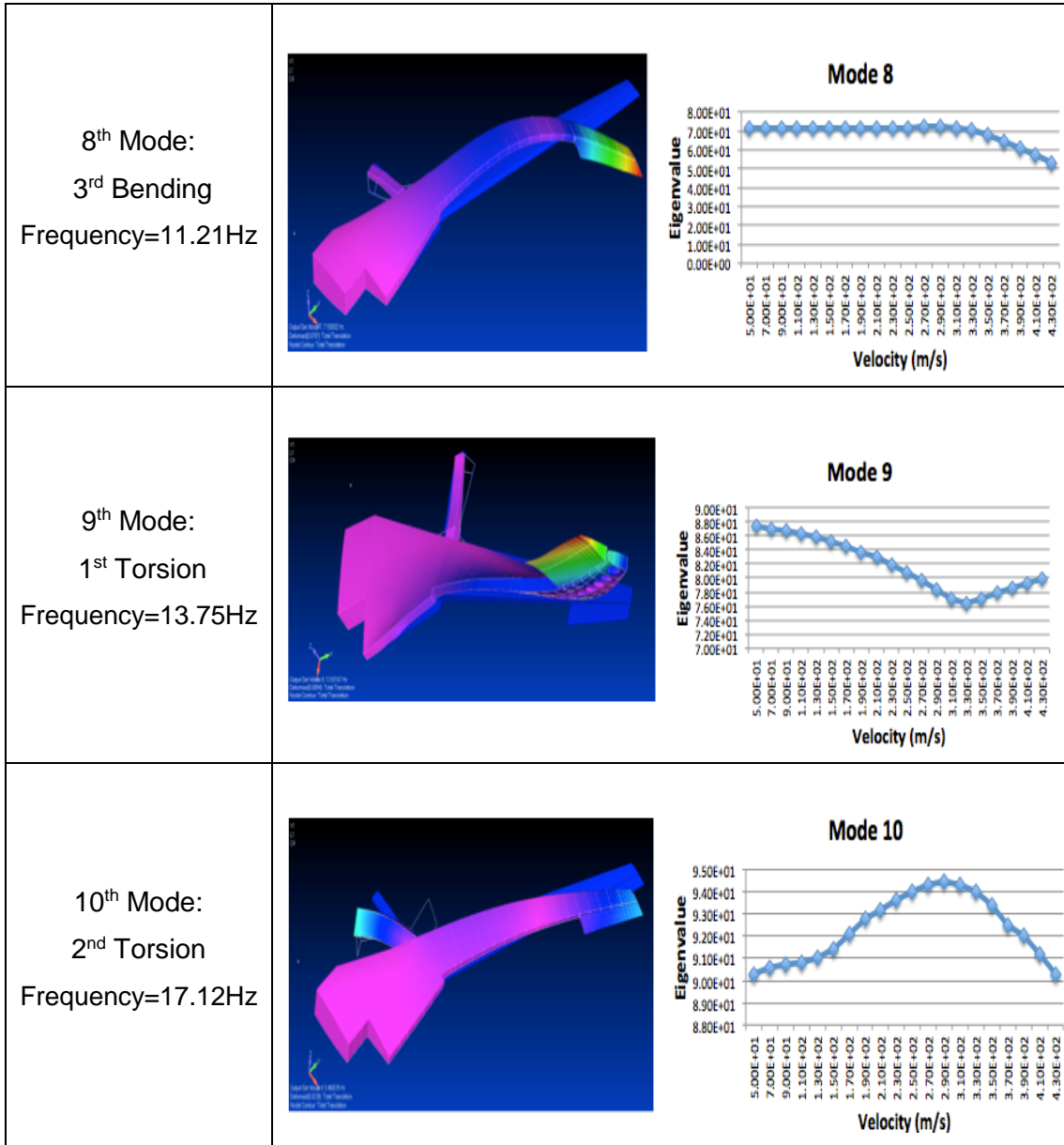


**Figure 6.23 The first ten natural frequencies and modes**

Figure 6.23 presents the first ten natural frequencies and mode shape for this analysis. The natural frequency for each mode can be obtained from the modal analysis results. The result is used to identify the first resonance effect during flutter analysis.



#### 6.4.4 Flutter Analysis

Flutter is a dynamic instability of an elastic body in an airstream. Flutter occurs at a critical or flutter speed,  $V_f$ , which in turn is defined as the lowest airspeed at which a given structure will oscillate with sustained harmonic motion. Flight at speeds below and above the flutter speed represents conditions of stable and unstable (which is divergent) structural oscillation, respectively [1,101]. The basic equation for flutter analysis by the P-K method can be described as follows [102].

$$\left[ -M_{hh}P^2 + \left( B_{hh} - \frac{0.25\rho cV Q_{hh}^I(m,k)}{k} \right) P + \left( K_{hh} - \frac{1}{2}\rho V^2 Q_{hh}^R(m,k) \right) \right] \{u_h\} \quad (6.6)$$

$$P = \gamma k + ik$$

where

$M_{hh}$  = modal mass matrix

$B_{hh}$  = modal damping matrix

$K_{hh}$  = modal stiffness matrix

$m$  = Mach number

$k$  = reduced frequency

$V$  = airspeed

$Q_{hh}^I$  = generalised aerodynamic damping matrix

$Q_{hh}^R$  = generalised aerodynamic stiffness matrix

$u_h$  = modal displacements or modal amplitude vector

One common form of flutter analysis is the V-g analysis. In V-g analysis, the structural damping of all the modes of vibration is assumed to have one unknown value,  $g$ . The velocity at which the upper curve passes through  $g=0$  corresponds to the flutter velocity of the model if assumption of zero structural damping is made. Then, from the V-f plot, using flutter speed obtained from V-g plot, the flutter frequency can be determined. In this research, the flutter analysis is carried out using 10 normal modes. However for presentational purposes, only four and

two selected modes are shown in the V-g plots, see Figure 6.24 and Figure 6.25, respectively. For Figure 6.24, only 4 modes, which is near  $g=0$  are selected. For Figure 6.25, only modes which the upper curve passes through  $g=0$  are selected.

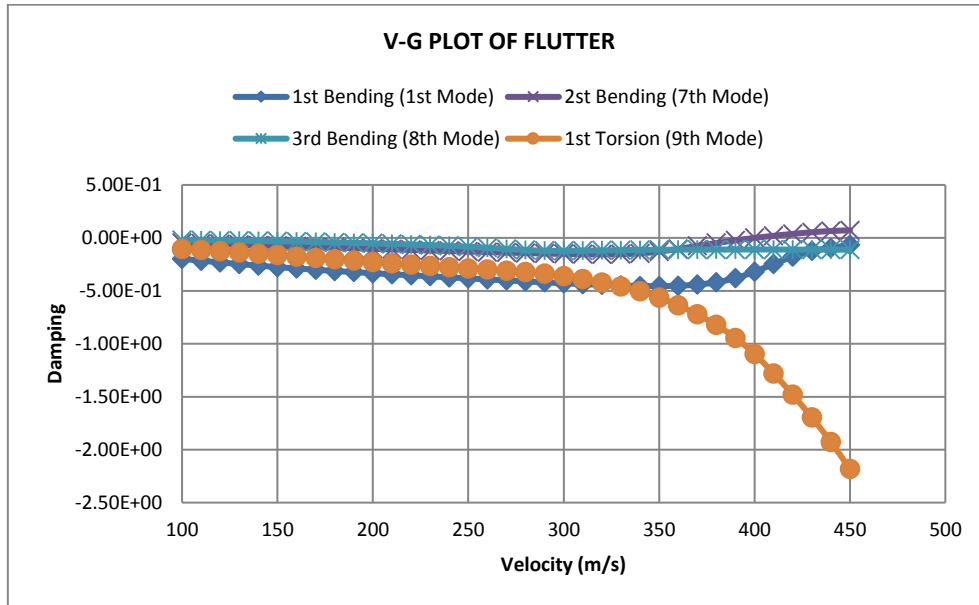


**Figure 6.24 V-g plot of flutter analysis 4 modes**

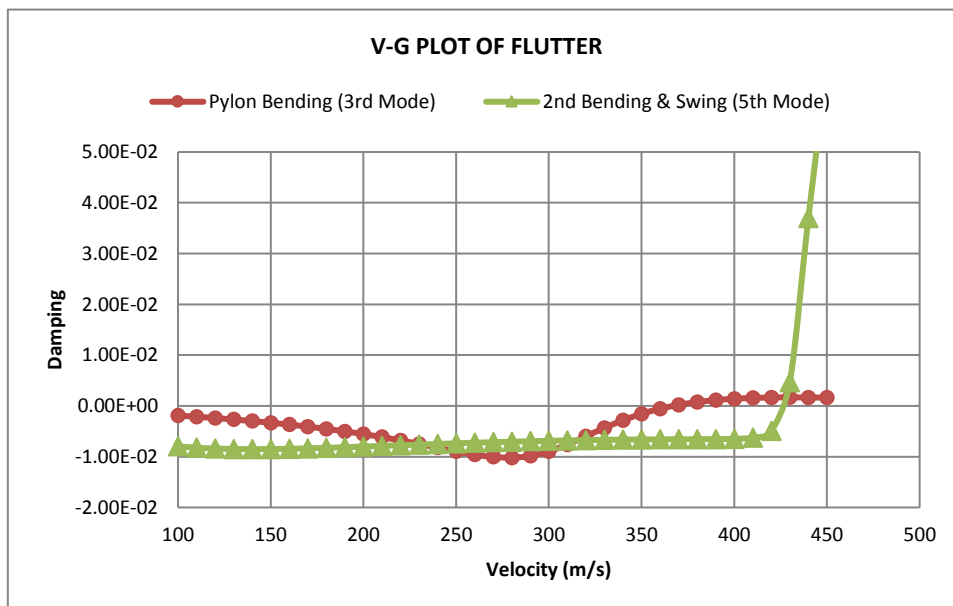


**Figure 6.25 V-g plot of flutter analysis for damping,  $g$  greater than 1**

The associated V-f plot including six modes is shown in Figure 6.26. The flutter frequency can be obtained from V-f plot by taking the frequency at flutter speed. From Figure 6.25, the flutter speed,  $V_f$  that the upper curve passes through  $g=0$

is 360 m/s. From V-f plot in Figure 6.26, at flutter speed, the flutter frequency is 3.70Hz.

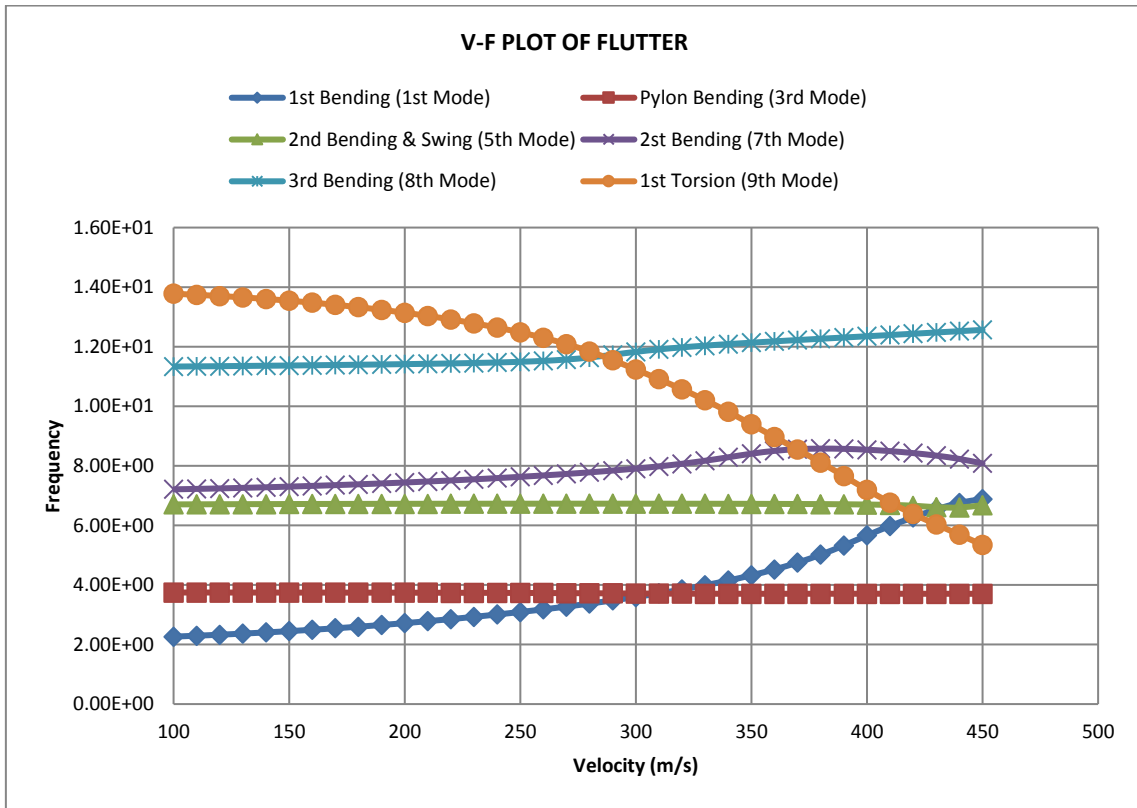


**Figure 6.26 V-f plot of flutter analysis for baseline wing (6 modes)**

**Table 6.13 Flutter results summary**

Dominant Mode	Flutter Speed (m/s)	Flutter Frequency (Hz)
Pylon Pitching (Mode 3)	360	3.70
2 <sup>nd</sup> Bending & Swing (Mode 5)	430	6.61
2 <sup>nd</sup> Bending (Mode 7)	400	8.54

The slope of the damping versus velocity curve as it passes through the flutter velocity can be assumed as a qualitative measure of how violently the oscillations would occur during accelerated flight. From Table 6.13, the first resonance is identified at Mode 3, which is pylon pitching mode. Flutter occurs at  $V_f=360$  m/s, at frequency  $f_1=3.70$ Hz. For interaction of higher modes, the expected flutter speed would be  $V_{f2}=400$  m/s for second bending (Mode 7) at frequency  $V_{f2}=8.54$  Hz, and  $V_{f3}=430$  m/s for 2<sup>nd</sup> bending & swing (Mode 5) at frequency  $f_3=6.61$  Hz.

### 6.4.5 Effect of Stringer Addition to Flutter Speed

In aircraft wing structure, the thin wing skin is reinforced by the stiffeners. The stiffeners or stringers are placed at upper and lower skin, across the multi-ribs to support the pressure, compression and shear loads to reduce buckling. T shape stringer has been selected for this analysis. Subject to manufacturing constraint, thickness of stringer foot to skin thickness ratio must be greater than 0.5. This condition must be satisfied to mitigate against crack propagation [59].

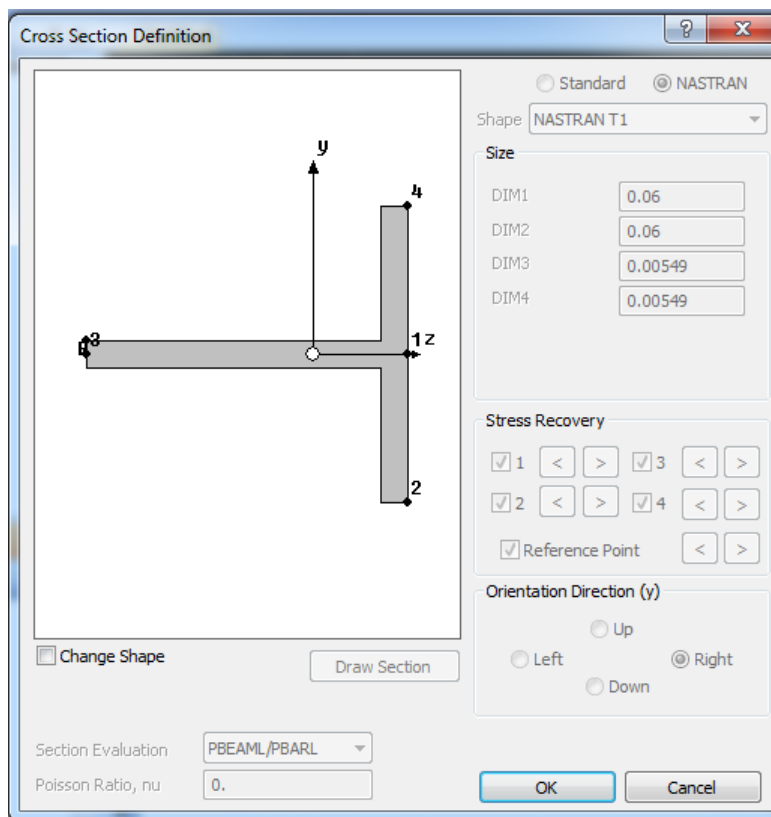


Figure 6.27 NASTRAN T1 has been chosen for this analysis

Refer Figure 6.27, the dimension of the stringer used in this analysis is as below.

$$b_w = \text{DIM1} = 0.06\text{m}$$

$$b_{fl} = \text{DIM2} = 0.06\text{m}$$

$$t_w = \text{DIM3} = 0.00549\text{m}$$

$$t_{fl} = \text{DIM4} = 0.00549\text{m}$$

where  $b_w$ ,  $b_{fl}$ ,  $t_w$ ,  $t_{fl}$  are web width, flange width, web thickness and flange thickness respectively. For the wing box, the minimum skin thickness found in Box 1, which is 0.00366m. Since the flange thickness is more than 0.5 ratio of skin thickness, the requirement for manufacturing met and this stringer dimension size is applicable for this analysis.

The objective of this analysis is to see the effect of stringer addition to the flutter speed. The bending stiffness value of stringer must first be calculated and then added to bending stiffness of the wing in order to get the total bending stiffness values. The material chosen for stringer is aluminium Al 2024.

**Table 6.14 Mechanical properties of Al 2024**

Material	Modulus of Elasticity (GPa)	Shear Modulus (GPa)	Poisson's ratio $\nu_{12}$
Al 2024	70	26.9	0.33

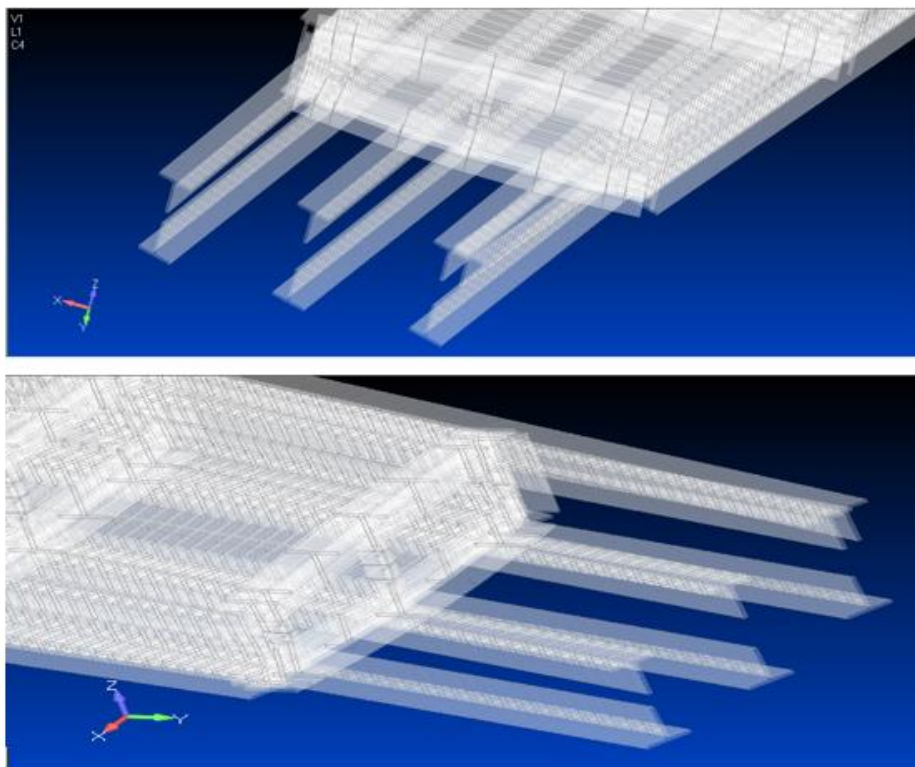


**Figure 6.28 Example of stringers location**

Moment of inertia must be calculated first to obtain the bending stiffness values for this stringer. Based on the axis shown in Figure 6.29, moment of inertia is in

$x$  axis. From parallel axis theorem, the second moment of area,  $I_X$  is calculated using Equation (6.7).

$$I_X = I_{xx} + Ac^2 \quad (6.7)$$

$$I_{xx} = \frac{bh^3}{12} \quad (6.8)$$

where  $b$  is the width and  $h$  is the height of the stringer flange and web.  $c$  is the distance from the centre of the mass to the parallel axis of rotation and  $I_{xx}$  is the moment of inertia about the centre of mass parallel to the current axis.

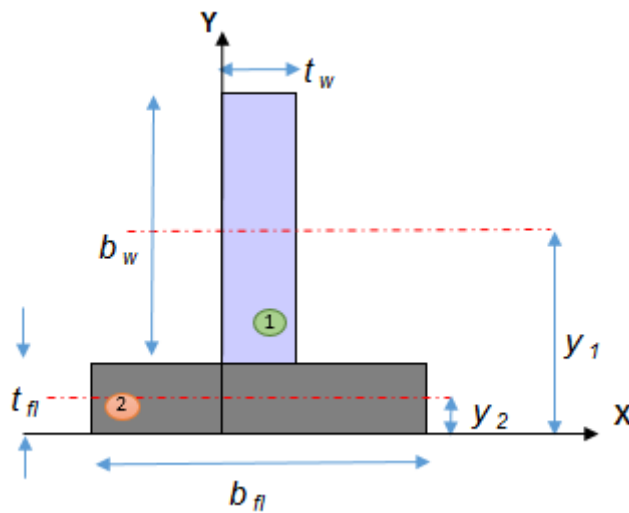


Figure 6.29 Cross-section of the stringer

$$(\sum A_i) \bar{y} = \sum A_i y_i$$

$$(A_1 + A_2) \bar{y} = A_1 y_1 + A_2 y_2$$

$$\bar{y} = \left( \frac{A_1 y_1 + A_2 y_2}{A_1 + A_2} \right) \quad (6.9)$$

Stringer dimension:

$b_{fl}$ : 0.06 m

$t_{fl}$ : 0.00549 m

$b_w$ : 0.06 m

$t_w$ : 0.00549 m

**Table 6.15 Web and flange sections**

Stringer Section	Area	$A_i$ (m <sup>2</sup> )	$y_i$ (m)	$A_i y_i$ (m <sup>3</sup> )	$A_1 + A_2$ (m <sup>2</sup> )
Web	$A_1$	0.000329	0.032745	0.000011	0.000012
Flange	$A_2$	0.000329	0.002745	0.0000009	

From Equation (6.9) and Table 6.15

$$\begin{aligned}\bar{y} &= \left( \frac{A_1 y_1 + A_2 y_2}{A_1 + A_2} \right) \\ &= \left( \frac{0.000011 + 0.0000009}{0.000012} \right) = 0.99m\end{aligned}$$

Use principle from Equation (6.7) and (6.8) to the second moment of area for  $x$  axis.

$$I_X = I_{xx} + A\bar{y}^2 \text{ and } I_{xx} = \frac{bh^3}{12}$$

For web:

$$\begin{aligned}I_{Xw} &= I_{xxw} + A_1 \bar{y}^2 \\ &= \frac{b_w h_w^3}{12} + A_1 \bar{y}^2 \\ &= \frac{(0.00549 \times 0.06^3)}{12} + (0.000329 \times (0.032745 - 0.99)^2) \\ &= 3.024E - 04 \text{ m}^4\end{aligned}$$

For flange:

$$\begin{aligned}I_{Xfl} &= I_{xxfl} + A_2 \bar{y}^2 \\ &= \frac{b_{fl} h_{fl}^3}{12} + A_2 \bar{y}^2 \\ &= \frac{(0.06 \times 0.00549^3)}{12} + (0.000329 \times (0.99 - 0.002745)^2) \\ &= 3.21E - 04 \text{ m}^4\end{aligned}$$



Total second moment of area,  $I_x$  :

$$I_x = I_{xw} + I_{xfl} = 3.024E - 04 + 3.21E - 04 = 6.23E - 04 m^4$$

Bending stiffness of the stringer,  $EI$ :

$$EI = 70E09Pa \times 6.23E - 04 = 4.36E07 Nm^2$$

The calculated  $EI$  is added in each box and the result is presented in Table 6.16.

**Table 6.16 Bending stiffness,  $EI$  for stringers**

		Number of stringers			EI (Nm <sup>2</sup> )	Average EI (Nm <sup>2</sup> )
		Upper Skin	Lower Skin	Total		
Box 1	Section 1	3	2	5	8.99E+04	8.99E+04
	Section 2	3	2	5	8.99E+04	
	Section 3	3	2	5	8.99E+04	
Box 2	Section 4	3	2	5	8.99E+04	9.89E+04
	Section 5	3	2	5	8.99E+04	
	Section 6	3	2	5	8.99E+04	
	Section 7	4	3	7	1.26E+05	
Box 3	Section 8	5	4	9	1.62E+05	1.62E+05
	Section 9	5	4	9	1.62E+05	
	Section 10	5	4	9	1.62E+05	
	Section 11	5	4	9	1.62E+05	
Box 4	Section 12	5	4	9	1.62E+05	1.89E+05
	Section 13	5	4	9	1.62E+05	
	Section 14	6	5	11	1.98E+05	
	Section 15	7	6	13	2.34E+05	
Box 5	Section 16	7	6	13	2.34E+05	2.43E+05
	Section 17	7	6	13	2.34E+05	
	Section 18	8	6	14	2.52E+05	
	Section 19	8	6	14	2.52E+05	
Box 6	Section 20	9	8	17	3.06E+05	3.36E+05
	Section 21	10	8	18	3.24E+05	
	Section 22	11	10	21	3.77E+05	
Box 7	Section 23	12	8	20	3.60E+05	3.82E+05
	Section 24	13	8	21	3.77E+05	
	Section 25	14	8	22	3.95E+05	
	Section 26	14	8	22	3.95E+05	

The flutter speed for wing skin with stringers was calculated using Comflut program [99]. Comflut is a FORTRAN based program that calculate flutter speed, natural frequency and main surface mode. The purpose of this analysis is to identify the effect of stringer addition to the flutter speed. Initial layup has been used as the input for this purpose. The percentage difference of flutter speed before and after the stringer addition is presented in Table 6.17.

**Table 6.17 Flutter speed and frequency with and without stringers**

	Without Stringer	With Stringer	Different of Percentage (%)
Flutter Speed (m/s)	331.50	279.5	15.7
Flutter frequency (rad/s)	53.75	60.5	11.2

From Table 6.17, result shows that the stringers have given the aeroelastic penalty to the wing structure where in this analysis the flutter speed for the baseline wing has been reduced by 15.7%. For the same baseline wing, the stringers addition has increased the flutter frequency by 11.2%.

The example of the stringer locations at the wing tip is shown in Figure 6.30.

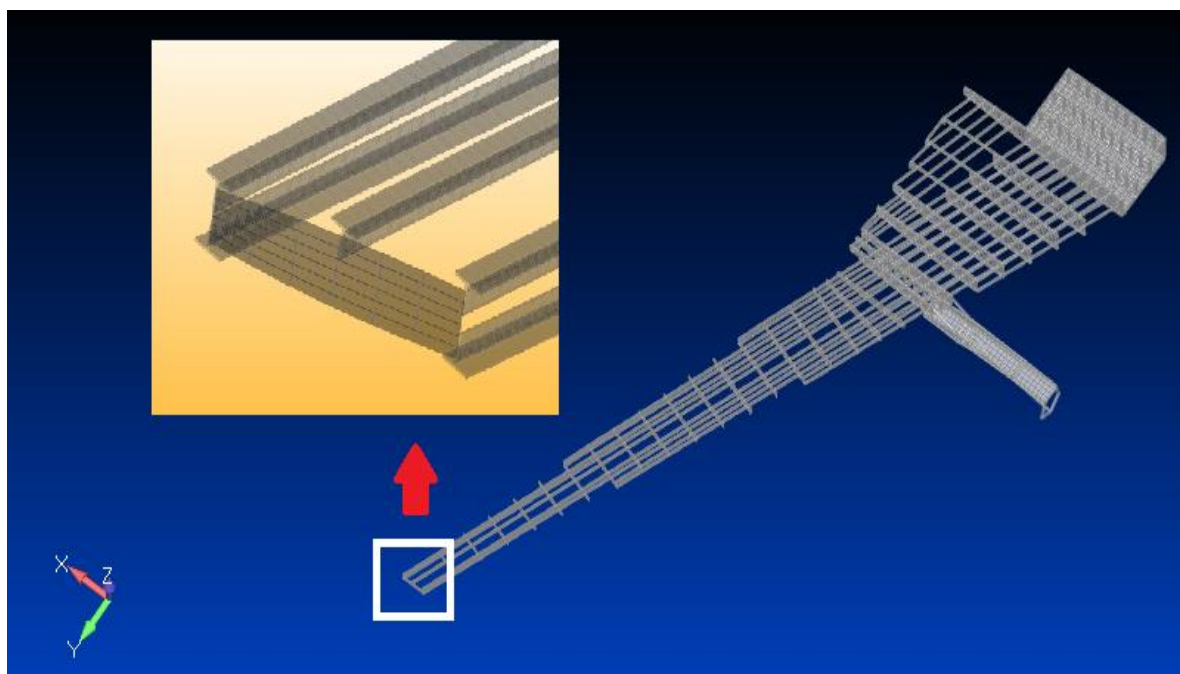


**Figure 6.30 Example of stringers location at wing tip**

# **7 OPTIMISATION OF COMPOSITE WING SUBJECT TO MULTI DESIGN AND MANUFACTURING CONSTRAINTS**

## **7.1 Wing Optimisation**

The static, buckling, modal, and flutter analysis of the baseline wing has been carried out in previous chapter using combination of low fidelity and high fidelity methods. Maximum von Mises stress and strain, critical buckling load including the representative mode shapes, normal modes, flutter speed and the main contributory modes to flutter were all computed and identified.

Analysis carried out in this chapter is a significant extension of the previous study and indeed, is essential because it is an important step towards the proposed major investigation on the design, analysis and optimisation of a transport airliner composite wing from an aeroelastic perspective. The present analysis has established and improved fundamental understanding of the current baseline wing. The investigation will then continue with optimisation of the baseline composite wing subject to multi design and manufacturing constraints.

Guo et al. [103,104] stated that the Gradient-Based Deterministic Method (GBDM) is more reliable and more efficient compared to the Genetic Algorithm (GA) based on a stochastic procedure. Guo et al. also discovered that the optimised result yield by GBDM method relied on the initial design variable set before the optimisation process begin [55]. This is a significant discovery since composite laminate can be tailored based on desired requirement. A NASA report, FORTRAN program for automated design synthesis (ADS) [105] has categorised the FORTRAN program into three levels; the optimisation strategy, optimiser and one-dimensional search for the solution of the nonlinear constrained optimisation problems.

The optimisation of baseline wing used the GBDM method and the objective is to increase the flutter speed. In this optimisation, the laminate layup is the design variable. No constraint has been set up in this analysis.

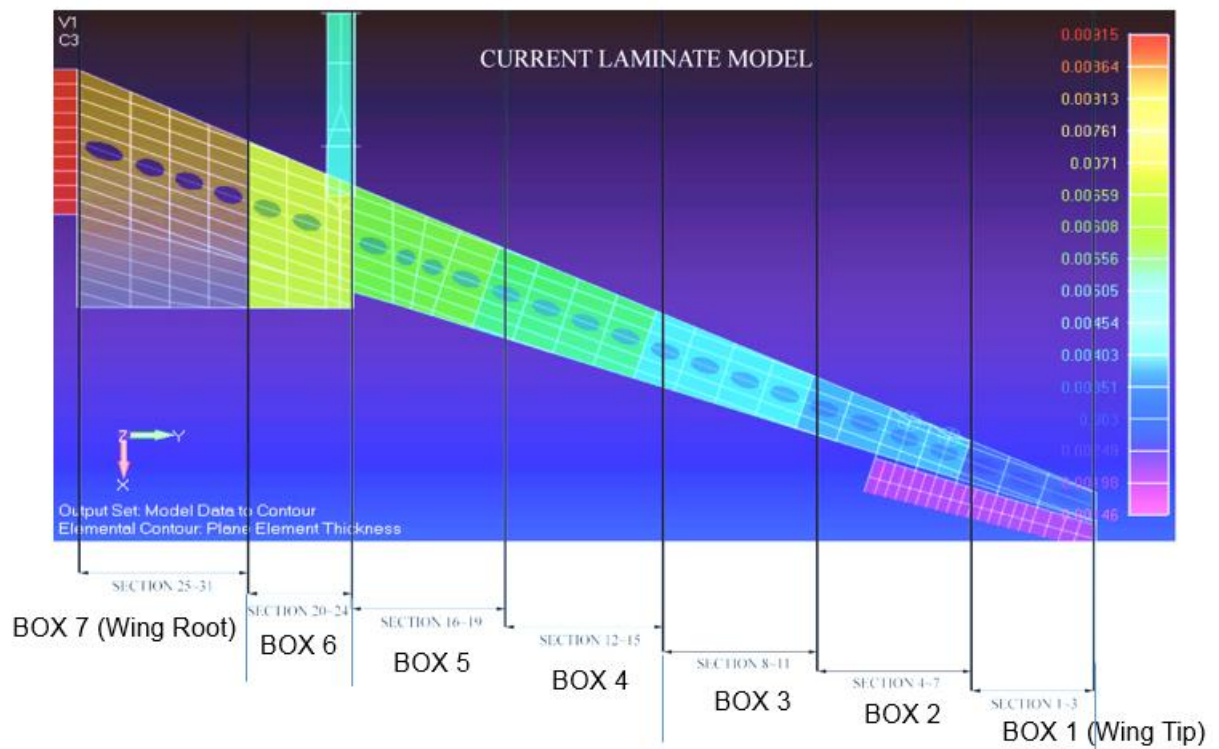


**Figure 7.1 Wing division for optimisation**

The wing is divided into 7 boxes, grouped by the same laminate thickness between each section. Refer Table 6.5 in previous chapter for details of laminate layup and stacking sequence.

## Optimisation Flowchart

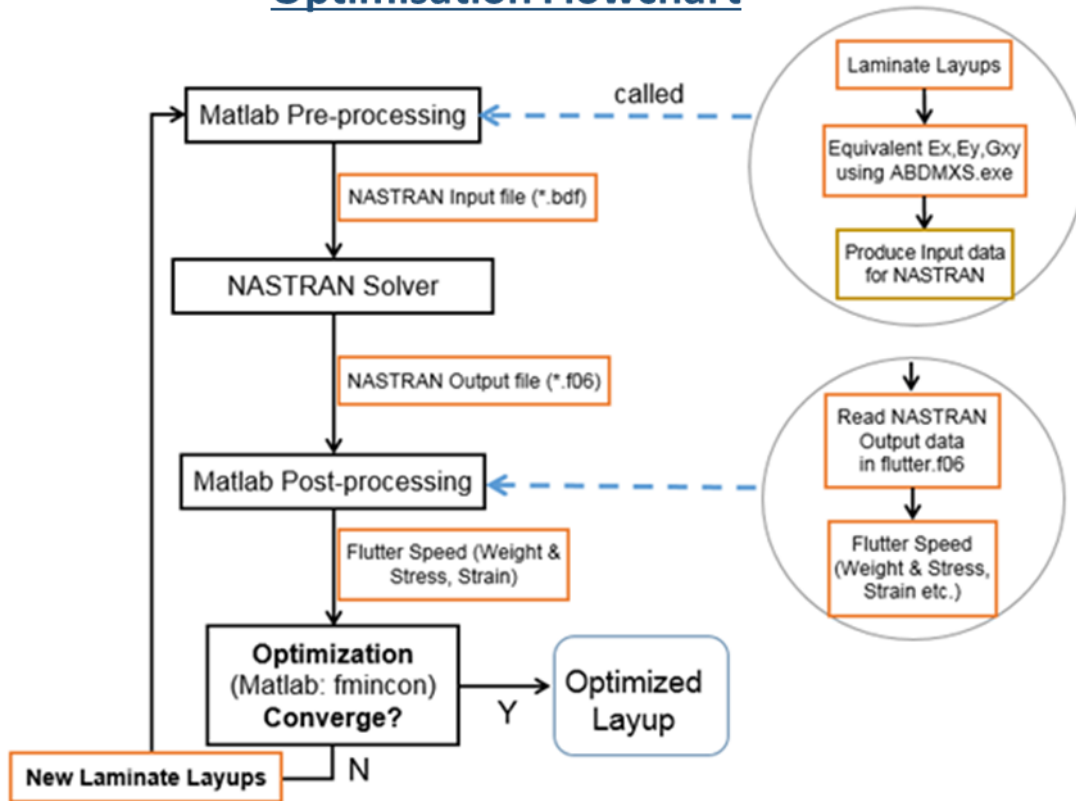


**Figure 7.2 Optimisation process using ABD Matrix Program, MATLAB and NASTRAN**

Figure 7.2 shows the optimisation process for the baseline model. The optimisation was run in NASTRAN, and MATLAB *fmincon* is used as the optimiser. The objective function is to increase the flutter speed by optimising the skin layup, by changing the ply orientation. A FORTRAN program called ABD Matrix Program [94] has been used to expedite the process. This program is developed based on composite laminate theory. Data generated from this program is a result of data analysed from macromechanics of composite laminate, the strength and stiffness of materials where the constitutive relationship of each parameter will be used in laminated composite structure analysis. This program will generate the laminate equivalent engineering elastic constant and produce input data for NASTRAN. The optimiser uses Gradient-Based Method where it will stop when the result of the slope is at zero value. This means there should be no flutter speed increment when the gradient is zero. The ply orientation will

keep changing until the slope reaches zero gradient, ergo the optimised layup will be decided when the slope becomes a fully nil value.

### Matlab Optimiser-fmincon

fmincon- Gradient-based optimiser

$$\min_x f(x) \text{ such that } \begin{cases} c(x) \leq 0 \\ ceq(x) = 0 \\ A \cdot x \leq b \\ Aeq \cdot x = beq \\ lb \leq x \leq ub \end{cases}$$

$f(x)$ - nonlinear objective function  
 $c(x)$ ,  $ceq(x)$ - nonlinear constraint functions  
 $A$ ,  $Aeq$ - matrices (linear constraints)  
 $lb$ ,  $ub$ - lower and upper bounds for variables

**Figure 7.3 The *fmincon*, MATLAB optimiser has been used in this optimisation**

Figure 7.3 shows *fmincon*, the MATLAB optimiser which used the Gradient-Based Method and the mathematical equation and function involved in this optimisation. In this research, A “NASTRAN-MATLAB-FORTRAN” based aeroelastic tailoring program has been developed as a tool for optimal design and analysis of composite wing (See Appendix D for MATLAB code).

## 7.2 Result

### 7.2.1 Convergence History

The convergence history during the optimisation process is shown in the following graphs. Results for Box 1 to Box 7 are presented in Figure 7.4 to Figure 7.10, respectively. These graphs are captured from MATLAB output. The top left graph shows the number of function involved, the bottom left graph represents the flutter speed result (m/s) and the bottom right shows the constraint. No constraint has been set up for this optimisation thus the value is constant for every graph. Note that for the function value graphs (bottom left), the  $y$  axis shows the positive function which indicates that the lower the value in the graph, the higher flutter speed is. For example in Figure 7.4, the initial flutter speed is 305.6m/s. After the

optimisation, the flutter speed increases and reach maximum value of 305.7m/s for Box 1.

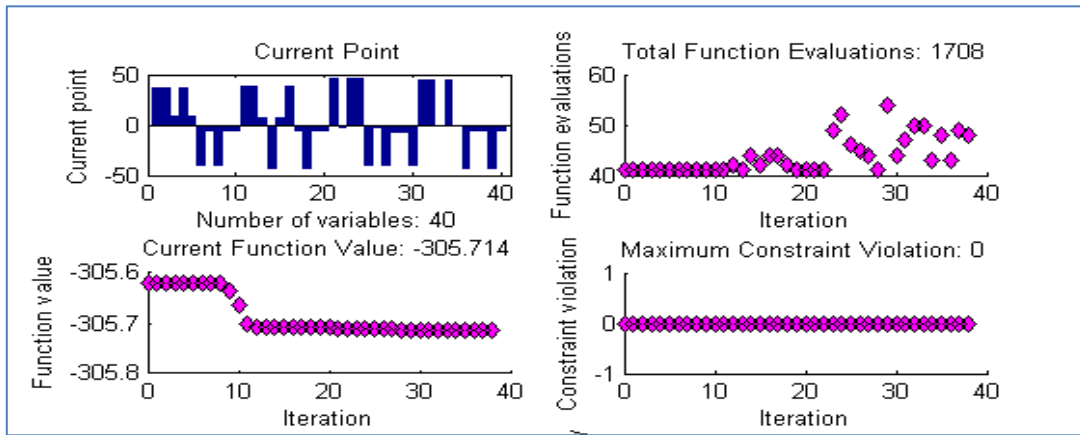


Figure 7.4 Result Box 1

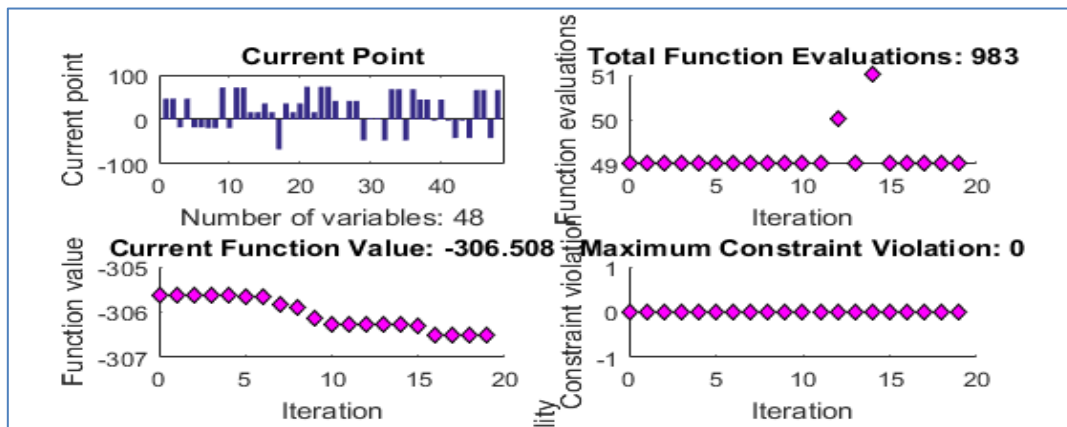


Figure 7.5 Result Box 2

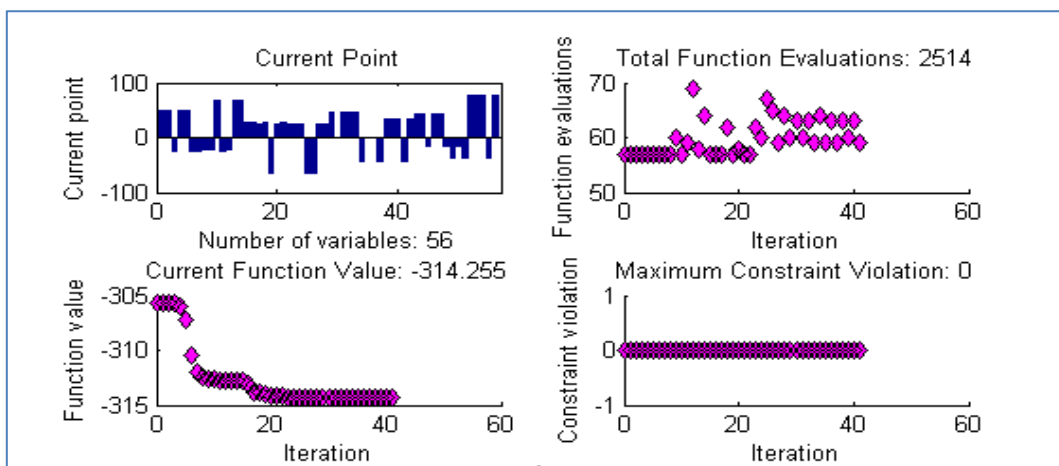


Figure 7.6 Result Box 3

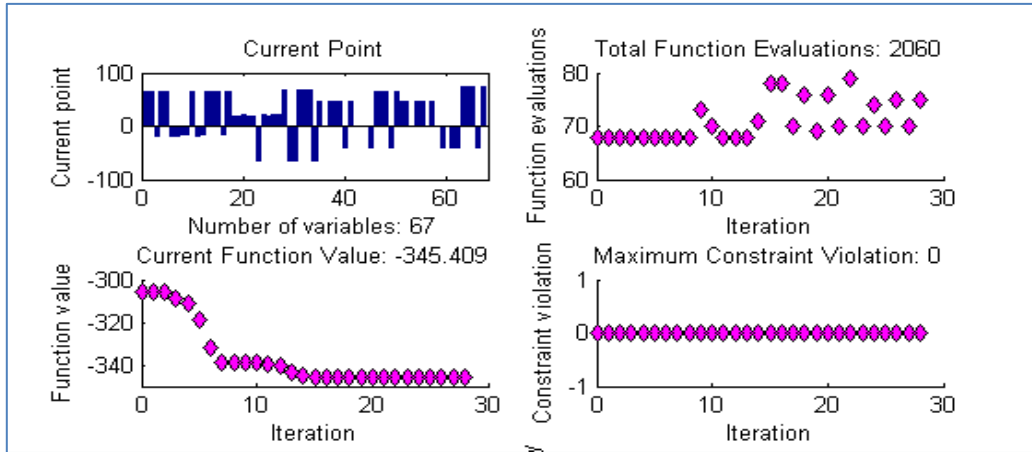


Figure 7.7 Result Box 4

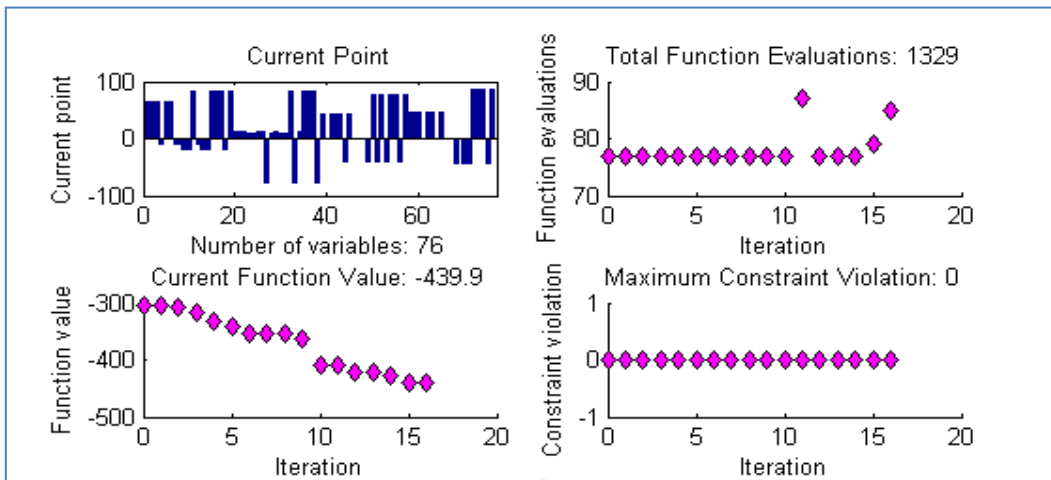


Figure 7.8 Result Box 5

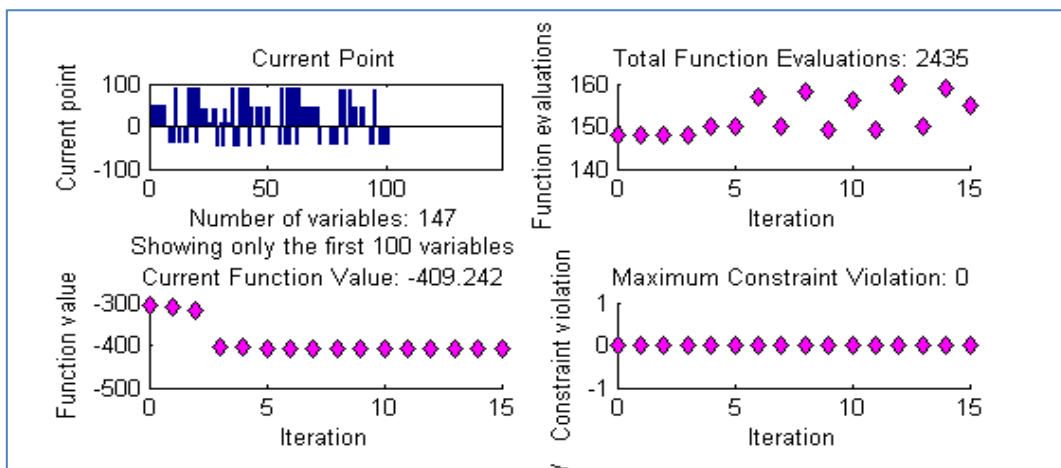
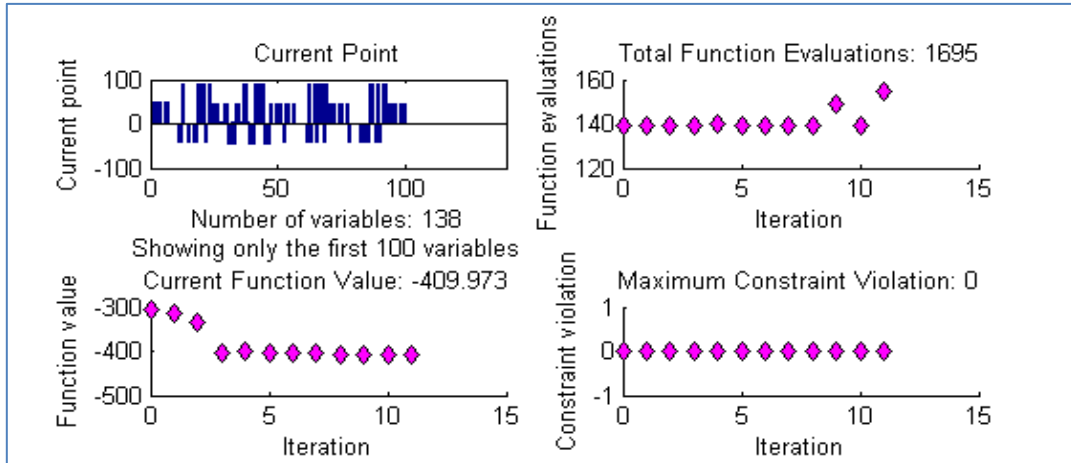


Figure 7.9 Result Box 6





**Figure 7.10 Result Box 7**

### 7.2.2 Flutter Speed

From the optimised flutter speed results obtained in Figure 7.4 to Figure 7.10, the flutter speed results for initial and optimum layup for every box is presented in Table 7.1 and graphs are illustrated in Figure 7.11. The percentage difference between initial and optimised design is plotted in Figure 7.12.

**Table 7.1 Flutter speed result for initial and optimised design**

	Initial flutter speed (m/s)	Optimised flutter speed (m/s)	Different of Percentage (%)
BOX 1	305.6	305.7	0.03
BOX 2	305.6	306.5	0.29
BOX 3	305.6	314.3	2.77
BOX 4	305.6	345.4	11.52
BOX 5	305.6	439.9	30.53
BOX 6	305.6	409.2	25.32
BOX 7	305.6	410	25.46

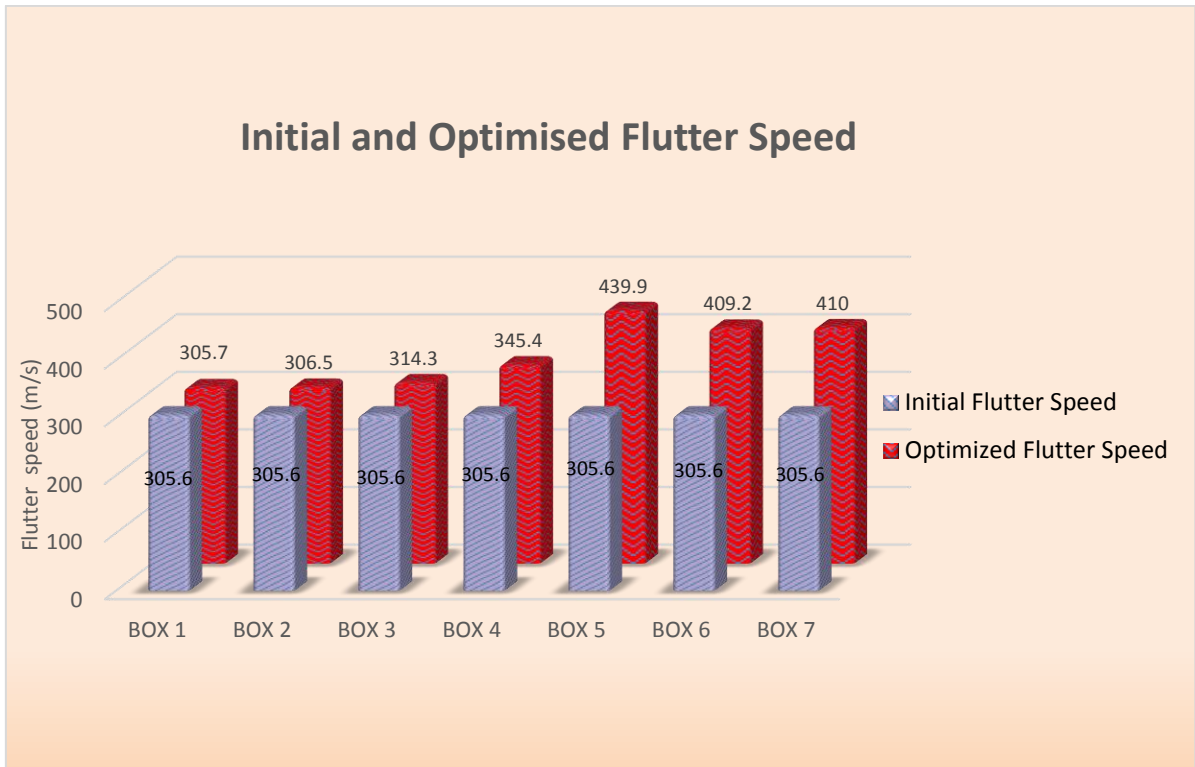


**Figure 7.11 Flutter speed results for initial and optimised layout**

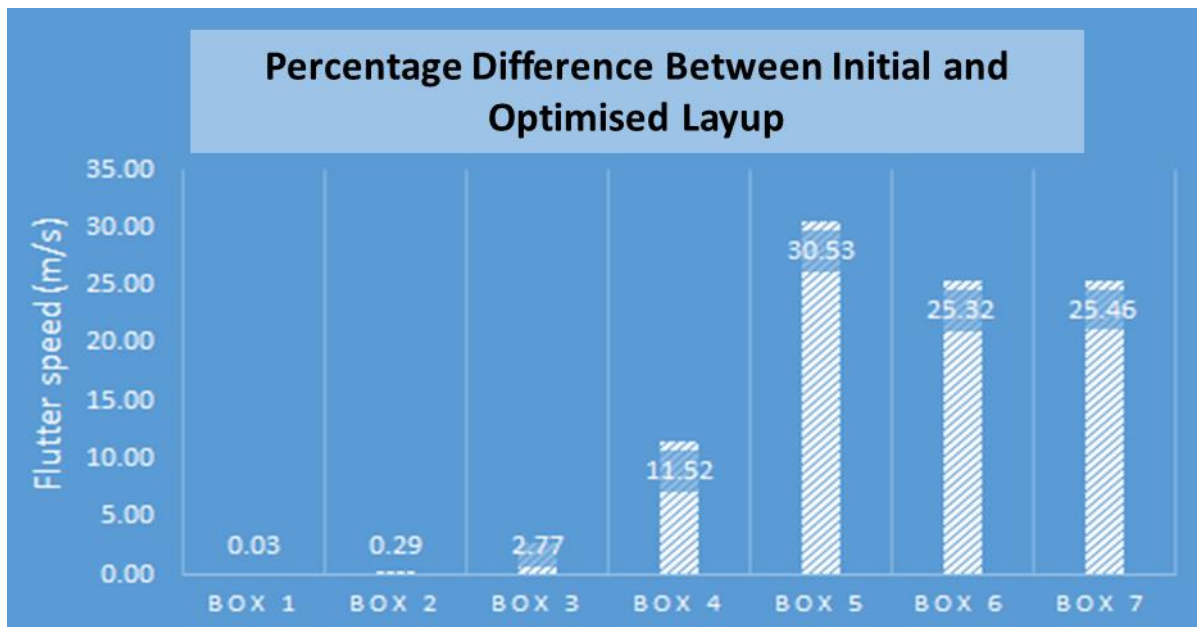


**Figure 7.12 The percentage difference between initial and optimised layout design**

The highest percentage difference occurs at Box 5. Note that Box 5 is located before pylon. The results show that the wing sections around the engine are more sensitive and effective to aeroelastic tailoring. Layup optimisation of Box 5 leads to an increased flutter speed by 30.53% from the initial  $V_f=305.6\text{m/s}$  to an optimised  $V_f= 439.9\text{m/s}$ .

### 7.2.3 Laminate Layup

The initial layup has been modified to meet the manufacture constraints. According to Liu and Richard [60] the design to manufacture of composite structure must follow the four rules given below as the manufacturing constraints.

1. The outer plies of the skin must be  $\pm 45^\circ$ . This rule is applied to reduce the damage tolerant after impact.
2. Only maximum of four consecutive ply layers with the same fibre orientation are allowed. If this constraint is neglected, the laminate will induce more transverse shear and the structure will be exposed to the edge splitting after produced.
3. Each orientation must contain at least 10% of the total laminate thickness. This constraint is significant and cannot be ignored to ensure the laminate will have sufficient damage tolerance, aeroelastic stiffness, bolted joint strength and strong enough to carry secondary load.
4. The ply drop-off rate as well as discontinuity between each adjacent laminates cannot be too large to reduce stress concentration. This constraint will also simplify the manufacturing process and can significantly reduce the manufacture cost.

Table 7.2 shows the initial baseline layup and Table 7.3 presents the optimised layup subject to manufacturing constraints. Optimised layup produced in Table 7.3 were trimmed in Table 7.4 to simplify the manufacturing process.

Table 7.2 Initial laminate layups subject to manufacturing constraints

Box	Laminate parts	Initial layups subject to manufacturing constraints
Box 1	Upper skin	[45/ -45/ 0/ 45/ 0/ 45/ 90/ -45/ 90/ 90]s
	Lower skin	[45/ -45/ 0/ 45/ 0/ 45/ 90/ -45/ 90/ 90]s
	Front spar	[45/ -45/ 45/ 45/ 0/ 0/ -45/ 90/ 90/ -45]s
	Rear spar	[45/ -45/ 0/ 45/ 0/ 45/ 90/ 90/ -45/ 90]s
Box 2	Upper skin	[45/ -45/ 0/ 45/ 0/ 0/ 45/ -45/ 90/ -45/ 90/ 90]s
	Lower skin	[45/ -45/ 0/ 45/ 45/ 0/ 45/ 0/ 90/ 45 90/ 90]s
	Front spar	[45/ -45/ 45/ 45/ 0/ 0/ 0/ -45/ 90/ 90/ -45 90]s
	Rear spar	[45/ -45/ 0/ 45/ 0/ 45/ 0/ -45/ 90/ 90/ -45 90]s
Box 3	Upper skin	[45/ -45/ 0/ 45/ 45/ 0/ 0/ 45/ -45/ 90/ 0/ -45/ 90/ 90]s
	Lower skin	[45/ -45/ 0/ 45/ 45/ 0/ 45/ 0/ 0/ 90/ -45/ -45/ 90/ 90]s
	Front spar	[45/ -45/ 45/ 45/ 45/ 0/ 0/ 0/ -45/ 90/ 90/ 90/ -45/ 90]s
	Rear spar	[45/ -45/ 0/ 45/ 45/ 0/ 45/ 0/ -45/ 90/ 90/ 90/ -45 90]s
Box 4	Upper skin	[45/ -45/ 0/ 45/ 45/ 0/ 0/ 45/ -45/ 90/ 0/ -45/ 90 90/ 90/ -45/ 90]s
	Lower skin	[45/ -45/ 0/ 45/ 45/ 45/ 0/ 45/ 0/ 0/ 90/ -45/ -45/ 90/ 90/ 90/ -45]s
	Front spar	[45/ -45/ 45/ 45/ 45/ 0/ 45/ 0/ 0/ 0/ -45/ 90/ 90/ 90/ -45 -45]s
	Rear spar	[45/ -45/ 0/ 45/ 45/ 0/ 45/ 0/ 45 0/ -45/ -45 90/ 90/ 90/ -45/ 90]s
Box 5	Upper skin	[45/ -45/ 45/ 0/ 45/ 45/ 0/ 0/ 45/ -45/ 90/ 0/ -45/ -45/ 90/ 90/ 90/ -45/ 90]s
	Lower skin	[45/ -45/ 45/ 0/ 0/ 45/ 45/ 45/ 0/ 45/ 0/ 0/ 90/ -45/ 45 90/ 90/ 90/ -45]s
	Front spar	[45/ -45/ 45/ 45/ 45/ 0/ 45/ 0/ 0/ 0/ -45/ 90 -45/ 90/ -45/ 90/ 90/ -45/ 90]s
	Rear spar	[45/ -45/ 45/ 0/ 45/ 45/ 0/ 45/ 0/ 0/ 45/ 0/ -45/ -45/ 90 90/ 90/ -45/ 90]s
Box 6	Upper skin cell-1	[45/ -45/ 45/ 0/ 45/ 45/ 0/ 0/ 45/ -45/ 90/ 0/ -45/ 0/ -45/ -45/ 90/ 90/ 90/ -45/ 90]s
	Lower skin cell-1	[45/ -45/ 45/ 0/ 0/ 45/ 45/ 45/ 0/ -45/ 45/ 0/ 0 90/ -45/ -45/ 90/ 90/ 90/ 90/ -45]s
	Front spar	[45/ -45/ 45/ 45/ 45/ 0/ 45/ 45/ 0/ 0/ 0/ 0/ -45/ 90/ -45/ 90/ -45 90/ 90/ -45/ 90]s
	Midwall	[45/ -45/ 45/ 0/ 45/ 45/ 0/ 45/ 45/ 0/ 0/ 0/ -45/ 0/ -45/ -45/ 90/ 90/ 90/ -45/ 90]s
	Upper skin cell-2	[45/ -45/ 45/ 0/ 45/ 45/ 0 0/ 45/ -45/ 90/ 0/ -45/ 0/ -45/ -45/ 90/ 90/ 90/ -45/ 90]s
	Lower skin cell-2	[45/ -45/ 45/ 0/ 0/ 45/ 45/ 45/ 0/ -45/ 45/ 0/ 0/ 90/ -45/ -45/ 90/ 90/ 90/ 90/ -45]s
Box 7	Rear spar	[45/ -45/ 45/ 45/ 0/ 0/ 45/ 45/ 0/ 0/ 45/ -45/ 0/ -45/ 90/ -45/ 0 90/ 90/ 90/ 90/ -45]s
	Upper skin cell-1	[45/ -45/ 45/ 45/ 0/ 45/ 45/ 0/ 0/ 0/ 45/ -45/ 90 0/ -45/ 0/ -45/ -45/ 90/ 90/ 90/ -45/ 90]s
	Lower skin cell-1	[45/ -45/ 45/ 0/ 0/ 45/ 45/ 45/ 0/ -45/ 45/ 0/ 0/ 90/ 0/ -45/ -45/ 90/ 90/ 90/ 90/ -45/ -45]s
	Front spar	[45/ -45/ 45/ 45/ 45/ 0/ 45/ 45/ 0/ 45/ 0/ 0/ 0/ 0/ -45/ 90/ -45/ 90/ -45 90/ 90/ -45/ 90]s
	Midwall	[45/ -45/ 45/ 0/ 45/ 45/ 0/ 45/ 45/ 0/ 0/ 0 0 -45/ 0/ -45/ 90/ 90/ 90/ -45 90/ -45/ 90 90]s
	Upper skin cell-2	[45/ -45/ 45/ 45/ 0/ 45/ 45/ 0/ 0/ 0/ 45/ 0/ 90/ 0/ -45/ 0/ -45/ -45/ 90/ 90/ 90/ -45/ 90]s

**Table 7.3 Optimised laminate layups subject to manufacturing constraints**

Box	Laminate parts	Optimum laminate layup subject to manufacturing constraints																			
Box 1	Upper skin	[45/ -45/ 13.08/ 30.35/ 13.08 30.3/ -6.3/ -41.11/ -6.34/ -6.34]s																			
	Lower skin	[45/ -45/ 16.24/ 34.92/ 16.24/ 34.93/ -7.11/ -45.13/ -7.11/ -7.11]s																			
	Front spar	[45/ -45/ 46.68/ 46.68/ -6.66/ -6.66/ -38.41/ 4.99/ -14.99/ -38.41]s																			
	Rear spar	[45/ -45/ -0.77/ 44.66/ -0.77/ 44.66/ -12.68/ -12.68/ -43.64/ -12.68]s																			
Box 2	Upper skin	[45/ -45/ -19.63/ 46.18/ -19.63/ -19.63/ 46.18/ -17.84/ 74.09/ -17.84/ 74.09/ 74.09]s																			
	Lower skin	[45/ -45/ 16.94/ 19.46/ 19.46/ 16.94/ 19.46/ 16.94/ 84.35/ 19.46/ 84.35/ 84.35]s																			
	Front spar	[45/ -45/ 42.06/ 42.06/ 3.53/ 3.53/ -46.96/ 78.4/ 78.41/ -46.96/ 78.41]s																			
	Rear spar	[45/ -45/ 3.28/ 44.71/ 3.28/ 44.71/ 3.28/ -41.96/ 76.13/ 76.13/ -41.9/ 76.13]s																			
Box 3	Upper skin	[45/ -45/ -23.77/ 60.02/ 60/ -23.77/ -23.76/ 60.01/ -23.28/ 63.54/ -23.76/ -23.28/ 63.54/ 63.5]s																			
	Lower skin	[45/ -45/ 25.95/ 18.83/ 18.83/ 26.33/ 18.83/ 26.33/ 25.99/ 26.58/ -78.62/ -78.62/ 26.58/ 26.58]s																			
	Front spar	[45/ -45/ 47.46/ 47.46/ 47.46/ 1.51/ 1.5/ 1.50/ -44.70/ 39.70/ 39.70/ 39.70/ -44.70/ 39.70]s																			
	Rear spar	[45/ -45/ -10.76/ 43.36/ 43.36/ -10.71/ 43.36/ -10.71/ -38.77/ 69.17/ 69.17/ 69.17/ -38.8/ 69.17]s																			
Box 4	Upper skin	[45/ -45/ -19.65/ 57.22/ 57.22/ -19.65/ -19.65/ 57.21/ -18.50/ 72/ -19.6/ -18.50/ 72/ 72/ 72/ -18.50/ 72]s																			
	Lower skin	[45/ -45/ 21.78/ 19.03/ 19.03/ 19.03/ 21.78/ 19.02/ 21.78/ 21.78/ 68.53/ -64.20/ -64.20/ 68.53/ 68.53/ 68.53/ -64.20]s																			
	Front spar	[45/ -45/ 44.88/ 44.88 44.88/ -0.15/ 44.87/ -0.14/ -0.14/ -0.14/ -43.93/ 66.61/ 66.61/ 66.61/ -43.93/ 66.61]s																			
	Rear spar	[45/ -45/ -1.44/ 44.95/ 44.95/ -1.44/ 44.95/ -1.44/ 44.95/ -1.44/ -42.88/ -42.88/ 77.66/ 77.66/ 77.66/ -42.89/ 77.66]s																			
Box 5	Upper skin	[45/ -45/ 64.60/ -9.50/ 64.60/ 64.60/ -9.50/ -9.50/ 64.60/ -9.76/ 82.58/ -9.50/ -9.76/ -9.76/ 82.54/ 82.54/ 82.54/ -9.76/ 82.54]s																			
	Lower skin	[45/ -45/ 20.47/ 23.07/ 23.08/ 20.47/ 20.47/ 20.47/ 23.07/ 20.47/ 23.07/ 23.07/ 83.70/ -87.19/ 20.47/ 83.70/ 83.70/ 83.70/ -87.19]s																			
	Front spar	[45/ -45/ 42.11/ 42.11/ 42.11/ 0.81/ 42.11/ 0.81/ 0.81/ 0.81/ -43.61/ 73.83/ -43.61/ 73.83/ -43.61/ 73.8/ 73.83/ -43.61/ 73.83]s																			
	Rear spar	[45/ -45/ 44.63/ -0.15/ 44.63/ 44.63/ -0.15/ 44.63/ -0.15/ -0.15/ 44.63/ -0.15/ -44.94/ -44.94/ 79.66/ 79.66/ 79.66/ -44.94]s																			
Box 6	Upper skin cell-1	[45/ -45/ 49.13/ -0.16/ 49.13/ 49.13 -0.16/ -0.16/ 49.13/ -41.75/ 89.92/ -0.16/ -41.75/ -0.16/ -41.75/ -41.7/ 89.9/ 89.92/ 89.92/ -41.75/ 89.92]s																			
	Lower skin cell-1	[45/ -45/ 39.79/ 11.50/ 11.50/ 39.79 39.79/ 39.79/ 11.50/ -49.70/ 39.79/ 11.50/ 11.50/ 86.99/ -49.70/ -49.70/ 86.99/ 86.99/ 86.99/ 86.99/ -49.70]s																			
	Front spar	[45/ -45/ 44.98/ 44.98 44.98/ -0.4 44.97/ 44.97/ -0.39/ -0.39/ -0.39/ -0.39/ -44.42/ 89.88/ -44.42/ 89.88/ -44.42/ 89.88/ 89.88/ -44.42/ 89.88]s																			
	Midwall	[45/ -45/ 44.93/ 0.06/ 44.93/ 44.94/ 0.05/ 44.92/ 44.92/ 0.05/ 0.05/ 0.05/ -45.03/ 0.05/ -45.03/ -45.03/ 85.37/ 85.37/ 85.37/ -45.03/ 85.37]s																			
	Upper skin cell-2	[45/ -45/ 45.11/ -0.82/ 45.11/ 45.11/ -0.82/ -0.82/ 45.10/ -44.86/ 85.40/ -0.82/ -44.86/ -0.82/ -44.86/ -44.86/ 85.4/ 85.40/ 85.40/ -44.86/ 85.40]s																			
	Lower skin cell-2	[45/ -45/ 44.58/ 1.44/ 1.44/ 44.58/ 44.57/ 44.57/ 1.44/ -45.21/ 44.57/ 1.44/ 1.44/ 85.28/ -45.21/ -45.21/ 85.28/ 85.28/ 85.28/ 85.28/ -45.21]s																			
Rear spar	[45/ -45/ 45.01/ 45.0/ -0.03/ -0.03/ 45/ 45/ -0.03/ -0.03/ 45.00/ -44.96/ -0.03/ -44.96/ 89.93/ -44.96/ 89.93/ 89.93/ 89.93/ 89.93/ -44.96]s																				
Box 7	Upper skin cell-1	[45/ -45/ 48.61/ 48.61/ -4.43/ 48.61/ 48.61/ -4.43/ -4.43/ -4.43/ 48.61/ -43.19/ 85.20/ -4.43/ -43.19/ -4.43/ -43.19/ -43.19/ 85.20/ 85.20/ 85.20/ -43.19/ 85.20]s																			
	Lower skin cell-1	[45/ -45/ 42.02/ 6.17/ 6.17/ 42.02/ 42.02/ 42.02/ 6.17/ -48.92/ 42.02/ 6.17/ 6.17/ 85.49/ 6.17/ -48.92/ -48.92/ 85.49/ 85.49/ 85.49/ 85.49/ -48.92/ -48.92]s																			
	Front spar	[45/ -45/ 45.13/ 45.13/ 45.13/ -0.11/ 45.12/ 45.12/ -0.10/ 45.12/ -0.10/ -0.10/ -0.10/ -0.10/ -44.82/ 85.21/ -44.82/ 85.21/ -44.82/ 85.21/ 85.21/ -44.82/ 85.21]s																			
	Midwall	[45/ -45/ 44.98/ 0.16/ 44.98/ 44.98/ 0.16/ 44.97/ 44.97/ 0.16/ 0.16/ 0.16/ -45.09/ 0.16/ -45.09/ -45.09/ 85.43/ 85.43/ -45.09/ 85.43/ -45.09/ 85.43/ 85.43]s																			
	Upper skin cell-2	[45/ -45/ 44.69/ 44.69/ 0.10/ 44.67/ 44.68/ 0.10/ 0.10/ 0.10/ 44.6/ -44.84/ 84.90/ 0.10/ -44.84/ 0.10/ -44.84/ -44.84/ 84.90/ 84.90/ 84.90/ -44.84/ 84.90]s																			
	Rear spar	[45/ -45/ 45/ 45/ -0.06/ -0.06/ 45/ 45/ -0.05/ -0.05/ 45 -44.95/ -0.05/ -44.95/ -44.95/ 85.30/ -44.95/ -0.05/ 85.30/ 85.30/ 85.30/ -44.95]s																			

Table 7.4 Trimmed optimum laminate layup for manufacturing considerations

Box	Laminate parts	Trimmed optimum laminate layup for manufacture considerations
Box 1	Upper skin	[45/ -45/ 13/ 30/ 13/ 30/ -6/ -41/ -6/ -6]s
	Lower skin	[45/ -45/ 16/ 35/ 16/ 35/ -7/ -45/ -7/ -71]s
	Front spar	[45/ -45/ 47/ 47/ -7/ -7/ -39/ 5/ -15/ -38]s
	Rear spar	[45/ -45/ -0.1/ 45/ -1/ 45/ -13/ -13/ -44/ -13]s
Box 2	Upper skin	[45/ -45/ -19/ 46/ -20/ -20/ 46/ -18/ 74/ -18/ 74/ 75]s
	Lower skin	[45/ -45/ 17/ 19/ 20/ 17/ 20/ 17/ 84/ 19/ 84/ 84]s
	Front spar	[45/ -45/ 42/ 42/ 4/ 4/ 4/ -47/ 78/ 78/ -47/ 78]s
	Rear spar	[45/ -45/ 3/ 45/ 3/ 45/ 3/ -42/ 76/ 76/ -42/ 76]s
Box 3	Upper skin	[45/ -45/ -24/ 60/ 60/ -24/ -24/ 60/ -23/ 64/ -24/ -23/ 63/ 63]s
	Lower skin	[45/ -45/ 26/ 19/ 19/ 26/ 19/ 26/ 26/ 27/ -79/ -79/ 27/ 26]s
	Front spar	[45/ -45/ 47/ 47/ 47/ 2/ 2/ 2/ -45/ 40/ 40/ 40/ -45/ 40]s
	Rear spar	[45/ -45/ -11/ 43/ 43/ -11/ 43/ -11/ -39/ 69/ 69/ 69/ -39/ 69]s
Box 4	Upper skin	[45/ -45/ -20/ 57/ 57/ -20/ -20/ 57/ -19/ 72/ -20/ -19/ 72/ 72/ 72/ -19/ 72]s
	Lower skin	[45/ -45/ 212/ 19/ 19/ 19/ 22/ 19/ 22/ 22/ 69/ -64/ -64/ 68/ 69/ 69/ -64]s
	Front spar	[45/ -45/ 45/ 45/ 45/ 0/ 45/ 0/ 0/ 0/ -44/ 67/ 67/ 66/ -44/ 67]s
	Rear spar	[45/ -45/ -1/ 45/ 45/ -1/ 45/ -1/ 45/ -1/ -43/ -43/ 78/ 78/ 78/ -42.89/ 78]s
Box 5	Upper skin	[45/ -45/ 65/ -10/ 65/ 65/ -10/ -10/ 65/ -10/ 83/ -10/ -10/ -10/ 83/ 83/ 83/ -10/ 83]s
	Lower skin	[45/ -45/ 20/ 23/ 23/ 20/ 20/ 20/ 23/ 20/ 23/ 23/ 84/ -87/ 20/ 84/ 84/ 84/ -87]s
	Front spar	[45/ -45/ 42/ 42/ 42/ 1/ 42/ 1/ 1/ 1/ -44/ 74/ -44/ 74/ -44/ 74/ 74/ -44/ 74]s
	Rear spar	[45/ -45/ 45/ 0/ 45/ 45/ 0/ 45/ 0/ 0/ 45/ 0/ -45/ -45/ 80/ 80/ 80/ -45/ 80]s
Box 6	Upper skin cell-1	[45/ -45/ 49/ 0/ 49/ 49/ 0/ 0/ 49/ -42/ 90/ 0/ -42/ 0/ -42/ -42/ 90/ 90/ 90/ -42/ 90]s
	Lower skin cell-1	[45/ -45/ 40/ 12/ 12/ 40/ 40/ 40/ 12/ -50/ 40/ 12/ 12/ 87/ -50/ -50/ 87/ 87/ 90/ 87/ -50]s
	Front spar	[45/ -45/ 45/ 45/ 45/ 0/ 45/ 45/ 0/ 0/ 0/ 0/ -44/ 90/ -44/ 90/ -44/ 90/ 90/ 90/ -44/ 90]s
	Midwall	[45/ -45/ 45/ 0/ 45/ 45/ 0/ 45/ 45/ 0/ 0/ 0/ -45/ 0/ -45/ -45/ 85/ 85/ 85/ -45/ 85]s
	Upper skin cell-2	[45/ -45/ 45/ -1/ 45/ 45/ -1/ -1/ 45/ -45/ 85/ -1/ -45/ -1/ -45/ -45/ 85/ 85/ 85/ -45/ 85]s
	Lower skin cell-2	[45/ -45/ 45/ 1/ 1/ 45/ 45/ 45/ 1/ -45/ 45/ 1/ 1/ 85/ -45/ -45/ 85/ 85/ 85/ 85/ -45]s
Rear spar	[45/ -45/ 45/ 45/ 0/ 0/ 45/ 45/ 0/ 0/ 45/ -45/ 0/ -45/ 90/ -45/ 90/ 90/ 90/ 90/ -45]s	
Box 7	Upper skin cell-1	[45/ -45/ 49/ 49/ -4/ 49/ 49/ -4/ -4/ -4/ 49/ -43/ 85/ -4/ -43/ -4/ -43/ -43/ 85/ 85/ 85/ -43/ 85]s
	Lower skin cell-1	[45/ -45/ 42/ 6/ 6/ 42/ 42/ 42/ 6/ -49/ 42/ 6/ 6/ 85/ 6/ -49/ -45/ 85/ 85/ 85/ 85/ -49/ -49]s
	Front spar	[45/ -45/ 45/ 45/ 45/ 1/ 45/ 45/ 0/ 45/ 0/ 0/ 0/ 0/ -44/ 85/ -45/ 85/ -45/ 85/ 85/ -45/ 85]s
	Midwall	[45/ -45/ 45/ 0/ 45/ 45/ 0/ 45/ 45/ 0/ 0/ 0/ -45/ 0/ -45/ -45/ 8/ 85/ -45/ 85/ -45/ 85/ 85]s
	Upper skin cell-2	[45/ -45/ 45/ 45/ 0/ 45/ 45/ 0/ 0/ 0/ 45/ -45/ 85/ 08/ -45/ 0/ -45/ -45/ 85/ 85/ 85/ -45/ 85]s
	Rear spar	[45/ -45/ 45/ 45/ 0/ 0/ 45/ 45/ 0/ 0/ 45/ -45/ 0/ -45/ -45/ 85/ -45/ 0/ 85/ 85/ 85/ 85/ -45]s

## 7.2.4 Natural Modes and Frequency

---

### 1<sup>st</sup> Mode

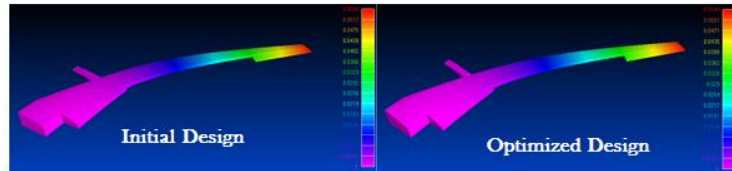
---

#### Initial design

Mode shape: 1<sup>st</sup> bending  
Natural frequency: 2.11Hz

#### Optimised design

Mode shape: 1<sup>st</sup> bending  
Natural frequency: 2.13Hz




---

### 2<sup>nd</sup> Mode

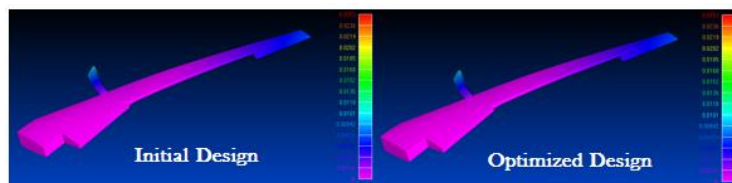
---

#### Initial design

Mode shape: Pylon Swing  
Natural frequency: 2.89Hz

#### Optimised design

Mode shape: Pylon Swing  
Natural frequency: 2.90Hz




---

### 3<sup>rd</sup> Mode

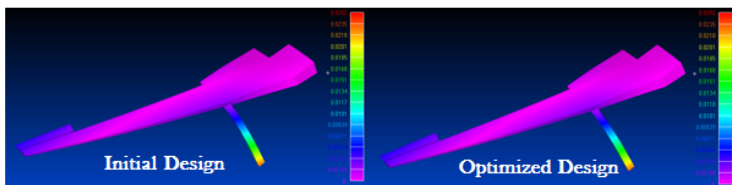
---

#### Initial design

Mode shape: Pylon Pitching  
Natural frequency: 3.75Hz

#### Optimised design

Mode shape: Pylon Pitching  
Natural frequency: 3.76Hz




---

### 4<sup>th</sup> mode

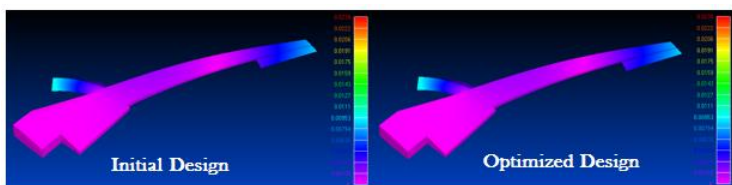
---

#### Initial design

Mode shape: 1<sup>st</sup> Bending and Swing  
Natural frequency: 5.47Hz

#### Optimised design

Mode shape: 1<sup>st</sup> Bending & Swing  
Natural frequency: 5.47Hz




---

### 5<sup>th</sup> Mode

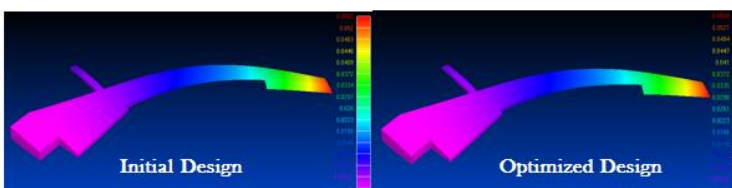
---

#### Initial design

Mode shape: 2<sup>nd</sup> Bending & Swing  
Natural frequency: 6.67Hz

#### Optimised design

Mode shape: 2<sup>nd</sup> Bending & Swing  
Natural frequency: 6.71Hz



---

6<sup>th</sup> Mode

---

**Initial design**

Mode shape: 3<sup>rd</sup> Bending & Swing

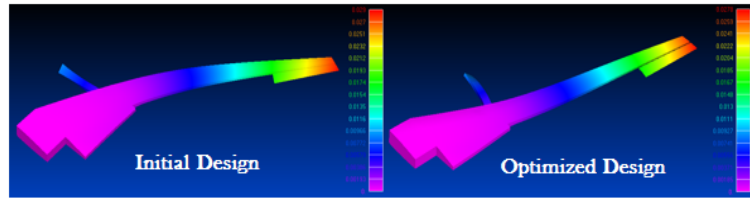
Natural frequency: 7.07Hz

**Optimised design**

Mode shape: 3<sup>rd</sup> Bending & Swing

Natural frequency: 7.08Hz

---



---

7<sup>th</sup> Mode

---

**Initial design**

Mode shape: 2<sup>nd</sup> Bending

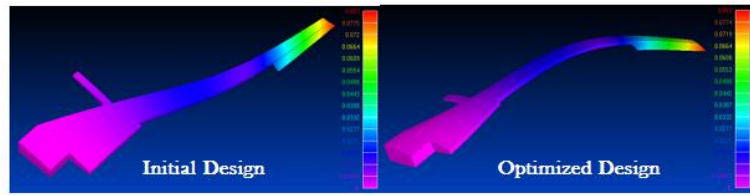
Natural frequency: 7.18Hz

**Optimised design**

Mode shape: 2<sup>nd</sup> Bending

Natural frequency: 7.19Hz

---



---

8<sup>th</sup> Mode

---

**Initial design**

Mode shape: 3<sup>rd</sup> Bending

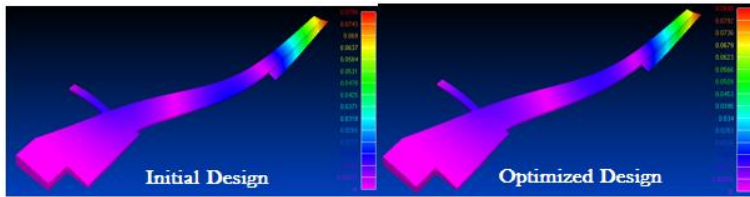
Natural frequency: 11.36Hz

**Optimised design**

Mode shape: 3<sup>rd</sup> Bending

Natural frequency: 11.38Hz

---



---

9<sup>th</sup> Mode

---

**Initial design**

Mode shape: 1<sup>st</sup> Torsion

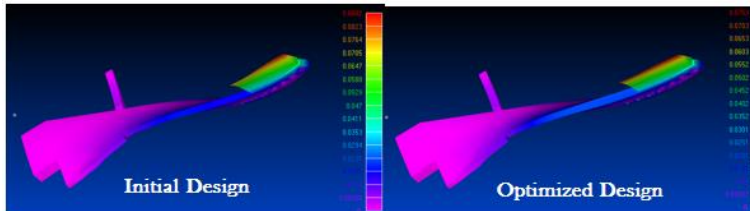
Natural frequency: 13.51Hz

**Optimised design**

Mode shape: 1<sup>st</sup> Torsion

Natural frequency: 13.96Hz

---



---

10<sup>th</sup> Mode

---

**Initial design**

Mode shape: 2<sup>nd</sup> Torsion

Natural frequency: 17.12Hz

**Optimised design**

Mode shape: 2<sup>nd</sup> Torsion

Natural frequency: 17.20Hz

---

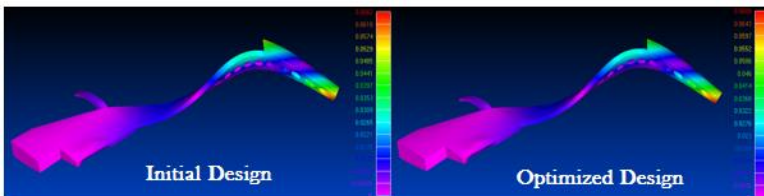
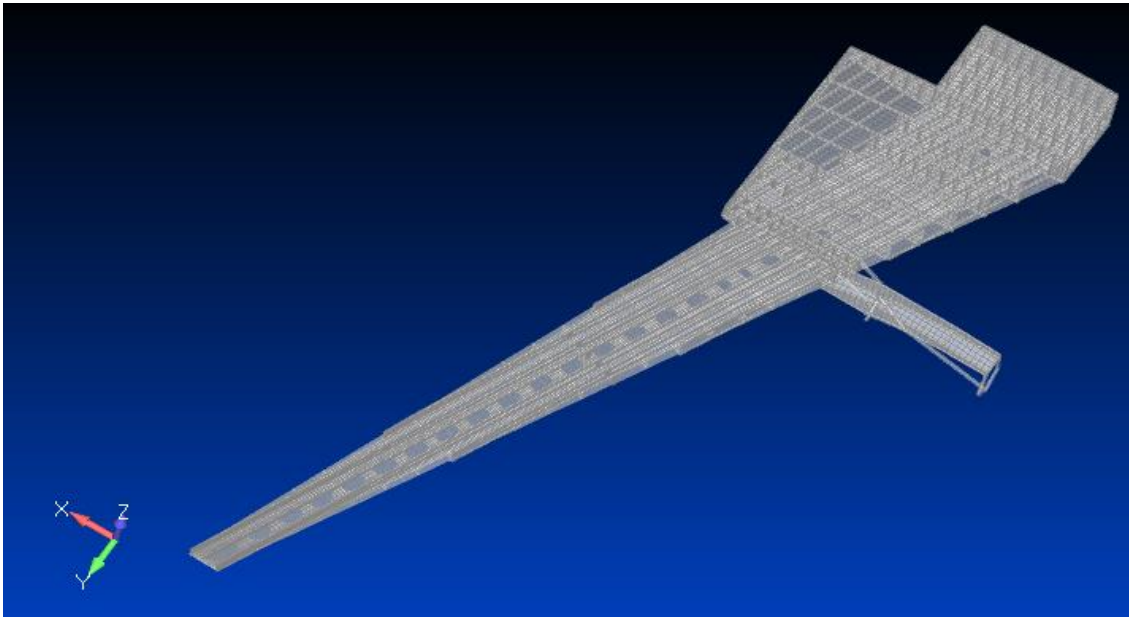




Figure 7.13 shown below is the final design of the wing cover panel which has been optimised based on the multi design constraints.



**Figure 7.13 The optimised composite wing cover panel subject to multi design constraints**

## 8 CONCLUSIONS AND SCOPE FOR FUTURE WORK

### 8.1 Conclusions

1. The K-BOAT tool developed at the beginning of the research has been demonstrated in the study of a composite wing. Results show that the optimised design has increased 30.5% flutter speed compared to initial design.
2. Detailed research on individual element for stiffness matrix has been carried out. There is no clear explanation as to why coupling in symmetrical and balance layup is zero. Analysis shows that the extension-shear coupling is eliminated in symmetrical balance layup by the plus and minus fibre angle, which contributes to the additional knowledge to shear theory.
3. Analysis for factors effecting coupling and uncoupling terms for symmetrical laminate is developed. When coupled terms combined with uncoupled terms, the trend is same as uncoupled term. Eg;  $A_{22}A_{33}$  has the same trend as  $A_{23}$ . When all coupled terms combined,  $A_{33}$  will dominate the trend.
4. Correlation between laminate and composite thin-wall beam structure has been developed. A new conceptual framework for design tool has been developed to correlate 1-dimensional to 2-dimensional beam structure. FE model was created to correlate 2-dimensional and 3-dimensional beam structure. Relationships amongst composite laminates and composite wing box structures of the same material have been developed. These correlations will be guidelines for the design engineers to predict the stiffness of the wing box structure during the material selection process and laminate design stage.
5. Three important factors have been identified as starting point for aircraft designer to design and have quick assessment on structural rigidity. Designers can start to design an aircraft composite structure by using symmetrical and balance layup, use ply orientation at  $45^\circ$  ply angle and use a closed double-cell box for type of the structure. By adopting these

criteria as a guideline at early design stage, aircraft designer will get benefit by minimising the cost and development time and the performance of end product can be predicted at early design stage. This initial input however can be tailored subject to the design requirements and constraints.

6. A “NASTRAN-MATLAB-FORTRAN” based aeroelastic tailoring program has been developed as a tool to optimise the design of a composite wing. FE model of a composite wing panel has been created for analysis and to represent the optimised wing structure. The optimisation of the wing panel skin has been performed by applying the K-BOAT structure with the practical design constraints taken into account. The optimisation has improved the aeroelastic stability by increasing the flutter speed from the initial  $V_f=305.6\text{m/s}$  to an optimised  $V_f=439.9\text{m/s}$ .

## **8.2 Scope for Future Work**

1. To demonstrate K-BOAT for different aircraft parts. In future, a case study to optimise a blended wing body of the aircraft will be carried out by using K-BOAT framework.
2. For beam box, there is no theory or formulation to calculate bending stiffness and torsional stiffness for box with cut-out. Up to now, the relationship of box with cut-out can be found in the stress-strain relation but not for stiffness. For future work, a theory for box with cut-out or manhole will be developed since in reality, most of the wing box are designed with manhole for maintenance purpose.

## REFERENCES

1. Megson THG. Aircraft Structures for Engineering Students Fifth Edition. Fifth Edit. Oxford, Elsevier Ltd.; 2012.
2. Sharma S., Iyengar NGR., Murthy PN. A study of coupling in laminated plates. *Fibre Science and Technology*. 1983; 18(4): 287–299. DOI:10.1016/0015-0568(83)90022-2
3. Tsai SW., Wu EM. A general theory of strength for anisotropic materials. *Journal of Composite Materials*. 1971; 5(1): 58–80. DOI:10.1177/002199837100500106
4. Guo S. Introduction to Basic Material Type and FRP Terminology. Lecture Notes. Cranfield University. 2012.
5. York CB. On extension-shearing coupled laminates. *Composite Structures*. 2015; 120: 472–482. DOI:10.1016/j.compstruct.2014.10.019
6. Bartholomew P. Ply stacking sequences for laminated plates having in-plane and bending orthotropy. *Fibre Science and Technology*. 1977; 10(4): 239–253. DOI:10.1016/0015-0568(77)90001-X
7. Li J., Li D. Extension-shear coupled laminates with immunity to hygro-thermal shearing distortion. *Composite Structures*. 2015; 123: 401–407. DOI:10.1016/j.compstruct.2014.12.032
8. Nakayama M., Uda N., Ono K., Takeda S-I., Morimoto T. Design-oriented strength of mechanical joints in composite laminate structures and reliability-based design factor. *Composite Structures*. 2015; 132: 1–11. DOI:10.1016/j.compstruct.2015.04.044
9. Bendemra H., Compston P., Crothers PJ. Optimisation study of tapered scarf and stepped-lap joints in composite repair patches. *Composite Structures*. 2015; 130: 1–8. DOI:10.1016/j.compstruct.2015.04.016
10. Mansfield EH. Stiffness of a two-cell anisotropic tube. *Aeronautical Quarterly*. 1981; 32(pt 4): 338–353.
11. Banerjee J. R., Williams F. W. Coupled bending-torsional matrix for timoshenko dynamic stiffness. *Mechanical Engineering*. 1992; 42(3): 301–310.
12. Armanios EA., Badir AM. Free vibration analysis of anisotropic thin-walled closed-section beams. *AIAA Journal*. 1995; 33(10): 1905–1910.
13. Berdichevsky V., Armanios E., Badir A. Theory of anisotropic thin-walled closed-cross-section beams with hygrothermal effects. *Composites Engineering*. 1992; 2(5–7): 411–432. DOI:10.1016/0961-9526(92)90035-5

14. Berdichevsky V., Armanios E., Badir A. Theory of anisotropic thin-walled closed-cross-section beams. *Composites Engineering*. 1992; 2(5–7): 411–432. DOI:10.1016/0961-9526(92)90035-5
15. Bauchau OA., Coffenberry BS., Rehfield LW. Composite box beam analysis - Theory and experiments. *ASME*. 1987; 6: 25–35.
16. Chandra R., Chopra I., Chandra, R.; Chopra I. Structural behavior of two-cell composite rotor blades with elastic couplings. *AIAA Journal*. 1992; 30(12): 2914–2921.
17. Badir AM. Analysis of two-cell composite beams. *Proceedings of the 36th AIAA/ASME/ASCE/AHS/ASC Structures, Structural Dynamics, and Materials Conference and AIAA/ASME Adaptive Structures Forum. Part 1 (of 5)*. 1995. pp. 419–424.
18. Boothroyd G. Product design for manufacture and assembly. *Computer-Aided Design*. 1994; 26(7): 505–520. DOI:10.1016/0010-4485(94)90082-5
19. Roy R., Hinduja S., Teti R. Recent advances in engineering design optimisation: Challenges and future trends. *CIRP Annals - Manufacturing Technology*. 2008; 57(2): 697–715. DOI:10.1016/j.cirp.2008.09.007
20. Wang K., Wang L., Yuan Q., Luo S., Yao J., Yuan S., et al. Construction of a generic reaction knowledge base by reaction data mining. *Journal of Molecular Graphics and Modelling*. 2001; 19(5): 427–433. DOI:10.1016/S1093-3263(00)00102-9
21. Bobbie PO. Grouping knowledge-base data into distributable clusters. *Knowledge-Based Systems*. 1990; 3(4): 230–235.
22. Velásquez JD., Palade V. A Knowledge Base for the maintenance of knowledge extracted from web data. *Knowledge-Based Systems*. 2007; 20(3): 238–248. DOI:10.1016/j.knosys.2006.05.015
23. Chapman CB., Pinfold M. The application of a knowledge based engineering approach to the rapid design and analysis of an automotive structure. *Advances in Engineering Software*. 2001; 32(12): 903–912. DOI:10.1016/S0965-9978(01)00041-2
24. Ong YS., Keane AJ. A domain knowledge based search advisor for design problem solving environments. *Engineering Applications of Artificial Intelligence*. 2002; 15(1): 105–116. DOI:10.1016/S0952-1976(02)00016-7
25. Curran R., Verhagen WJC., Van Tooren MJL., Van Der Laan TH. A multidisciplinary implementation methodology for knowledge based engineering: KNOMAD. *Expert Systems with Applications*. 2010; 37(11): 7336–7350. DOI:10.1016/j.eswa.2010.04.027

26. Choi J-W. Architecture of a knowledge based engineering system for weight and cost estimation for a composite airplane structures. *Expert Systems with Applications*. 2009; 36(8): 10828–10836. DOI:10.1016/j.eswa.2008.10.049
27. Li BM., Xie SQ., Xu X. Recent development of knowledge-based systems, methods and tools for One-of-a-Kind Production. *Knowledge-Based Systems*. 2011; 24(7): 1108–1109. DOI:10.1016/j.knosys.2011.05.005
28. Rocca G La. Knowledge based engineering: Between AI and CAD. Review of a language based technology to support engineering design. *Advanced Engineering Informatics*. 2012; 26(2): 159–179. DOI:10.1016/j.aei.2012.02.002
29. Verhagen WJC., Bermell-Garcia P., Van Dijk REC., Curran R. A critical review of Knowledge-Based Engineering: An identification of research challenges. *Advanced Engineering Informatics*. 2012; 26(1): 5–15. DOI:10.1016/j.aei.2011.06.004
30. Thuraisingham MB. Towards the design of a secure data/knowledge 11 base management system. *Data and Knowledge Engineering*. 1990; 5(1): 59–72.
31. Lai Y-L. A constraint-based system for product design and manufacturing. *Robotics and Computer-Integrated Manufacturing*. 2009; 25(1): 246–258. DOI:10.1016/j.rcim.2007.12.003
32. Nguyen N-V., Choi S-M., Kim W-S., Lee J-W., Kim S., Neufeld D., et al. Multidisciplinary unmanned combat air vehicle system design using multi-fidelity model. *Aerospace Science and Technology*. 2013; 26(1): 200–210. DOI:10.1016/j.ast.2012.04.004
33. Lin C-C., Lee Y-J. Stacking sequence optimization of laminated composite structures using genetic algorithm with local improvement. *Composite Structures*. 2004; 63(3–4): 339–345. DOI:10.1016/S0263-8223(03)00182-X
34. Kogiso N., Watson LT., Gürdal Z., Haftka RT. Genetic algorithms with local improvement for composite laminate design. *Structural Optimization*. 1994; 7(4): 207–218. DOI:10.1007/BF01743714
35. Park JH., Hwang JH., Lee CS., Hwang W. Stacking sequence design of composite laminates for maximum strength using genetic algorithms. *Composite Structures*. 2001; 52(2): 217–231. DOI:10.1016/S0263-8223(00)00170-7
36. Todoroki A., Haftka RT. Stacking sequence optimization by a genetic algorithm with a new recessive gene like repair strategy. *Composites Part B: Engineering*. 1998; 29(3): 277–285. DOI:10.1016/S1359-8368(97)00030-9

37. Nagendra S., Jestin D., Gürdal Z., Haftka RT., Watson LT. Improved genetic algorithm for the design of stiffened composite panels. *Computers and Structures*. 1996; 58(3): 543–555. DOI:10.1016/0045-7949(95)00160-I
38. Le Riche R., Haftka RT. Optimization of laminate stacking sequence for buckling load maximization by genetic algorithm. *AIAA Journal*. 1993; 31(5): 951–956. DOI:10.2514/3.11710
39. An H., Chen S., Huang H. Simultaneous optimization of stacking sequences and sizing with two-level approximations and a genetic algorithm. *Composite Structures*. 2015; 123: 180–189. DOI:10.1016/j.compstruct.2014.12.041
40. Jing Z., Fan X., Sun Q. Stacking sequence optimization of composite laminates for maximum buckling load using permutation search algorithm. *Composite Structures*. 2015; 121: 225–236. DOI:10.1016/j.compstruct.2014.10.031
41. Wang W., Guo S., Chang N., Yang W. Optimum buckling design of composite stiffened panels using ant colony algorithm. *Composite Structures*. 2010; 92(3): 712–719. DOI:10.1016/j.compstruct.2009.09.018
42. Wang W., Guo S., Yang W. Simultaneous partial topology and size optimization of a wing structure using ant colony and gradient based methods. *Engineering Optimization*. 2011; 43(4): 433–446.: DOI:10.1080/0305215X.2010.493936
43. Zhao Q., Ding Y., Jin H. A layout optimization method of composite wing structures based on carrying efficiency criterion. *Chinese Journal of Aeronautics*. *Chinese Journal of Aeronautics*; 2011; 24(4): 425–433. DOI:10.1016/S1000-9361(11)60050-2
44. Hao W., Ying Y., Wei Y., Baohua L. Adaptive approximation-based optimization of composite advanced grid-stiffened cylinder. *Chinese Journal of Aeronautics*. August 2010; 23(4): 423–429. DOI:10.1016/S1000-9361(09)60237-5
45. Omkar SN., Senthilnath J., Khandelwal R., Narayana Naik G., Gopalakrishnan S. Artificial Bee Colony (ABC) for multi-objective design optimization of composite structures. *Applied Soft Computing*. 2011; 11(1): 489–499. DOI:10.1016/j.asoc.2009.12.008
46. Hansen LU., Horst P. Multilevel optimization in aircraft structural design evaluation. *Computers & Structures*. 2008; 86(1): 104–118. DOI:10.1016/j.compstruc.2007.05.021
47. S. Guo.; C.W. Cheung; J.R. Banarjee; R. Butler. Gust alleviation and flutter suppression of an optimized composite wing. *Proceedings of the International Forum: Aeroelasticity and Structural Dynamic*. 1995; : 41.1-41.

48. ISOGAI K. Direct search method to aeroelastic tailoring of a composite wing under multiple constraints. *Journal of Aircraft*. 1989; 26(12): 1076–1080. DOI:10.2514/3.45883
49. Guo S. Aeroelastic optimization of an aerobatic aircraft wing structure. *Aerospace Science and Technology*. 2007; 11(5): 396–404. DOI:10.1016/j.ast.2007.01.003
50. Guo S., Cheng W., Cui D. Aeroelastic tailoring of composite wing structures by laminate layup optimization. *AIAA Journal*. 2006; 44(12): 3146–3150. DOI:10.2514/1.20166
51. Mastroddi F., Tozzi M., Capannolo V. On the use of geometry design variables in the MDO analysis of wing structures with aeroelastic constraints on stability and response. *Aerospace Science and Technology*. 2011; 15(3): 196–206. DOI:10.1016/j.ast.2010.11.003
52. Banerjee JR., Williams FW. Free vibration of composite beams-an exact method using symbolic computation. *Journal of Aircraft*. 1995; 32(3): 636–642. DOI:10.2514/3.46767
53. Lillico, M., Butler, R., Guo, S., and Banerjee JR. Aeroelastic Optimization of Composite Wings Using the Dynamic Stiffness Method. *Aeronautical Journal*. 1997; 101(2161): 77–86.
54. Butler R., Lillico M., Banerjee JR., Guo S. Optimum design of high aspect ratio wings subject to aeroelastic constraints. *Collection of Technical Papers - AIAA/ASME/ASCE/AHS/ASC Structures, Structural Dynamics and Materials Conference*. 1995; 1. DOI:10.2514/6.1995-1223
55. Guo SJ., Bannerjee JR., Cheung CW. The effect of laminate lay-up on the flutter speed of composite wings. *Proceedings of the Institution of Mechanical Engineers, Part G: Journal of Aerospace Engineering* . 2003; 217(3): 115–122. DOI:10.1243/095441003322297225
56. Guo S., Li D., Liu Y. Multi-objective optimization of a composite wing subject to strength and aeroelastic constraints. *Proceedings of the Institution of Mechanical Engineers, Part G: Journal of Aerospace Engineering*. 2012; 226(9): 1095–1106. DOI:10.1177/0954410011417789
57. Fu Q. *Optimization of a Composite Wing Subject to Multi Constraints*. Cranfield University; 2013.
58. Niu MC-Y. *Airframe Structural Design - Practical Design Information and Data on Aircraft Structures (2nd Edition)*. AD Adaso/Adastra Engineering LLC. Hong Kong: Conmilit Press Limited; 1999. 282-284, 406-412 p.
59. Phillips BJ. *Multidisciplinary Optimisation of a CFRP Wing Cover*. Design. PhD Thesis. Cranfield University; 2009. DOI:10.1260/0957456042880200



60. Liu W., Butler R. Optimum buckling design of composite wing cover panels. *AIAA/ASME/ASCE/ASC Structures, Structural Dynamics, and Materials Conference*. 2007. pp. 1–11. DOI:10.2514/6.2007-2215
61. Vidyashankar BR., Krishna Murty A V. Analysis of laminates with ply drops. *Composites Science and Technology*. 2001; 61(5): 749–758. DOI:10.1016/S0266-3538(01)00010-0
62. Kradinov V., Hanauska J., Barut A., Madenci E., Ambur DR. Bolted patch repair of composite panels with a cutout. *Composite Structures*. 2002; 56(4): 423–444. DOI:10.1016/S0263-8223(02)00027-2
63. Costin DP., Wang BP. Optimum design of a composite structure with manufacturing constraints. *Thin-Walled Structures*. 1993; 17(3): 185–202. DOI:10.1016/0263-8231(93)90002-R
64. Costin DP., Wang BP. Optimum design of a composite structure with ply-interleaving constraints. *Thin-Walled Structures*. 1993; 17: 185–202.
65. Henderson JL., Gürdal Z., Loos AC., Henderson, J. L.; Gurdal, Z.; Alfred CL. Combined Structural and Manufacturing Optimization of Stiffened Composite Panels. *Journal of Aircraft*. 1999; 36(1): 246–254.
66. Yin H., Yu X. Integration of manufacturing cost into structural optimization of composite wings. *Chinese Journal of Aeronautics*. *Chinese Journal of Aeronautics*; 2010; 23(6): 670–676. DOI:10.1016/S1000-9361(09)60269-7
67. Mohd Maulana II BIN., Al-Ashaab A., Flisiak J., Araci ZC., Lasisz P., Shehab E., et al. The set-based concurrent engineering application: A process of identifying the potential benefits in the surface jet pump case study. *27th CIRP Design Conference*. 2017. pp. 350–355. DOI:10.1016/j.procir.2017.01.026
68. Araci ZC., Al-Ashaab A., Lasisz PW., Flisiak JW., Maulana MIIM., Beg N., et al. Trade-off Curves Applications to Support Set-based Design of a Surface Jet Pump. *Procedia CIRP*. 2017. pp. 356–361. DOI:10.1016/j.procir.2017.01.028
69. Court M. The Application of Set-Based Concurrent Engineering to Enhance the Design Performance of Surface Jet Pump 2 A review of the SBCE related literature 3 The Surface Jet Pump Case Study. 2016. pp. 634–643.
70. Khan MS., Al-Ashaab A., Shehab E., Haque B., Ewers P., Sorli M., et al. Towards lean product and process development. *International Journal of Computer Integrated Manufacturing*. 2013; 26(12): 1105–1116. DOI:10.1080/0951192X.2011.608723
71. Robinson HS., Carrillo PM., Anumba CJ., Al-Ghassani a. M. Developing a business case for knowledge management: the IMPaKT approach. *Construction Management and Economics*. 2004; 22(9): 733–743. DOI:10.1080/0144619042000226306

72. Bert CW. Classical Lamination Theory. In: Pendleton RL, Tuttle ME (eds.) Manual on Experimental Methods for Mechanical Testing of Composites. Dordrecht: Springer Netherlands; 1989. pp. 11–16. DOI:10.1007/978-94-009-1129-1\_3
73. Lu P., He LH., Lee HP., Lu C. Thin plate theory including surface effects. International Journal of Solids and Structures. 2006; 43(16): 4631–4647. DOI:10.1016/j.ijsolstr.2005.07.036
74. Kubiak T. Chapter 2 Theory of thin plates for laminates. Static and Dynamic Buckling of Thin-Walled Plate Structures. Springer International Publishing Switzerland; 2013. p. 188. DOI:10.1007/978-3-319-00654-3
75. Bauchau OA., Craig JI. Kirchhoff plate theory. Structural Analysis. 2009; 163: 819–914. DOI:10.1007/978-90-481-2516-6\_16
76. eFunda. Classical Lamination Theory. 2017. Available at: [http://www.efunda.com/formulae/solid\\_mechanics/composites/comp\\_laminate.cfm](http://www.efunda.com/formulae/solid_mechanics/composites/comp_laminate.cfm) (Accessed: 30 April 2017)
77. NPTEL. Laminate Theory: Introduction to Classical Plate Theory. 2017. Available at: [http://nptel.ac.in/courses/101104010/lecture16/16\\_3.htm](http://nptel.ac.in/courses/101104010/lecture16/16_3.htm) (Accessed: 30 April 2017)
78. Ashton, J. E., J.C. Halpin PHP. Primer on Composite Materials: Analysis, Technomic Press. Westport, CT: CRC Press; 1992. 242 p.
79. Powell P. Engineering with Polymers. London: Chapman and Hall; 1983.
80. McComb G., Boysen E. Electronics for Dummies. Wiley Publishing, Inc. John Wiley & Sons; 2005. 1-433 p.
81. Jones RM. Mechanics of composite materials. Mechanics of Composite Materials. 1999. p. 519. DOI:10.1007/BF00611782
82. Roylance D. Laminated Composite Plates. Lecture Notes. Massachusetts Institute of Technology Cambridge. 2000.
83. Jung SN., Park I-J., Shin ES. Theory of thin-walled composite beams with single and double-cell sections. Composites Part B: Engineering. 2007; 38(2): 182–192. DOI:10.1016/j.compositesb.2006.07.001
84. Adams DB., Watson LT., G??rdal Z., Anderson-Cook CM. Genetic algorithm optimization and blending of composite laminates by locally reducing laminate thickness. Advances in Engineering Software. 2004; 35(1): 35–43. DOI:10.1016/j.advengsoft.2003.09.001
85. Almeida FS., Awruch AM. Design optimization of composite laminated structures using genetic algorithms and finite element analysis. Composite Structures. Elsevier Ltd; 2009; 88(3): 443–454. DOI:10.1016/j.compstruct.2008.05.004

86. Omkar SN., Mudigere D., Naik GN., Gopalakrishnan S. Vector evaluated particle swarm optimization (VEPSO) for multi-objective design optimization of composite structures. *Computers & Structures*. 2008; 86(1–2): 1–14. DOI:10.1016/j.compstruc.2007.06.004
87. Soremekun G., Gürdal Z., Haftka RT., Watson LT. Composite laminate design optimization by genetic algorithm with generalized elitist selection. *Computers & Structures*. 2001; 79(2): 131–143. DOI:10.1016/S0045-7949(00)00125-5
88. Walker M., Smith RE. A technique for the multiobjective optimisation of laminated composite structures using genetic algorithms and finite element analysis. *Composite Structures*. 2003; 62(1): 123–128. DOI:10.1016/S0263-8223(03)00098-9
89. Suresh S., Sujit PB., Rao AK. Particle swarm optimization approach for multi-objective composite box-beam design. *Composite Structures*. 2007; 81(4): 598–605. DOI:10.1016/j.compstruct.2006.10.008
90. Muc A., Gurba W. Genetic algorithms and finite element analysis in optimization of composite structures. *Composite Structures*. 2001; 54(2–3): 275–281. DOI:10.1016/S0263-8223(01)00098-8
91. Fu Q. Optimisation of a composite wing subject to multi constraints. PhD Thesis. Cranfield University; 2013.
92. Ghiasi H., Pasini D., Lessard L. Optimum stacking sequence design of composite materials Part I: Constant stiffness design. *Composite Structures*. 2009. pp. 1–11. DOI:10.1016/j.compstruct.2009.01.006
93. Butler R. The Optimisation of wing structures-theory or practise. *Aircraft Engineering and Aerospace Technology*. 1998; 70(1): 4–8.
94. Guo S. ABD Matrix Program. Computer Program. Cranfield University; 2004.
95. Guo S. BOXMX Program. Computer Program. Cranfield University; 2004.
96. Rehfield LW., Atilgan AR., Hodges DH. Nonclassical Behavior of Thin-Walled Composite Beams with Closed Cross Sections. *Journal of the American Helicopter Society*. 1990; 35(2): 42. DOI:10.4050/JAHS.35.42
97. Hodges DH., Atilgan AR., Fulton M V., Rehfield LW. Free-Vibration Analysis of Composite Beams. *Journal of the American Helicopter Society*. 1991; 36(3): 36. DOI:10.4050/JAHS.36.36
98. Hart-Smith L J D. 2054. The Ten-Percent Rule for Preliminary Sizing of Fibrous Composite Structures. 51st Annual Conference, Hartford, Connecticut, May 18-20. 1992. p. 28.
99. Guo S. COMFLUT. Computer Program. Cranfield University; 2004.

100. Harakare P., Heblikar VK. Evaluation of Static and Buckling load carrying capability of the Wing box through FEM approach. Proceedings of National Conference on 'Women in Science & Engineering. 2013. pp. 6–9.
101. Hodges DH., Pierce GA. Introduction to Structural Dynamics and Aeroelasticity. Cambridge University Press; 2011.
102. J. R. Wright JEC. Introduction to Aircraft Aeroelasticity and Loads. Second Edi. John Wiley & Sons; 2014.
103. Guo S. Aeroelastic optimization of an aerobatic aircraft wing structure. Aerospace Science and Technology. 2007; 11(5): 396–404. DOI:10.1016/j.ast.2007.01.003
104. Guo SJ., Cheng W., Cui D. Optimization of composite wing structures for maximum flutter speed. 46th AIAA/ASME/ASCE/AHS/ASC Structures, Structural Dynamics & Materials Conference. 2005. pp. 1–10. DOI:AIAA 2005-2132
105. Vanderplaats GN. ADS-A Fortran program for automated design synthesis. NASA Contractor Report. NASA-CB-177985; 1985.

## APPENDICES

### Appendix A: ABD Matrix Program (Example data file)

Input example:

8 **Line 1**  
--- *Number of layers of the plate*

135E09 10.0E09 0.3 5.0E09 5.0E09 5.0E09 **Line 2**  
--- *Young's Modulus  $E_1$ ;  $E_2$ ; Poisson's Ratio  $\nu_{12}$ ; Shear modulus  $G_{12}$ ;  $G_{23}$ ;  $G_{13}$*

1 15.0 0.125E-3  
2 15.0 0.125E-3  
3 15.0 0.125E-3  
4 15.0 0.125E-3  
5 15.0 0.125E-3 **Line 3**  
6 15.0 0.125E-3  
7 15.0 0.125E-3  
8 15.0 0.125E-3  
--- *Layer number; fibre orientation (degree); layer thickness*

1.0 **Line 4**  
--- *The width of the composite beam*

100000.0 30000.0 50000.0 0.0 0.0 0.0 **Line 5**  
--- *In-plane force in X; Y; XY; moment about X; Y; torque applied*

1370E+03 1000E+03 42E+03 200E+03 60E+03 **Line 6**  
--- *Material strength input data. Tensile and compressive strength in fibre direction (1); tensile and compressive strength in off-fibre direction (2); shear strength in 1-2 direction*

1 **Line 7**  
--- *Failure index criteria for maximum stress and Tsai-Hill criteria)*

**Output example:**

ABD Matrix Program produces the following results for a laminate plate (beam)

1. [ABD] matrix;

```
***** THE ELASTICITY MATRIX [ABD] *****
0.1200E+09 0.1052E+08 0.2871E+08 0.0000E+00 0.0000E+00 0.0000E+00
0.1052E+08 0.1100E+08 0.2747E+07 0.0000E+00 0.0000E+00 0.0000E+00
0.2871E+08 0.2747E+07 0.1250E+08 0.0000E+00 0.0000E+00 0.0000E+00
0.0000E+00 0.0000E+00 0.0000E+00 0.9998E+01 0.8763E+00 0.2393E+01
0.0000E+00 0.0000E+00 0.0000E+00 0.8763E+00 0.9167E+00 0.2289E+00
0.0000E+00 0.0000E+00 0.0000E+00 0.2393E+01 0.2289E+00 0.1041E+01
**** THE TRANSFORMED [D] MATRIX ****
0.9998E+01 0.8763E+00 0.2393E+01
0.8763E+00 0.9167E+00 0.2289E+00
0.2393E+01 0.2289E+00 0.1041E+01
***** THE COMPLIANCE MATRIX [abd] *****
0.1912E-07 -0.7731E-08 -0.4223E-07 0.0000E+00 0.0000E+00 0.0000E+00
-0.7731E-08 0.9931E-07 -0.4064E-08 0.0000E+00 0.0000E+00 0.0000E+00
-0.4223E-07 -0.4064E-08 0.1780E-06 0.0000E+00 0.0000E+00 0.0000E+00
0.0000E+00 0.0000E+00 0.0000E+00 0.2294E+00 -0.9278E-01 -0.5068E+00
0.0000E+00 0.0000E+00 0.0000E+00 -0.9278E-01 0.1192E+01 -0.4876E-01
0.0000E+00 0.0000E+00 0.0000E+00 -0.5068E+00 -0.4876E-01 0.2136E+01
```

2. Equivalent elastic constants  $E_x$ ,  $E_y$ ,  $G_{xy}$ ,  $\nu_{xy}$ ,  $\nu_{yx}$ ,  $m_x$ ,  $m_y$ ;

Equ Elastic Constant	Ex	Ey	Gxy	vxy	vyx	mx	my
MEMBRANE:	0.523E+11	0.101E+11	0.562E+10	0.404E+00	0.779E-01	0.221E+01	0.409E-01
BENDING :	0.523E+11	0.101E+11	0.562E+10	0.404E+00	0.779E-01	0.221E+01	0.409E-01

3. Bending, torsional and coupling stiffness parameters EI, GJ, K;

BENDING STIFFNESS EI= 0.9161E+01  
TORSION STIFFNESS GJ= 0.3937E+01

COUPLING CONSTANT CK= 0.4348E+01

4. Strength analysis with F.I. based on various criteria subjected to a set of input load Nx, Ny, Nxy, B.M.

\*\*\*\*\* THE STRESS IN EACH LAYER \*\*\*\*\*

PLY-NO	S1	S2	t12
1	0.1203E+09	0.9689E+07	0.2580E+08
2	0.1203E+09	0.9689E+07	0.2580E+08
3	0.1203E+09	0.9689E+07	0.2580E+08
4	0.1203E+09	0.9689E+07	0.2580E+08
5	0.1203E+09	0.9689E+07	0.2580E+08
6	0.1203E+09	0.9689E+07	0.2580E+08
7	0.1203E+09	0.9689E+07	0.2580E+08
8	0.1203E+09	0.9689E+07	0.2580E+08

Max Stress in 1, 2, 1-2: 0.1203E+09 0.9689E+07 0.2580E+08 N/m<sup>2</sup>

Ply-No.	FI from Max Stress in 1, 2 & 1-2	TSAI-HILL	HOFFMAN	TSAI-WU
1	87.8182	230.6931	430.0212245228.4748205958.6225195943.0211	
2	87.8182	230.6931	430.0212245228.4748205958.6225195943.0211	
3	87.8182	230.6931	430.0212245228.4748205958.6225195943.0211	
4	87.8182	230.6931	430.0212245228.4748205958.6225195943.0211	
5	87.8182	230.6931	430.0212245228.4748205958.6225195943.0211	
6	87.8182	230.6931	430.0212245228.4748205958.6225195943.0211	
7	87.8182	230.6931	430.0212245228.4748205958.6225195943.0211	
8	87.8182	230.6931	430.0212245228.4748205958.6225195943.0211	

Max FI from Max Stress Criterion in 1, 2 & 1-2: 87.81822 30.69314 30.0212

in the layers: 1 1 1

Max FI from TSAI-HILL, HOFFMAN & TSAI-WU CRITERIA:\*\*\*\*\*

in the layers: 1 1 1

## Appendix B: BOX Program (Example data file)

Input example:

2 7 1 2

Line 1

--- Option factor for Single-cell (=1) or Double-cell (=2) box beam;

--- Number of parts (panel) divided along the circumference of the box section for loop integral (for 2-cell box, the last part represents the mid-wall. This applies to the following data for material properties, layup and coordinates);

--- Control factor for unit system (=1 for SI unit; =2 for IM unit)

--- Control factor for CUS (ICUS=1) or for CAS (ICUAS=2) layup

8 8 8 8 8 8

Line 2

--- Number of layers in the *ith* part of the curve

1.47E11 0.95E10 0.28 0.58E10 0.58E10 0.58E10 1562.0

1.47E11 0.95E10 0.28 0.58E10 0.58E10 0.58E10 1562.0

1.47E11 0.95E10 0.28 0.58E10 0.58E10 0.58E10 1562.0

1.47E11 0.95E10 0.28 0.58E10 0.58E10 0.58E10 1562.0

Line 3

1.47E11 0.95E10 0.28 0.58E10 0.58E10 0.58E10 1562.0

1.47E11 0.95E10 0.28 0.58E10 0.58E10 0.58E10 1562.0

1.47E11 0.95E10 0.28 0.58E10 0.58E10 0.58E10 1562.0

--- Young's Modulus  $E_1$ ;  $E_2$ ; Poisson's Ratio  $\nu_{12}$ ; Shear modulus  $G_{12}$ ;  $G_{23}$ ;  $G_{13}$ ; material density of the *ith* part respectively

45.0 45 45 45 45.0 45.0 45 45

45.0 45 45 45 45.0 45.0 45 45

45.0 45 45 45 45.0 45.0 45 45

45.0 45 45 45 45.0 45.0 45 45

Line 4

45.0 45 45 45 45.0 45.0 45 45



45.0 45 45 45 45.0 45.0 45 45

45.0 45 45 45 45.0 45.0 45 45

--- *Fibre direction of the Lth layer in the lth part of the section curve (There are total NLAYER(i) layers in the lth part or column)*

0.125E-03 0.125E-03 0.125E-03 0.125E-03 0.125E-03 0.125E-03 0.125E-03  
0.125E-03 0.125E-03 0.125E-03

0.125E-03 0.125E-03 0.125E-03 0.125E-03 0.125E-03 0.125E-03 0.125E-03  
0.125E-03 0.125E-03 0.125E-03

0.125E-03 0.125E-03 0.125E-03 0.125E-03 0.125E-03 0.125E-03 0.125E-03  
0.125E-03 0.125E-03 0.125E-03

0.125E-03 0.125E-03 0.125E-03 0.125E-03 0.125E-03 0.125E-03 0.125E-03  
0.125E-03 0.125E-03 0.125E-03 0.125E-03 0.125E-03 0.125E-03 0.125E-03  
0.125E-03 0.125E-03 0.125E-03 0.125E-03 0.125E-03 0.125E-03

0.125E-03 0.125E-03 0.125E-03 0.125E-03 0.125E-03 0.125E-03 0.125E-03  
0.125E-03 0.125E-03 0.125E-03

0.125E-03 0.125E-03 0.125E-03 0.125E-03 0.125E-03 0.125E-03 0.125E-03  
0.125E-03 0.125E-03 0.125E-03

**Line 5**

--- *Thickness of the Lth layer in the lth part of the section curve (There are total NLAYER(i) layers in the lth part or column)*

0.0 0.0 0.325

**Line 6**

0.0 0.61 0.018

0.0 0.61 -0.25

0.0 0.0 -0.325

0.0 -2.99 -0.31

0.0 -2.99 0.2

0.0 0.0 0.325

3.6 0.65 15.0

--- The x,y,z coordinates (in column) of the lth node (INTEGP number of nodes in total. The last node represents the mid-wall on top skin

0.0 0.0 5.0E+04 0.0000E+00 0.0000E+00 0.0000E+00 0.0000E00 **Line 7**

--- In-plane force in X; Y; XY; moment about X; Y; torque applied to each laminate

1.5E+9 -1.2E+9 0.05E+09 -0.250E+09 0.07E+09 **Line 8**

--- Xt, Xc, Yt, Yc, S : Tensile and compressive strength in fibre direction (1); tensile and compressive strength in off-fibre direction (2); shear strength in 1-2 direction

1 4 **Line 9**

--- The upper and lower Node number connecting the mid-wall (in 1-cell box case, these data will not be read and the above input data representing the mid-wall should be taken away)

#### **Output:**

1. [ABD] matrix for each part (as in Appendix A);
2. Equivalent elastic constants  $E_x$ ,  $E_y$ ,  $G_{xy}$ ,  $\nu_{xy}$ ,  $\nu_{yx}$ ,  $m_x$ ,  $m_y$  (as in Appendix A);
3. Bending, torsional and coupling stiffness parameters EI, GJ, K (as in Appendix A);

## **Appendix C: Comflut Program (Example data file)**

#### **Input example:**

7 0 **Line 1**

--- Total number of main surface modes; control surface modes selected for flutter analysis

1 2 3 4 5 6 7 **Line 2**

--- Mode number of selected modes

23.5 **Line 3**

--- Swept angle (in degree)

7 **Line 4**

--- Total number of span-wise beam elements taken for wing modelling

7 1

**Line 5**

--- Beam element number counted from tip to root; unit system (1= SI unit, 0= IMP unit system)

1	1.11E+06	8.21E+05	3.73E+04	41.18	3.01	-0.07	0.75	1.79
2	3.21E+06	2.47E+06	1.73E+05	147.50	10.28	0.04	0.91	2.16
3	8.27E+06	6.55E+06	2.19E+05	381.45	80.76	-0.05	0.91	2.16
4	1.61E+07	1.47E+07	1.79E+05	418.89	76.18	-0.06	0.91	2.16
5	3.06E+07	3.01E+07	6.71E+05	557.80	30.48	0.01	0.69	1.80
6	9.72E+07	2.21E+08	2.23E+05	1032.58	796.75	0.13	0.29	1.44
7	2.88E+08	6.51E+08	5.21E+05	1183.48	1235.30	0.02	0.55	2.32

**Line 6**

--- Beam element number counted from tip to root; EI; GJ; CK; Mass per unit length (M/L); Polar mass moment of inertia per unit length (Ip/L); Distance between elastic axis and mass axis (negative when elastic axis is forward of the mass exist which is the usual case); The project of the element length on the X-axis and Y-axis respectively Xp, Yp

1

**Line 7**

--- Number of nodes where lump mass exist

6 3110 152.63 520.18 -2.47 0.06 -0.91

**Line 8**

--- Node number where lumped mass exist; lump mass; inertia around the local X and Y axis (origin locates at lumped mass centre); distances between the lumped mass centre and node in X, Y and Z direction respectively

1 0.73 -0.073

2 0.92 -0.092

3 1.14 -0.114

4 1.35 -0.135

5 1.55 -0.155

**Line 9**

6 1.84 -0.184

7 2.28 -0.228

8 2.65 -0.265

--- Node number counted from tip to root; aerodynamic centre position of the lth strip section; lifting-curve slope of the lth strip

1 **Line 10**

--- =1 for modal and flutter analysis, =0 for modal analysis only

10.0 2.0 250.0 **Line 11**

--- Starting frequency; step size (DWF); maximum frequency for flutter search using determinant method (frequency in rad/s)

250.0 2.0 500.0 **Line 12**

--- Starting speed; step size (DU); maximum speed for flutter search used in both determinant and V-g methods

1 2 **Line 13**

--- =1 when input iteration step length 'DWF' and 'DU' are used; =0 when size 'DWF' and 'DU' will take the default values set in the program according to the range

--- =0 when no accuracy is required for both flutter speed and frequency; =1 when the accuracy requirement for flutter speed set in the next group of data will be used; =2 when the accuracy requirements for both flutter speed and frequency set in the next group of data are used

0.5 0.5 **Line 14**

--- Specified accuracy tolerances for flutter frequency and flutter speed respectively

2 1 **Line 15**

--- =0 print flutter speed and frequency only; =1 print flutter results plus modal data; =2 print above results plus result details in the iteration

--- = -1 for divergence using normal mode method; =0 for divergence using static analysis method; =1 for flutter using determinant V-G method; =2 for flutter analysis using V-G method

--- =1 using strip theory; =2 using lifting-surface theory

**Output example:**

1) Mode shape (Bending Torsion)

Mode no	Frequency(rad/s)	Freq.(Hz)
1	10.582	1.684

Node	Distance from root	Vertical Displacement	Pitching Rotation
(i)	(m)	(Bending)	(Torsion)
1	13.830	-1.000	-0.055
2	12.040	-0.742	-0.052

3	9.880	-0.455	-0.043
4	7.720	-0.228	-0.030
5	5.560	-0.081	-0.015
6	3.760	-0.024	-0.004
7	2.320	-0.008	-0.002
8	0.000	0.000	0.000

Mode no	Frequency(rad/s)	Freq.(Hz)
2	31.690	5.044

Node	Distance from root	Vertical Displacement	Pitching Rotation
(i)	(m)	(Bending)	(Torsion)
1	13.830	-1.000	-0.130
2	12.040	-0.449	-0.108
3	9.880	0.036	-0.048
4	7.720	0.209	0.000
5	5.560	0.164	0.020
6	3.760	0.077	0.019
7	2.320	0.030	0.009
8	0.000	0.000	0.000

Mode no	Frequency(rad/s)	Freq.(Hz)
3	51.468	8.191

Node	Distance from root	Vertical Displacement	Pitching Rotation
(i)	(m)	(Bending)	(Torsion)
1	13.830	-1.000	-0.236
2	12.040	-0.269	-0.180
3	9.880	0.201	-0.055
4	7.720	0.141	0.005
5	5.560	-0.043	-0.010
6	3.760	-0.067	-0.039
7	2.320	-0.031	-0.017
8	0.000	0.000	0.000

Mode no	Frequency(rad/s)	Freq.(Hz)
4	86.696	13.798

Node Distance from root Vertical Displacement Pitching Rotation

(i)	(m)	(Bending)	(Torsion)
1	13.830	1.000	-0.017
2	12.040	0.038	-0.139
3	9.880	-0.236	-0.326
4	7.720	0.124	-0.241
5	5.560	0.198	-0.099
6	3.760	0.082	-0.068
7	2.320	0.027	-0.024
8	0.000	0.000	0.000

Mode no	Frequency(rad/s)	Freq.(Hz)
5	100.064	15.926

Node Distance from root Vertical Displacement Pitching Rotation

(i)	(m)	(Bending)	(Torsion)
1	13.830	0.520	1.000
2	12.040	-0.054	0.840
3	9.880	-0.105	0.577
4	7.720	0.075	0.337
5	5.560	0.019	0.126
6	3.760	-0.025	0.000
7	2.320	-0.013	-0.001
8	0.000	0.000	0.000

Mode no	Frequency(rad/s)	Freq.(Hz)
6	129.929	20.679

Node Distance from root Vertical Displacement Pitching Rotation

(i)	(m)	(Bending)	(Torsion)
1	13.830	1.000	-0.032
2	12.040	-0.166	-0.256
3	9.880	-0.108	-0.425

4	7.720	0.185	-0.109
5	5.560	-0.079	0.054
6	3.760	-0.138	0.064
7	2.320	-0.066	0.019
8	0.000	0.000	0.000
Mode no	Frequency(rad/s)	Freq.(Hz)	
7	185.561	29.533	

Node	Distance from root	Vertical Displacement	Pitching Rotation
(i)	(m)	(Bending)	(Torsion)
1	13.830	-1.000	-0.864
2	12.040	0.382	-0.283
3	9.880	-0.150	0.047
4	7.720	0.034	0.027
5	5.560	0.110	0.119
6	3.760	-0.111	0.041
7	2.320	-0.090	0.004
8	0.000	0.000	0.000

## 2) Flutter speed and flutter frequency

-----  
Flutter Speed (m/s);      Flutter Frequency (rad/s)

279.5000                  60.5000  
-----

## Appendix D: Optimisation (MATLAB Code)

### 1) Material Input Data

```
% -----Initial Layup for each Section(1~NoSec)-----
LP1=[45 45 0 45 0 -45 90 -45 90 90 ...
     45 45 0 -45 0 45 90 -45 90 90 ...
     45 0 45 45 -45 0 -45 90 90 -45 ...
```

```

    45 45 0 45 0 -45 90 90 -45 90];
% -----
LP2=[45 45 0 45 0 0 -45 -45 90 -45 90 90 ...
      45 45 0 45 -45 0 45 0 90 45 90 90 ...
      45 0 45 45 -45 0 0 -45 90 90 -45 90 ...
      45 45 0 45 0 -45 0 -45 90 90 -45 90];
% -----
LP3=[45 45 0 45 45 0 0 -45 -45 90 0 -45 90 90 ...
      45 45 0 45 -45 0 45 0 0 90 -45 -45 90 90 ...
      45 0 45 45 45 -45 0 0 -45 90 90 90 -45 90 ...
      45 45 0 45 45 0 -45 0 -45 90 90 90 -45 90];
% -----
LP4=[45 45 0 45 45 0 0 -45 -45 90 0 -45 90 90 90 -45 90
...
      45 45 0 45 45 -45 0 45 0 0 90 -45 -45 90 90 90 -
45 ...
      45 0 45 45 45 -45 45 0 0 0 -45 90 90 90 -45 90 ...
      45 45 0 45 45 0 45 0 -45 0 -45 -45 90 90 90 -45
90];
% -----
LP5=[45 45 45 0 45 45 0 0 -45 -45 90 0 -45 -45 90 90 90
-45 90 ...
      45 45 45 0 0 45 45 -45 0 45 0 0 90 -45 45 90 90
90 -45 ...
      45 0 45 45 45 -45 45 0 0 0 -45 90 -45 90 -45 90 90
-45 90 ...
      45 45 45 0 45 45 0 45 0 0 -45 0 -45 -45 90 90 90
-45 90];
% -----
LP6=[45 45 45 0 45 45 0 0 -45 -45 90 0 -45 0 -45 -45 90
90 -45 90 ...
      45 45 45 0 0 45 45 -45 0 -45 45 0 0 90 -45 -45 90
90 90 90 -45 ...
      45 0 45 45 45 -45 45 45 0 0 0 0 -45 90 -45 90 -
45 90 90 -45 90 ...
      45 45 45 0 45 45 0 45 -45 0 0 0 -45 0 -45 -45 90
90 90 -45 90 ...
      45 45 45 0 45 45 0 0 -45 -45 90 0 -45 0 -45 -45 90
90 90 -45 90 ...
      45 45 45 0 0 45 45 -45 0 -45 45 0 0 90 -45 -45 90
90 90 90 -45 ...
      45 45 45 45 0 0 45 45 0 0 -45 -45 0 -45 90 -45 90
90 90 90 -45];
% -----
LP7=[45 45 45 45 0 45 45 0 0 0 -45 -45 90 0 -45 0 -
45 -45 90 90 90 -45 90 ...
      45 45 45 0 0 45 45 -45 0 -45 45 0 0 90 0 -45 -
45 90 90 90 90 -45 -45 ...
      45 0 45 45 45 -45 45 45 0 45 0 0 0 0 -45 90 -
45 90 -45 90 90 -45 90 ...
      45 45 45 0 45 45 0 45 -45 0 0 0 -45 0 -45 -45 90
90 -45 90 -45 90 90 ...
      45 45 45 45 0 45 45 0 0 0 -45 -45 90 0 -45 0 -
45 -45 90 90 90 -45 90 ...
      45 45 45 45 0 0 45 45 0 0 -45 -45 0 -45 -45 90 -
45 0 90 90 90 90 -45];
% -----
LP=[LP1,LP2,LP3,LP4,LP5,LP6,LP7];
% --Material DEF--

```



```

MAT=[1.48E+11,1.03E10,0.27,5.93E9,5.93E9,5.93E9];
THK=0.183E-3;
DENSITY=1580;
% -----
% --NO of Layers of each Panel on each SEC: upper, lower, front, rear,
(upper, lower, rear of box2)--
Sec.Layer(1,:)= [10 10 10 10 0 0 0];
Sec.Layer(2,:)= [12 12 12 12 0 0 0];
Sec.Layer(3,:)= [14 14 14 14 0 0 0];
Sec.Layer(4,:)= [17 17 16 17 0 0 0];
Sec.Layer(5,:)= [19 19 19 19 0 0 0];
Sec.Layer(6,:)= [21 21 21 21 21 21 21];
Sec.Layer(7,:)= [23 23 23 23 23 0 23];
% -----

```

## 2) Layup Process

```

MAT=M_T_D(1:6);
THK=M_T_D(7);
DENS=M_T_D(8);
EModulus_T_D=zeros(Nnt,8);
ILp=[1,1];%--Layup indicator--
for Ni=1:Nnt
    %-----write ABDMXS.IN-----
    fid1=fopen('ABDMXS.IN','w');
    %---Getting Sequence by indicator--
    ILp(2)=ILp(1)+Sec.Layers(Ni)-1;
    SEQ=LP(ILp(1):ILp(2));
    ILp(1)=ILp(1)+Sec.Layers(Ni);
    %-----
    SEQ=[SEQ,flip(SEQ)'];
    NUML = length(SEQ);
    fprintf(fid1,'%d\n',NUML);
    fprintf(fid1,'%E %E %E %f %E %E\n',MAT);
    for i=1:NUML
        fprintf(fid1,'%d %f %E\n',[i,SEQ(i),THK]);
    end
    fprintf(fid1,'%f\n',1);
    fprintf(fid1,'%f %f %f %f %f %f\n', [680000.0,0.0,0.0,0.0,0.0,0.0]);
    fprintf(fid1,'%E %E %E %E %E %E\n', [1.0E9,0.85E9,0.4E08,0.2E09,0.6E08]);
    fclose(fid1);
    % -----
    %---SOLVE EModulus and Skin Thickness of Single Skin---
    sta=system('ABDMXS.exe');
    fid3=fopen('abdmxs.out','r');
    fid4=fopen('SModulus.txt','w');
    ST=0;
    while ~ST
        tline = fgetl(fid3);
        ST = length(strfind(tline,'MEMBRANE'));
    end
    fprintf(fid4,'%s\n',tline);
    fclose(fid3);
    fclose(fid4);
    SkinThk=NUML*THK;%--Skin Thickness----
    %-----

```

```

%----Write EModulus and Skin Thickness for whole wing----
EM=importdata('SModulus.txt');
Ec=EM.data;
CMatrix=[1/Ec(1),-Ec(5)/Ec(2),-Ec(6)/Ec(1); ...
         -Ec(4)/Ec(1),1/Ec(2),-Ec(7)/Ec(2); ...
         -Ec(6)/Ec(1),-Ec(7)/Ec(2),1/Ec(3)];
SMatrix=inv(CMatrix);

EModulus_T_D(Ni,:)=[SMatrix(1,1:3),SMatrix(2,2:3),SMatrix(3,3),SkinThk
,DENS];
% -----
end

```

### 3) Flutter Speed Process

```

clear
NS=importdata('NS_fvel.txt');
LastFlutter=NS(length(NS(:,1)),:);
fid=fopen('flutter.f06');
fidout=fopen('vgdata.txt','w');
while ~feof(fid)
    tline = fgetl(fid);
    ST = length(strfind(tline,'1./KFREQ'));
    if ST
        tline = fgetl(fid);
        EN=0;
        while ~EN
            fprintf(fidout,'%s\n',tline);
            tline = fgetl(fid);
            EN = length(strfind(tline,'FLUTTER'));
        end
        fprintf(fidout,'\n');
    end
end
fclose(fid);
fclose(fidout);

DAT=importdata('vgdata.txt');
if ~isempty(DAT)
    ind=find(DAT(:,4)>=0);
    [~,mI]=min(DAT(ind,3));
    FI=ind(mI);
    if FI>1
        fvel=linterp(DAT(FI-1:FI,4),DAT(FI-1:FI,3),0);
    else
        fvel=DAT(FI,3);
    end
    fvel=-fvel;
else
    fvel=-LastFlutter(2);
end
NS_fvel=[LastFlutter(1)+1,-fvel];

```

#### 4) Pre-process Optimisation

```
Input_Data;
NoSec=length(Sec.Layer);%--No of Sections----
Nlayers=sum(Sec.Layer,2);%--No of Layers in each Section--
N=sum(Nlayers);%--Total no of layers--
ID=zeros(1,NoSec+1);%--Section Indicator--
for i=1:NoSec
    ID(i+1)=ID(i)+Nlayers(i);
end

fidi=fopen('LPi.txt','w');
fidr=fopen('LPr.txt','w');
% ---
fprintf(fidr,'%d\n',N);
fprintf(fidr,'%d\n',NOPSec);
for i=1:NOPSec
    fprintf(fidr,'%d ',OSec(i));
end
fprintf(fidr,'\n');
for i=1:NoSec+1
    fprintf(fidr,'%d ',ID(i));
end
fprintf(fidr,'\n');
% ---
k=zeros(1,NOPSec);
for i=1:N
    for j=1:NOPSec
        k(j)=(i>ID(OSec(j)) && i<=ID(OSec(j)+1));
    end
    if sum(k)
        fprintf(fidi,'%f ',LP(i));
    else
        fprintf(fidr,'%f ',LP(i));
    end
end
end
LPi=importdata('LPi.txt');
fclose(fidi);
fclose(fidr);
```

#### 5) Post-process Optimisation

```
clear
% --Indicate Section(s) been Optimized (OSec=0~NoSec, put 0 for all
Sections)--
% --Multiple input of section No is allowed, should put in ascending
order--
OSec=[6];
% ----
NOPSec=length(OSec);%--No of section for optimization--
Name=char(zeros(1,2*NOPSec));
for i=1:NOPSec
    Name(2*i-1:2*i)=[ '_',num2str(OSec(i))];
end
PreprocessOPT
LPr=importdata('LPr.txt');
LPi=importdata(['Optimized LP',Name, '.txt']);
```

```

LPi=round(LPi);
% -----Organizing Input-----
N=LPr(1);%--Total no of layers--
NoSec=length(Sec.Layer);%--No of Sections----
NOPSec=LPr(2);%--No of section for optimization--
OSec=LPr(3:2+NOPSec);%--Section(s) to Optimize--
ID=LPr(3+NOPSec:3+NOPSec+NoSec);%--Section Indicator--
LPr=LPr(4+NOPSec+NoSec:end);
M_T_D=[MAT,THK,DENSITY];%--Material Matrix----
% -----
k=zeros(1,NOPSec);
LP=zeros(1,N);
ii=1;jj=1;
for i=1:N
    for j=1:NOPSec
        k(j)=(i>ID(OSec(j)) && i<=ID(OSec(j)+1));
    end
    if sum(k)
        LP(i)=LPi(ii);
        ii=ii+1;
    else
        LP(i)=LPr(jj);
        jj=jj+1;
    end
end
Nnt=Sec.Layer|0;
Nnt=sum(sum(Nnt));%--No of Nontrivial panels--
Sec.Layers=zeros(1,Nnt);%--Nontrivial panels--
NPanel=zeros(1,NoSec);%--No of Panels in each section---
k=1;
for i=1:NoSec
    NPanel(i)=length(Sec.Layer(i,:));
    for j=1:NPanel(i)
        if Sec.Layer(i,j)>0
            Sec.Layers(k)=Sec.Layer(i,j);
            k=k+1;
        end
    end
end
end
% -----
% -Processing Skin Properties-
layupprocess
% -----
% -Write Optimized NASTRAN Input-
Optimized_NASin
% -----

```

## 6) NASTRAN Input Data

```

% -----Format Material Properties-----
MPin=zeros(Nnt,16);
for i=1:Nnt;
    MProperties=[i,EModulus_T_D(i,1:6),EModulus_T_D(i,8)];
    SignMP=MProperties<0;
    DigitMP=-SignMP+2;
    for j=1:8
        MPin(i,2*j-1:2*j)=[DigitMP(j),MProperties(j)];
    end
end
end

```

```

% -----
% -----Write NASTRAN INPUT BDF file-----
fid=fopen('flutterin.bdf','r');
fidout=fopen('flutter.bdf','w');
i=1;
while ~feof(fid)
    tline = fgetl(fid);
    MT = length(strfind(tline,'EMBRAERSEC'));
    TT = length(strfind(tline,'PSHELL'));
    if MT% -----Write Material Properties-----
        fprintf(fidout,'%s\n',tline);
        fgetl(fid);
        fgetl(fid);
        fprintf(fidout,'%-
8s%8.*d%8.*E%8.*E%8.*E%8.*E%8.*E%8.*E%8.*f%s\n%-
8s%8.1f%8.1f%8.1f%8.1f\n','MAT2',MPin(i,:),'+','+',[0,0,0,0]);
        i=i+1;
    elseif TT% -----Write Skin Thickness-----
        fidt=fopen('thicknesstemp.txt','w');
        fprintf(fidt,'%s\n',tline);
        fclose(fidt);
        thickt=importdata('thicknesstemp.txt');
        matno=thickt.data(2);
        if matno<=Nnt
            fprintf(fidout,'%-
8s%8.0d%8.0d%8.6f%8.0d%32.2f\n','PSHELL',thickt.data(1:2),EModulus_T_D
(matno,7),thickt.data(4:5));
        else
            fprintf(fidout,'%s\n',tline);
        end
    else% -----Copy Rest-----
        fprintf(fidout,'%s\n',tline);
    end
end
fclose(fid);
fclose(fidout);
% -----

```

## 7) NASTRAN Input for Optimisation

```

% -----Format Material Properties-----
MPin=zeros(Nnt,16);
for i=1:Nnt;
    MProperties=[i,EModulus_T_D(i,1:6),EModulus_T_D(i,8)];
    SignMP=MProperties<0;
    DigitMP=-SignMP+2;
    for j=1:8
        MPin(i,2*j-1:2*j)=[DigitMP(j),MProperties(j)];
    end
end
% -----
% -----Write NASTRAN INPUT BDF file-----
fid=fopen('flutterin.bdf','r');
fidout=fopen(['Optimized_NASin',Name,'.bdf'],'w');
i=1;

```

```

while ~feof(fid)
    tline = fgetl(fid);
    MT = length(strfind(tline, 'EMBRAERSEC'));
    TT = length(strfind(tline, 'PSHELL'));
    if MT% -----Write Material Properties-----
        fprintf(fidout, '%s\n', tline);
        fgetl(fid);
        fgetl(fid);
        fprintf(fidout, '%-
8s%8.*d%8.*E%8.*E%8.*E%8.*E%8.*E%8.*E%8.*f%s\n%-
8s%8.1f%8.1f%8.1f%8.1f\n', 'MAT2', MPin(i, :), '+', '+', [0,0,0,0]);
        i=i+1;
    elseif TT% -----Write Skin Thickness-----
        fidt=fopen('thicknesstemp.txt', 'w');
        fprintf(fidt, '%s\n', tline);
        fclose(fidt);
        thickt=importdata('thicknesstemp.txt');
        matno=thickt.data(2);
        if matno<=Nnt
            fprintf(fidout, '%-
8s%8.0d%8.0d%8.6f%8.0d%32.2f\n', 'PSHELL', thickt.data(1:2), EModulus_T_D
(matno, 7), thickt.data(4:5));
        else
            fprintf(fidout, '%s\n', tline);
        end
    else% -----Copy Rest-----
        fprintf(fidout, '%s\n', tline);
    end
end
fclose(fid);
fclose(fidout);
% -----

```

## 8) Optimisation Code (Flutter)

```

% --Indicate Section(s) to Optimize (OSec=0~NoSec, put 0 for all
Sections)--
% --Multiple input of section No is allowed, should put in ascending
order-
OSec=[0];
% -----
% -----
% -----
if OSec(1)==0
    OSec=[1,2,3,4,5,6,7];
end
NOPSec=length(OSec);%--No of section for optimization--
% -----
PreprocessOPT
Nv=length(LPi);
LB=zeros(1,Nv);UB=zeros(1,Nv);%--Variable bounds--
LB=LB-90.0001;UB=UB+90.0001;
MaxFunEvals=1e4;%--Max Fun Evaluation--
MaxIter=500;%--Max Iteration--
DiffMaxChange=10;%--Max Step--
RelStep=0.15;%--Step length--
% -----

```

```

fidstep=fopen('NS_fvel.txt','w');
NS_fvel=[0,0];
fprintf(fidstep,'%d %8.3f\n',NS_fvel);
fclose(fidstep);
% ---
[x,fval,exitflag,output,lambda,grad,hessian] =
OPT_Setting(LPi, LB, UB, MaxFunEvals, MaxIter, DiffMaxChange, RelStep);
NLpi=length(x);
Name=char(zeros(1,2*NOPSec));
for i=1:NOPSec
    Name(2*i-1:2*i)=[ '_', num2str(OSec(i))];
end
fidout=fopen(['Optimized LP',Name, '.txt'],'w');
for i=1:NLpi
    fprintf(fidout,'%8.3f',x(i));
end
fclose(fidout);

```